19960503 103

STUDIES OF MECHANICS OF FILAMENTARY COMPOSITES

by Norris F. Dow, B. Walter Rosen, and Zvi Hashin

Prepared by
GENERAL ELECTRIC COMPANY
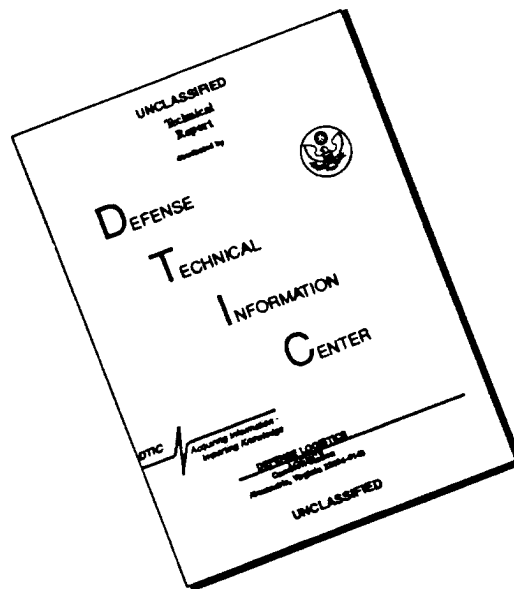Philadelphia, Pa.
for

DISCLAIMER NOTICE

"The aeronautical and space activities of the United States shall be conducted so as to contribute . . . to the expansion of human knowledge of phenomena in the atmosphere and space. The Administration shall provide for the widest practicable and appropriate dissemination of information concerning its activities and the results thereof."

—NATIONAL AERONAUTICS AND SPACE ACT OF 1958

NASA SCIENTIFIC AND TECHNICAL PUBLICATIONS

TECHNICAL REPORTS: Scientific and technical information considered important, complete, and a lasting contribution to existing knowledge.

TECHNICAL NOTES: Information less broad in scope but nevertheless of importance as a contribution to existing knowledge.

TECHNICAL MEMORANDUMS: Information receiving limited distribution because of preliminary data, security classification, or other reasons.

CONTRACTOR REPORTS: Technical information generated in connection with a NASA contract or grant and released under NASA auspices.

TECHNICAL TRANSLATIONS: Information published in a foreign language considered to merit NASA distribution in English.

SPECIAL PUBLICATIONS: Information derived from or of value to NASA activities. Publications include conference proceedings, monographs, data compilations, handbooks, sourcebooks, and special bibliographies.

TECHNOLOGY UTILIZATION PUBLICATIONS: Information on technology used by NASA that may be of particular interest in commercial and other nonaerospace applications. Publications include Tech Briefs; Technology Utilization Reports and Notes; and Technology Surveys.

Details on the availability of these publications may be obtained from:

SCIENTIFIC AND TECHNICAL INFORMATION DIVISION

NATIONAL AERONAUTICS AND SPACE ADMINISTRATION

Washington, D.C. 20546

STUDIES OF MECHANICS OF FILAMENTARY COMPOSITES

By Norris F. Dow, B. Walter Rosen, and Zvi Hashin

ABSTRACT

Studies are reported relating to the enhancement of understanding of the roles played by both binders and reinforcements in the attainment of advanced properties with fibrous composites. Previous analyses of properties and of efficiency of application are reviewed and extended. New analyses are developed for viscoelastic behavior and for three-dimensional reinforcement. Results of mechanical and photoelastic evaluations of transverse effectivenesses of filamentary reinforcement are presented.

FOREWORD

This document is the annual report on the program entitled "Study of
the Relationship of Properties of Composite Materials to Properties of
Their Constituents" for the period from September 27, 1964 to September
26, 1965. The program was performed for the National Aeronautics and
Space Administration under Contract NASw-1144, and was monitored by
Mr. Norman Mayer of that agency.

In this report the section "STATUS OF MICROMECHANICS STUDIES"
was prepared by Mr. Rosen. The sections "THREE DIMENSIONAL RE-
INFORCEMENT and "EXPERIMENTAL EVALUATIONS OF TRANSVERSE
EFFECTIVENESS" were prepared by Mr. Dow, and the section "STRUC-
TURAL EFFICIENCY" was the result of joint efforts of these two authors.
Professor Zvi Hashin of the University of Pennsylvania prepared the sec-
tion entitled "VISCOELASTIC FIBER-REINFORCED MATERIALS".

The authors wish to acknowledge the contributions of the following:
A. Redner of Photolastic, Inc. who did the photoelastic studies; R. L.
O'Brien who performed the experiments on transverse effectiveness, and
O. Winter for computer programming.

TABLE OF CONTENTS

INTRODUCTION

Evaluations of composite materials past and present continue to emphasize the impediment provided to the attainment of dramatic advances in material properties by the relatively weak and flexible plastic binder materials of current technology. The researches described in this report are accordingly directed toward the delineation and evaluation of the role of the binder material as well as the filaments in the determination of the mechanical properties - both as regards strength and stiffness -, and then toward the definition and investigation of various ways of alleviating binder deficiencies.

The present report covers both the areas outlined in the first paragraph. The first part of the report is concerned with extending and carrying to a logical conclusion the efficiency evaluations begun in Reference 1. Then, in the area of delineation and evaluation of the role played by the binder material, a review is made of the state of the art of micromechanics as applied to composites, particularly in the light of the researches already accomplished in associated programs (References 1 and 2) to the present study, in order to tie together the various accomplishments and extend them as required to solidify the base for further advances. As a result of this review, progress in the understanding of the mechanics of tension and compression failure, as well as the determination of elastic properties, is reported in the section "STATUS OF MICROMECHANICS STUDIES".

1

The second part of the report is concerned with advancing the knowledge of the binder-reinforcement mechanics. Researches on viscoelastic behavior are reported in the section "VISCOELASTIC FIBER-REINFORCED MATERIALS", and experiments on the transverse properties of filament-binder combinations are described in the section "EXPERIMENTAL EVALUATIONS OF TRANSVERSE EFFECTIVENESSES OF FILAMENTS OF VARIOUS CROSS-SECTIONS". Finally a method of analysis in the section "THREE-DIMENSIONAL REINFORCEMENT" is developed for three-dimensionally reinforced composites to permit the evaluation of the elimination of all planes of weakness through proper filament orientation.

STRUCTURAL EFFICIENCY

In the previous contract studies, (Reference 1) the structural efficiency of various materials for shell structures subjected to the axial compression loads representative of launch vehicles was treated. In this approach a non-dimensional measure of the structural weight is plotted as a function of a non-dimensional measure of the design load (the structural index) in such fashion that the structure having the least value of the ordinate at any value of the abscissa is the one of minimum weight for that design load. Numerical treatment of fibrous composites indicated that fiber winding patterns which resulted in a material that was isotropic in the plane of the shell produced the most efficient composite structures. The present contract studies have resulted in the simplification of the structural efficiency relations to a form which clarifies the reason for the previous result. Also the studies have been extended to provide a definitive evaluation of the influence of individual constituent properties upon the composite structural efficiency.

Methods of Efficiency Analysis

A composite laminate can now be characterized by two material properties, when considered for application to a cylindrical shell in axial compression. These parameters are the effective modulus, $\bar{E}$, and the shear stiffness ratio, γ, given by:

$$\bar{E} = \left[\frac{E_L E_T}{1 - \nu_{LT} \nu_{TL}} \right]^{1/2} \tag{1a}$$

3

$$\gamma = \frac{G_{LT}}{\left[\frac{\sqrt{E_L E_T}}{2(1 + \sqrt{\nu_{LT} \nu_{TL}})} \right]}$$

(1a)

Where L & T denote longitudinal (axial) and transverse (circumferential) directions, the results of the analysis of Ref. 3 have been applied (Ref. 4) to laminates which are effectively homogeneous through the thickness. When transverse shear deformations are neglected, the resulting instability equation is of the form:

$$\sigma_{cr} = \frac{K}{\sqrt{3}} \left(\frac{t}{R} \right) \overline{E} \; \overline{\phi}$$

(2)

where

$\overline{\phi}$ is the smaller of $\gamma^{1/2}$ and unity

$\dfrac{t}{R}$ is the shell thickness (or effective thickness for a sandwich shell) to radius ratio

K   empirical factor to account for initial imperfections, etc. (herein, K is assumed unity throughout)

The buckle pattern is either of the symmetric-or bellows type-or the asymmetric-or checkerboard type-as γ is greater or less than one, respectively. Thus, shells having a low shear stiffness ratio will buckle in a checkerboard pattern. As the shear stiffness is increased, while the effective modulus, $\overline{E}$, is held constant, the shell will reach the point where the lowest buckling stress is associated with the symmetric mode. Beyond this, any further increases in the shear stiffness ratio will have no effect on the buckling stress.

In terms of the structural efficiency, the elastic behavior can now be represented by the following simple expression:

4

$$\frac{W}{R} = \frac{\rho_s \sqrt[4]{3}}{\sqrt{\overline{E}\,\Phi}} \sqrt{\frac{N_x}{R}} \tag{3}$$

where

W   shell weight per unit surface area

R   shell radius

ρ_s shell material density

N_x shell load per unit circumferential length

In the above equations it is seen that for an isotropic material:

$$\Phi = \gamma = 1$$

and:

$$\overline{E} = \frac{E}{\sqrt{1 - \nu^2}}$$

An isotropic material can be obtained with a fibrous composite by selecting a fiber orientation pattern in which one n^{th} of the fibers are oriented in each of n equally spaced directions (with $n \geq 3$) and with many layers so that the material is effectively homogeneous through the thickness. Such a material has been shown to be the most efficient for the launch vehicle application (Ref. 1). Typical results which illustrate both the benefits of an isotropic pattern and also the influence of shear stiffness are shown in Fig. 1. Here the elastic efficiency is characterized by the slope, F, of the curve relating weight to the square root of the loading index, i. e. :

$$F = \frac{\dfrac{W}{R}}{\sqrt{\dfrac{N_x}{R}}} \tag{4}$$

5

E-glass reinforced epoxy composites containing seventy percent fibers, by volume, are considered for various fiber orientations. The upper curve is a longitudinal/circumferential (or $0°/90°$) laminate of varying fractions of the material in each direction. The next curve is for a symmetric helical pattern ($\pm\theta$) of varying helix angle. The straight line is the isotropic pattern and the weight reduction associated with this pattern is evident.

It is of interest to note also that the efficiency of a $\pm45°$ laminate and a half and half $0°-90°$ laminate are identical. These structures are of the same material but one has the material principal axes rotated 45° with respect to the other. This rotation does not have any effect on the buckling strength of the composite shell. However, the shear stiffness ratios differ substantially and the buckle modes are different. The helical pattern shell buckles symmetrically at this point and the $0°-90°$ shell buckles asymmetrically. When a shell is made with a material containing equal parts of these two biaxial laminates the result is a material which has 25% of its material every $45°$. This is an isotropic pattern and has the high strength (or low weight) shown by the lowest line of Fig. 1. The halves of the two biaxial materials when put together buckle at higher loads than shells of each alone because of the conflict in buckle patterns.

Equations (2) and (3) apply to simple monocoque shells. As has been shown, for the majority of cases of interest for launch vehicles, stiffened shells are more efficient than monocoque construction. Accordingly, to investigate the potential of fibrous composites for stiffened shells, an

6

idealized stiffening was hypothesized; the shells were assumed made in the form of a sandwich with an ideal core material having adequate stiffness properties through the thickness to stabilize the faces, but having no ability to carry axial load. The elastic buckling efficiency for sandwich shells with such a core is given by Reference 4.

$$\frac{W}{R} = \frac{\left[\rho_s + \rho_c\left(\frac{t_c}{2t_s}\right)\right]}{\left[\left(1 + \frac{t_c}{2t_s}\right)^3 - \left(\frac{t_c}{2t_s}\right)^3\right]^{1/4}} \left[\frac{\frac{N_x}{R}}{\frac{K}{\sqrt{3}} E \phi}\right]^{1/2} \quad (5)$$

where

ρ_s, ρ_c densities of face and core materials

t_s, t_c thicknesses of face and core materials

In all cases, minimum-weight sandwich proportions were used, with the optimum ratio of $\frac{t_c}{2t_s}$ found from the equation

$$\frac{\rho_c}{\rho_s} = \frac{2\left(\frac{t_c}{2t_s}\right) + 1}{2\left(\frac{t_c}{2t_s}\right)^2 + 3\left(\frac{t_c}{2t_s}\right) + \frac{4}{3}} \quad (6)$$

For stresses above the elastic range (as in Reference 4)

$$\frac{W}{R} = \frac{\rho_s + \rho_c\left(\frac{t_c}{2t_s}\right)}{\sigma_y} \cdot \left(\frac{N_x}{R}\right) \quad (7)$$

where

σ_y is the compressive "yield" or failure stress for the face materials

As brought out in Reference 1, the determination of a really adequate

7

value of σ_y for fibrous composites is a problem for further research, and conclusions drawn regarding the potential of these materials for those (limited) applications for which Equation 7 is used must be somewhat qualified. For launch vehicles, however, elastic buckling is the dominant criterion.

Equations 1 through 7 were used in References 1 and 5 to evaluate the efficiency of composite shells having a wide range of constituent properties and geometries. The present extension of these studies concentrates upon the presentations of the influence of individual constituent properties upon the composite structural efficiency.

The elastic constants of Equation 1 were evaluated by the methods of Reference 6. The range of loading intensities used in Equations 3 and 5 were based on the boosters described in Table 1.

Materials and Configurations Considered

The materials and configurations considered for the launch-vehicle shell application fell into several classes, as follows:

(a) <u>Metals</u> - First a family of metal shells was analyzed to provide a basis for comparison with the composite shells. This metal family comprised a steel, titanium, aluminum, magnesium, and beryllium alloy with the advanced properties postulated in Table 2. These properties were deliberately chosen to be high relative to present technological values to insure

a high standard for the comparisons with composites.

(b) Filaments - A family of eight filamentary materials was selected for use in the composites. These materials began with the presently used E-glass in both solid and hollow fibers and ranged upward in characteristics, including:

High-Modulus Glass
Asbestos
Steel
Beryllium
Boron
·and Alumina

The properties used for these various filamentary materials are given in Table 3.

(c) Binders - A family of eight binder materials was also selected into which the various filaments were incorporated. The binders began with the presently used epoxy resin and ranged upward in properties, as follows:

Magnesium
Three hypothetical "Light Alloys"
Titanium
Steel
Boron

The properties used for these various binder materials are also listed in Table 4.

(d) Configurations - All shell composites were considered to be laminates with each lamina unidirectionally reinforced by the filamentary material. The directions of reinforcement of the laminae were varied in symmetric fashion such that the principal stiffnesses of the laminate always coincided with the axial and circumferential shell directions. The number of laminae

9

was supposed great enough so that the laminate acted like a homogeneous medium, -i.e., no attempt was made to dispose internal and external laminae in different fashions. Thus typical configurations included: (1) longitudinal reinforcement; (2) transverse reinforcement; (3) longitudinal and transverse reinforcement; (4) reinforcement at equal angles ($\pm\,\theta$) to the longitudinal or transverse directions; and (5) three way ($\pm\,30^{\circ}$, 90°) reinforcement to provide in-plane isotropy.

In order to help isolate the importance of various factors on the end efficiency of composites, the filamentary and binder materials were selected to provide several interrelated systematic types of variations. These interrelationships are indicated on Figure 2. The matrix material properties plotted in Figure 2 show that:

(1) The magnesium, titanium, and steel materials provide a variation in modulus at constant modulus-to-density ratio.

(2) The magnesium, "light alloy II", "light alloy III", and boron materials provide a variation in modulus at constant density.

(3) The "light alloy I", "light alloy II", and titanium provide a variation in density at constant modulus, as do the "light alloy III", and steel at a different constant modulus.

The fiber materials were selected to cover the range of actual prospects from those now in actual use like E-glass to those which are more in the nature of laboratory curiousities like alumina. (The fiber properties are presented in Figure 2b.) Thus approximately the entire spectrum of

10

properties of current interest is surveyed as well as those portions

of the spectrum which provide systematic variations.

Results and Discussion

The results of the evaluations of composite shell efficiencies are

discussed here in sections. In the first section the interplay between

the magnitude of the design loading and the structural configuration

employed to support the load is considered, to insure that the results

are not inequitably influenced by the configurations chosen. In the

second section, the conclusions drawn from this consideration of the

significance of configuration are focussed upon the evaluation of hol-

low fiber reinforcement. Here some of the aspects of the importance

of fiber stiffness are first demonstrated, and then they are examined in

detail in the third section. Finally, the importance of binder stiffness

is assessed.

Effects of Configuration

Metal Shells - The basis used for the evaluations of fibrous composite

shells is established in Figure 3. Here are plotted the weights of cylin-

drical shells of a wide range of types of metals, and fabricated in a variety

of sandwich proportions, designed to carry intensities of loadings of from

a small fraction of-to many time those-appropriate for launch vehicles,

as shown. Characteristically a shell of any material is heavier than the

the weight required to carry the design load at the material yield stress

(represented by the lines of 45° slope at the right of Figure 3) by the

weight of the additional material needed to stabilize the shell against

buckling. Generally speaking the greatest weight is required with the

stiffening added simply as increased shell thickness, giving a pure mono-

coque construction (the upper curves on the figure). For the monocoque

buckling below the yield stress, the weight is proportional to $\dfrac{\rho}{\sqrt{E}}$ as is

well known, and beryllium is a currently recognized minimum-weight metal

for the idealized monocoque shell, - especially in the low loading intensity

regime of interest for launch vehicles.

Clearly, however, Figure 3 shows that for the metal shell more is to

be gained by a change from a monocoque to an efficient stiffening configur-

ation like a low-density-core-material sandwich than by the use of even

such an efficient material as beryllium. In fact a steel faced sandwich with

a light core may be lighter than a beryllium monocoque shell, -indeed will

be lighter than a beryllium faced sandwich on the same core if the core

densities are low enough or the loading intensities high enough (the area

shown to the right of Figure 3) so that the higher strength-to-weight ratio

of steel compared to beryllium can be utilized.

Important to the composite evaluations to which this study is directed is

the implication of the preceding paragraph that the optimum material de-

pends upon both loading that must be carried and upon the structural config-

uration employed. In consequence both the range of loadings and range of

configurations of interest must be surveyed for proper assessment of the

potentials of composites. Herein the effect of varying overall configuration

12

is determined by a variation in the hypothetical sandwich core density. The results of this variation are generally the same as variations in the effectiveness of other types of stiffening. Thus, a very light weight core represents to a degree, for example, very efficient integral ribbing on the shell, or highly efficient ring-stringer reinforcement.

One further aspect of the importance of configuration in the evaluation of material efficiency is brought out by the reference shell efficiencies calculated for the variables included in Figure 3. Whereas for the elastic monocoque shell the weight is proportional to $\frac{\rho}{\sqrt{E}}$ as previously noted, this relationship does not apply for sandwich shells even for the heaviest core density given in Figure 3. For values of the ratio of face sheet to core densities large compared with unity, it can be shown that the shell weight for a given core density is proportional to $\sqrt{\rho/E}$. The shell weight required in the elastic buckling range may be measured simply by the efficiency parameter, F, of Equation 4. Here F is a function of shell moduli and density. Values of F are plotted in Figure 4 for monocoque and sandwich shells of the five metals used in Figure 3. As shown, values of F for the monocoque configuration plot on the expected straight line of 45° slope when the abscissa is $\rho/\sqrt{E}$, but for the sandwich the abscissa must be changed to $\left(\frac{\rho}{E}\right)^{1/2}$. Thus even for elastic buckling the configuration affects the relationship between material properties and shell efficiency, though perhaps not as profoundly as when a change from elastic to plastic behavior is involved.

Composite Shells - With fibrous composites additional degrees of

freedom are available compared to metal construction. Not only may

each reinforcing material be employed in a variety of binder materials,

but also various volume fractions of the constituents and fiber orientations

may be used. Typical effects of binder content are illustrated in Figure 5.

Figure 5 shows the elastic buckling efficiences at a typical sandwich core

density, and hence applies to the low load end of the range. Variations in

elastic buckling efficiency as measured by the values of F plotted in Figure 5

are rather surprising in that relatively small concentrations of the high-

modulus filaments are sufficient to produce materials with buckling effective-

ness comparable to structural metals. Accordingly, for the very light

loading for which strength is not important, low volume fractions of advanced

filaments may be of interest.

Disappointingly inefficient are the results for the hollow E-glass filaments.

These results have sufficiently sweeping implications regarding geometrical

effects to warrant special attention, and some of these implications are there-

fore reviewed in the following section on the effects associated with the use

of hollow fibers.

Effects of Hollow Fibers

Hollow fibers provide a reduction in density, ρ_s, of composite material

together with a high ultimate compressive stress-density ratio (Reference 7).

At the same time the hollows reduce the elastic stiffnesses and the absolute

values of strength. Because of these reductions, with E-glass, as pointed out in the preceding section, for sandwich shell faces the hollows are not effective, and indeed compared to metal shells, hollow E-glass reinforcements appear attractive only for monocoque shells.

Factors which combine to make hollow E-glass ineffective are (1) the fact that for a sandwich face material, density is not as important a characteristic as for a monocoque shell, and (2) the low transverse stiffness properties calculated for the hollow fibers. As previously pointed out, for a sandwich the efficiency varies inversely as only the square root of the face material density, where for the monocoque the efficiency varies as the inverse first power of the density. The low transverse stiffness found for the hollow glass is a less obvious problem, however, that deserves further consideration. Perhaps, for example, the analysis of the hollow fiber transverse stiffness is more open to question than the solid fiber calculations. For both types of fibers the values used are the average of upper and lower bounds but in the case of the solids the bounds are not far apart so that this procedure is open to no substantial variation no matter which bound is the more applicable. For the hollows, on the other hand the upper-bound transverse stiffness at 30% binder is approximately twice the value for the lower bound. Thus, the hollow fibers may be appreciably better (or even worse) than the mean value indicates.

Regardless of the accuracy of analysis, perhaps of greater significance

for future prospects is the fact that stiffer materials than E-glass should

perform better transversely in an epoxy matrix. This effect is illustrated

in Figure 6 where the calculated ratios of transverse stiffness (upper and

lower bounds) for hollows and solids are plotted against volume fraction

of binder for alumina and E-glass fibers. The curves for the alumina are

above those for E-glass over the entire range of concentrations, being

about twice as great at the normal 30 volume percent binder. In other words

not only is the transverse stiffness inherently higher for alumina than E-

glass reinforcement, but also the hollow alumina performs twice as well

compared to solid as the E-glass does. In sum, hollow E-glass fibers in

epoxy binder appear promising only for increasing the efficiency of shells

in applications for which material density is of prime importance, as for

monocoque construction. Hollow filaments of higher modulus than E-glass

may be relatively more favorable.

The Importance of Fiber Stiffness and Density

That the use of high modulus/density ratio filaments like boron should

increase the elastic buckling efficiency of composite shells is to be expected,

and the effect is demonstrated by the values of F given in Figure 5 for

sandwiches and Figure 7 for monocoque construction. In order to determine

just how effective improvements in filaments may be, the filament density

and modulus will be treated separately. The face sheet density is related to

the fiber and binder densities by a simple mixtures rule. When the fiber

weight is a large fraction of the composite weight, as it is for high volume

fractions of most fiber materials, then the variation of F with fiber density

16

is of essentially the same form as that of the variation with face density
(i.e., with ρ_f for monocoque and $\rho_f^{1/2}$ for sandwich construction). The
variation of weight with modulus is most readily studied by plotting F as
a function of E_f for the family of constant density fibers shown in
Figure 2b. For example, Figure 8 presents such results for sandwich
shells having isotropic and uniaxial face sheets. The slope of the best
fit straight lines can be used to determine the exponent of fiber modulus
in the assumed weight variation:

$$F = K \rho_f^{\ m} E_f^{\ n} \tag{8}$$

These results are combined to yield the results shown in Figure 9. The
exponents have been rounded off to fractional powers as greater accuracy
is certainly not justified at the present. Similar results are presented in
Figure 10 for the monocoque shell. Correlation of the data are indicated
by comparison with curves of 45° slope on the log-log plots of the figures.
Approximate correlation is found if the following powers of Young's modulus
are employed:

(1) $F \propto \dfrac{1}{E_f^{\ 1/6}}$ for 0° reinforced monocoque shells

(2) $F \propto \dfrac{1}{E_f^{\ 1/3}}$ for Isotropic monocoque shells

(3) $F \propto \dfrac{1}{F_f^{\ 1/6}}$ for 0° reinforced sandwich shells

(4) $F \propto \dfrac{1}{E_f^{\ 1/2}}$ for Isotropic sandwich shells

17

(Correlation is established as for the metal shells by comparison with curves of 45° slope on the log-log plots of the figures.)

Thus it appears that the elastic buckling efficiency of composite shells is a rather insensitive function of the modulus of the fibers. For the configuration of greatest probable interest, however, (the isotropic sandwich), the sensitivity is greatest, and in this case an increase in fiber modulus is nearly as effective as a decrease in fiber density.

Throughout this section only epoxy binder at 30% volume fraction has been considered. Effects of binder changes will be considered in the following section.

The Importance of Binder Stiffness and Density

The use of improved binder material compared to epoxy resin can have several important effects. First, by enhancing the transverse and shearing stiffnesses, it can reduce the difference in buckling efficiencies of the 0° and Isotropic reinforcement configurations. This effect is illustrated in Figure 11.

In Figure 11 are plotted the buckling effectivenesses of composite sandwiches made with very high modulus filaments like alumina embedded in a variety of metallic binders. The plots show that for all binder volume fractions there is little difference in efficiency for the 0° and Isotropic configurations, although the Isotropic cases are always the lighter. For

18

comparison, the F value for beryllium sandwiches is also given on the figure; for purely elastic buckling it is exceeded in efficiency only at high volume fractions by the boron-like binder. However, it should be recalled that, even for the low loading intensities of launch vehicles, such beryllium sandwiches would be stressed beyond the elastic limit, and any of the alumina-reinforced composites would therefore be more efficient in application.

The effectiveness of improvements in binder material properties is similar to that of filament properties. Even with an advanced filament like boron, the buckling efficiency is improved compared to epoxy binder by either an increase in binder modulus or a decrease in binder density (see Figure 12). Evaluation of the magnitudes of the improvements (Figure 13) show that they depend only on the one-sixth power of the modulus, for monocoque rather than sandwich shells again the density is of greater significance, $F \propto \sqrt[3]{\dfrac{\rho_b}{\sqrt[3]{E_b}}}$, approximately.

Conclusions

The conclusions derived from the complete investigation of the influence of constituent properties upon the efficiency of composite shells are as follows:

1. Loading intensities for launch vehicles are so low that elastic buckling governs the compression design for all but the most efficient stiffening configurations.

2. For sandwich construction the elastic shell buckling efficiency
is no longer proportional to the ratio of shell density to the square
root of Young's modulus $\frac{\rho}{\sqrt{E}}$ as for a monocoque shell, but rather
is proportional to $\sqrt{\frac{\rho}{E}}$ for the sandwich face material.

3. Composites reinforced in an isotropic laminate configuration
by advanced filaments like boron and alumina are superior to the best
metal shells for the most structurally efficient applications for launch
vehicles.

4. Relatively small concentrations of high-modulus filaments in an
isotropic configuration produce materials with buckling effectiveness
comparable to structural metals.

5. Hollow fibers appear promising only for shell buckling applications
for which density is of prime importance, (for example; monocoque shells,
minimum-gage cases).

6. The relation between shell buckling efficiency and filament properties
varies with configuration. In general the efficiency is a weak function of
the filament modulus and a stronger function of filament density. For the
most efficient configuration (isotropic laminate sandwich) the efficiency
is proportional to the square root of the filament density and slightly less
than the square root of the inverse of the modulus.

7. The relation between shell buckling efficiency and binder properties
is similar to that for filaments but is an even weaker function. Thus, for
the isotropic sandwich shells the efficiency is approximately proportional

20

to the one-sixth power of the density/modulus ratio.

8. Failure criteria for composite shells need further intensive investigation. Such problems as those of maximum shear stresses in laminates in compression need evaluation.

STATUS OF MICROMECHANICS STUDIES

During the course of this NASA sponsored program for the study of
composites (see Refs. 1 and 2), the authors have undertaken studies of those
aspects of the mechanics of composites which are on the one hand necessary
to provide an understanding of the synthesis, design and response of compo-
site structural laminates and which, on the other hand, have not been ade-
quately treated in the existing literature. It is, therefore, appropriate
at this time to discuss the relationship of these NASA contract results to
other related studies in the open literature. The aim of this review is not
to provide a comprehensive critical literature survey, but rather to examine
a limited number of existing solutions of problems of interest for subsequent
studies. The status of the micromechanics studies to be used in this program
will thus be defined.

A concept which simplifies many aspects of the analysis of composite
materials is the recognition that for most static loading conditions, the fiber
cross-sectional dimension is small compared to the structural dimension
and to the dimension over which a significant variation in applied load or dis-
placement occurs. Thus it is reasonable to consider the average stress and
strain in the composite, rather than the actual stress and strain distribution.
This permits the representation of the inhomogeneous isotropic composite
by an equivalent homogeneous anisotropic material where the response of the
latter to imposed boundary tractions or displacements is equal to the average
response of the former to the same boundary conditions. Several approaches

to the problem of relating the elastic constants of the "effective" material to the properties (mechanical and geometrical) of the constituents are treated in the following section. Although the understanding of average response is adequate for many structural applications, a treatment of composite strength generally requires a knowledge of some details of the internal stress distribution. Analyses of these stresses are described under "Internal Stresses". The utilization of the internal stress solutions in the treatment of composite strength is described in the "Failure Mechanics" section.

The elastic constants analyses define the moduli of the individual layers of a composite laminate. The failure mechanics studies likewise define lamina strength criteria. The results of these studies can then be used to define overall laminate stiffness, strength and structural performance. For this aspect of the study, a substantial body of literature developed for plywood-type materials, among others, is in existence. The applicability of these studies is presently being evaluated (an indication of this is given elsewhere in this report in connection with the stability of laminated shells). For this reason and because of the existence of several recent literature reviews on this subject (e.g., Ref. 8 and 9). The present survey does not include the subject of laminate analysis.

Elastic Constants

The direct approach to the evaluation of elastic constants is to determine the stress distribution in the inhomogeneous composite medium subjected to various simple boundary conditions and then to obtain appropriate body averages. These boundary value problems require the complete specification of the phase geometry (e.g., the relative location of fibers over the cross-sectional

plane normal to the fiber axes) and the extensive application of numerical methods. This approach has recently been utilized for a hexagonal array (Ref. 10) and a square array (Ref. 11) of circular fibers. These methods produce the desired results for a known geometry (although requiring the use of high speed computers). However, they do leave unanswered the question of the magnitude of possible variations in moduli associated with the variation in cross-sectional location of fibers.

A second approach to this problem utilizes known and regular phase geometries and gross approximations to the nature of the stress field. Thus the materials are usually represented as various combinations of simple elements in series and in parallel with one another (e.g., Ref. 12 and 13). Papers of this type range from simple approximations of the stiffness parallel to the fibers to transverse Young's and shear moduli obtained by assuming uniform strain or by assuming that the material can be represented by a truss, etc. These methods can be justified as providing working estimates only if no better methods are available. Thus at the present state of development they are not of major importance.

The third approach to the elastic constants problem is the use of variational principles to obtain bounds on the desired moduli. In this method the effective elastic moduli are expressed in terms of the strain energy and bounds on the strain energy are found for simple applied average stress and strain fields, thus also bounding the elastic moduli. This definition of moduli in terms of strain energy is directly equivalent to the definition in terms of average stress and strain. In the previous contract studies

(Ref. 2), strain energy methods were used to evaluate elastic constants as functions of constituent moduli and volume fractions. Uniaxially oriented circular fibers randomly distributed over a cross-sectional plane were considered. Such a material is transversely isotropic and is defined by five independent elastic constants. These constants can be bounded for several different types of geometries.

Several geometries of interest are shown in Fig. 14. The hexagonal array is typical of the ordered arrays which are susceptible to rigorous bounding procedures. The contrast between such orderly arrays and the arrays which result from common manufacturing procedures are indicated by comparison of the upper two sketches in Fig. 14. Indeed, the contiguity between the fibers shown in cross sections of real fibrous composites has motivated some interest in the possible effect of continuous or semi-continuous load transmission paths through the fiber material. The extreme of such geometric considerations is represented by the arbitrary phase geometry in which both phases are cylindrical but a cross-section perpendicular to the generator of the phase geometry interfaces is completely arbitrary and a distinction between the two materials enabling one to identify a fiber and a binder is no longer possible. Rigorous bounds can also be obtained for this arbitrary geometry material (see Ref. 14 and 15). The problem, however, is that the distance between such bounds is usually quite large and the value of the upper bound for application to the case of rigid fibers in relatively less

rigid binder materials is questionable. That is to say, it appears intu-

itively that a continuous binder phase will result in modulus values closer

to the lower bound of the arbitrary phase geometry material. Another set

of bounds exists. These are those of Ref. 6 for the special material also

shown in Fig. 14. This material is composed by taking concentric circular

cylinders of fiber and binder with the fiber material as the core and the

volume fractions of fiber and binder in this typical composite cylinder are

equal to those of the volume fractions of the two materials in the bulk com-

posite. These volume fractions are maintained in a set of cylinders

having various diameters which are used to completely fill out the entire

volume by going to an infinitesimally small fiber diameter. The bounds

for this material coincide for four of the five independent elastic constants.

These are the so-called random array results. For the real material,

it is always possible to surround each circular fiber with a cylinder of

binder material such that the fiber binder composite has the proper volume

fractions. However, the outer surface of the binder will not be a circular

cylinder. The results of the random array can be used as an approximation

to this real material by assuming that the strain energy in this irregularly

shaped composite cylinder can be approximated by the strain energy in a con-

centric circular cylinder having the same areas of fiber and binder. This as-

sumption makes the random array results directly applicable to the real material

behavior. However, there is some uncertainty associated with this assumption and

alternate assumptions have been proposed in the form of interpolating fac-

tors between the upper and lower bounds of the arbitrary phase geometry

results. It should be noted that for those cases where the bounds of the

random array moduli are coincident, they also coincide with the arbitrary

phase geometry bounds when the binder and fiber materials are alternately

used as the core of the typical composite cylinder. This information is

of value in that it establishes for those cases the fact that the arbitrary

phase geometry bounds are the best possible bounds.

Various interpolation schemes have been proposed to yield a set of

values for elastic constants which can be used in structural analysis. Tsai

(Ref. 16) has proposed that a linear interpolation between the upper and lower

bounds is a proper approach. The contiguity factor represents the inter-

polation between the bounds. Wu (Ref. 17) has proposed an interpolation

factor based on physical reasoning which has recently been shown to be

equivalent to a linear interpolation factor between the bounds. Such approaches

assume that a single interpolation between the bounds will be valid for all

volume fractions when dealing with a pair of constituents in a fibrous com-

posite. Further, their value is quite limited unless the interpolation factor

is also insensitive to the ratio of the elastic constants of the two phases.

Such questions can only be answered by comparison with experimental data.

The experimental data for the moduli in question, which are notably those

in the transverse plane, are quite limited.

An indication of the relative position of the various bounding curves discussed above is provided in Fig. 15. The transverse bulk modulus is plotted here as a function of the binder volume fraction for constituents having a ratio of elastic moduli of 100. This ratio is appropriate, for example, for boron reinforced epoxy. For the transverse bulk modulus the random array results coincide, and as pointed out earlier, this result is also equal to the lower bound for the arbitrary cylindrical phase geometry. These curves are also shown on the figure, and note that at reasonable volume fractions the upper and lower bounds differ by about an order of magnitude. Also shown on this figure are the results obtained by Paul (Ref. 18) for isotropic composites of these same materials. That is, an upper bound equal to the popular "rule of mixtures" and a lower bound which is essentially the equivalent of the two materials located in a series path in resistance to the load. The proximity of these latter two curves to the arbitrary phase geometry results emphasizes the problem of using the arbitrary phase geometry results. When these bulk modulus results are used with the shear modulus results to obtain results for the transverse Young's modulus, distinct bounds occur since the bounds for the shear modulus are not coincident. This is shown in Fig. 16 where the transverse Young's modulus for glass reinforced plastics is plotted as a function of the binder volume fraction. Again the random array upper and lower bounds are shown, the arbitrary cylindrical phase geometries upper and lower bounds are shown, and the experimental data available in the literature (Ref.

16) are plotted. An interpolation curve two-tenths of the distance between the lower and upper arbitrary phase geometry bounds is plotted. This value is suggested in Ref. 16. Note that both the C = 0.2 and the random array upper bound are good approximations to the experimental data over the range for which such data are available. No rational choice between these two curves for use as design data can be made on the basis of this comparison. However, a different result occurs when experimental data for boron reinforced plastics (Ref. 19) are plotted as in Fig.17. Here the greater distance between upper and lower arbitrary phase geometry bounds results in a greater separation of the C = 0.2 curve from the lower bound. Here it is seen that C = 0.2 is now a poor approximation to the experimental data while the random array upper bound remains a good result. Although these data are too limited to justify the conclusion that interpolation schemes are not useful, they do seem to indicate that the random array result is at this time a more rational choice. A comparison between these random array results and the few existing exact solutions is also of interest. For this purpose we can compare the Hashin/Rosen bounds (Ref. 6) to numerical solutions for hexagonal arrays obtained in Ref.10, and to solutions obtained for random arrays of circular holes and rigid fibers in an elastic plate (Ref. 20).

The data of Ref.10 are in the form of a computed matrix of elastic constants, g_{ij}, in the form:

$$\sigma_i = g_{ij} \, \epsilon_j$$

$$\text{or} \qquad [\sigma] = [g][\epsilon] \tag{9}$$

The comparison of these results with those of Ref. 6 is best accomplished by transforming the former according to the following relations:

$$K_{23} = \frac{1}{4}(g_{11} + g_{22} + g_{12} + g_{21})$$

$$G_{23} = \frac{1}{4}(g_{11} + g_{22} - g_{12} - g_{21})$$

$$E_1 = g_{33} - \frac{(g_{13} + g_{23} + g_{31} + g_{32})^2}{4(g_{11} + g_{22} + g_{12} + g_{21})} \tag{10}$$

$$\nu_{21} = \frac{g_{13} + g_{31}}{g_{11} + g_{22} + g_{12} + g_{21}}$$

$$G_{12} = \frac{1}{2}(g_{44} + g_{55})$$

where the left-hand side of the above equations is in the nomenclature of the present paper and the right-hand side is in that of Ref. 10. Note that where different numerical results were obtained for symmetric terms of the elastic constant matrix, they were averaged. The comparison between the results of Refs. 10 and 6 appears in Table 5.

The results of Ref. 20 which lend themselves to comparison are those for the plane stress bulk modulus, K^1_{23}. These can be obtained from Ref. 20 by reading values for Young's modulus and Poisson's ratio from curves

presented in that paper (with limited accuracy because of the small size of the graphs) and computing.

$$K^1_{23} = \frac{E}{2(1-\nu)} \tag{11}$$

Similarly, the plane stress bulk modulus, K^1_{23}, is related to the plane strain bulk modulus, $\overline{K}_{23}$, from Ref. 6, by:

$$K^1 = \frac{\overline{K}}{\phi} \tag{12}$$

$$\text{where } \phi = 1 + \frac{4\overline{K}\nu^2_{21}}{E_1}$$

The resulting values are plotted in Fig. 18.

Because of the greater flexibility and simplicity of the strain energy results of Ref. 6 , the curves in Fig. 18 and the data of Table 5 can be interpreted as supporting the use of the Hashin/Rosen Bounds for computation of the effects of variation in any of the constituent properties. The numerical methods (i.e., Ref. 10 and 11) are also limited to very specific regular arrays in the sense that the existant complexity would be greatly multiplied if it were necessary to use a typical element involving more than one fiber as the basis for the numerical analysis. In conclusion, it appears that the methods of Ref. 6 are the most suitable results presently available for use to obtain average elastic response of fibrous composites. Utilization of these results in laminate and structural analysis has been discussed

31

elsewhere. It should be emphasized that the discussion heretofore has related to the elastic constants of a matrix stiffened by a uniaxial set of fibers. The application of these results to the study of a matrix stiffened by a three-dimensional array of fibers is discussed elsewhere.

In addition to the references described above, one should also consult the comprehensive critical bibliography of the mechanics of heterogeneous materials contained in Ref. 21.

Internal Stresses

The evaluation of the details of the stress distribution in a fibrous composite can be important for the study of failure mechanisms. Overall inelastic response or failure may be studied without knowledge of the local stresses, by the use of limit analysis theorems, for example. However, models such as that of the statistical tensile failure study (Ref. 1) do serve to emphasize the usefulness of a knowledge of the stress distribution, particularly in the vicinity of initial small internal fractures. This attempt to relate failure processes to constituent characteristics is based on the hypothesis that given a complete set of constitutive relations for a uniaxial fibrous composite, it will be possible to determine the behavior of a laminate of layers of uniaxial composites and thereby to have relations defining material behavior which are suitable for complete structural analysis. In this

section we will be concerned with studies of the internal stress distribution

of the heterogenous material represented by a fibrous composite. The appli-

cation of these studies to the definition of failure mechanisms and the estab-

lishment of rational failure criteria will be treated in the subsequent section.

Here, as in the case of the elastic constants a complete solution of

the stress problem is a complex undertaking; hence, the literature consists

of a limited number of exact and approximate solutions based on idealized

constituent geometry. Numerical methods for determining the elastic stress

distribution when the fiber array is a regular one have been discussed in the pre-

vious section. Further work is required to obtain the influence of non-uniform

fiber spacing upon the stress distribution. These results would be of prin-

cipal value for consideration of the failure mechanisms associated with loads

applied in a plane transverse to the fiber axes. For loads applied parallel to

the fiber axes, the initial internal failure is generally considered to result

from a flaw or imperfection in the fibers. Thus, the stress analysis of inter-

est for the discussion of failure mechanisms for loads in the fiber direction

is the one associated with the perturbed stress field in the vicinity of a fiber.

The stresses in the vicinity of such a discontinuity do not lend themselves

readily to analysis. This has resulted in a variety of approximate treat-

ments most of which assume that radial symmetry exists. The work of

Dow (Ref. 22) appears to be the initial treatment of this problem. His

analysis utilizes the shear lag approximation that extensional stresses in

the binder are negligible with respect to those in the fiber and that the shear

strains in the fiber are small compared to those in the matrix. This analysis

has since been repeated in other studies and has also been utilized as the

basis for a three-concentric cylinder model (Ref. 2) where the third

cylinder attempts to represent an average effect of the surrounding material.

These models generally retain some realism with regard to the constituent

geometry but involve gross approximations of the stress field. An alternate

approach utilized by Sadowski (Ref. 23) considers an exact plasticity analysis

for fiber geometries which approximate the true configuration. Thus, fibers

having ends of an ellipsoidal shape which are perfectly bonded to the surround-

ing matrix material have been studied. The results of these studies, however,

indicate that a large portion of the load carried in the fiber is transmitted

to the matrix by stress components normal to the interface and localized

at the end of the fiber. These results are thus perhaps most appropriate for

discontinuous fibers prior to an interface failure. The influence of interface

shear stresses appears to be better represented in the shear lag type models.

Sadowsky has also presented a two-dimensional analysis for rigid fibers

with alternate fibers discontinuous (Ref. 24). A two-dimensional model

has also been utilized by Hedgepeth (Ref. 25) for extensional fibers

using the shear lag analysis assumptions to approximate the stress field

in the matrix. In a general way, all of the studies described above support

the conclusion that the load is transferred around a discontinuity in a fiber,

in a very short distance by relatively high stresses. However, the details

of the load transmission, which is the important consideration in a failure

34

mechanism analysis, can be quite different, as will be shown by a comparison of the results of Refs. 2 and 22.

The interface shear stress is given in Ref. 2 (with some changes in notation) as:

$$\tau = \frac{\sigma_{fo}}{2}\left(\frac{G_b}{E_f}\right)^{1/2}\left(\frac{v_f}{1-v_f^{1/2}}\right)^{1/2}\left[\cosh\beta_1 x - \sinh\beta_1 x\right] \qquad (13)$$

$$\text{where } \beta_1^2 = \frac{G_b}{E_f}\left(\frac{v_f^{1/2}}{1-v_f^{1/2}}\right)\left(\frac{\ell}{r_f}\right)^2$$

G_b = Shear modulus of binder (matrix)

E_f = Young's modulus of fiber

v_f = Fiber volume fraction

x = Distance from fiber end

r_f = Fiber radius

σ_{fo} = Extensional stress in the fiber at a large distance from the fiber end

τ = Interface shear stress

The interface shear stress is given in Ref. 22 (again with some changes of nomenclature), as:

$$\tau = \frac{\lambda}{4}\left[\frac{P/A_f}{v_b\frac{E_b}{E_f}+v_f}\right]\left[\frac{\sinh\left(\lambda\frac{z}{d_f}\right)}{\cosh\left(\lambda\frac{\ell}{d_f}\right)}\right] \qquad (14)$$

where   P = the effective load differential between filament and binder

A = Filament area E_b = Young's modulus of binder

2ℓ = Fiber length z = Coordinate from fiber midpoint

35

For a comparison between this solution and that of Ref. 2, the stress distribution at a large distance from the filament end should be the same. Thus:

$$\frac{P}{A} = V_f \sigma_{fo} + (1 - V_f) \sigma_{fo} \frac{E_b}{E_f} \tag{15}$$

And, for long fibers

$$\frac{\tau}{\sigma_{fo}} = \frac{\lambda}{4} \left[\cosh\left(\lambda \frac{x}{d_f}\right) - \sinh\left(\lambda \frac{x}{d_f}\right) \right] \tag{16}$$

where, λ, is given in Ref. 22 by:

$$\lambda = 2 \left\{ \frac{2\sqrt{2}\left(\frac{G_f}{E_f}\right)\left[1 + \left(\frac{V_f}{1 - V_f}\right)\left(\frac{E_f}{E_b}\right)\right]}{\sqrt{2} - 1 + \frac{G_f}{G_b}\left[\left(\frac{1 + V_f}{V_f}\right)^{1/2} - \sqrt{2}\right]} \right\}^{1/2} \tag{17}$$

This value is based on an assumed distribution of shear strain across the binder material. For a constant shear strain the above expression would be altered to yield:

$$\lambda = \left\{ \frac{24 \frac{G_f}{E_f}\left(1 + \frac{V_f E_f}{V_b E_b}\right)}{1 - 3 \frac{G_f}{G_b} + 2 \frac{G_f}{G_b}\left[\frac{V_f^{-1/2} - V_f}{1 - V_f}\right]} \right\}^{1/2} \tag{18}$$

The results of Ref. 25 can be utilized to yield

$$\frac{\tau_{max}}{\sigma_{fo}} = \frac{\pi}{4}\left(\frac{G_b}{E_f}\right)^{1/2}\left(\frac{V_f}{1 - V_f}\right)^{1/2} \tag{19}$$

The maximum shear stresses as found from the three references can then be compared. The values of λ given by Equations (17) and (18) are found to be essentially identical for the cases considered and therefore only one result of Ref. 22 will be plotted. Fig. 19 shows the variation of the normalized maximum shear stress with fiber volume fraction for elastic constants appropriate to glass reinforced plastic. The results for the two-dimensional model of Ref. 25 (Equation 19) and the three-dimensional model of Ref. 2 are nearly identical and, although similar in shape, substantially smaller in magnitude than those of Ref. 22. In Fig. 20 the effect of constituent moduli ratio at a fixed fiber volume fraction is presented. Here the results of Ref. 22 differ in form as well as in magnitude from those of Refs. 2 and 25. It appears that a well conceived set of experiments would be a desirable contribution.

Failure Mechanics

The efforts to analyze the failure mechanisms in composites have met with most success in the problems of load applied parallel to the fibers of a composite containing a uniaxial fiber set. It is on this subject that attention will be focussed in the present review, treating both tensile and compressive loads.

Tension - The results of some of those studies which need not be considered here can be found in Ref. 26. One of the early models which still retains popular appeal is that of Ref. 27. That model is based on the assumption

that constant strain exists throughout the composites and that fracture occurs at the failure strain of the fibers alone. Although this model offers many conveniences, for example, it permits the use of the "rule of mixtures" as an estimate of composite strength, it must in general be discarded for the following reason alone: The high strength and stiffness filaments which make the potential for composites seem high generally have brittle failure characteristics, which are subject to the statistical distribution of flaws and imperfections inherent in brittle materials. Some way of coupling the statistical nature of the strength of a filament to that of the composite is essential. Such an approach was suggested by Parratt (Ref. 28) who proposed that composite failure occurs when the accumulation of fiber fractures resulting from increasing load shortens the fiber lengths to the point that further increases in load could not be transmitted to the fibers because the maximum matrix shear stress was exceeded. Thus the fiber fractures were eventually followed by a shear failure of the matrix, producing composite failure.

It seems reasonable to treat a model which contains a set of parallel fibers which are strong and stiff with respect to the matrix material in which they are imbedded. The fibers are brittle and their strength varies substantially from point to point along their length. When such a composite is subjected to a tensile load a fiber fracture will occur at one of the serious flaws or imperfections. When such a fiber breaks, the stress in the vicinity of the broken fiber is perturbed substantially so that the axial stress in the fiber

vanishes at the fiber break and gradually builds back up to its undisturbed stress value due to shear stresses being transferred across the fiber matrix interface. The general form of the fiber stress is disturbed for only a short dimension. When such a break occurs, several possibilities for the future behavior of the composite exist. First, the high interface shear stresses could produce interface failure which could propagate along the length of the fiber reducing the fiber effectiveness over a substantial fiber length. In order to achieve the potential of the fiber strength it is necessary to study and determine the fabrication conditions which will yield an inter- face sufficiently strong to prevent this interface shear failure. This can be done either through the use of a high strength bond or a ductile matrix which permits redistribution of the shear stresses. In the latter case the length of fiber which is affected by the break will increase as it will take a longer distance to retransmit the stresses back into the fiber at the low stress level of a ductile matrix. With a strong bond, the interface conditions can be overcome as a potential source of failure. The fracture toughness of the matrix must also be considered to prevent the propagation of a crack through the matrix and parallel to the filaments. A second possibility is that the initial crack will propagate across the composite resulting in failure. This is influenced by the fracture toughness of the matrix and again, since it is clear that with brittle fibers one can always expect a fracture to occur at a relatively low stress level, it is important that the fracture toughness of the matrix material be sufficient to prevent the propagation of this crack across the composite. If these two potential modes of failure are arrested,

39

it will then be possible to continue to increase the applied tensile load and to obtain breaks at other points of imperfection along the fibers. Increasing the load will produce a statistical accumulation of fiber fractures until a sufficient number of ineffective fiber lengths in the vicinity of one cross-section interact to provide a weak surface. At the point of incipient fracture all of the failure modes described may very well interact to produce the final fracture. The desirable approach might well be to establish a statistical tensile failure model (as in Ref. 29) and to incorporate the possibility of crack propagation failure modes, as defined in Ref. 30 - 32, prior to the statistical fracture.

This statistical model of failure has been discussed in some detail in Ref. 29. The model which was used to evaluate the influence of constituent properties upon the tensile strength considers that in the vicinity of an individual break a portion of each fiber may be considered ineffective, as discussed previously. The composite may then be considered to be composed of layers of dimension equal to the ineffective length. Any fiber which fractures within this layer will be unable to transmit a load across the layer. The applied load at that cross-section would then be uniformly distributed among the unbroken fibers in each layer. The effective stress concentrations which would introduce a non-uniform redistribution of these loads is not considered initially. A segment of a fiber within one of these layers may be considered as a link in the chain which constitutes an individual fiber. Each layer of the composite

is then a bundle of such links and the composite itself a series of such bundles. Treatment of a fiber as a chain of links is appropriate to the hypothesis that fracture is due to local imperfections. The links may be considered to have a statistical strength distribution which is equivalent to the statistical flaw distribution along the fibers. The realism of such a model is demonstrated by the length dependence of fiber strength. That is, longer chains have a high probability of having a weaker link than shorter chains, and this is supported by experimental data for brittle fibers which demonstrate that mean fiber strength is a monotonically decreasing function of fiber length. For this model it is first necessary to define a link dimension by consideration of the perturbed stress field in the vicinity of a broken fiber. It is then necessary to define the statistical strength distribution of the individual links which can be obtained indirectly from the experimental data for the fiber-strength-length relationship. These results can then be used in the statistical study of a series of bundles and utilized to define the distribution for the strength of the fibrous composite.

For fibers which can be characterized by a Weibull distribution of the strength of a series of individual fibers of a specified gage length tested to failure, it is possible to represent the fiber reinforced composite strength with a closed form solution. In particular, the statistical mode of the composite tensile strength, σ_t^*, is found to be:

$$\sigma_t^* = V_f (\alpha \delta \beta e)^{-1/\beta} \tag{20}$$

where v_f The fiber volume fraction

α , β The two parameters in the Weibull frequency distribution,

$g(\sigma)$, for strength of individual filaments.

e   The base of natural logarithms.

δ A characteristic length for the perturbation of the stress

field produced by a fiber break (the "ineffective length").

This is based on individual filaments characterized statistically by the frequency

distribution function given by:

$$g(\sigma) = L \alpha \beta \sigma^{\beta-1} exp\left(- L \alpha \sigma^{\beta}\right)$$

(21)

where L   gage length for individual fiber tests.

σ stress at fiber fracture

Certain results of this analysis are presented in Fig. 21 (reproduced

from Ref. 1, with typographical errors corrected). Here the composite

strength, normalized with respect to the mean strength, $\overline{\sigma_L}$, of individual

fibers of length, L, is plotted as a function of the coefficient of variation,

μ , of individual fiber strength values. The variation, μ , is the standard

deviation divided by the mean fiber strength. Curves are shown for various

values of the ratio of fiber test length to "ineffective length". It is seen

that for reference fibers of length equal to the "ineffective length", that

is for the basic bundle of fiber links of the model described previously,

the statistical mode of the composite strength is lower than the mean fiber

strength by an amount which increases as the coefficient of variation of

the strength of the individual fibers increases. For more practical length

ratios, L/δ, (that is, for single fibers tested at gage lengths large compared

to the "ineffective length") the analysis indicates that composite strength

is larger than the mean fiber strength. In order to explain these results,

consider the size effect on composite and on fiber individually. The prac-

tical composite specimen is large as compared with the fiber link. That

is a composite cross-section contains many fibers and the composite length

is many times the ineffective length. For this composite, the strength is

insensitive to changes in composite dimension. Thus the composite strength

defined by equation 20 is valid for practical composites regardless of size.

However, an individual fiber has a strength which is a strong function

of length. There is an increasing likelihood of encountering serious flaws

as fiber length increases and hence mean fiber strength decays monotonically

with increasing fiber test length. A very long fiber can have a low strength,

but when this fiber is incorporated into a composite the fiber break which

occurs at a low stress level will have a relatively unimportant effect on

composite strength. Thus the ratio of composite strength to mean fiber

strength is strongly dependent upon the length of the individual fiber specimens.

Note that the normalized strength ratio is close to unity for coefficients

of variation as large as 15%. However, the fact that the magnitudes of com-

posite strength and mean fiber strength are close to one another should not

be taken to justify the hypothesis that composite performance is some

fraction of fiber performance. The frequently quoted "strength conversion"

results becloud the importance of fiber coefficient of variation and fiber

test length.

Another way of viewing the significance of the result of the statistical

tensile failure model arises from the fact that the statistical mode of the

composite strength is equal to the mode of a bundle of filaments whose

length is equal to the characteristic or "ineffective length". Thus, the

difference between the strengths of a composite and a bundle of filaments is

equal to the difference between the strength of a bundle of fibers whose

length is equal to the composite length and that of a bundle of fibers whose

length is equal to the "ineffective" length. Since the latter is on the order

of 10 fiber diameters and the former many multiples of the latter, this is

a large effect. A plot of bundle strength, σ_b^*, normalized with respect to com-

posite strength, σ_t^*, (the statistical modes of both) is presented in Fig. 22

as a function of the ratio of composite length, L, to "ineffective" length,

δ, for a given value of the coefficient of variation, μ. The merits

of the compositing process are apparent herein.

With this information it is possible now to treat, as a final evaluation,

the composite tensile strength on a weight basis as a function of the consti-

tuent characteristics. The strength to density ratio of a fibrous compo-

site, normalized with respect to the strength to density ratio of the

44

individual fibers tested, can be expressed as a function, ψ , of the fiber

volume fraction, v_f, the fiber to binder modulus ratio, E_f/G_b, the fiber to

binder density ratio, ρ_f/ρ_b, the single fiber test gage length to diameter

ratio, L/d_f, and the fiber strength coefficient of variation, μ . It has pre-

viously been shown, that for this model, the effect of fiber volume fraction

is very nearly a linear one. The effects of the other variables are presented

in parametric form in Fig.23. Here, the normalized strength-density ratio,

ψ , is plotted as a function of fiber coefficient of variation, μ . The

product of the ratio, ψ , and the mean single fiber strength to density

ratio defines composite strength-density. Hence, the ratio ψ will be larger

than unity when the compositing process results in a material which is for-

giving of scattered low strength fiber elements, and it will be less than unity

when even short gage length single fibers show a large strength dispersion.

These effects are illustrated in Fig.23 where it is shown that the larger the

gage length on which a given fiber strength level is achieved the higher the

composite strength will be. Also indicated is the fact that even for moderate

dispersions of fiber strength, the composite can achieve a large fraction of

the strength associated with very short length filaments. The effect of constit-

uent moduli is also shown and the beneficial effect of increased matrix modulus

is indicated.

This format provides materials design criteria for this mode of tensile

failure. For low fiber strength dispersions it is seen that the curves are nearly

horizontal and crack propagation effect is the more likely occurrence.

It is of interest to note that the statistical tensile failure model can be used to provide insight into the stress concentration effect. That is, it is possible to account for a non-uniform redistribution of the load which had been carried in a now broken filament. For example, a computation has been performed for a simple triangular distribution function for the links of the statistical model. This function is shown in the upper portion of Fig. 11. The model assumed that for every broken fiber there were two adjacent fibers which carried a load equal to a multiple, k, the stress concentration factor, of the load carried in the other fibers. The model was a gross simplification of the real material, but it was intended to qualitatively indicate a phenomenon. The maximum load in a bundle of links having the given frequency distribution function is defined by the average stress at failure, $\bar{\sigma}$. Fig. 24 presents a plot of $\bar{\sigma}/b$, as a function of the stress concentration factor, k, for two ratios of b/a, where a and b are the limiting stresses of the triangular distribution function, $f(\sigma)$. Also shown are the fraction of fibers which are broken at incipient bundle failure. Thus it is seen that for high stress concentration factors the bundle strength decreases as expected. In this case, the minimum bundle strength, for large k is of course $\bar{\sigma}$ = a. More important is the sharp decrease in the fraction of broken fibers at incipient failure as k increases. It is this effect which clearly signals the change from a statistical fracture accumulation failure mode to a crack propagation mode. In the latter it would be expected that the fracture toughness studies would be of principal importance.

Compression - The existing studies of compressive strength (Ref. 33 and 34) are based on the hypothesis advanced by Dow (Ref. 35) that the mode of failure for a fibrous composite subjected to compression parallel to the filaments is a small wavelength fiber instability. This mechanism is analogous to the buckling of a column on an elastic foundation. As presented in the previous annual report (Ref. 1) a simple strain energy evaluation of two possible buckling patterns yields the following results:

For the "extension" mode:

$$\sigma_c = 2 V_f \left[\frac{V_f E_b E_f}{3 (1 - V_f)} \right]^{1/2} \tag{22}$$

For the "shear" mode:

$$\sigma_c = \frac{G_b}{1 - V_f} \tag{23}$$

A more exact approach to this would be to consider the model composite of elastic layers and use the methods of Ref. 36. For this case the results obtained are

$$\sigma_c = \frac{G_b}{1 - V_f} \left[\frac{1 + n \left(\frac{1 - V_f}{V_f} \right)}{1 + n^2 + \frac{n (1 - 2 V_f)^2}{2 V_f (1 - V_f)}} \right]^{1/2} \tag{24}$$

where $n = \dfrac{G_b}{G_f}$

47

It can be seen that for fibers having a modulus that is large compared to that of the binder: $n \to o$. For this case, Equation (24) reduces to Equation (23).

The studies of composite structural efficiency described elsewhere in this report conclude that minimum-weight structures demand optimum stiffening efficiencies, stresses beyond the elastic range and consequent analysis of all possible failure modes--with attendant improvement of the criteria for failure. A rational extension of the above compression model is thus the inelastic case. This can be obtained by considering the matrix to have a characteristic or maximum stress level as well as an initial elastic modulus. For an elastic-perfectly plastic matrix, the characteristic stress level would be the yield stress. With the use of a secant modulus as the measure of effective material stiffness, the elastic result can be extended to give a composite compressive strength for inelastic matrices. This result, for the generally dominant "shear" mode of compressive micro-instability is given by:

$$\sigma_c = \left[\frac{v_f E_f \sigma_y}{3(1-v_f)} \right]^{1/2} \tag{25}$$

where:

σ_c = Composite compressive strength

E_f = Fiber Young's modulus

G_b = Binder shear modulus

σ_y = Binder characteristic stress level

v_b = Binder volume fraction

v_f = Fiber volume fraction

Typical results are plotted in Fig. 25, which shows the compressive strength predictions for the elastic case as a function of the binder modulus. The inelastic cutoff curves depend on both the fiber modulus and binder "strength." Computations for glass and boron filaments in two different binders are shown. It can be seen that the relative importance of changes in binder modulus, binder "strength", and fiber modulus are greatly dependent upon the initial or reference condition. For example, a composite containing glass filaments in a matrix having a modulus of 0.25×10^3 psi and a "yield" stress of 15 ksi can be improved (in the sense of higher compressive strength) by improving the strength of the binder, but is unaffected by an increase in binder modulus and essentially unaltered by a change in fiber modulus. However, composites of boron fibers in the same matrix could be improved substantially by improvements in binder modulus but would be unaffected by a change in binder strength or fiber modulus. This quantitative measure of the influence of constituent properties upon composite performance can be used in an efficiency analysis as being representative of the potential compressive strength of uniaxial composites.

Some measure of experimental qualification of this analysis has been obtained by a study of single filaments in a matrix subjected to compressive loads. In the previous study (Ref. 1) photoelastic stress patterns were shown for individual glass filaments embedded in epoxy matrix after a high

temperature (250° F) cure. The resulting fiber instability was exactly

the type assumed in the present analysis. This instability has been observed

previously by other investigators (e.g., Ref. 37) but there has been some

question as to whether a loading strain applied subsequent to a room tempera-

ture cure would produce the same effect as the thermally induced strain.

In the present program a series of single filaments were imbedded in a

room temperature curing silicone rubber (GE RTV 615) and subsequently

loaded. The results are shown in Fig. 26 for glass, tungsten and boron

filaments. The wave lengths have been measured and they can be correlated

with the simple beam on an elastic foundation results of Ref. 38. From

those results it can be shown that the wave length, λ , is given by

$$\lambda = \frac{\pi d}{2} \sqrt[4]{\frac{E}{\beta}} \qquad\qquad (26)$$

where

d fiber diameter

E   fiber modulus

β "foundation" modulus.

The "foundation" modulus is unknown (not to be confused with the

Young's modulus of the matrix, which in this case is 70 psi) but it can

safely be assumed to be the same for all three fibers. Thus one would

predict that the buckling wave length would be proportional to diameter and

the fourth root of fiber modulus. In the previous study of buckling due to

thermally induced strains (Ref. 1), a set of glass filaments of different

diameters was treated and it was shown that, in accordance with Equation

25, the buckling wave length varied linearly with fiber diameter. Here

the results have been normalized with respect to the tungsten filament

wave length so that:

$$\frac{\lambda}{\lambda_W} = \frac{d}{d_W} \left(\frac{E}{E_W} \right)^{1/4}$$

(27)

where subscript W denotes Tungsten

The results for the specimens of Fig. 26 are as follows:

Table A - RTV - 615 Matrix Composites

Fiber Material	Fiber Modulus, E	Fiber Diameter, d	Fiber Wavelength, λ	$\left(\frac{\lambda}{\lambda_W} \right)_{theo.}$	$\left(\frac{\lambda}{\lambda_W} \right)_{exp.}$
Tungsten	50×10^6 psi	0.0020"	0.195"	1.00	1.00
Glass	10.5×10^6	0.0038"	0.230	1.29	1.18
Boron	57.5×10^6	0.0051"	0.460	2.64	2.36

Further confirmation was attempted with the use of a different matrix.

GE RTV-602 was selected for its nominally higher Young's modulus. The

test, however, yielded a modulus of only 110 psi and the correlation of these

results is inexplicably poor, as shown below.

Table B - RTV - 662 Matrix Composites

Fiber Material	Fiber Modulus, E	Fiber Diameter, d	Fiber Wavelength, λ	$\left(\dfrac{\lambda}{\lambda_w}\right)_{theo.}$	$\left(\dfrac{\lambda}{\lambda_w}\right)_{exp.}$
Tungsten	50×10^6 psi	0.0020"	0.260	1.00	1.00
Glass	10.5×10^6 psi	0.0038"	0.195	1.29	0.75
Boron	57.5×10^6 psi	0.0048"	0.430	2.49	1.65

Further study is required in this experimental area. Indeed no report on the status of micromechanics of fibrous composites would be complete without a statement emphasizing the serious shortage of both reliable experimental results and experimental methods for these materials. (See also Ref. 39).

VISCOELASTIC FIBER REINFORCED MATERIALS

Introduction

Present fibrous composites contain very strong and stiff fibers which are embedded in a relatively soft matrix. The use of these materials for long times under load raises the question of time-dependent material properties. An approach to this problem is described herein. Considered here is uniaxial random reinforcement in which case is obtained an anisotropic material which has very great strength in fiber direction and is relatively weak in the transverse direction. A recent comprehensive appraisal and survey of the subject of mechanics of fiber reinforced materials is given in [18].

It seems that at the present time the best understood aspect of mechanical behavior of fiber reinforced materials is prediction of their elastic moduli in terms of fiber and matrix moduli and internal geometry, though even here much remains to be done. In the event of uniaxial random reinforcement, the material is transversely isotropic and has five independent effective elastic moduli. Hashin and Rosen [6] considered an idealized model of a random array of parallel hollow or solid fibers embedded in a matrix. This model of a fiber reinforced material will hence forth be referred to as a composite cylinder assemblage. Closed form expressions for four elastic moduli and bounds for a fifth modulus, of such an assemblage, were obtained in [6].

In the general case of irregularly shaped and randomly placed fibers the problem is a statistical one. The first steps in the treatment of this difficult

reference to the present case, assume that a cylindrical specimen of fiber reinforced material, whose generators are parallel to the fibers, and which contains very many fibers, is subjected to boundary displacements of the form

$$u_i^o \ (S, t) \ = \ \tilde{\epsilon}_{ij} \ (t) \ x_j$$

$$(o \leq t \leq \infty)$$

(2.1)

Here the range of subscripts is 1, 2, 3, a repeated subscript denotes summation, S is the bounding surface, t is time, $\tilde{\epsilon}_{ij}(t)$ are space constant strains and x_i are cartesian coordinates. Here and in what follows it is assumed that the material is unstressed and undeformed for t< o. For (2.1) applied the volume average strains are $\tilde{\epsilon}_{ij}(t)$ and because of assumed statistical homogeneity they also are the local strain averages over large enough subregions of the specimen. In the present case these subregions are cylinders extending from base to base in the specimen. They are small parts of the specimen, yet large enough to be representative of the material.

Assume now that $\tilde{\epsilon}_{ij}(t)$ are given in the special form

$$\tilde{\epsilon}_{ij} (t) \ = \ \epsilon_{ij}^o \ H \ (t)$$

(2.2)

where ϵ_{ij}^o are constant and H(t) is the Heaviside step function. Because of assumed phase linearity the average stresses are linearly related to ϵ_{ij}^o.
In general

$$\bar{\sigma}_{ij} (t) \ = \ C_{ijkl}^* (t) \, \epsilon_{kl}^o$$

(2.3)

problem have been taken by Hill [15] and Hashin [14] who have given

bounds for the five effective moduli, in terms of phase moduli and phase

volume fractions only. Moreover, it has been shown in [14] on the basis

of the results obtained in [6] that all pairs of bounds, except perhaps one,

are best possible in terms of phase moduli and volume fractions. In other

words, to improve the bounds more information about the phase geometry

is required.

The motivation for the present study is the fact that the matrix in fiber

reinforced materials is in many cases a resin which exhibits time effects.

The simplest model for such a time dependent material is a linear visco-

elastic one. Accordingly, the problem to be considered is that of the

prediction of macroscopic viscoelastic properties of a material composed

of a linear viscoelastic matrix which is uniaxially reinforced by elastic fibers.

It has recently been shown by Hashin [40] that elastic moduli and visco-

elastic relaxation moduli (and creep compliances) of heterogeneous materials

of identical phase geometry, are related by the analogy which has become

known as the correspondence principle. The purpose of the present investi-

gation is to exploit this analogy and the results given in [6] in order to derive

macroscopic viscoelastic properties for the composite cylinder assemblage

model of a fiber reinforced material which has been introduced and described

in [6].

2. GENERAL THEORY

The effective relaxation moduli and creep compliances of linear viscoelastic

heterogeneous media have been defined in [40]. To recapitulate, with special

where overbar denotes average. The components of the fourth rank tensor C_{ijkl}^{*} are defined as the effective relaxation moduli. They depend in general upon the entire phase geometry.

Dually, let tractions of the form

$$T_{i}^{o}(S, t) = \tilde{\sigma}_{ij}(t) x_{j} \tag{2.4}$$

be prescribed. Here $\tilde{\sigma}_{ij}(t)$ are space constant stresses and x_{i} are the components of the outward unit normal. Then the average stresses are $\tilde{\sigma}_{ij}(t)$. Again assume the special form

$$\tilde{\sigma}_{ij}(t) = \sigma_{ij}^{o} H(t) \tag{2.5}$$

where σ_{ij}^{o} are constant. Then the average strains may be written in the form

$$\bar{\epsilon}_{ij}(t) = J_{ijkl}^{*}(t) \; \sigma_{ij}^{o} \tag{2.6}$$

The J_{ijkl}^{*} are defined as the effective creep compliances.

For the general boundary conditions (2.1) and (2.4) it follows by superposition in time that

$$\bar{\sigma}_{ij}(t) = \int_{0}^{t} C_{ijkl}^{*}(t - \tau) \; \frac{d\bar{\epsilon}_{kl}(\tau)}{d\tau} \; d\tau \tag{2.7}$$

$$\bar{\epsilon}_{ij}(t) = \int_{0}^{t} J_{ijkl}^{*}(t - \tau) \; \frac{d\bar{\sigma}_{kl}(\tau)}{d\tau} \; d\tau \tag{2.8}$$

56

where in (2.7) $\overline{\epsilon}_{ij}$ is $\widetilde{\epsilon}_{ij}$ and in (2.8) $\overline{\sigma}_{ij}$ is $\widetilde{\sigma}_{ij}$.

It is, however, clear that (2.3), (2.6) and (2.7-8) have a more general interpretation. They apply in any case where the specimen is subjected to statistically homogeneous states of stress and strain. The boundary conditions (2.1) and (2.4) are merely a device to produce such statistically homogeneous fields. Therefore, the average stresses in (2.7-8) may be interpreted as the same quantities and the same is true for the average strains. In the case of the present specific boundary conditions such equivalence would fail only in a very narrow layer near the boundary, and would hold further away.

In order to account for discontinuities in time of applied average strains or stresses, primarily at t = o, the stress-strain relations (2.7-8) may be written as Stieltjes convolutions. (Compare e.g. [41].) Here the Riemann convolution form of (2.7-8) will be used with the understanding that the integrands may involve delta functions.

The one sided Laplace transform (LT) of (2.7-8) is given by

$$\hat{\overline{\sigma}}_{ij}(p) = p\,\hat{\overline{C}}^{*}_{ijkl}(p)\,\hat{\overline{\epsilon}}_{kl}(p) \tag{2.9}$$

$$\hat{\overline{\epsilon}}_{ij}(p) = p\,\hat{\overline{J}}^{*}_{ijkl}(p)\,\hat{\overline{\sigma}}_{kl}(p) \tag{2.10}$$

where p is the transform variable and the circumflex above a symbol denotes LT. Because of the formal resemblance to an elastic stress-strain law the quantities $p\hat{\overline{C}}^{*}_{ijkl}(p)$ are termed transform domain (TD) effective moduli and the quantities $p\hat{\overline{J}}^{*}_{ijkl}$ are termed TD effective compliances. Substituting

(2.10) into (2.9) it follows immediately that the TD effective moduli tensor and the TD effective compliances tensor are reciprocal.

The fiber reinforced materials here considered are transversely isotropic, the fiber direction being the axis of axial symmetry. Taking into account this symmetry and also reflectional symmetry with respect to the transverse plane, normal to the fibers, it follows exactly as for an elastic stress-strain law that there remain only five independent TD effective moduli in (2.9). Referring the fiber reinforced specimen to a cartesian system of axes x_1 x_2 x_3, where x_1 is in fiber direction and $x_2 x_3$ are in the transverse plane, and adopting for convenience a six by six matrix notation for the effective TD moduli, Equation (2.9) can be rewritten in precisely the same form as given in [6]. Thus

$$\bar{\sigma}_{11}(p) = p\, C_{11}^{*}(p)\, \bar{\epsilon}_{11}(p) + p\, C_{12}^{*}(p)\, \bar{\epsilon}_{22}(p) + p\, C_{12}^{*}(p)\, \bar{\epsilon}_{33}(p) \tag{2.11}$$

$$\bar{\sigma}_{22}(p) = p\, C_{12}^{*}(p)\, \bar{\epsilon}_{11}(p) + p\, C_{22}^{*}(p)\, \bar{\epsilon}_{22}(p) + p\, \bar{C}_{23}^{*}(p)\, \bar{\epsilon}_{33}(p) \tag{2.12}$$

$$\bar{\sigma}_{33}(p) = p\, C_{12}^{*}(p)\, C_{12}^{*}(p)\, \bar{\epsilon}_{11}(p) + p\, C_{23}^{*}(p)\, \bar{\epsilon}_{22}(p) + p\, C_{22}^{*}(p)\, \bar{\epsilon}_{33}(p) \tag{2.13}$$

$$\bar{\sigma}_{12}(p) = 2\, p\, C_{44}^{*}(p)\, \bar{\epsilon}_{12}(p) \tag{2.14}$$

$$\bar{\sigma}_{13}(p) = 2\, p\, C_{44}^{*}(p)\, \bar{\epsilon}_{13}(p) \tag{2.15}$$

$$\bar{\sigma}_{23}(p) = p\, [C_{22}^{*}(p) - C_{23}^{*}(p)]\, \bar{\epsilon}_{23}(p) \tag{2.16}$$

The TD stress-strain relation (2.10) can of course be written in entirely analogous form.

Again, as in the elastic case, it is convenient to define the following four physically significant TD moduli.

58

$$p \hat{K}_{23}^* = \frac{1}{2} \, p \, (\hat{C}_{22}^* + \hat{C}_{23}^*) \tag{2.17}$$

$$p \hat{G}_{23}^* = \frac{1}{2} \, p \, (\hat{C}_{22}^* - \hat{C}_{23}^*) \tag{2.18}$$

$$p \hat{G}_{12}^* = p \hat{G}_{13}^* = p \hat{G}_1^* = p \hat{C}_{44}^* \tag{2.19}$$

$$p \hat{E}_1^* = p \hat{C}_{11}^* - \frac{2p^2 \hat{C}_{12}^{*2}}{p \, (\hat{C}_{22}^* + \hat{C}_{23}^*)} \tag{2.20}$$

and to choose $p\hat{C}_{11}^*$ as the fifth independent TD modulus.

Here $p\hat{K}_{23}^*$ is the plane strain effective TD bulk modulus, $p\hat{G}_{23}^*$ the effective TD transverse shear modulus, $p\hat{G}_1^*$ the effective TD axial shear modulus, $p\hat{E}_1^*$ the effective TD Young's modulus and $p\hat{C}_{11}^*$ is associated with uniaxial stress in fiber direction, with transverse deformation prevented by a rigid bonded enclosure.

The TD effective compliances associated with (2.17 - 2.20) and $p\hat{C}_{11}^*$ will be consistently denoted by corresponding small letters. From the reciprocity of the TD moduli and compliance tensors stem the following simple relations:

$$p \hat{k}_{23}^* (p) = \frac{1}{pK_{23}^*(p)} \tag{2.21}$$

$$p \hat{g}_{23}^* (p) = \frac{1}{pG_{23}^*(p)} \tag{2.22}$$

$$p \, g_1^* (p) = \frac{1}{p G_1^* (p)} \qquad\qquad (2.23)$$

$$p \, e_1^* (p) = \frac{1}{p E_1^* (p)} \qquad\qquad (2.24)$$

$$p \, c_{11}^* (p) = \frac{1}{p C_{11}^* (p)} \qquad\qquad (2.25)$$

The physical significance of the chosen effective relaxation moduli and creep compliances will be further brought out in applications, below.

A correspondence principle for effective relaxation moduli and creep compliances of viscoelastic heterogeneous media has been given in [40] for the specific case of statistical isotropy. However, as stated there the correspondence holds equally well for anisotropic heterogeneous media, the proof being completely analogous to the isotropic case. Therefore, this correspondence principle can be immediately written down for the present case of a viscoelastic fiber reinforced material of transverse isotropy.

Consider first the case of a two phase elastic fiber reinforced specimen, whose phases are linearly elastic, homogeneous, and for simplicity, isotropic. Let it be assumed that for some specific geometry the five effective elastic moduli C_{ijkl}^{*E} are exactly known in terms of phase elastic moduli and geometrical phase details. Consider now a specimen of entirely identical phase geometry whose phases, however, are linearly viscoelastic, homogeneous and isotropic.

60

Then the TD effective moduli, or in other words the LT of the effective

relaxation moduli and creep compliances, of the viscoelastic specimen

can be directly written down by making certain replacements in the expres-

sions for the effective elastic moduli of the elastic fiber reinforced material.

To explain these replacements, two different cases have to be considered

separately. First assume that the viscoelastic phase stress-strain relations

are of the differential operator type, thus at any point $\underline{x}$ in the rth phase

$$R_r (D) \, \sigma^r (\underline{x}, t) = S_r (D) \, \epsilon^r (\underline{x}, t) \tag{2.26}$$

$$P_r (D) \, s_{ij}^r (\underline{x}, t) = Q_r (D) \, e_{ij}^r (\underline{x}, t) \tag{2.27}$$

where $r = 1, 2$ is the phase number, $D = d/dt$, σ^r and s_{ij}^r are isotropic and

deviatoric parts of the stress σ_{ij}^r, ϵ^r and e_{ij}^r are isotropic and deviatoric

parts of the strain ϵ_{ij}^r, and R_r, S_r, P_r, Q_r, are polynomials in D. Then in

order to obtain the TD moduli of the viscoelastic specimen the following

replacement scheme should be used:

$$K_r^E \rightarrow \frac{1}{3} \frac{S_r (p)}{R_r (p)} = \varkappa_r (p) \tag{2.28}$$

$$G_r^E \rightarrow \frac{1}{2} \frac{Q_r (p)}{P_r (p)} = \Gamma_r (p) \tag{2.29}$$

where K_r^E and G_r^E are the phase bulk and shear moduli appearing in the

expressions for the effective elastic moduli C_{ijkl}^{*E} of the elastic specimen.

61

In the second case assume that the phase stress-strain relations are specified in the more general, hereditary integral form. For the $_r$th phase

$$\sigma^r(\underline{x}, t) = 3 \int_0^t K_r(t-\tau) \frac{\partial}{\partial \tau} \epsilon^r(\underline{x}, \tau) \, d\tau \qquad (2.30)$$

$$s_{ij}^r(\underline{x}, t) = 2 \int_0^t G_r(t-\tau) \frac{\partial}{\partial \tau} e_{ij}^r(\underline{x}, \tau) \, d\tau \qquad (2.31)$$

where $K_r(t)$ and $G_r(t)$ are the bulk and shear relaxation moduli, respectively, of the $_r$th phase. Dually

$$\epsilon^r(\underline{x}, t) = \frac{1}{3} \int_0^t I_r(t-\tau) \frac{\partial}{\partial \tau} \sigma^r(\underline{x}, \tau) \, d\tau \qquad (2.32)$$

$$e_{ij}^r(\underline{x}, t) = \frac{1}{2} \int_0^t J_r(t-\tau) \frac{\partial}{\partial \tau} s_{ij}^r(\underline{x}, \tau) \, d\tau \qquad (2.33)$$

where $I_r(t)$ and $J_r(t)$ are the bulk and shear creep compliances, respectively. Then the replacement scheme analogous to (2.28-2.29) becomes

$$K_r^E \rightarrow p \, \hat{K}_r(p) = \varkappa_r(p) \qquad (2.34)$$

$$G_r^E \rightarrow p \, \hat{G}_r(p) = \Gamma_r(p) \qquad (2.35)$$

It is important to note that when the viscoelastic specimen has an elastic phase, as in the case to be considered here, the replacement schemes (2.28-2.29) and (2.34-2.35) show that the elastic moduli of that phase are left unmodified in the replacement scheme.

Thus the problem of finding effective relaxation moduli, when effective elastic moduli are known, is reduced to Laplace transform inversion. The effective creep compliances are found in a similar way on using relations of type (2.21-2.25).

The analogy which has been outlined above will be used to find the viscoelastic counterparts of the elastic results obtained in [6]. While the procedure is straightforward, analytical inversion of the transforms is in general only possible if the phase stress-strain relations are of type (2.26-2.27). Even for the simplest cases of Maxwell or Kelvin models the inversion requires heavy calculations. It becomes prohibitively cumbersome for more complicated models. The situation is worse for stress-strain relations of type (2.30-2.33) since in general the kernels are only known numerically from experiment, whence the inversion must be performed numerically, which generally requires a computer. Unfortunately, the stress-strain relations of type (2.30-2.33) are the more important ones from the practical point of view. It turns out, however, that important conclusions about the effective relaxation moduli and creep functions can be reached without LT inversion. This can be done on the

basis of some general theorems relating the value of a function to its
transform which are known as Abel-Tauber theorems. The theorems
can be written in the following form (compare e.g. [42]).

$$\lim \left[\frac{f(t)}{t^n} \right] = \lim \left[\frac{p^{n+1} \hat{f}(p)}{\Gamma(n+1)} \right] \tag{2.36}$$

$$t \to o_+ \qquad\qquad p \to +\infty$$

$$t \to +\infty \qquad\qquad p \to o_+ \quad n >-1$$

where $\hat{f}(p)$ is the one sided LT of a function $f(t)$, and Γ is the Gamma
function. Of particular importance for the present purpose is the special
case $n = o$. Then (2.36) reduces to

$$\lim f(t) = \lim p\hat{f}(p) \tag{2.37}$$

$$t \to o_+ \qquad\qquad p \to +\infty$$

$$t \to +\infty \qquad\qquad p \to o_+$$

It should now be remembered that the TD effective moduli which are
directly given by the correspondence principle are of the form $p\hat{C}^*_{ijkl}(p)$;
compare (2.9) and also (2.17-2.20). Thus from (2.37)

$$C^*_{ijkl}(o) = \lim p\, \hat{C}^*_{ijkl}(p) \tag{2.38}$$

$$p \to +\infty$$

$$C^*_{ijkl}(\infty) = \lim p\, \hat{C}^*_{ijkl}(p) \tag{2.39}$$

$$p \to o_+$$

(Henceforth, an argument o as in the left side of (2.38) is to be interpreted as o_+.) Now $p\,\dot{C}^*_{ijkl}(p)$ are found from the effective elastic moduli C^{*E}_{ijkl} by the replacement scheme (2.34-2.35). Hence to find the right sides of (2.38-2.39) it is necessary to substitute in C^{*E}_{ijkl} the limiting values of (2.34-2.35) for $p \to +\infty$, o_+. Applying (2.37) again

$$\lim_{p \to +\infty} p\,\dot{G}_r(p) = G_r(o) \tag{2.40}$$

$$\lim_{p \to o_+} p\,\hat{G}_r(p) = G_r(\infty) \tag{2.41}$$

and similarly for $p\,\dot{K}_r(p)$.

It follows that in order to find $C^*_{ijkl}(o_+)$ all that is needed is to replace K^E_r and G^E_r in C^{*E}_{ijkl}, by $K_r(o)$ and $G_r(o)$, respectively. Similarly, in order to find $C^*_{ijkl}(\infty)$, K^E_r and G^E_r in C^{*E}_{ijkl}, are replaced by $K_r(\infty)$ and $G_r(\infty)$. Thus, the initial and final asymptotic relaxation moduli can be simply found in terms of direct experimental information.

The result concerning the initial values of the moduli is physically almost obvious since it merely asserts that the initial response is an elastic one in terms of the initial elastic responses of the phases. The result for infinite time is more interesting and quite important, since in many applications the behavior after long time is all that is needed.

Once the relaxation moduli for t = o$_+$, ∞ are known, the creep compli-
ances for the same times can be easily found, for as has been pointed out
above the tensors pC^*_{ijkl} (p) and pJ^*_{ijkl} (p) in (2.9-2.10) are reciprocal,
whence it follows from (2.37) that C^*_{ijkl} (o) and J^*_{ijkl} (o) are reciprocal
and that C^*_{ijkl} (∞) and J^*_{ijkl} (∞) are reciprocal. For the special TD moduli
and compliances defined in (2.21-2.25), the values of a relaxation modulus
and a creep compliance at o$_+$, ∞ are simply mutually reciprocal.

3. PLANE STRAIN DILATION

Assume that the fiber reinforced specimen is subjected to the average
strains

$$\bar{\epsilon}_{11} (t) = 0 \qquad \bar{\epsilon}_{22} (t) = \bar{\epsilon}_{33} (t) = \bar{\epsilon} (t) \tag{3.1}$$

by choice of (3.1) as the strains in (2.1). Then the only non-vanishing
average stresses are $\bar{\sigma}_{11}$ (t), $\bar{\sigma}_{22}$ (t) = $\bar{\sigma}_{33}$ (t) = $\bar{\sigma}$ (t). The stress-strain
law (2.11-2.13), in the time domain, then becomes

$$\bar{\sigma}_{11}(t) = 2 \int_o^t C^*_{12} (t-\tau) \frac{d\bar{\epsilon}(\tau)}{d\tau} d\tau \tag{3.2}$$

$$\bar{\sigma}(t) = 2 \int_o^t K^*_{23} (t-\tau) \frac{d\bar{\epsilon} (\tau)}{d\tau} d\tau \tag{3.3}$$

Now assume average stresses

$$\bar{\sigma}_{22} (t) = \bar{\sigma}_{33}(t) = \bar{\sigma} (t) \tag{3.4}$$

retaining the plane strain condition $\bar{\epsilon}_{11}$ (t) = 0. Then

$$\bar{\epsilon}_{22}(t) = \bar{\epsilon}_{33} (t) = \bar{\epsilon} (t) = \frac{1}{2} \int_o^t k^*_{23} (t-\tau) \frac{d\bar{\sigma}(\tau)}{d\tau} d\tau \tag{3.5}$$

where $K_{23}^*(t)$ and $k_{23}^*(t)$ are related by (2.21). To compute $\bar{\sigma}_{11}(t)$, (3.5) now has to be inserted into (3.2).

In order to use the correspondence principle for evaluation of K_{23}^* and k_{23}^*, the results for the plane strain bulk modulus of an elastic fiber-reinforced material are needed. For the composite cylinder assemblage model introduced in ⌊2⌋, the results will be given for convenience in the form used in ⌊4⌋ [(*)]. Thus

$$K_{23}^{*E} = k_m^E + \cfrac{v_f}{\cfrac{1}{k_f^E - k_m^E} + \cfrac{v_m}{k_m^E + G_m^E}} \tag{3.6}$$

Here and henceforward, subscripts f and m denote fibers and matrix, respectively. The symbol k^E in (3.6) denotes plane strain elastic bulk modulus which for the present isotropic phases is given by

$$k^E = K^E + \frac{1}{3} G^E \tag{3.7}$$

in terms of usual bulk and shear moduli, K^E and G^E.

[(*)] Note that the expression equivalent to (3.6), which was given in ⌊6⌋, contained errors. See errata of ⌊6⌋, J. Appl. Mech. 32E, 219, (1965).

Assuming elastic fibers and using (3.7) and the correspondence

principle, (3.6) transforms into

$$pK_{23}^{*}(p) = \varkappa_m(p) + \frac{1}{3}\,\Gamma_m(p) + v_f\left\{\frac{1}{K_f + \frac{1}{3}G_f - \varkappa_m(p) - \frac{1}{3}\,\Gamma_m(p)} + \frac{v_m}{\varkappa_m(p) + \frac{4}{3}\,\Gamma_m(p)}\right\}^{-1} \tag{3.8}$$

Here $\varkappa_m(p)$ and $\Gamma_m(p)$ are given by (2.28-2.29) or (2.34-2.35), and

(3.8) then defines the LT of the relaxation modulus $K_{23}^{*}(t)$.

To simplify (3.8) let it first be assumed that the matrix is elastic

in dilatation. It is easily shown that in this event

$$\varkappa_m(p) = K_m^{E} \tag{3.9}$$

where K_m is the elastic bulk modulus. A very simple case representing

(2.28-2.29) is a Maxwell model, for which

$$\Gamma_m(p) = G_m^{M}\,\frac{pT}{1 + pT} \tag{3.10}$$

where

$$T = \frac{\eta_m^{M}}{G_m^{M}} \tag{3.11}$$

68

and η_m^M and G_m^M are the viscosity coefficient and shear modulus respectively.

It is a straight forward matter to insert (3.9-3.11) into (3.8) and to then find $K_{23}^*(t)$ by the method of partial fractions, but the resulting expressions are very complicated. Instead, another simplified procedure will be here used. Because of the considerable stiffness of the fibers relative to the matrix, in practice, the former will be assumed to be perfectly rigid. In that event (3.6) simplifies to

$$K_{23}^{*E} = K_m^E + \frac{1}{3} G_m^E + (K_m^E + \frac{4}{3} G_m^E)\frac{c}{1-c} \qquad (3.12)$$

where (3.7) has been used, and

$$v_f = c \qquad v_m = 1-c \qquad (3.13)$$

Using the correspondence principle with the general replacement (2.34-2.35), (3.21) transforms to

$$p\hat{K}_{23}^*(p) = p\hat{K}_m(p) + \frac{1}{3} p\hat{G}_m(p) + \left[p\hat{K}_m(p) + \frac{4}{3} p\hat{G}_m(p)\right]\frac{c}{1-c} \qquad (3.14)$$

which on cancelling the common factor p, immediately yields by inversion into the time domain

$$K_{23}^*(t) = K_m(t) + \frac{1}{3} G_m(t) + \left[K_m(t) + \frac{4}{3} G_m(t) \right] \frac{c}{1-c} \qquad (3.15)$$

Thus the plane strain effective relaxation modulus is explicitly expressed for the whole time range in terms of the matrix relaxation moduli by the same formula as (3.12). Equation (3.15) is a very attractive result since it permits the direct use of measured relaxation moduli. A similar result has been found in [40] for the three-dimensional bulk relaxation modulus of a rigid particle suspension. However, no result similar to (3.15) exists for the effective creep compliance k_{23}^*. This compliance is related to K_{23}^* by the transform relation (2.21), which may be inverted into a convolution type Volterra integral equation of the second kind, which in general must be solved numerically. (Compare [40] .)

To show a simple result for the creep compliance $k_{23}^*(t)$, let it be assumed that the fibers are rigid and that the matrix is elastic in dilatation and viscoelastic in shear according to the simple Maxwell model. Then to find $p\hat{K}_{23}^*(p)$, replace G_m in (3.12) by (3.10) while K_m remains unchanged. Then use (2.24) to find

$$\hat{k}_{23}^*(p) = \frac{1 + Tp}{p \left[K_m^E / (1-c) + TK_{23}^{*E} p \right]} \qquad (3.16)$$

where K_{23}^{*E} is given by (3.12). Inversion of (3.16) yields immediately

$$k_{23}^{*}(t) = \frac{1-c}{K_m^E} H(t) + \left[\frac{1}{K_{23}^{*E}} - \frac{1-c}{K_m^E} \right] \exp \left\{ - \frac{K_m^E(1-c)}{K_{23}^{*E}} \frac{t}{T} \right\} \qquad (3.17)$$

To provide a check on the general results obtained with use of the Abel-Tauber theorems it is easily found from (3.17) that

$$k_{23}^{*}(0) = \frac{1}{K_{23}^{*E}} \qquad (3.18)$$

$$k_{23}^{*}(\infty) = \frac{1-c}{K_m^E} \qquad (3.19)$$

Now (3.18) is simply the elastic compliance, whereas (3.19) can be directly found from the reciprocal of (3.12) by replacing K_m^E and G_m^E by $K_m(\infty)$ and $G_m(\infty)$, respectively. In the present case $K_m(\infty) = K_m^E$ and for a Maxwell material $G_m(\infty) = 0$. Then, (3.19) follows immediately.

Finally, the Abel-Tauber theorems will be applied in the case where the fibers are not assumed rigid. The initial value $K_{23}^{*}(0)$ is simply given by replacement of the matrix moduli in (3.6) by the corresponding initial viscoelastic relaxation moduli. To obtain a simplified expression for $K_{23}^{*}(\infty)$ let it be assumed that the matrix is elastic in dilatation. Furthermore, for many materials the relaxation moduli reduce to a small

fraction of their initial values, after long time. Accordingly, $G_m(\infty)$

will be neglected in (3.6) in comparison to other moduli. Under these

circumstances the following result is easily found

$$K_{23}^*(\infty) = \frac{k_f K_m^E}{k_f(1-c) + cK_m^E} \tag{3.20}$$

4. AXIAL SHEAR

Let the fiber reinforced specimen be subjected to the average shear

strains

$$\bar{\epsilon}_{12}(t) = \bar{\epsilon}_{21}(t) = \alpha \tag{4.1}$$

and all other average strain components vanish. The system (4.1) is a

shearing action on planes normal and parallel to the fibers. The trans-

formed effective stress-strain relation is given by (2.14) or (2.15) which

becomes in the time domain

$$s(t) = 2 \int_o^t G_1^*(t-\tau) \frac{d\alpha(\tau)}{d\tau} d\tau \tag{4.2}$$

where

$$s(t) = \bar{\sigma}_{12}(t) = \bar{\sigma}_{21}(t) \tag{4.3}$$

and all other average stresses vanish. Dually, the specimen may be

subjected to the average stress system (4.3), the resulting average strains

being (4.1) and the effective creep type stress-strain relation is then

$$\alpha(t) = \frac{1}{2} \int_0^t g_1^*(t-\tau) \frac{ds(\tau)}{d\tau} d\tau \tag{4.4}$$

The quantities G_1^* and g_1^* are the effective axial shear relaxation modulus and creep compliance, respectively, and are related by (2.23).

For an elastic composite cylinder assemblage the expression for G_1^{*E} obtained by Hashin and Rosen, [6] (Equation 71 for solid fibers) may be rewritten as follows:

$$G_1^{*E} = \frac{G_f(1+c) + G_m^E(1-c)}{G_f(1-c) + G_m^E(1+c)} G_m^E \tag{4.5}$$

where c is the fractional volume of fibers. This is a particularly simple expression since only the phase shear moduli are involved.

Let it first be assumed that the fibers are elastic and that the matrix is represented by a Maxwell model. Note that it does not matter in this case whether or not the matrix exhibits volume viscoelasticity. As an example the creep compliance $g_1^*(t)$ will be calculated. Using the correspondence rule (2.29), with (3.10) and (2.23), a straightforward calculation yields

$$\hat{g}_1^*(p) = \frac{1}{G_m^M} \frac{1+Tp}{Tp^2} \frac{G_f(1-c) + \left[G_f(1-c) + G_m^M(1+c)\right]}{G_f(1+c) + \left[G_f(1+c) + G_m^M(1-c)\right]} \tag{4.6}$$

Inverting by partial fractions,

$$G_m^M g_1^*(t) = \frac{1-c}{1+c} \left[H(t) + \frac{t}{T}\right] + \frac{4c}{o\,(1+c)^2} H(t)$$

$$\frac{4(1-c)c}{(1+c)^2 \phi[\phi(1+c) + 1 - c]} \exp\left\{-\frac{\phi(1+c)}{\phi(1+c) + 1 - c} \frac{t}{T}\right\} \tag{4.7}$$

73

where

$$\phi = \frac{G_f}{G_m^M} \qquad (4.8)$$

It is seen that the first term in the right side of (4.7) does not contain ϕ, the second is of order ϕ^{-1}, and the third of order ϕ^{-2}. For fibers which are much stiffer than the matrix ϕ is large. Hence in that case the third or both the second and third terms can be neglected in comparison to the first. For the ϕ usually encountered in practice retainment of the first term only, involves but a few percent error. It is seen that the first term is the exact solution for $\phi \to \infty$, i.e., rigid fibers. Because of the linear term in t, the creep compliance becomes unbounded for infinite time.

A very simple result is obtained if it is assumed at the outset that the fibers are rigid. The elastic result (4.5) then reduces to

$$G_1^{*E} = \frac{1+c}{1-c} \, G_m^E \qquad (4.9)$$

whence, by the correspondence rule (2.41)

$$p\hat{G}_1^*(p) = \frac{1+c}{1-c} \, p\hat{G}_m(p) \qquad (4.10)$$

which on cancelling p directly inverts into

$$G_1^*(t) = \frac{1 + c}{1 - c} \, G_m(t) \tag{4.11}$$

Thus, the relaxation modulus of the fiber reinforced material is merely

the relaxation modulus of the matrix multiplied by $\frac{1 + c}{1 - c}$. A similar

result can be obtained for the creep compliance, for it follows from (2.23)

and an analogous relation for $p\hat{G}_m(p)$ and $p\hat{g}_m(p)$, that

$$\frac{1}{p\,\hat{g}_1^*(p)} = \frac{1 + c}{1 - c} \; \frac{1}{p\,g_m(p)} \tag{4.12}$$

where $\hat{g}_m(p)$ is the LT of the matrix creep compliance. Again (4.12) can

be directly inverted to yield

$$g_1^*(t) = \frac{1 - c}{1 + c} \, g_m(t) \tag{4.13}$$

Note as a check that the first part of the right side of (4.7) could have

been directly deduced from (4.13), since the former is the creep compliance

of the Maxwell matrix multiplied by the factor $\frac{1 - c}{1 + c}$. Equations (4.11)

and (4.13) are particularly useful results since they permit simple, direct

determination of viscoelastic creep and relaxation functions on the basis

of measured matrix behavior.

To illustrate the use of the Abel-Tauber theorems, $G_1^*(\infty)$ will be calcu-

lated from (4.5). The result is

$$G_1^*(\infty) = \frac{G_f(1 + c) + G_m(\infty)(1 - c)}{G_f(1 - c) + G_m(\infty)(1 + c)} \, G_m(\infty) \tag{4.14}$$

Even if $G_m(0)$ is of the order of magnitude of G_f, usually a relaxation modulus decreases at $t = \infty$ to a small fraction of its initial value, so that the rigid fiber approximation becomes applicable to (4.14) whence it reduces with sufficient accuracy to

$$G_1^*(\infty) \cong \frac{1+c}{1-c} G_m(\infty) \quad .$$
(4.15)

which is of course in accordance with (4.11). Similarly, by the same reasoning

$$g_1^*(\infty) \cong \frac{1-c}{1+c} \frac{1}{G_m(\infty)}$$
(4.16)

which is in accordance with (4.13). Thus, in general, if $G_m(\infty)$ goes to zero, $g_1^*(\infty)$ becomes unbounded. The important point to remember is that (4.15-4.16) will hold even if fibers and matrix are initially of comparable stiffness.

5. UNIAXIAL STRESS IN FIBER DIRECTION

The fiber reinforced specimen is first subjected to uniaxial average strain

$$\overline{\epsilon}_{11}(t) = \overline{\epsilon}(t)$$
(5.1)

while the lateral surface is free of load. Then

$$\overline{\sigma}_{22}(t) = \overline{\sigma}_{33}(t) = 0$$
(5.2)

76

and all average shear strains and shear stresses vanish. The relation

between axial average stress and strain is then given by

$$\bar{\sigma}_{11}(t) = \bar{\sigma}(t) = \int_0^t E_1^*(t - \tau) \frac{d\bar{\epsilon}(\tau)}{d\tau} \tag{5.3}$$

where E_1^* is the axial Young's relaxation modulus.

If instead of (5.1) the specimen is subjected to average axial stress

$$\bar{\sigma}_{11}(t) = \bar{\sigma}(t) \tag{5.4}$$

while (5.2) continues to hold, then the axial average strain is given by

$$\bar{\epsilon}_{11}(t) = \bar{\epsilon}(t) = \int_0^t e_1^*(t - \tau) \frac{d\bar{\sigma}(\eta)}{d\tau} d\tau$$

where e_1^* is the axial Young's creep compliance. The functions E_1^* and

e_1^* are related by (2.24).

An expression for the effective Young's modulus E_1^{*E} of the composite

cylinder assemblage has been given by Hashin and Rosen [6]. Hill [15]

has given an equivalent expression [Equation (3.9)] which is of much

simpler algebraic form. Therefore the latter form will be here used. In

the present notation this expression can be written as

$$E_1^{*E} = v_m E_m^E + v_f E_f^E + v_m v_f G_m^E \frac{(G_f^E / \mathcal{R}_f^E - G_m^E / \mathcal{R}_m^E}{v_m \mathcal{R}_f^E / G_m^E + v_f \mathcal{R}_m^E / G_m^E + 1} \tag{5.6}$$

where $\mathcal{R}^E$ is the elastic plane strain bulk modulus defined by (3.7). It

should be noted that simplification to rigid fibers is not permitted here, since this would result in infinite effective Young's modulus.

Application of the correspondence rules to find $E_1^*(t)$ from (5.6), although straightforward, involves very heavy calculations, even for a simple Maxwell matrix. Therefore such derivations will not be given here. Equation (5.6) will only be used to find $E_1^*(o)$ and $E_1^*(\infty)$ by the Abel-Tauber theorems and as will be seen from the results calculation of $E_1^*(t)$ for the full time range is hardly needed for fiber reinforced materials used in practice.

The initial relaxation modulus $E_1^*(o)$ is simply given by inserting in (5.6) the initial phase relaxation moduli. The third term in (5.6) is negligible in most cases, and thus

$$E_1^*(o) \cong v_m E_m(o) + v_f E_f \qquad (5.7)$$

A sample calculation for a typical fiber reinforced material with

$$E_m(o) = 0.5 \times 10^6 \text{ psi} \qquad E_f = 10.5 \times 10^6 \text{ psi}$$

$$\nu_m(o) = 0.35 \qquad \nu_f = 0.20$$

$$v_m = 0.3 \qquad v_f = 0.7$$

shows that the error due to this approximation is 0.013% of (5.7).

Generally in fiber reinforced materials

$$E_m << E_f \qquad\qquad v_m = 0 \, (v_f)$$

In this case the first term in the right side of (5.7) can also be

neglected, and then

$$E_1^*(o) \tilde{=} v_f E_f \qquad\qquad (5.8)$$

Turning now to $t \to \infty$, it is seen that the dominant term in (5.6) is

the middle one since all matrix relaxation moduli become less than

their initial values. Thus to a better approximation than (5.8)

$$E_1^*(\infty) \tilde{=} v_f E_f \qquad\qquad (5.9)$$

Assuming that $E_1^*(t)$ is monotonic it is seen that the viscoelastic effect

is negligible and $E_1^*(t)$ is practically constant.

By the same reasoning the creep compliance e_1^* is practically con-

stant for the whole time range and is given by

$$e_1^* \tilde{=} \frac{1}{v_f E_f} \qquad\qquad (5.10)$$

To define an axial Poisson's ratio $v_1^*(t)$ assume that the average applied

axial stress (5.4) has the form

$$\overline{\sigma}(t) = \sigma^{o} H(t) \tag{5.11}$$

while (5.2) continues to hold. The average strains produced are then (5.1) and

$$\overline{\epsilon}_{22}(t) = \overline{\epsilon}_{33}(t) = \overline{\epsilon}_{s}(t) \tag{5.12}$$

Then $\overset{*}{\nu}_{1}(t)$ is defined by

$$\overset{*}{\nu}_{1}(t) = -\frac{\overline{\epsilon}_{s}(t)}{\overline{\epsilon}(t)} \tag{5.13}$$

It should be noted that $\overset{*}{\nu}_{1}(t)$ cannot be found from an expression for an elastic Poisson's ratio, by the correspondence rules, since it is not a constant which relates stress to strain. To compute $\overset{*}{\nu}_{1}(t)$, $\overline{\epsilon}(t)$ and $\overline{\epsilon}_{s}(t)$ have first to be calculated. Introducing the transforms of the present average stresses and strains into (2.11-13) and solving for the transformed strains, there follows

$$p\,\overline{\epsilon}(p) = \sigma^{o}\,\frac{p\,\overset{\wedge}{\overset{*}{K}}_{23}(p)}{p^{2}\overset{\wedge}{\overset{*}{C}}_{11}\,\overset{\wedge}{\overset{*}{K}}_{23} - p^{2}\overset{*}{C}_{12}^{2}} \tag{5.14}$$

$$p\,\overline{\epsilon}_{s}(p) = \sigma^{o}\,\frac{p\,\overset{\wedge}{\overset{*}{C}}_{12}}{2\left[p^{2}\overset{\wedge}{\overset{*}{C}}_{11}\,\overset{\wedge}{\overset{*}{K}}_{23} - p^{2}\overset{\wedge}{\overset{*}{C}}_{12}^{2}\right]} \tag{5.15}$$

The TD moduli entering into the right sides of (5.14 - 15) are determined from their elastic counterparts by the correspondence rules, whence result

the transforms of the average strains which now have to be inverted to the time domain. Note that (5.14) defines the TD axial Young's modulus which has already been discussed. The inversion being in general very complicated, attention will again be directed to evaluation at times o, ∞ by the Abel-Tauber theorems. Application of these theorems immediately shows that

$$\nu_1^*(o) = -\frac{\overline{\epsilon}_s(o)}{\overline{\epsilon}(o)} = \frac{C_{12}^*(o)}{2K_{23}^*(o)} \tag{5.16}$$

$$\nu_1^*(\infty) = -\frac{\overline{\epsilon}_s(\infty)}{\overline{\epsilon}(\infty)} = \frac{C_{12}^*(\infty)}{2K_{23}^*(\infty)} \tag{5.17}$$

Recalling that the elastic Poisson's ratio ν_1^{*E} is given by (see [2])

$$\nu_1^{*E} = \frac{C_{12}^{*E}}{2K_{23}^{*E}} \tag{5.18}$$

it is concluded that $\nu_1^*(o)$ and $\nu_1^*(\infty)$ can simply be calculated from ν_1^{*E} by replacement of the elastic moduli by the initial and final values of the relaxation moduli, respectively.

An expression for ν_1^{*E} of a cylinder assemblage has been given in [6] and an equivalent expression of simpler form in [15]. The last expression is

$$\nu_1^{*E} = v_m \nu_m^E + v_f \nu_f^E + \frac{v_m v_f (\nu_f^E - \nu_m^E)(1/\hbar_m^E - 1/\hbar_f^E)}{v_m/\hbar_f^E + v_f/\hbar_m^E + 1/G_m^E} \tag{5.19}$$

81

To find ν_1^* (o) and ν_1^* (∞) it is necessary to replace the elastic moduli in (5.19) by the initial and final values of the relaxation moduli. Note in this respect that ν_m (o) and ν_m (∞) have to be interpreted as

$$\nu_m \text{ (o)} = \frac{1}{2}\left(1 - \frac{G_m(o)}{k_m(o)}\right) \tag{5.20}$$

$$\nu_m \text{ (∞)} = \frac{1}{2}\left(1 - \frac{G_m(\infty)}{k_m(\infty)}\right) \tag{5.21}$$

Considerable simplification is achieved if it is assumed that the matrix is incompressible and that G_m (∞) can be neglected relative to fiber moduli. Then

$$\nu_1^* \text{ (∞)} \frac{1}{2} v_m + \nu_f v_f \tag{5.22}$$

6. TRANSVERSE SHEAR

When the fiber reinforced specimen is subjected to the average shear strain

$$\bar{\epsilon}_{23} \text{ (t)} = \bar{\epsilon}_{32} \text{ (t)} = \alpha \tag{6.1}$$

and all other average strains vanish, the resulting average stresses are

$$\bar{\sigma}_{23} \text{ (t)} = \bar{\sigma}_{32} \text{ (t)} = s \tag{6.2}$$

and all others vanish. The stress is given by

$$s(t) = 2 \int_0^t G^*_{23} (t-\tau) \frac{d\alpha(\tau)}{d\tau}$$

(6.3)

If, on the other hand, (6.2) is prescribed, the strain is given by

$$\alpha(t) = \frac{1}{2} \int_0^t g^*_{23} (t-\tau) \frac{ds(\tau)}{d\tau} d\tau$$

(6.4)

The effective transverse shear relaxation modulus and creep compliance, G^*_{23} and g^*_{23}, are related by (2.22).

Unfortunately an expression for G^{*E}_{23} of an elastic composite cylinder assemblage is not known. In the treatment given in [6], this modulus could only be bounded from above and below. It is at present not known how to establish such bounds for visco-elastic fiber reinforced materials for the whole time range.

It has, however, been shown by Schulgasser [43], on the basis of the Abel-Tauber theorems, that elasticity bounds on effective moduli can be transcribed into bounds on visco-elastic effective relaxation moduli at times zero and infinity, simply by replacement of phase elastic moduli in the bound expressions, by initial and ultimate values of the phase relaxation moduli. Consequently the bounds on G^{*E}_{23}, obtained in [6], can be used to find bounds on $G^{*E}_{23}(o)$ and $G^*_{23}(\infty)$ of a composite cylinder assemblage.

If results for intermediate times are needed, the following observation may be of some value. It has been shown in [14] that a lower bound for G_{23}^{*E} of a fiber reinforced material, with arbitrary fiber shapes, is given by the expression

$$G_{23 \, (-)}^{*E} = G_m^E + \cfrac{v_f}{\cfrac{1}{G_f^E - G_m^E} + \cfrac{(k_m^E + 2G_m^E) v_m}{2G_m^E (k_M^E + G_m^E)}} \qquad (6.5)$$

It may be shown that (6.5) is always between the bounds for G_{23}^{*E} of a cylinder assemblage which have been derived in [6]. Furthermore, for v_f very close to zero or very close to unity, these bounds coincide and reduce to (6.5). Therefore, if the bounds for the elastic case are reasonably close, there may be some merit in replacing the phase moduli in (6.5) by TD phase moduli and inverting into the time domain. It may then be hoped that the resulting expression will give $G_{23}^*(t)$ of a composite cylinder assemblage, approximately.

7. APPLICATION OF RESULTS

As an example of the application of the results of this study, the time dependent properties of a Maxwell body will be treated. For this material the stress-strain relations are of the form:

$$\dot{e}_{ij} = \frac{\dot{s}_{ij}}{2G} + \frac{s_{ij}}{2\eta} \qquad (7.1)$$

84

The relaxation modulus is defined as the stress associated with a constant unit strain. Thus:

$$e_{ij}(t) = 1$$

$$\dot{e}_{ij}(t) = 0$$

$$\therefore \quad \frac{\dot{s}_{ij}}{2G} + \frac{s_{ij}}{2\eta} = 0 \qquad (7.2)$$

The solution to this equation is:

$$s_{ij} = Ce^{-t/\tau} \qquad (7.3)$$

$$\text{where} \quad \tau = \frac{\eta}{G}$$

Since

$$s_{ij}(o) = 2G^E e_{ij}(o)$$

$$s_{ij} = 2G^E e^{-t/\tau}$$

And the relaxation modulus, $G(t)$, is given by:

$$G(t) = G^E e^{-t/\tau} \qquad (7.4)$$

In particular, the plane strain bulk modulus, $K^*_{23}(t)$, for a composite of rigid fibers is given by eq. (3.15). The matrix will be assumed elastic in dilation. Thus:

$$K_m(t) = K_m^E \qquad (7.5)$$

From (7.4): $\quad G_m(t) = G_m^E e^{-t/\tau}$ (7.6)

Substitution of eqs. (7.5) and (7.6) into (3.15) yields:

$$\frac{K_{23}^*(t)}{K_m^E} = \frac{1}{1-c} + \left(\frac{1+3c}{1-c}\right) \frac{G_m^E}{K_m^E} e^{-t/\tau}$$ (7.7)

where $\quad \dfrac{G_m^E}{K_m^E} = \dfrac{3(1-2\nu_m)}{2(1+\nu_m)}$

The normalized plane strain bulk modulus is presented as a function of the non-dimensional time parameter in fig. 27 for several values of c. The lowest curve represents an unreinforced matrix.

Similarly, the relaxation modulus for shear in a fiber plane, $G_1^*(t)$ is given by eq. (4.11). Thus from eqs. (7.4) and (4.11):

$$\frac{G_1^*(t)}{G_m^E} = \frac{1+c}{1-c} e^{-t/\tau}$$ (7.8)

Results for the same values of c used previously are presented in fig. 28

Another example of the application of this viscoelastic analysis is obtained by evaluating the creep compliance. For this case we consider the strain associated with the stresses:

$$s_{ij}(t) = 1$$

$$\therefore \dot{s}_{ij}(t) = 0$$

86

and from eq. 7.1:

$$\dot{e}_{ij}(t) = \frac{1}{2\eta}$$
(7.9)

$$\therefore e_{ij}(t) = \frac{t}{2\eta} + C$$

$$e_{ij}(o) = \frac{s_{ij}(o)}{2G^E} = \frac{1}{2G^E}$$

$$e_{ij}(t) = \frac{t}{2\eta} + \frac{1}{2G^E}$$

or
$$e_{ij}(t) = \frac{1}{2G^E}\left(\frac{t}{\tau} + 1\right)$$

The creep compliance, $g(t)$ is thus:

$$g(t) = g^E\left(\frac{t}{\tau} + 1\right)$$
(7.10)

The creep compliance, k_{23}^* for rigid fibers is given by (3.17). Thus

$$\frac{k_{23}^*(t)}{(1/K_m^{*E})} = (1-c) H(t) + \left[\frac{K_m^*}{K_{23}^{*E}} - (1-c)\right] \exp\left\{-\frac{K_m^E (1-c)}{K_{23}} \frac{t}{\tau}\right\}$$
(7.11)

It can be shown (ref. 6) that for this case

$$\frac{k_{23}^{*E}}{K_m^E} = \frac{3(1+2c\,\nu_m)}{2(1-c)(1+\nu_m)}$$
(7.12)

Substituting eq. (7.12) into (7.11) yields:

$$\frac{k_{23}^{*}(t)}{(1/K_m^{*}{}^{E})} = (1-c)\left\{H(t) + \left[\frac{2(1+\nu_m)}{3(1+2c\,\nu_m)} - 1\right]\exp\left[-\frac{2(1-c)^2(1+\nu_m)}{3(1+2c\,\nu_m)}\frac{t}{\tau}\right]\right\} \quad (7.13)$$

A simple illustration is obtained for the case $\nu_m = o$, namely;

$$\frac{k_{23}^{*}(t)}{(1/K_m^{*}{}^{E})}\bigg|_{\nu_m = o} = (1-c)\left\{H(t) - \frac{1}{3}\exp\left[-\frac{2}{3}(1-c)^2\frac{t}{\tau}\right]\right\} \quad (7.14)$$

Eq. (7.14) is plotted in fig. 29.

The creep compliance in shear, $g_1^{*}(t)$ is given by eq. (4.13), which with the aid of eq. (7.10) yields:

$$\frac{g_1^{*}(t)}{\dfrac{E}{g_m}} = \frac{1-c}{1+c}\left(\frac{t}{\tau} + 1\right) \quad (7.15)$$

These results are presented in fig. 30.

8. CONCLUSIONS

The analysis given here may be regarded as a first step in the theoretical evaluation of the viscoelastic properties of fiber reinforced materials in terms of phase properties. It should be remembered that the composite cylinder assemblage model is only a geometrical idealization of a real fiber reinforced material.

In the elastic case the results obtained on the basis of this model were in many cases close to experimental results. It may therefore be hoped that the viscoelastic results will exhibit similar features. To the author's knowledge, systematic experimental investigation of the viscoelastic properties of fiber reinforced materials has not been performed.

THREE-DIMENSIONAL REINFORCEMENT

Filamentary reinforcement of composites has generally been of two-dimensional character. That is, the filaments are usually disposed to provide reinforcement in the plane of a plate-like composite, or around the circumference of a shell, for example. Reinforcements through the thickness of plates and shells have not often been attempted. Thus the composites have most often had a laminate-like structure, similar to plywood.

Lack of reinforcement through the thickness, while leading to simplifications in both composite fabrication and analysis also introduces undesirable planes of weakness in the material. Probably mis-named "interlaminar shear" failures have been encountered in compression; "shredding" failures of hoop-wound pressure vessels have occurred in tension and both analytical and experimental models (Ref. 11) have supported the desirability of added reinforcement in the thickness direction for thin-walled as well as thick composites.

In this section of this report analytical procedures are developed for the evaluation of the elastic constants of filamentary composites having three-dimensional reinforcements. Formulas for these constants are derived for orthogonal filaments, and for skewed filaments having symmetries about three orthogonal axes. In the derivations some symplifying assumptions are employed; these assumptions (or the symmetries considered) are not

essential to the development,-their importance will be discussed and directions for more rigorous and general extensions will be given. The formulas derived, however, encompass a wide new range of reinforcement possibilities, and they will be employed in the evaluation of some of the potentialities accessible through the use of a three-dimensional reinforcing system.

Analytical Approach

The approach used for the three-dimensional analysis relates to that followed in Reference 44 to determine the properties of integrally stiffened plates. Therein the reinforcement provided by integral stiffening is evaluated as fully effective in the direction of the stiffening but reduced in stretching effectiveness transverse to the stiffening by a factor β. Similarly the transverse shearing effectiveness is evaluated as reduced, - in this case by a different factor β'. With the longitudinal and transverse effectivenesses established, the remainder of the analysis is a straight-forward elasticity problem of trigonometric resolution and summation of stiffnesses to yield the desired elastic constants.

The basis for the extension of the integral stiffening analysis to fila-mentary composites is illustrated schematically in Figure 31. In this figure the portion of the binder material between filaments in a uni-directionally reinforced filamentary composite is shown to be similar to the skin and inte-gral ribbing of integrally stiffened plates. Neglecting the filaments (i.e.,

91

treating them for the moment as holes) the stiffness of such a two-dimensional array may be written according to the analysis of Reference 44 either as

$$E_{T_0} = E_b \left[\frac{t_S}{1-\nu^2} + \beta_\perp \left(\frac{A_{w_\perp}}{b_x} \right) - \frac{\left(\frac{\nu}{1-\nu^2} \right)^2 t_S^2}{\frac{t_S}{1-\nu^2} + \frac{A_{w_\perp}}{b_x}} \right] \quad (28)$$

or converting to the nomenclature for composites

$$E_{T_0} = E_b \left[\frac{1}{1-\nu^2} - \beta_0 (1-v_b) - \frac{\left(\frac{\nu}{1-\nu^2} \right)^2}{\frac{1}{1-\nu^2} - (1-v_b)} \right] \quad (29)$$

In these equations

E_{T_0} stiffness transverse to round holes in binder

E_b Young's modulus of binder material

t_S "skin thickness" - thickness of straight elements of binder (if any) between holes

ν Poisson's ratio

$\beta_\perp$ transverse effectiveness of $\perp$-shaped material between holes in binder

$A_{w_\perp}$ cross-sectional area of $\perp$-shaped material between holes

b_x hole spacing

β_0 transverse effectiveness lost by making holes in binder

v_b volume fraction of binder material

92

The next step is evidently to fill the holes with filaments to yield

an equation for the two-dimensional composite as follows:

$$E_{T_e} = E_b \left[\frac{1}{1-\nu^2} - \beta_e (1-\nu_b) + \beta_e (1-\nu_b)\frac{E_f}{E_b} - \frac{\left(\frac{\nu}{1-\nu^2}\right)^2}{\frac{1}{1-\nu^2} - (1-\nu_b) + (1-\nu_b)\frac{E_f}{E_b}} \right] \quad (30)$$

where for simplicity the Poisson's ratios of filaments and binder have been

assumed equal; β_e represents the transverse effectiveness of the filament,

and E_f is the Young's modulus of the filamentary material.

Extension of this type of analysis to three dimension and for appli-

cation to filaments and binders of different Poisson's ratios is discussed in

the following sections.

Equations for Elastic Constants

General Equations - The elastic constants evaluated in the three-

dimensional analysis are those applicable to an orthotropic composite having

reinforcements symmetrically disposed about the three principal axes at plus

and minus the angles indicated in Figure 32. For such a composite there are

nine elastic constants defined by the following equations:

$$\sigma_1 = A_1 \epsilon_1 + A_2 \epsilon_2 + A_3 \epsilon_3$$

$$\sigma_2 = A_2 \epsilon_1 + A_4 \epsilon_2 + A_5 \epsilon_3$$

$$\sigma_3 = A_3 \epsilon_1 + A_5 \epsilon_2 + A_6 \epsilon_3 \quad (31)$$

93

$$\tau_{12} = A_7 \gamma_{12}$$

$$\tau_{23} = A_8 \gamma_{23}$$

$$\tau_{13} = A_9 \gamma_{13}$$

(31)
Cont'd.

where

σ_1, σ_2, σ_3 direct stresses in the 1-, 2-, and 3-directions

ε_1, ε_2, ε_3 direct strains in the 1-, 2-, and 3-directions

τ_{12}, τ_{23}, τ_{13} shear stresses in the 1-2, 2-3, and 1-3 planes

γ_{12}, γ_{23}, γ_{13} shear strains in the 1-2, 2-3, and 1-3 planes

and the A's are the elastic constants given by the equations in the following

section. These constants are related to the conventional stretching and

shearing stiffnesses E_1, E_2, and E_3, G_{12}, G_{23}, and G_{13}, and Poisson's

ratios ν_{21}, ν_{32}, and ν_{31}, by the following equations:

$$E_1 = A_1 - \frac{A_2^2 A_6 - A_2 A_3 A_5}{A_4 A_6 - A_5^2} - \frac{A_3^2 A_4 - A_2 A_3 A_5}{A_4 A_6 - A_5^2}$$

(32)

$$E_2 = A_4 - \frac{A_2^2 A_6 - A_2 A_3 A_5}{A_1 A_6 - A_3^2} - \frac{A_1 A_5^2 - A_2 A_3 A_5}{A_1 A_6 - A_3^2}$$

$$E_3 = A_6 - \frac{A_3^2 A_4 - A_2 A_3 A_5}{A_1 A_4 - A_2^2} - \frac{A_1 A_5^2 - A_2 A_3 A_5}{A_1 A_4 - A_2^2}$$

$$\nu_{21} = \frac{A_2 A_6 - A_3 A_5}{A_1 A_6 - A_3^2}$$

94

$$\nu_{32} = \frac{A_1 A_5 - A_2 A_3}{A_1 A_4 - A_2^2}$$

$$\nu_{31} = \frac{A_3 A_4 - A_2 A_5}{A_1 A_4 - A_2^2}$$

$$G_{12} = A_7$$

$$G_{23} = A_8$$

$$G_{13} = A_9$$

General equations like (31) and (32) may be found in the literature of three-dimensional elasticity for application to any orthotropic solid with the specified symmetries (so that couplings among shears and displacements are avoided). The evaluation of the constants employed in these equations for filamentary composites, however, involves less standard procedures. These special characteristics are discussed and illustrated for specific cases in the following sections.

<u>Derivations</u> - The elastic constants for the three-dimensionally rein-forced composites are derived by partial differentiations of the general expression for the strain energy of a repeating rectangular element b_1 by b_2 by b_3 of the composite. This derivation is analogous to that in Reference 44 for integrally-stiffened plates with the following differences:

(1) It is a three-dimensional rather than a two-dimensional analysis.

(2) Properties of binder and filaments are different, whereas ribs and skin in Reference 44 were of the same material.

(3) Only extension and shearing are considered. Reference 44 also evaluated bending and twisting stiffnesses. Thus the implicit assumption is made that the composite is homogeneous, and bending and twisting stiffnesses can be evaluated in terms of the stretching and shearing constants. Non-homogeneities through the thickness direction could be readily taken into account, if desired, with a re-derivation extended in further analogy to the waffle-stiffening of Reference 44. Non-homogeneities in the other two directions, however, would require such major modifications that they can hardly be considered in terms of the present analysis.

The general expressions for the strain energy of stretching of a composite subjected to the strains ϵ_1, ϵ_2, and ϵ_3, may be written as follows:

$$V = \frac{1}{2} \int_0^{b_1} \int_0^{b_2} \int_0^{b_3} \frac{E_b}{(1+\nu_b)(1-2\nu_b)} \left[\left(\epsilon_1^2 + \epsilon_2^2 + \epsilon_3^2\right)(1-\nu_b) + \left(\epsilon_1 \epsilon_2 + \epsilon_2 \epsilon_3 + \epsilon_1 \epsilon_3\right)(2\nu_b) \right] d_{(1)} d_{(2)} d_{(3)}$$

$$+ \frac{1}{2} \int_0^{b_1} \left[\left[\frac{E_1(1-\nu_{f_1})}{(1+\nu_{f_1})(1-2\nu_{f_1})} - \frac{E_b(1-\nu_b)}{(1+\nu_b)(1-2\nu_b)} \right] \left[\epsilon_1^2 (V_{f_1}) \right] \right] d_{(1)}$$

(33)

$$+ \frac{1}{2} \int_0^{b_1} \left[\left[\frac{\nu_{f_1} E_{f_1} \beta_{o_1}}{(1+\nu_{f_1})(1-2\nu_{f_1})} - \frac{\nu_b E_b \beta_{-o}}{(1+\nu_b)(1-2\nu_b)} \right] \left[\left(\epsilon_1 \epsilon_2 + \epsilon_2 \epsilon_3 + \epsilon_1 \epsilon_3\right)(2 V_{f_1}) \right] \right] d_{(1)}$$

$$+ \frac{1}{2} \int_0^{b_1} \left[\left[\frac{E_{f_1}(1-\nu_{f_1})\beta_{o_1}}{(1+\nu_{f_1})(1-2\nu_{f_1})} - \frac{E_b(1-\nu_b)\beta_{-o}}{(1+\nu_b)(1-2\nu_b)} \right] \left[\left(\epsilon_2^2 + \epsilon_3^2\right)(V_{f_1}) \right] \right] d_{(1)}$$

96

$$+ \frac{1}{2} \int_0^{b_2} \left[\left[\frac{E_{f_2}(1-\nu_{f_2})}{(1+\nu_{f_2})(1-2\nu_{f_2})} - \frac{E_b(1-\nu_b)}{(1+\nu_b)(1-2\nu_b)} \right] \left[\epsilon_2^2 (V_{f_2}) \right] \right] d(2)$$

$$+ \frac{1}{2} \int_0^{b_2} \left[\left[\frac{\nu_{f_2} E_{f_2} \beta_{o_2}}{(1+\nu_{f_2})(1-2\nu_{f_2})} - \frac{\nu_b E_b \beta_{-o}}{(1+\nu_b)(1-2\nu_b)} \right] \left[(\epsilon_1 \epsilon_2 + \epsilon_2 \epsilon_3 + \epsilon_1 \epsilon_3)(2 V_{f_2}) \right] \right] d(2)$$

$$+ \frac{1}{2} \int_0^{b_2} \left[\left[\frac{E_{f_2}(1-\nu_{f_2})\beta_{o_2}}{(1+\nu_{f_2})(1-2\nu_{f_2})} - \frac{E_b(1-\nu_b)\beta_{-o}}{(1+\nu_b)(1-2\nu_b)} \right] \left[(\epsilon_1^2 + \epsilon_3^2)(V_{f_2}) \right] \right] d(2)$$

$$+ \frac{1}{2} \int_0^{b_3} \left[\left[\frac{E_{f_3}(1-\nu_{f_3})}{(1+\nu_{f_3})(1-2\nu_{f_3})} - \frac{E_b(1-\nu_b)}{(1+\nu_b)(1-2\nu_b)} \right] \left[\epsilon_3^2 (V_{f_3}) \right] \right] d(3)$$

$$+ \frac{1}{2} \int_0^{b_3} \left[\left[\frac{\nu_{f_3} E_{f_3} \beta_{o_3}}{(1+\nu_{f_3})(1-2\nu_{f_3})} - \frac{\nu_b E_b \beta_{-o}}{(1+\nu_b)(1-2\nu_b)} \right] \left[(\epsilon_1 \epsilon_2 + \epsilon_2 \epsilon_3 + \epsilon_1 \epsilon_3)(2 V_{f_3}) \right] \right] d(3)$$

$$+ \frac{1}{2} \int_0^{b_3} \left[\left[\frac{E_{f_3}(1-\nu_{f_3})\beta_{o_3}}{(1+\nu_{f_3})(1-2\nu_{f_3})} - \frac{E_b(1-\nu_b)\beta_{-o}}{(1+\nu_b)(1-2\nu_b)} \right] \left[(\epsilon_1^2 + \epsilon_2^2)(V_{f_3}) \right] \right] d(3)$$

$$+ \frac{1}{2} \int_0^{b_s} \left[\left[\frac{E_{f_s}(1-\nu_{f_s})}{(1+\nu_{f_s})(1-2\nu_{f_s})} - \frac{E_b(1-\nu_b)}{(1+\nu_b)(1-2\nu_b)} \right] \left[\epsilon_{S_L}^2 (V_{f_s}) \right] \right] d(s)$$

$$+ \frac{1}{2} \int_0^{b_s} \left[\left[\frac{\nu_{f_s} E_{f_s} \beta_{os}}{(1+\nu_{f_s})(1-2\nu_{f_s})} - \frac{\nu_b E_b \beta_{-o}}{(1+\nu_b)(1-2\nu_b)} \right] \left[(\epsilon_{S_L} \epsilon_{S_{T_1}} + \epsilon_{S_{T_1}} \epsilon_{S_{T_2}} + \epsilon_{S_L} \epsilon_{S_{T_2}})(2 V_{f_s}) \right] \right] d(s)$$

$$+ \frac{1}{2} \int_0^{b_s} \left[\left[\frac{E_{f_s}(1-\nu_{f_s})\beta_{os}}{(1+\nu_{f_s})(1-2\nu_{f_s})} - \frac{E_b(1-\nu_b)\beta_{-o}}{(1+\nu_b)(1-2\nu_b)} \right] \left[(\epsilon_{S_{T_1}}^2 + \epsilon_{S_{T_2}}^2)(V_{f_s}) \right] \right] d(s)$$

97

$$+ \frac{1}{2} \int_0^{b_s} \left[\left[G_{f_s} \beta'_{\bullet_s} - G_b \beta'_{-\bullet} \right] \left[\gamma^2_{S_{LT_1}} + \gamma^2_{S_{LT_2}} \right] (v_{f_s}) \right] d(s)$$

$$+ \frac{1}{2} \int_0^{b_s} \left[\left[G_{f_s} \beta''_{\bullet_s} - G_b \beta''_{-\bullet} \right] \left[\gamma^2_{S_{T_1 T_2}} \right] (v_{f_s}) \right] d(s)$$

(33)
Conc.

where

    V = strain energy of distortion

    E = Young's modulus

    G = shear modulus

    ν = Poisson's ratio

    ϵ = extensional strain

    γ = shear strain

    v = volume fraction

Subscripts

    f = filament

    b = binder

    1, 2, 3, s = 1-, 2-, 3-, skew directions

    S_L = along skew direction

    S_T = transverse to skew direction

98

Evident in the foregoing expression are the various β's representative of the transverse effectivenesses of the filaments and binder elements among filaments. For simple extension, such that the energy is measured by an expression of the form

$$\frac{1}{2}\int_0^b \frac{E_f(1-\nu_f)}{(1+\nu_f)(1-2\nu_f)}(\beta_0 V_f)(\epsilon^2)d(n) \tag{34}$$

for example, the analogy between the β's of Reference 44 and those used herein is complete. For Poisson extensions of the form

$$\frac{1}{2}\int_0^b \frac{\nu_f E_f}{(1+\nu_f)(1-2\nu_f)}(\beta_0 V_f)(2\epsilon_1\epsilon_2)d(n) \tag{35}$$

however, the physical model of reduced effectiveness is somewhat different, and strictly speaking a different effectiveness factor, as $(\beta_0 + \delta)$ should perhaps be employed. For simplicity herein such a refinement is not considered. In consequence slight errors are introduced which show up primarily as slightly high calculated values of E_1 for uni-directionally reinforced (in the 1-direction) composites. Inasmuch as this E_1 is the most easily calculated of all the constants, via the rule of mixtures, so it can be readily corrected, if desired, and since the other values of stiffnesses appear accurately calculated ($\pm 5\%$) with one β for direct and for Poisson strains, only one β is used in the following development.

(The use of a single transverse effectiveness factor also affects the values of Poisson's ratios calculated by this analysis. It will be shown later that expressions may be derived for the adjustment of the β-value for a more precise description of the transverse effectiveness. For most purposes, however, such an adjustments appears unwarranted.)

In order to evaluate the strain energy as given in Equation (35) expressions are required for ϵ_{S_L}, $\gamma_{S_{LT_1}}$, etc. in terms of the imposed distortions ϵ_1, ϵ_2, and ϵ_3. These expressions are:

(1) The strain along a skew filament

$$\epsilon_{S_L} = \epsilon_1 \cos^2\phi + \epsilon_2 \cos^2\psi + \epsilon_3 \cos^2\Omega \tag{36}$$

(2) The strain perpendicular to a skew filament and in the plane of the filament and the 1-axis

$$\epsilon_{S_{T_1}} = \epsilon_1 \sin^2\phi + \epsilon_2 \cos^2\psi \cot^2\phi + \epsilon_3 \cos^2\Omega \cot^2\phi \tag{37}$$

(3) The strain perpendicular to ϵ_{S_L} and $\epsilon_{S_{T_1}}$

$$\epsilon_{S_{T_2}} = \epsilon_2 \frac{\cos^2\Omega}{\sin^2\phi} + \epsilon_3 \frac{\cos^2\psi}{\sin^2\phi} \tag{38}$$

100

Similar expressions can be written for the orthogonal shearing

strains as:

$$\gamma_{S_{LT_1}} = 2\left[\epsilon_1 \sin\phi\cos\phi - \epsilon_2 \cot\phi\cos^2\phi - \epsilon_3 \cot\phi\cos^2\Omega\right] \tag{39}$$

$$\gamma_{S_{LT_2}} = 2\left[\epsilon_2 \frac{\cos\Omega}{\sin\phi} - \epsilon_3 \frac{\cos\phi\cos\Omega}{\sin\phi}\right] \tag{40}$$

$$\gamma_{S_{T_1 T_2}} = 2\left[\epsilon_2 \cot\phi \frac{\cos\phi\cos\Omega}{\sin\phi} - \epsilon_3 \cot\phi \frac{\cos\phi\cos\Omega}{\sin\phi}\right] \tag{41}$$

Substituting Equations (36) - (41) in Equation (33), integrating and

simplifying, yields -

$$\frac{V}{b_1 b_2 b_3} = \epsilon_1^2 \left\{ \frac{E_b(1-\nu_b)}{2(1+\nu_b)(1-2\nu_b)} + \left[\frac{E_{f_1}(1-\nu_{f_1})}{2(1+\nu_{f_1})(1-2\nu_{f_1})} - \frac{E_b(1-\nu_b)}{2(1+\nu_b)(1-2\nu_b)} \right](\nu_{f_1}) \right.$$

$$+ \left[\frac{E_{f_2}(1-\nu_{f_2})\beta_{\bullet 2}}{2(1+\nu_{f_2})(1-2\nu_{f_2})} - \frac{E_b(1-\nu_b)\beta_{\bullet\bullet}}{2(1+\nu_b)(1-2\nu_b)} \right](\nu_{f_2}) + \left[\frac{E_{f_3}(1-\nu_{f_3})\beta_{\bullet 3}}{2(1+\nu_{f_3})(1-2\nu_{f_3})} - \frac{E_b(1-\nu_b)\beta_{\bullet\bullet}}{2(1+\nu_b)(1-2\nu_b)} \right](\nu_{f_3})$$

$$+ \left[\frac{E_{f_5}(1-\nu_{f_5})}{2(1+\nu_{f_5})(1-2\nu_{f_5})} - \frac{E_b(1-\nu_b)}{2(1+\nu_b)(1-2\nu_b)} \right]\left[(\cos^4\phi)(\nu_{f_5})\right] \tag{42}$$

$$+ \left[\frac{E_{f_5}(1-\nu_{f_5})\beta_{\bullet 5}}{2(1+\nu_{f_5})(1-2\nu_{f_5})} - \frac{E_b(1-\nu_b)\beta_{\bullet\bullet}}{2(1+\nu_b)(1-2\nu_b)} \right]\left[(\sin^4\phi)(\nu_{f_5})\right]$$

$$\left. + \left[\frac{\nu_{f_5}E_{f_5}\beta_{\bullet 5}}{(1+\nu_{f_5})(1-2\nu_{f_5})} - \frac{\nu_b E_b \beta_{\bullet\bullet}}{(1+\nu_b)(1-2\nu_b)} \right]\left[\sin^2\phi\cos^2\phi)(\nu_{f_5})\right] + 2\left[G_{f_5}\beta_5' - G_b\beta_{\bullet\bullet}' \right]\left[\sin^2\phi\cos^2\phi)(\nu_{f_5})\right] \right\}$$

101

$$+ \epsilon_2^2 \left\{ \frac{E_b(1-\nu_b)}{2(1+\nu_b)(1-2\nu_b)} + \left[\frac{E_{f_1}(1-\nu_{f_1})\beta_{o_1}}{2(1+\nu_{f_1})(1-2\nu_{f_1})} - \frac{E_b(1-\nu_b)\beta_{-o}}{2(1+\nu_b)(1-2\nu_b)} \right](\nu_{f_1}) \right.$$

$$+ \left[\frac{E_{f_2}(1-\nu_{f_2})}{2(1+\nu_{f_2})(1-2\nu_{f_2})} - \frac{E_b(1-\nu_b)}{2(1+\nu_b)(1-2\nu_b)} \right](\nu_{f_2}) + \left[\frac{E_{f_3}(1-\nu_{f_3})\beta_{o_3}}{2(1+\nu_{f_3})(1-2\nu_{f_3})} - \frac{E_b(1-\nu_b)\beta_{-o}}{2(1+\nu_b)(1-2\nu_b)} \right](\nu_{f_3})$$

$$+ \left[\frac{E_{f_5}(1-\nu_{f_5})}{2(1+\nu_{f_5})(1-2\nu_{f_5})} - \frac{E_b(1-\nu_b)}{2(1+\nu_b)(1-2\nu_b)} \right](\cos^4\psi)(\nu_{f_5}) + \left[\frac{E_{f_5}(1-\nu_{f_5})\beta_{o_5}}{2(1+\nu_{f_5})(1-2\nu_{f_5})} - \frac{E_b(1-\nu_b)\beta_{-o}}{2(1+\nu_b)(1-2\nu_b)} \right]\left[\frac{\cos^4\phi\cos^4\psi + \cos^4\Omega}{\sin^4\phi} \right](\nu_{f_5})$$

$$+ \left[\frac{\nu_{f_5}E_{f_5}\beta_{o_5}}{2(1+\nu_{f_5})(1-2\nu_{f_5})} - \frac{\nu_b E_b\beta_{-o}}{2(1+\nu_b)(1-2\nu_b)} \right]\left[\left(2\cot^2\phi\cos^4\psi + \frac{\cot^2\phi\cos^2\psi\cos^2\Omega}{\sin^4\phi} \right)(\nu_{f_5}) \right]$$

$$+ 2\left[G_{f_5}\beta_{o_5}' - G_b\beta_{-o}' \right]\left[\left(\cot^2\phi\cos^4\psi + \frac{\cos^2\psi\cos^2\Omega}{\sin^2\phi} \right)(\nu_{f_5}) \right] + \left. 2\left[G_{f_5}\beta_{o_5}'' - G_b\beta_{-o}'' \right]\left[\left(\frac{\cot^2\phi\cos^2\psi\cos^2\Omega}{\sin^4\phi} \right)(\nu_{f_5}) \right] \right\}$$

$$+ \epsilon_3^2 \left\{ \frac{E_b(1+\nu_b)}{2(1+\nu_b)(1-2\nu_b)} + \left[\frac{E_{f_1}(1-\nu_{f_1})\beta_{o_1}}{2(1+\nu_{f_1})(1-2\nu_{f_1})} - \frac{E_b(1-\nu_b)\beta_{-o}}{2(1+\nu_b)(1-2\nu_b)} \right](\nu_{f_1}) + \left[\frac{E_{f_2}(1-\nu_{f_2})\beta_{o_2}}{2(1+\nu_{f_2})(1-2\nu_{f_2})} - \frac{E_b(1-\nu_b)\beta_{-o}}{2(1+\nu_b)(1-2\nu_b)} \right](\nu_{f_2}) \right.$$

$$+ \left[\frac{E_{f_3}(1-\nu_{f_3})}{2(1+\nu_{f_3})(1-2\nu_{f_3})} - \frac{E_b(1-\nu_b)}{2(1+\nu_b)(1-2\nu_b)} \right](\nu_{f_3}) + \left[\frac{E_{f_5}(1-\nu_{f_5})}{2(1+\nu_{f_5})(1-2\nu_{f_5})} - \frac{E_b(1-\nu_b)}{2(1+\nu_b)(1-2\nu_b)} \right](\cos^4\Omega)(\nu_{f_5})$$

$$+ \left[\frac{E_{f_5}(1-\nu_{f_5})\beta_{o_5}}{2(1+\nu_{f_5})(1-2\nu_{f_5})} - \frac{E_b(1-\nu_b)\beta_{-o}}{2(1+\nu_b)(1-2\nu_b)} \right]\left[\left(\frac{\cos^4\phi\cos^4\Omega + \cos^4\psi}{\sin^4\phi} \right)(\nu_{f_5}) \right]$$

$$+ \left[\frac{\nu_{f_5}E_{f_5}\beta_{o_5}}{2(1+\nu_{f_5})(1-2\nu_{f_5})} - \frac{\nu_b E_b\beta_{-o}}{2(1+\nu_b)(1-2\nu_b)} \right]\left[\left(2\cot^2\phi\cos^4\Omega + \frac{\cot^2\phi\cos^2\psi\cos^2\Omega}{\sin^4\phi} \right)(\nu_{f_5}) \right]$$

$$+ 2\left[G_{f_5}\beta_{o_5}' - G_b\beta_{-o}' \right]\left[\left(\cot^2\phi\cos^4\Omega + \frac{\cos^2\psi\cos^2\Omega}{\sin^2\phi} \right)(\nu_{f_5}) \right] + \left. 2\left[G_{f_5}\beta_{o_5}'' - G_b\beta_{-o}'' \right]\left[\left(\frac{\cos^2\phi\cos^2\psi\cos^2\Omega}{\sin^4\phi} \right)(\nu_{f_5}) \right] \right\}$$

$$+\epsilon_1\epsilon_2\left\{\frac{\nu_b E_b}{(1+\nu_b)(1-2\nu_b)}+\left[\frac{\nu_{f_1}E_{f_1}\beta_{\circ_1}}{(1+\nu_{f_1})(1-2\nu_{f_1})}-\frac{\nu_b E_b\beta_{-\circ}}{(1+\nu_b)(1-2\nu_b)}\right](V_{f_1})+\left[\frac{\nu_{f_2}E_{f_2}\beta_{\circ_2}}{(1+\nu_{f_2})(1-2\nu_{f_2})}-\frac{\nu_b E_b\beta_{-\circ}}{(1+\nu_b)(1-2\nu_b)}\right]V_{f_2})\right.$$

$$+\left[\frac{\nu_{f_3}E_{f_3}\beta_{\circ_3}}{(1+\nu_{f_3})(1-2\nu_{f_3})}-\frac{\nu_b E_b\beta_{-\circ}}{(1+\nu_b)(1-2\nu_b)}\right]V_{f_3})+\left[\frac{E_{f_3}(1-\nu_{f_3})\beta_{\circ_3}}{(1+\nu_{f_3})(1-2\nu_{f_3})}-\frac{E_b(1-\nu_b)\beta_{-\circ}}{(1+\nu_b)(1-2\nu_b)}\right]2\cos^2\phi\cos^2\psi)(V_{f_3})$$

$$+\left[\frac{\nu_{f_3}E_{f_3}\beta_{\circ_3}}{(1+\nu_{f_3})(1-2\nu_{f_3})}-\frac{\nu_b E_b\beta_{-\circ}}{(1+\nu_b)(1-2\nu_b)}\right]\left(\sin^2\phi\cos^2\psi+\cos^2\Omega+\cot^2\phi\{\cos^2\phi\cos^2\psi+\cos^2\Omega\}\right)(V_{f_3})\right]$$

$$\left.-4\left[G_{f_3}\beta'_{\circ_3}-G_b\beta'_{-\circ}\right]\left(\cos^2\phi\cos^2\psi\right)(V_{f_3})\right\}$$

$$+\epsilon_2\epsilon_3\left\{\frac{\nu_b E_b}{(1+\nu_b)(1-2\nu_b)}+\left[\frac{\nu_{f_1}E_{f_1}\beta_{\circ_1}}{(1+\nu_{f_1})(1-2\nu_{f_1})}-\frac{\nu_b E_b\beta_{-\circ}}{(1+\nu_b)(1-2\nu_b)}\right](V_{f_1})+\left[\frac{\nu_{f_2}E_{f_2}\beta_{\circ_2}}{(1+\nu_{f_2})(1-2\nu_{f_2})}-\frac{\nu_b E_b\beta_{-\circ}}{(1+\nu_b)(1-2\nu_b)}\right]V_{f_2})\right.$$

$$+\left[\frac{\nu_{f_3}E_{f_3}\beta_{\circ_3}}{(1+\nu_{f_3})(1-2\nu_{f_3})}-\frac{\nu_b E_b\beta_{-\circ}}{(1+\nu_b)(1-2\nu_b)}\right](V_{f_3})+\left[\frac{E_{f_3}(1-\nu_{f_3})\beta_{\circ_3}}{(1+\nu_{f_3})(1-2\nu_{f_3})}-\frac{E_b(1-\nu_b)\beta_{-\circ}}{(1+\nu_b)(1-2\nu_b)}\right]\left(\cos^2\psi\cos^2\Omega\right)\left(\frac{\sin^4\phi+\cos^4\phi+1}{\sin^4\phi}\right)(V_{f_3})$$

$$+\left[\frac{\nu_{f_3}E_{f_3}\beta_{\circ_3}}{(1+\nu_{f_3})(1-2\nu_{f_3})}-\frac{\nu_b E_b\beta_{-\circ}}{(1+\nu_b)(1-2\nu_b)}\right]\left(\frac{\cos^2\phi\cos^2\psi\cos^2\Omega}{\sin^4\phi}+\frac{\cos^4\psi+\cos^4\Omega}{\sin^2\phi\cos^2\phi}(V_{f_3})\right]$$

$$+4\left[G_{f_3}\beta'_{\circ_3}-G_b\beta'_{-\circ}\right]\left(\cos^2\psi\cos^2\Omega\right)(V_{f_3})\right]-4\left[G_{f_3}\beta''_{\circ_3}-G_b\beta''_{-\circ}\right]\left(\frac{\cos^2\phi\cos^2\psi\cos^2\Omega}{\sin^4\phi}\right)(V_{f_3})\right]\right\}$$

103

$$+ \epsilon_1 \epsilon_3 \left\{ \frac{\nu_b E_b}{(1+\nu_b)(1-2\nu_b)} + \left[\frac{\nu_{f_1} E_{f_1} \beta_{o_1}}{(1+\nu_{f_1})(1-2\nu_{f_1})} - \frac{\nu_b E_b \beta_{-o}}{(1+\nu_b)(1-2\nu_b)} \right](\nu_{f_1}) \right.$$

$$+ \left[\frac{\nu_{f_2} E_{f_2} \beta_{o_2}}{(1+\nu_{f_2})(1-2\nu_{f_2})} - \frac{\nu_b E_b \beta_{-o}}{(1+\nu_b)(1-2\nu_b)} \right](\nu_{f_2}) + \left[\frac{\nu_{f_3} E_{f_3} \beta_{o_3}}{(1+\nu_{f_3})(1-2\nu_{f_3})} - \frac{\nu_b E_b \beta_{-o}}{(1+\nu_b)(1-2\nu_b)} \right](\nu_{f_3})$$

$$\quad\quad\quad\quad\quad\quad\quad\quad\quad\quad\quad\quad\quad\quad\quad\quad\quad (42) \text{ Conc.}$$

$$+ \left[\frac{E_{f_s}(1-\nu_{f_s})\beta_{o_s}}{(1+\nu_{f_s})(1-2\nu_{f_s})} - \frac{E_b(1-\nu_b)\beta_{-o}}{(1+\nu_b)(1-2\nu_b)} \right]\left[(2\cos^2\phi \cos^2\Omega)\right](\nu_{f_s})$$

$$+ \left[\frac{\nu_{f_s} E_{f_s} \beta_{o_s}}{(1+\nu_{f_s})(1-2\nu_{f_s})} - \frac{\nu_b E_b \beta_{-o}}{(1+\nu_b)(1-2\nu_b)} \right]\left[\left(\sin^2\phi \cos^2\Omega + \cos^2\psi + \cot^2\phi \left\{\cos^2\phi \cos^2\Omega + \cos^2\psi\right\}\right)\right](\nu_{f_s})$$

$$\left. - 4\left[G_{f_s}\beta'_{o_s} - G_b \beta'_{-o} \right]\left[(\cos^2\phi \cos^2\Omega)(\nu_{f_s})\right] \right\}$$

Differentiating successively with respect to ϵ_1, ϵ_2, and ϵ_3, and collecting the factors of each of these strains for each partial derivative yields the desired elastic constants, as follows:

$$\frac{\partial\left(\frac{V}{b_1 b_2 b_3}\right)}{\partial \epsilon_1} = \sigma_1$$

as before

$$\sigma_1 = A_1 \epsilon_1 + A_2 \epsilon_2 + A_3 \epsilon_3$$

104

and

$$A_1 = \frac{E_b(1-\nu_b)}{(1+\nu_b)(1-2\nu_b)} + \left[\frac{E_{f_1}(1-\nu_{f_1})}{(1+\nu_{f_1})(1-2\nu_{f_1})} - \frac{E_b(1-\nu_b)}{(1+\nu_b)(1-2\nu_b)}\right](V_{f_1})$$

$$+ \left[\frac{E_{f_2}(1-\nu_{f_2})\beta_{o_2}}{(1+\nu_{f_2})(1-2\nu_{f_2})} - \frac{E_b(1-\nu_b)\beta_{-o}}{(1+\nu_b)(1-2\nu_b)}\right](V_{f_2}) + \left[\frac{E_{f_3}(1-\nu_{f_3})\beta_{o_3}}{(1+\nu_{f_3})(1-2\nu_{f_3})} - \frac{E_b(1-\nu_b)\beta_{-o}}{(1+\nu_b)(1-2\nu_b)}\right](V_{f_3})$$

(43)

$$+ \left[\frac{E_{f_5}(1-\nu_{f_5})}{(1+\nu_{f_5})(1-2\nu_{f_5})}\right]\left\{\cos^4\phi + \beta_{o_5}\sin^4\phi + \left[\nu_{f_5}\beta_{o_5} + (1-2\nu_{f_5})\beta'_{o_5}\right]\left[\frac{2\sin^2\phi\cos^2\phi}{1-\nu_{f_5}}\right]\right\}(V_{f_5})$$

$$- \left[\frac{E_b(1-\nu_b)}{(1+\nu_b)(1-2\nu_b)}\right]\left\{\cos^4\phi + \beta_{-o}\sin^4\phi + \left[\nu_b\beta_{-o} + (1-2\nu_b)\beta'_{-o}\right]\left[\frac{2\sin^2\phi\cos^2\phi}{1-\nu_b}\right]\right\}(V_{f_5})$$

Similarly,

$$A_2 = \frac{\nu_b E_b}{(1+\nu_b)(1-2\nu_b)} + \left[\frac{\nu_{f_1} E_{f_1}\beta_{o_1}}{(1+\nu_{f_1})(1-2\nu_{f_1})} - \frac{\nu_b E_b\beta_{-o}}{(1+\nu_b)(1-2\nu_b)}\right](V_{f_1})$$

$$+ \left[\frac{\nu_{f_2} E_{f_2}\beta_{o_2}}{(1+\nu_{f_2})(1-2\nu_{f_2})} - \frac{\nu_b E_b\beta_{-o}}{(1+\nu_b)(1-2\nu_b)}\right](V_{f_2}) + \left[\frac{\nu_{f_3} E_{f_3}\beta_{o_3}}{(1+\nu_{f_3})(1-2\nu_{f_3})} - \frac{\nu_b E_b\beta_{-o}}{(1+\nu_b)(1-2\nu_b)}\right](V_{f_3})$$

(44)

$$+ \left[\frac{E_{f_5}(1-\nu_{f_5})}{(1+\nu_{f_5})(1-2\nu_{f_5})}\right]\left\{(1+\beta_{o_5})\cos^2\phi\cos^2\psi + \frac{\nu_{f_5}\beta_{o_5}}{1-\nu_{f_5}}\left[\sin^2\phi\cos^2\psi + \cos^2\Omega + \cot^2\psi(\cos^2\phi\cos^2\psi + \cos^2\Omega)\right] - (1-2\nu_{f_5})\beta'_{o_5}\left(\frac{2\cos^2\phi\cos^2\psi}{1-\nu_{f_5}}\right)\right\}(V_{f_5})$$

$$- \left[\frac{E_b(1-\nu_b)}{(1+\nu_b)(1-2\nu_b)}\right]\left\{(1+\beta_{-o})\cos^2\phi\cos^2\psi + \frac{\nu_b\beta_{-o}}{1-\nu_b}\left[\sin^2\phi\cos^2\psi + \cos^2\Omega + \cot^2\psi(\cos^2\phi\cos^2\psi + \cos^2\Omega)\right] - (1-2\nu_b)\beta'_{-o}\left(\frac{2\cos^2\phi\cos^2\psi}{1-\nu_b}\right)\right\}(V_{f_5})$$

· and

$$A_3 = \frac{\nu_b E_b}{(1+\nu_b)(1-2\nu_b)} + \left[\frac{\nu_{f_1}E_{f_1}\beta_{o_1}}{(1+\nu_{f_1})(1-2\nu_{f_1})} - \frac{\nu_b E_b \beta_{-o}}{(1+\nu_b)(1-2\nu_b)}\right](v_{f_1})$$

$$+ \left[\frac{\nu_{f_2}E_{f_2}\beta_{o_2}}{(1+\nu_{f_2})(1-2\nu_{f_2})} - \frac{\nu_b E_b \beta_{-o}}{(1+\nu_b)(1-2\nu_b)}\right](v_{f_2}) + \left[\frac{\nu_{f_3}E_{f_3}\beta_{o_3}}{(1+\nu_{f_3})(1-2\nu_{f_3})} - \frac{\nu_b E_b \beta_{-o}}{(1+\nu_b)(1-2\nu_b)}\right](v_{f_3}) \tag{45}$$

$$+ \left[\frac{E_{f_s}(1-\nu_{f_s})}{(1+\nu_{f_s})(1-2\nu_{f_s})}\right]\left\{(1+\beta_s)\cos^2\!\phi\cos^2\!\Omega + \frac{\nu_{f_s}\beta_{o_s}}{1-\nu_{f_s}}\left[\sin^2\!\phi\cos^2\!\Omega + \cos^2\!\phi + \cot^2\!\phi(\cos^2\!\phi\cos^2\!\Omega + \cos^2\!\phi)\right] - (1-2\nu_{f_s})\beta_s'\left(\frac{2\cos^2\!\phi\cos^2\!\Omega}{1-\nu_{f_s}}\right)\right\}(v_{f_s})$$

$$- \left[\frac{E_b(1-\nu_b)}{(1+\nu_b)(1-2\nu_b)}\right]\left\{(1+\beta_{-o})\cos^2\!\phi\cos^2\!\Omega + \frac{\nu_b\beta_{-o}}{1-\nu_b}\left[\sin^2\!\phi\cos^2\!\Omega + \cos^2\!\phi + \cot^2\!\phi(\cos^2\!\phi\cos^2\!\Omega + \cos^2\!\phi)\right] - (1-2\nu_b)\beta_{-o}'\left(\frac{2\cos^2\!\phi\cos^2\!\Omega}{1-\nu_b}\right)\right\}(v_{f_s})$$

$$A_4 = \frac{E_b(1-\nu_b)}{(1+\nu_b)(1-2\nu_b)} + \left[\frac{E_{f_1}(1-\nu_{f_1})\beta_{o_1}}{(1+\nu_{f_1})(1-2\nu_{f_1})} - \frac{E_b(1-\nu_b)\beta_{-o}}{(1+\nu_b)(1-2\nu_b)}\right](v_{f_1})$$

$$+ \left[\frac{E_{f_2}(1-\nu_{f_2})}{(1+\nu_{f_2})(1-2\nu_{f_2})} - \frac{E_b(1-\nu_b)}{(1+\nu_b)(1-2\nu_b)}\right](v_{f_2}) + \left[\frac{E_{f_3}(1-\nu_{f_3})\beta_{o_3}}{(1+\nu_{f_3})(1-2\nu_{f_3})} - \frac{E_b(1-\nu_b)\beta_{-o}}{(1+\nu_b)(1-2\nu_b)}\right](v_{f_3}) \tag{46}$$

$$+ \left[\frac{E_{f_s}(1-\nu_{f_s})}{(1+\nu_{f_s})(1-2\nu_{f_s})}\right]\left\{\cos^4\!\psi + \beta_s\left[\frac{\cos^4\!\phi\cos^4\!\psi + \cos^4\!\Omega}{\sin^4\!\phi}\right]\right.$$

$$\left. + \left[\nu_{f_s}\beta_{o_s}(\cot^2\!\phi)(\sin^4\!\phi\cos^4\!\psi + \cos^2\!\Omega) + 2(1-2\nu_{f_s})\left\{\beta_s'(\cos^2\!\phi\cos^2\!\psi + \cos^2\!\Omega) + \beta_s''(\cot^2\!\phi\cos^2\!\Omega)\right\}\right]\frac{\frac{\cos^2\!\psi}{\sin^4\!\phi}}{1-\nu_{f_s}}\right\}(v_{f_s})$$

$$- \left[\frac{E_b(1-\nu_b)}{(1+\nu_b)(1-2\nu_b)}\right]\left\{\cos^4\!\psi + \beta_{-o}\left[\frac{\cos^4\!\phi\cos^4\!\psi + \cos^4\!\Omega}{\sin^4\!\phi}\right]\right.$$

$$\left. + \left[\nu_b\beta_{-o}(\cot^2\!\phi)(\sin^4\!\phi\cos^4\!\psi + \cos^2\!\Omega) + 2(1-2\nu_b)\left\{\beta_{-o}'(\cos^2\!\phi\cos^2\!\psi + \cos^2\!\Omega) + \beta_{-o}''(\cot^2\!\phi\cos^2\!\Omega)\right\}\right]\frac{\frac{\cos^2\!\psi}{\sin^4\!\phi}}{1-\nu_b}\right\}(v_{f_s})$$

106

$$A_5 = \frac{\nu_b E_b}{(1+\nu_b)(1-2\nu_b)} + \left[\frac{\nu_{f_1} E_{f_1}\beta_{o_1}}{(1+\nu_{f_1})(1-2\nu_{f_1})} - \frac{\nu_b E_b \beta_{-o}}{(1+\nu_b)(1-2\nu_b)}\right](V_{f_1}) \tag{47}$$

$$+ \left[\frac{\nu_{f_2} E_{f_2}\beta_{o_2}}{(1+\nu_{f_2})(1-2\nu_{f_2})} - \frac{\nu_b E_b \beta_{-o}}{(1+\nu_b)(1-2\nu_b)}\right](V_{f_2}) + \left[\frac{\nu_{f_3} E_{f_3}}{(1+\nu_{f_3})(1-2\nu_{f_3})} - \frac{\nu_b E_b}{(1+\nu_b)(1-2\nu_b)}\right](V_{f_3})$$

$$+ \left[\frac{E_{f_3}(1-\nu_{f_3})}{(1+\nu_{f_3})(1-2\nu_{f_3})}\right]\left\{(1+\beta_{o_3})\sin^2\phi + \frac{\nu_{f_3}\beta_{o_3}}{1-\nu_{f_3}}\left(\frac{\sin^2\phi\cos^2\psi+\cos^2\psi+\cos^2\Omega}{\sin^2\phi\cos^2\psi\cos^2\Omega}\right) - \frac{2(1+\nu_{f_3})}{1-\nu_{f_3}}\left(\beta'_{o_3}\sin^2\psi + \beta''_{o_3}\cot^2\psi\right)\left[\frac{\cos^2\psi\cos^2\Omega}{\sin^2\phi}\right]\right\}(V_{f_3})$$

$$- \left[\frac{E_b(1-\nu_b)}{(1+\nu_b)(1-2\nu_b)}\right]\left\{(1+\beta_{-o})\sin^2\phi + \frac{\nu_b\beta_{-o}}{1-\nu_b}\left(\frac{\sin^2\phi\cos^2\psi+\cos^2\psi+\cos^2\Omega}{\sin^2\phi\cos^2\psi\cos^2\Omega}\right) - \frac{2(1-2\nu_b)}{1-\nu_b}\left(\beta'_{-o}\sin^2\psi + \beta''_{-o}\cot^2\psi\right)\left[\frac{\cos^2\psi\cos^2\Omega}{\sin^2\phi}\right]\right\}(V_{f_3})$$

$$A_6 = \frac{E_b(1-\nu_b)}{(1+\nu_b)(1-2\nu_b)} + \left[\frac{E_{f_1}(1-\nu_{f_1})\beta_{o_1}}{(1+\nu_{f_1})(1-2\nu_{f_1})} - \frac{E_b(1-\nu_b)\beta_{-o}}{(1+\nu_b)(1-2\nu_b)}\right](V_{f_1}) \tag{48}$$

$$+ \left[\frac{E_{f_2}(1-\nu_{f_2})\beta_{o_2}}{(1+\nu_{f_2})(1-2\nu_{f_2})} - \frac{E_b(1-\nu_b)\beta_{-o}}{(1+\nu_b)(1-2\nu_b)}\right](V_{f_2}) + \left[\frac{E_{f_3}(1-\nu_{f_3})}{(1+\nu_{f_3})(1-2\nu_{f_3})} - \frac{E_b(1-\nu_b)}{(1+\nu_b)(1-2\nu_b)}\right](V_{f_3})$$

$$+ \left[\frac{E_{f_3}(1-\nu_{f_3})}{(1+\nu_{f_3})(1-2\nu_{f_3})}\right]\left\{\cos^4\Omega + \beta_{o_3}\left[\frac{\cos^4\phi\cos^2\Omega+\cos^4\psi}{\sin^4\phi}\right]\right.$$

$$\left. + \left[\nu_{f_3}\beta_{o_3}(\cot^2\psi)(\sin^4\phi\cos^2\Omega+\cos^4\psi) + 2(1-2\nu_{f_3})\left(\beta'_{3}(\cos^4\phi\cos^2\Omega+\cos^4\psi) + \beta''_{3}(\cot^4\phi\cos^4\psi)\right)\right]\frac{\cos^2\Omega}{\sin^4\phi}}{1-\nu_{f_3}}\right\}(V_{f_3})$$

$$- \left[\frac{E_b(1-\nu_b)}{(1+\nu_b)(1-2\nu_b)}\right]\left\{\cos^4\Omega + \beta_{-o}\left[\frac{\cos^4\phi\cos^4\Omega+\cos^4\psi}{\sin^4\phi}\right]\right.$$

$$\left. + \left[\nu_b\beta_{-o}(\cot^2\psi)(\sin^4\phi\cos^2\Omega+\cos^4\psi) + 2(1-2\nu_b)\left(\beta'_{-o}(\cos^4\phi\cos^2\Omega+\cos^4\psi) + \beta''_{-o}(\cot^4\phi\cos^4\psi)\right)\right]\frac{\cos^2\Omega}{\sin^2\phi}}{1-\nu_b}\right\}(V_{f_3})$$

The elastic constants for shearing are found in a similar fashion to those for stretching. Shears γ_{12}, γ_{23}, and γ_{13} are imposed and the strain energy is evaluated as

$$
V' = \frac{1}{2} \int_0^{b_1}\int_0^{b_2}\int_0^{b_3} G_b \left(\gamma_{12}^2 + \gamma_{23}^2 + \gamma_{13}^2 \right) d(n)
$$

$$
+ \frac{1}{2} \int_0^{b_n} \left[G_{f_n}\beta_{\bullet n}' - G_b \beta_{\bullet \bullet}' \right]\left[\gamma_{f_{n_{LT_1}}}^2 + \gamma_{f_{n_{LT_2}}}^2 \right]\left[V_{f_n} \right] d(n)
$$

$$
+ \frac{1}{2} \int_0^{b_n} \left[G_{f_n}\beta_{\bullet n}'' - G_b \beta_{\bullet \bullet}'' \right]\left[\gamma_{f_{n_{T_1 T_2}}}^2 \right]\left[V_{f_n} \right] d(n)
$$

$$
+ \frac{1}{2} \int_0^{b_s} \left[G_{f_s}\beta_{\bullet s}' - G_b \beta_{\bullet \bullet}'' \right]\left[\gamma_{f_{s_{LT_1}}}^2 + \gamma_{f_{s_{LT_2}}}^2 \right]\left[V_{f_s} \right] d(s) \qquad (49)
$$

$$
+ \frac{1}{2} \int_0^{b_s} \left[G_{f_s}\beta_{\bullet s}'' - G_b \beta_{\bullet \bullet}'' \right]\left[\gamma_{f_{s_{T_1 T_2}}}^2 \right]\left[V_{f_s} \right] d(s)
$$

$$
+ \frac{1}{2} \int_0^{b_s} \left[\frac{E_{f_s}(1-\nu_{f_s})}{(1+\nu_{f_s})(1-2\nu_{f_s})} - \frac{E_b(1-\nu_b)}{(1+\nu_b)(1-2\nu_b)} \right]\left[\epsilon_{f_{s_L}}^2 \right]\left[V_{f_s} \right] d(s)
$$

$$
+ \frac{1}{2} \int_0^{b_s} \left[\frac{E_{f_s}(1-\nu_{f_s})\beta_{\bullet s}}{(1+\nu_{f_s})(1-2\nu_{f_s})} - \frac{E_f(1-\nu_b)\beta_{\bullet \bullet}}{(1+\nu_b)(1-2\nu_b)} \right]\left[\epsilon_{f_{s_{T_1}}}^2 + \epsilon_{f_{s_{T_2}}}^2 \right]\left[V_{f_s} \right] d(s)
$$

$$
+ \frac{1}{2} \int_0^{b_s} \left[\frac{\nu_{f_s} E_{f_s}\beta_{\bullet s}}{(1+\nu_{f_s})(1-2\nu_{f_s})} - \frac{\nu_b E_b \beta_{\bullet \bullet}}{(1+\nu_b)(1-2\nu_b)} \right]\left[2\left(\epsilon_{f_{s_L}}\epsilon_{f_{s_{T_1}}} + \epsilon_{f_{s_{T_1}}}\epsilon_{f_{s_{T_2}}} + \epsilon_{f_{s_L}}\epsilon_{f_{s_{T_2}}} \right) \right]\left[V_{f_s} \right] d(s)
$$

In (49) n = 1, 2, 3; and

$$\gamma_{f_{S_{\perp T_1}}} = \gamma_{12}\left[\frac{\cos\psi}{\sin\phi}\left(\cos^2\phi - \sin^2\phi\right)\right]$$

$$+ \gamma_{23}\left[\frac{2\cos\phi\cos\psi\cos\Omega}{\sin\phi}\right] \tag{50}$$

$$+ \gamma_{13}\left[\frac{\cos\Omega}{\sin\phi}\left(\cos^2\psi - \sin^2\phi\right)\right]$$

$$\gamma_{f_{S_{\perp T_2}}} = \gamma_{12}\left[\frac{\cos\phi\cos\Omega}{\sin\phi}\right] + \gamma_{23}\left[\frac{\cos^2\psi - \cos^2\Omega}{\sin\phi}\right] + \gamma_{13}\left[\frac{\cos\phi\cos\psi}{\sin\phi}\right] \tag{51}$$

$$\gamma_{f_{S_{T_1 T_2}}} = -\gamma_{12}\cos\Omega + \gamma_{23}\left[\frac{\cos\phi\left(\cos^2 x - \cos^2\Omega\right)}{\sin^2\phi}\right] - \gamma_{13}\cos\psi \tag{52}$$

$$\epsilon_{f_{S_L}} = \pm\gamma_{12}\cos\phi\cos\psi \pm \gamma_{23}\cos\psi\cos\Omega \pm \gamma_{13}\cos\phi\cos\Omega \tag{53}$$

$$\epsilon_{f_{S_{T_1}}} = \mp\gamma_{12}\cos\phi\cos\psi \pm \gamma_{23}\cot^2\phi\cos\psi\cos\Omega \mp \gamma_{13}\cos\phi\cos\Omega \tag{54}$$

$$\epsilon_{f_{S_{T_2}}} = \pm\gamma_{23}\left[\frac{\cos\psi\cos\Omega}{\sin^2\phi}\right] \tag{55}$$

Substituting (50) - (55) in (49), carrying out the integrations

and differentiations, etc. yields

$$A_7 = G_b + \left[G_{f_1}\beta_{\cdot_1}' - G_b\beta_{\cdot_\bullet}'\right](v_{f_1}) + \left[G_{f_2}\beta_{\cdot_2}' - G_b\beta_{\cdot_\bullet}'\right](v_{f_2}) + \left[G_{f_3}\beta_{\cdot_3}'' - G_b\beta_{\cdot_\bullet}''\right](v_{f_3}) \tag{56}$$

$$+ \left[\frac{E_{f_s}(1-v_{f_s})}{(1+v_{f_s})(1-2v_{f_s})}\right]\left\{\left[1+\left(\frac{1-3v_{f_s}}{1-v_{f_s}}\right)\beta_{\cdot_s}\right]\left[\cos^2\psi\cos^2\psi\right] + \left[\frac{1-2v_{f_s}}{2(1-v_{f_s})}\right]\left[\beta_{\cdot_s}'\left(\frac{\cos^2\psi\cos^2 2\phi + \cos^2\phi\cos^2\Omega}{\sin^2\psi}\right)+\beta_3''\cos^2\Omega\right]\right\}(v_{f_s})$$

$$- \left[\frac{E_b(1-v_b)}{(1+v_b)(1-2v_b)}\right]\left\{\left[1+\left(\frac{1-3v_b}{1-v_b}\right)\beta_{\cdot_\bullet}\right]\left[\cos^2\psi\cos^2\psi\right] + \left[\frac{1-2v_b}{2(1-v_b)}\right]\left[\beta_{\cdot_\bullet}'\left(\frac{\cos^2\psi\cos^2 2\phi + \cos^2\phi\cos^2\Omega}{\sin^2\psi}\right)+\beta_{\cdot_\bullet}''\cos^2\Omega\right]\right\}(v_{f_s})$$

$$A_8 = G_b + \left[G_{f_1}\beta_{\cdot_1}'' - G_b\beta_{\cdot_\bullet}''\right](v_{f_1}) + \left[G_{f_2}\beta_{\cdot_2}' - G_b\beta_{\cdot_\bullet}'\right](v_{f_2}) + \left[G_{f_3}\beta_{\cdot_3}' - G_b\beta_{\cdot_\bullet}'\right](v_{f_3}) \tag{57}$$

$$+ \left[\frac{E_{f_s}(1-v_{f_s})}{(1+v_{f_s})(1-2v_{f_s})}\right]\left\{\left[1+\left(1+\frac{2v_{f_s}}{1-v_{f_s}}\{\cos^2\psi+\csc^2\psi\}\right)\beta_{\cdot_s}\right]\left[\cos^2\psi\cos^2\Omega\right]\right.$$

$$\left. + \left[\frac{1-2v_{f_s}}{2(1-v_{f_s})}\right]\left[\beta_{\cdot_s}'\left(\cot^2\phi\cos^2\psi\cos^2\Omega+\frac{\{\cos^2\psi-\cos^2\Omega\}^2}{\sin^2\psi}\right)+\beta_3''\cot^2\phi\left(\frac{\{\cos^2\psi-\cos^2\Omega\}^2}{\sin^2\psi}\right)\right]\right\}(v_{f_s})$$

$$- \left[\frac{E_b(1-v_b)}{(1+v_b)(1-2v_b)}\right]\left\{\left[1+\left(1+\frac{2v_b}{1-v_b}\{\cos^2\psi+\csc^2\psi\}\right)\beta_{\cdot_\bullet}\right]\left[\cos^2\psi\cos^2\Omega\right]\right.$$

$$\left. + \left[\frac{1-2v_b}{2(1-v_b)}\right]\left[\beta_{\cdot_\bullet}'\left(\cot^2\phi\cos^2\psi\cos^2\Omega+\frac{\{\cos^2\psi-\cos^2\Omega\}^2}{\sin^2\psi}\right)+\beta_{\cdot_\bullet}''\cot^2\phi\left(\frac{\{\cos^2\psi-\cos^2\Omega\}^2}{\sin^2\psi}\right)\right]\right\}(v_{f_s})$$

$$A_9 = G_b + \left[G_{f_1}\beta_{\cdot_1}' - G_b\beta_{\cdot_\bullet}'\right](v_{f_1}) + \left[G_{f_2}\beta_{\cdot_2}'' - G_b\beta_{\cdot_\bullet}''\right](v_{f_2}) + \left[G_{f_3}\beta_{\cdot_3}' - G_b\beta_{\cdot_\bullet}'\right](v_{f_3})$$

$$+ \left[\frac{E_{f_s}(1-v_{f_s})}{(1+v_{f_s})(1-2v_{f_s})}\right]\left\{\left[1+\left(\frac{1-3v_{f_s}}{1-v_{f_s}}\right)\beta_{\cdot_s}\right]\left[\cos^2\psi\cos^2\Omega\right] + \left[\frac{1-2v_{f_s}}{2(1-v_{f_s})}\right]\left[\beta_{\cdot_s}'\left(\frac{\cos^2\Omega\cos^2 2\phi+\cos^2\phi\cos^2\psi}{\sin^2\psi}\right)+\beta_{\cdot_s}''\cos^2\psi\right]\right\}(v_{f_s}) \tag{58}$$

$$- \left[\frac{E_b(1-v_b)}{(1+v_b)(1-2v_b)}\right]\left\{\left[1+\left(\frac{1-3v_b}{1-v_b}\right)\beta_{\cdot_\bullet}\right]\left[\cos^2\psi\cos^2\Omega\right] + \left[\frac{1-2v_b}{2(1-v_b)}\right]\left[\beta_{\cdot_\bullet}'\left(\frac{\cos^2\Omega\cos^2 2\phi+\cos^2\phi\cos^2\psi}{\sin^2\psi}\right)+\beta_{\cdot_\bullet}''\cos^2\psi\right]\right\}(v_{f_s})$$

Evaluation of β's - Equations relating the stiffnesses of uni-directionally reinforced composites to the effectiveness coefficients β, β', and β'' may be readily derived as special cases of the general equations developed in the preceding section. For the three-dimensional case, with the Poisson's ratio of the filaments ν_f not equal to those of the binder, these equations are:

$$(1-\beta_\bullet V_f) = \frac{1}{4}\left\{\left[\left(\frac{1-\nu_b}{\nu_b^2}\right)V_b + \left(1+\nu_b\right)\frac{E_{T_o}}{E_b}\right] - \sqrt{\left[\left(\frac{1-\nu_b}{\nu_b^2}\right)V_b + \left(1+\nu_b\right)\frac{E_{T_o}}{E_b}\right]^2 - 8\left(\frac{1-\nu_b}{\nu_b}\right)\left(V_b\right)\left(1+\nu_b\right)\frac{E_{T_o}}{E_b}}\right\} \qquad (59)$$

$$(\beta_\bullet V_f)^3 + \left\{(T+2T')(1-\beta_\bullet V_f) - \frac{1}{2}\left(\frac{1-\nu_f}{\nu_f}\right)V - \left(\frac{1+\nu_f}{2}\right)\frac{E_{T_o}}{E_f}\right\}(\beta_\bullet V_f)^2$$

$$+\left\{(T+2T)T'(1-\beta_\bullet V_f)^2 - \frac{1}{2}\left(\frac{1-\nu_f}{\nu_f}\right)V\left[T'+\frac{T}{\nu_f}+\left(\frac{1-\nu_f}{\nu_f}\right)T''\right](1-\beta_\bullet V_f)\right.$$

$$\left.+\left(\frac{1+\nu_f}{2}\right)\frac{E_{T_o}}{E_f}\left[\left(\frac{1-\nu_f}{\nu_f}\right)^2 V - 2T'(1-\beta_\bullet V_f)\right]\right\}(\beta_\bullet V_f) \qquad (60)$$

$$+\left\{(T')^2(1-\beta_\bullet V_f) - \frac{1}{2}\left(\frac{1-\nu_f}{\nu_f}\right)V\left[T'+\left(\frac{1-\nu_f}{\nu_f}\right)T''\right]\right\}T(1-\beta_\bullet V_f)^2$$

$$+\left\{\left(\frac{1+\nu_f}{2}\right)\frac{E_{T_o}}{E_f}\left[\left(\frac{1-\nu_f}{\nu_f}\right)^2 T''V - (T')^2(1-\beta_\bullet V_f)\right]\right\}(1-\beta_\bullet V_f) = 0$$

$$\left(1 - \beta_\bullet' V_f\right) = \frac{G_{12_\bullet}}{G_b} \tag{61}$$

$$\beta_\bullet' V_f = \frac{G_{12_\bullet}}{G_f} - \frac{G_b}{G_f}\left(1 - \beta_\bullet' V_f\right) \tag{62}$$

$$= \frac{G_{12_\bullet}}{G_f} - \frac{G_{12_0}}{G_f}$$

$$\left(1 - \beta_\bullet'' V_f\right) = \frac{G_{23_\bullet}}{G_b} \tag{63}$$

$$\beta_\bullet'' V_f = \frac{G_{23_\bullet}}{G_f} - \frac{G_{23_0}}{G_f} \tag{64}$$

where

$$T = \frac{\dfrac{E_b}{1 + \nu_b}}{\dfrac{E_f}{1 + \nu_f}} \tag{65}$$

$$T' = \frac{\dfrac{\nu_b E_b}{(1 + \nu_b)(1 - 2\nu_b)}}{\dfrac{\nu_f E_f}{(1 + \nu_f)(1 - 2\nu_f)}} \tag{66}$$

$$T'' = \frac{\dfrac{E_b(1 - \nu_b)}{(1 + \nu_b)(1 - 2\nu_b)}}{\dfrac{E_f(1 - \nu_f)}{(1 + \nu_f)(1 - 2\nu_f)}} \tag{67}$$

$$V = T'' \nu_b + \nu_f \tag{68}$$

V_f = volume fraction of filaments

v_f = Poisson's ratio of filaments

G_{12_0} = shear stiffness of binder having uni-directional round holes, in the plane of the holes

G_{23_0} = shear stiffness of binder having uni-directional round holes, transverse to the holes

Other symbols as before.

In essence equations (59) - (64) define factors (β) for transverse effectiveness for use in multi-directional reinforcement patterns - in terms of unidirectional reinforcement. Accordingly, any available data on the transverse effectiveness of unidirectional filamentary reinforcement may be employed via these equations, and those of the preceding section for multi-directional configurations.

In order to obtain values of the β's for use in the present evaluations of approaches to improvements in properties, the upper bounds of the elastic constant analysis of Reference 6 were used to yield values of β. Typical results are plotted in Figure 33.

From Equations (59)-(64) above the related equations of Ref. 6, and in Figure 33 the following characteristics of the β's are evident:

113

(1) The values of $\beta_{-\bullet}$, $\beta'_{-\bullet}$, and $\beta''_{-\bullet}$ are independent of the filament properties; $\beta'_{-\bullet}$ depends only upon V_b, and $\beta_{-\bullet}$ and $\beta''_{-\bullet}$ depend upon V_b and v_b.

(2) Values of $\beta_\bullet$, $\beta'_\bullet$, and $\beta''_\bullet$ are not greatly different one from another (c.f. Ref. 44 in which β' was suggested to be approximately $8/7\beta$). That is, the transverse effectivenesses as represented by the β-values are slightly - but not substantially - different for stretching and shearing.

Values of β's calculated using the upper bounds of Reference 6 will be employed in the following section to measure the merits of various reinforcement configurations.

Evaluations of Various Reinforcement Configurations

In order to illustrate the application of the equations derived in the fore-
going sections to specific configurations of fibrous reinforcement, a number
of examples will be evaluated, as follows:

(1) Elastic constant for uni-directional and for simple 2-dimensional
reinforcement configurations will be computed by the three-
dimensional analysis and compared with previous "laminate"
analyses to indicate the accuracy obtainable.

(2) Uni-directional triangular cross-section filaments will be
considered.

(3) Orthogonal elliptical filaments aligned in the 1- and 2- directions
and having all the minor axes of the elliptical cross-sections in
the 3-direction will be evaluated.

(4) Three-dimensional reinforcement patterns will be evaluated.

The equations for the elastic constants for these four cases are given in
Tables 6 - 13.

Two-Dimensional Uni-Directional Reinforcement - The initial application
of the equations derived in the previous section that will be reported covers
two-dimensional reinforcement in various configurations, for comparisons
with previous results obtained for quasi-homogeneous laminate constructions.
First simple, uni-directional reinforcement will be considered to show the
magnitudes of possible differences from other methods of calculation intro-
duced by the approximations associated with the transverse β-factors of the

present analysis. Also possible improvements associated with refined transverse factors will be discussed. Second, reinforcements at angles of $\pm\theta$ degrees to the 1-direction, orthogonal filaments in the 1- and 2-directions, and the 2-dimensionally-isotropic $(\pm30^\circ, 90^\circ)$ delta reinforcement pattern will be evaluated and compared to previous calculations. The reduced elastic constant equations derived from the general equations - that apply to these four reinforcement patterns are given in Tables 6 - 9.

For uni-directional reinforcement the present analysis naturally forces agreement in calculated elastic constants with other analyses for those constants which are direct functions of the β-values if the β-values themselves are based on the other analyses. Thus values of E_2, E_3, G_{12}, G_{23}, and G_{13} found from the equations of Table 1 must agree with the corresponding values from whatever source was used to determine the β's. Values of the stiffness along the reinforcement direction E_1, and of the three Poisson's ratios ν_{21}, ν_{32}, and ν_{31}, however, do not follow this forced correspondence. Generally the values of E_1 calculated from Table 1 are higher than from other approaches (or the rule of mixtures), and the Poisson's ratio values are lower. Typical differences are plotted in Figure 34.

That E_1 for uni-directional filaments in the 1-direction should correspond to the "rule-of-mixtures" value (see Fig. 34) has been generally accepted and indeed such correspondence appears conceptually satisfactory. The physical

concept of a "rule-of-mixtures" applying to the Poisson's ratio ν_{21},
however, is perhaps not as satisfying, nor is it supported by other
analyses. The fact that the Hashin-Rosen values on the Figure are so
close to the "rule-of-mixtures" line, for example, is just a coincidence
for this particular combination of constituents; for epoxy filaments in
glass binder, the corresponding Hashin-Rosen curve for ν_{21} is essentially
identical to that plotted for $\beta = \beta$ upper bound. In any event, the major
discrepancy appears in the calculation of E_1 via the present analysis
(circa 10% maximum difference between the calculation and the "rule-of-
mixtures" value for uni-directional reinforcement; as will be shown, for
all other reinforcement patterns the present analysis is in closer agree-
ment with accepted calculations for E_1 as well as the other stiffnesses).

Refined Equations for Uni-directional Reinforcement. - A likely source
of the above discrepancy is the use of a single value of β to apply to the
transverse effectiveness for strains introduced by Poisson's ratio effects,
as noted in the section describing the derivation of the equations for elas-
tic constants. A more refined analysis could be developed, for example,
which would result in equations of the nature given in Table 14 for uni-
directional reinforcement. The evaluation of the additional parameters
in a set of equations like those in Table 14 can be made through the imposi-
tion of additional conditions to be simultaneously satisfied, such as, that

$$A_5 = A_1 - 2A_8 \qquad (69)$$

(because of the transverse isotropy of uni-directional reinforcement)

and that

$$E_1 = E_f v_f + E_b (1 - v_f) \tag{70}$$

or by the direct evaluation of A_1, A_2, etc. in terms of the Hashin-Rosen

constants as by the equations of Table 15.

For most purposes refined equations of the nature of those in Table 14

do not appear justified. As will be shown the accuracy of the simpler

equations developed here should be adequate for most reinforcement pat-

terns, as judged by the following comparisons with available, 2-dimensional

laminate analyses.

<u>Two-Dimensional, Multi-Directional Reinforcement</u> - If the rein-
forcing filaments are disposed at right angles to each other but still
essentially in a single plane, two possible approaches suggest themselves
for the calculation of the elastic constants using the equations in Table 7.
In the first approach the β-values corresponding to the total volume con-
centration of filaments is used, as if the filaments were packed in individual,
uni-directionally reinforced laminae each of which had the volume fraction
packing of the laminate as a whole. In the second approach the β-values for
the lesser volume fractions corresponding to the fraction of filaments in
each direction are used, as if the filaments were truly mixed in a given
plane. Thus two slightly different results are obtainable for the elastic
constants, as shown in Figure 35.

As shown in Figure 35 the values of E_1 calculated by the present analysis
are slightly greater than those found from conventional laminate analysis.
The differences are less than for the uni-directional case, decreasing from
the maximum discrepancy at 0% filaments in the 2-direction to zero difference
at 100% transverse reinforcement. (The case chosen for comparison - that
is, 50% volume fraction with very different filament and binder materials, was
specifically selected to bring out the differences in results associated with the
β-value approximations. For filaments having Poisson's ratios and stiffnesses
less different from those of the binder than this example, and for higher volume
fractions of reinforcement, the present analyses may be expected to correspond

more closely to laminate analyses.)

For reinforcements running in one plane at angles of $\pm\theta$ to the 1-direction the correspondence between the present and laminate analyses is similar to that for orthogonal filaments. Thus as shown in Figure 36 the results of present and past analyses rapidly approach each other as θ diverges from zero degrees.

One more comparison will be made of two-dimensional calculations before passing to the investigations of three-dimensional effects that the new analysis facilitates. This last comparison (Figure 37) shows values of E_1 for the $\pm 30^\circ$ & 90° configuration that provides in-plane isotropy. Agreement between laminate and present analysis is shown generally satisfactory. An additional comforting result not shown on the figure, or obvious from the pertinent equations (Table 9), is that, as it should, for the present analysis of this configuration

$$G_{12} = \frac{E_1}{2(1 + \nu_{21})} \tag{71}$$

at least to four decimal places.

Triangular Filaments - As a first application of the three-dimensional analysis to the evaluation of reinforcements which affect the stiffnesses in all directions, let us consider filaments having an equilateral-triangle cross-section. This shape is of especial interest because, with ideal packing it permits straight-line binder elements among the filaments (Figure 38).

120

In the limit, the configuration shown in Figure 38 is akin to those

for which the waffle-type analysis was originated. That is, the material

between the triangular filaments is effective along the straight-line elements

as well as transverse to them; the components of stiffnesses both along and

transverse to each binder element thus contribute to the overall stiffness,

as described by the equations of Table 10

The ratio of transverse stiffnesses produced by straight-line continuous

binder elements of Figure 38(as represented by the equations of Table 10) to

the transverse stiffnesses of the usual discontinuous binder are plotted in

Figure 38 as representing triangular glass filaments in epoxy. More precisely,

the transverse stiffnesses of the two models shown in Figure 38 are those com-

pared in Figure 39. That is the stiffness of a composite of epoxy filaments

oriented in a delta configuration in a glass matrix is compared with that of

a dispersion of rounds transverse to the direction in which the stiffness is

calculated. The stiffness of the oriented epoxy filaments was evaluated via

the equations of Table 6 with β-values corresponding to the random-array

upper bounds of Ref. 6. The transverse stiffness of the dispersed rounds

was found directly as the random-array upper bounds of Ref. 6. Accordingly

the difference in stiffness between the two models is just that arising along

the oriented, straight-line elements found among the equilateral triangles.

Although the gains in transverse stiffness for the triangular filaments

shown in Figure 39 are only 20-25% in the volume fraction range of greatest

interest ($V_b \approx 0.33$), two factors tend to multiply the importance of this improvement. First the gain is bi-directional - i.e. if the triangular filaments are oriented in the 1-direction both E_2 and E_3 are equally enhanced. Second, the fact that the percent gain is greater at the higher volume fractions of binder suggest that as the binder properties become more significant (hence for better binders than epoxy) the improvement may be more significant. The value of enhancement of E_3 as well as E_2 will be discussed further in other sections of this report.

Elliptical Filaments - It was first shown in Ref. 2 and has been now thoroughly confirmed by the data herein that elliptical filaments can substantially increase the transverse properties in the direction of the ellipse major axis. In order to determine just how valuable such an increase is, however, a quantitative study is required of various approaches which are capable of affecting the same increase. Accordingly, the waffle-type analysis is here applied to the evaluation of elliptical filaments.

As a first example, let us compare the properties of round and elliptical-filament reinforced composites having comparable amounts of orthogonal reinforcement to provide biaxial stiffness. The comparison is made in Figure 40.

In Figure 40 the stretching stiffness in the 1-direction (E_1) is plotted against the percentage of reinforcement oriented transversely. In all cases the total amount of reinforcement (i.e. the sum of the reinforcements in the two directions) is held constant at 50% by volume of the composite. The values plotted were calculated from the equations of Table 11 and 7 for

$$E_f = 72.45 \text{ GN/m}^2$$
$$(10,500,000 \text{ psi,}) \quad \nu_f = 0.2$$
$$E_b = 3.45 \text{ GN/m}^2$$
$$(500,000 \text{ psi,}) \quad \nu_b = 0.35$$

that is for properties representative of E-glass filaments in epoxy binder.

Two curves are given for both the round and elliptical filaments, representing the two possible β -values as discussed for Figure 35. Differences between the upper and lower curves are small, as can be seen. The β -values for the round filaments are those plotted in Figure 33. Those for the ellipses were calculated to make $E_1 = 2E_1$ for 100% of the reinforcement in the 2-direction as appropriate for 4 to 1 aspect ratio ellipses at 50 volume percent reinforcement.

With the curves of Figure 40, it is possible to compare directly the relative effectiveness of the rounds and the ellipses for providing a given transverse stiffness. For example, suppose that transverse stiffnesses ranging upward from that for the uni-directional ellipses is to be obtained by the orthogonal rounds. To achieve these stiffnesses some of the longitudinal (1-direction) round filaments must be oriented in the 2-direction;

the stiffness in the 1-direction is thus reduced, and the reduction is substantial, - as shown by the "equivalent rounds" curve on Figure 40.

Each point on the "equivalent rounds" curve of Figure 40 has the same transverse (2-direction) stiffness as the elliptical filaments at the same value of the abscissa. Thus, for example, with 20% transverse reinforcement the ellipses provide an E_1 of 35.2 GN/m^2 approximately, whereas the equivalent rounds (i.e. the rounds giving the same E_2 (= 23.5 GN/m^2) as this configuration of ellipses) would provide only the E_1 given by the "equiv" curve at this abscissa (20%) or 26.9 GN/m^2.

While comparisons like those of Figure 40 suggest that, for glass-reinforced epoxy, -if the application requires transverse stiffness of one-half or more of the axial stiffness, -shaped filaments like 4 to 1 ellipses may provide substantial structural improvement. If advanced filaments like boron are considered, however, a different result is obtained.

In Figure 41, the curves of Figure 40 are replotted for boron instead of glass reinforcement. With the high ratio of longitudinal to transverse stiffness provided by the boron, the factor 2 improvement associated with the elliptical geometry for unidirectional reinforcement is nearly as readily attained with a few transverse round filaments. Hence, the "equivalent round" curve is only slightly below the curve for the ellipses.

A similar result is obtainable for changes in binder properties. Thus

124

the use of a hypothetical filled binder (properties like those of the alumina-filled epoxy of Reference 2 were used for calculation) can raise the overall stiffness level (i. e. the longitudinal as well as the transverse stiffnesses) of a glass-reinforced plastic as shown in Figure 42. Thus the binder improvement is more effective than the filamentary ellipses, for example, for they enhance only the transverse properties. If, however, the reinforcement were boron, the improvement arising from the stiffer binder would be a much smaller percentage of the overall stiffnesses. With boron, then, once again transverse stiffness properties could be attained nearly as readily with a few transverse filaments as with a binder twice as stiff as epoxy.

Reviewing the implications of Figures 40 to 42 one concludes that the merit of the elliptical shape depends on the associated conditions. It is perhaps most valuable when the ratio of E_f/E_b is not extreme - as extreme as boron in epoxy, for example.

An interesting future possibility might be a diamond-shaped filament (with slightly rounded corners) which could combine most of the attractive features of the equilateral triangles with those of the ellipse.

<u>Three-Dimensional Reinforcement</u> - Equations for the elastic constants for composites having reinforcing filaments in three orthogonal directions and filaments making equal angles ($\pm \theta$) to each of three orthogonal directions

are given in Tables 12 and 13 respectively.

The use of three-dimensional reinforcement raises new questions about the relative desirability of various reinforcement configurations. Most of these questions have not yet been answered. Hence, here we shall only indicate some of the problem areas to which equations like those of Tables 12 and 13 provide access.

(1) What is the proper balance for optimum reinforcement in the various directions? Strength criteria (Ref. 11) suggest the desirability of three-directional reinforcement, but any sacrifice in filaments in one direction to provide filaments for another direction produces a compound loss of properties in the first direction. For example, consider the following three glass filament-reinforced epoxy composites:

(a) 60 volume percent filaments in the 1-direction

(b) 50 volume percent filaments in the 1-direction,
10 volume percent filaments in the 2-direction

(c) 40 volume percent filaments in the 1-direction
10 volume percent filaments in the 2-direction
10 volume percent filaments in the 3-direction

Elastic constants for these configurations are

$$E_1 = 48.8 \ {}^{GN}\!/_{m^2} \qquad E_2 = 13.4 \ {}^{GN}\!/_{m^2} \qquad E_3 = 13.4 \ {}^{GN}\!/m^2.$$

(7,070,000 psi)   (1,940,000 psi)   (1,940,000 psi)

(a)

$$G_{12} = 4.42 \ {}^{GN}\!/_{m^2} \qquad G_{23} = 5.01 \ {}^{GN}\!/_{m^2} \qquad G_{13} = 4.42 \ {}^{GN}\!/_{m^2}$$

(640,000 psi)   (726,000 psi)   (640,000 psi)

$$E_1 = 42.2 \ {}^{GN}\!/_{m^2} \qquad E_2 = 18.1 \ {}^{GN}\!/_{m^2} \qquad E_3 = 11.2 \ {}^{GN}\!/_{m^2}$$

(6,120,000 psi)   (2,630,000 psi)   (1,620,000 psi)

(b)

$$G_{12} = 3.71 \ {}^{GN}\!/_{m^2} \qquad G_{23} = 4.08 \ {}^{GN}\!/_{m^2} \qquad G_{13} = 3.68 \ {}^{GN}\!/_{m^2}$$

(537,000 psi)   (592,000 psi)   (534,000 psi)

$$E_1 = 35.5 \ {}^{GN}\!/_{m^2} \qquad E_2 = 16.6 \ {}^{GN}\!/_{m^2} \qquad E_3 = 16.6 \ {}^{GN}\!/_{m^2}$$

(5,140,000 psi)   (2,410,000 psi)   (2,410,000 psi)

(c)

$$G_{12} = 3.26 \ {}^{GN}\!/_{m^2} \qquad G_{23} = 3.48 \ {}^{GN}\!/_{m^2} \qquad G_{13} = 3.26 \ {}^{GN}\!/_{m^2}$$

(472,000 psi)   (504,000 psi)   (472,000 psi)

The reductions in G_{12} from (a) to (c), and in E_3 from (a) to (b) are associated with the losses in transverse properties (c f., the two curve of Figure 35 associated with the reduction in filament packing density in the 1 - direction. Evidently a balance must be struck between multi-directional filaments and multi-directional reinforcing by transverse filament effectiveness.

(2)   Are skew filaments more effective than orthogonal filaments?

If one restricts oneself (to begin with) to the simple combination of pairs of skewed filaments indicated in Fig. 43, for which the equations of Table 13 apply, one finds, for example, that if all pairs make 30° angles with their

respective axes, and the volume fractions are 40% in the 1-direction,

and 10% in the other directions.

$$E_1 = 12.4 \; {}^{GN}\!/_{m^2}$$
$$(1,790,000 \; psi)$$

$$E_2 = 10.2 \; {}^{GN}\!/_{m^2}$$
$$(1,480,000 \; psi)$$

$$E_3 = 7.25 \; {}^{GN}\!/_{m^2}$$
$$(1,050,000 \; psi)$$

$$G_{12} = 4.69 \; {}^{GN}\!/_{m^2}$$
$$(680,000 \; psi)$$

$$G_{23} = 4.80 \; {}^{GN}\!/_{m^2}$$
$$(696,000 \; psi)$$

$$G_{13} = 8.49 \; {}^{GN}\!/_{m^2}$$
$$(1,230,000 \; psi)$$

By comparison with (c) above, it is evident that the skewing has decreased

the E's and increased the G's. Here the stretching stiffnesses in the three

directions are more nearly alike; with just the orthogonal filaments the

shearing stiffnesses were closer together. The differences of this nature

lead immediately to questions like the following:

(3) How do the various stiffnesses change with angular orientation, and

   what is the minimum number of reinforcement directions required

   for isotropy?

In order to illustrate some of the possibilities, Figs. 44 - 48 were pre-

pared. In Figs. 44 - 47, the variations in stretching and shearing stiffnesses

with angular orientation of reinforcement are presented for a constant volume

fraction of total reinforcement of 0.6. In general as the reinforcements

are changed to enhance the stretching stiffness, the shearing stiffness is

decreased and vice versa. In Figs. 46 and 47, however, there is evidence

that the correspondence between the two types of stiffnesses is not a simple

one. Thus for $\theta \approx 45^\circ$ in Fig. 46, the stretching stiffnesses in the 1-, 2-

and 3 - directions are about equal. The corresponding shearing stiffnesses

plotted on Fig. 47 , on the other hand, are substantially different at this

angle. Hence, obviously, equality of stretching stiffness in 3 orthogonal

directions does not constitute isotropy.

   One criterion for isotropy is that

$$G = \frac{E}{2(1+\nu)}.$$ (72)

   A plot of the ratio $\dfrac{\frac{E}{2(1+\nu)}}{G}$ for the reinforcements of Figs. 44 and

45, and for two other volume fractions is made in Fig. 48. For all volume

fractions, the ratio is unity at $\pm\Theta = 30^{\circ}$ or 60°. Accordingly, it appears

that six filamentary directions   ($\pm 30^{\circ}$ to three orthogonal axes) may be

sufficient to provide an essentially isotropic reinforcement pattern.

Concluding Remarks on Three-Dimensional Reinforcement

   The waffle-like analysis for elastic properties developed in this section

is sufficiently versatile to encompass most geometrical effects of composite

reinforcement. While written only in approximate form, the fact that its

results correlate reasonably with other analyses when two-dimensional

problems are considered lends confidence to the belief that it should be

adequate for the three-dimensional domain. Guidelines for improving the

accuracy of approximation, as by the employment of more precisely deter-

mined transverse effectiveness factors follow straight forwardly from the

same starting point used in the present derivations. Indeed there should be no major impediment to the development of an essentially rigorous general analysis analogous to that already completed. The desirability of such a derivation can perhaps be better determined after the present results have been capitalized upon to explore the three-dimensional reinforcement regime, determine its areas of prime interest, and relate these to accompanying studies of strength characteristics.

EXPERIMENTAL EVALUATIONS OF TRANSVERSE EFFECTIVENESSES OF FILAMENTS OF VARIOUS CROSS-SECTIONS

The use of filamentary cross-sections other than rounds to improve properties transverse to the filaments was proposed in Reference 2 and progress has been made by DeBell and Richardson since then in the development of techniques required to make shaped-filamentary composites feasible. Quantitative evaluations of the merits of shaped filaments, however, have still been inadequate to direct this development into most fruitful areas. Accordingly, both experiment and analysis has been conducted on the more attractive cross-sectional geometries proposed for filaments. The results of the experimental phases of these investigations, comprising photo-elastic studies and mechanical tests of ellipses and hollow rounds, are reported herewith.

Evaluations of Elliptical Filaments

In contrast to the relatively small increases found for triangular filaments in the preceding section, elliptical filaments have already demonstrated (Ref. 2) factors of two improvements in transverse stiffness for a specific aspect ratio ellipse in 50 volume percent binder ($E_f/E_b \approx 21$). Accordingly, an extensive experimental study of the transverse effectivenesses of ellipses compared to rounds has been made. The findings are reported forthwith.

<u>Tests of Transverse Stiffness</u> - A series of models (Figure 49) of "large" (typical diametral dimensions 5 mm) inclusions was made and tested in

compression (Figure 50) with systematic variations in volume fractions and inclusion shapes. Stiffnesses were measured in both transverse directions using Tuckerman optical strain gages, with the gage length adjusted to span even multiples of inclusions and associated binder. The results are presented in Table 16 and Figures 51-54.

Not surprising are the results shown in Figure 51. The solid rounds are in fair agreement with the predictions of Hashin and Rosen (Reference 6) and the ellipses provide substantial enhancement of transverse stiffness in the direction of their major axes.

More surprising are the results shown in Figure 52. Here the transverse stiffnesses in the direction of the ellipse minor axes are also shown greater than the rounds. Apparently, the round is one of the least effective shapes for providing transverse stiffness.

For hollow rounds (Figures 53-54) and for holes, Hashin-Rosen upper bounds are in better agreement with the test data than the previously used mean value (Reference 1). Here again ellipses are better in the direction of their major axes, but for holes the stiffnesses in the direction of the minor axes are much less than for rounds.

For completeness the measured values of Poisson's ratio for the specimens are presented in Figure 55.

Discussion of Test Results - The most significant results of the foregoing

tests appear to be the following:

1. For solid round inclusions the Hashin-Rosen bounds predict the

   transverse stiffnesses with reasonable accuracy.

2. For hollow rounds the Hashin-Rosen upper bounds are a better measure

   of the transverse stiffnesses than the average of the upper and lower

   bounds. Thus evaluations (Ref. 1) of hollow filaments which used the

   average of the bounds and concluded that the hollow was disappointing

   because of its poor transverse properties, unduly devalue the hollow

   filament.

3. Little relationship exists between the transverse effectiveness of binder

   between holes and binder between solid inclusions. This fact, amply

   demonstrated by the very low effectiveness in the direction of the minor

   axis of elliptical holes and the high effectiveness in the direction of the

   minor axis of elliptical solids, suggests that the β values of the pre-

   ceding section should not be evaluated on the basis of holes in the binder.

4. Ellipses are perhaps better than might have been anticipated for the

   enhancement of transverse properties, because they increase the stiff-

   ness in the direction of the minor axis (albeit only slightly) as well as

   in the direction of the major axis.

Photoelastic Studies

In order to study further the mechanics of filament-binder combina-
tions an additional series of models similar to those tested as described
in the preceding section was made and subjected to photoelastic analysis
at the Photolastic Corporation. Specimens comprised round and elliptical
holes and inclusions at several volume fractions. The resin used was
Photolastic type PS-2. Inclusions were aluminum, and they were bonded
in place with Photolastic type PC-IC cement. Typical fringe patterns are
illustrated in Figures 56-58, and typical results of the reduction of data
to yield isoclinics and isostatics are presented in Figures 59 and 60.

Results of Photoelastic Studies - The chief result of the photoelastic analysis
is that with inclusions, and especially with high volume fractions of filaments,
a nearly uniform stress state is produced for transverse loads, as illustrated
in the lower, right sides of Figures 59 and 60. This uniform stress state is
consistent with the high transverse effectivenesses found for solid inclusions
in the previous section (effectivenesses near the Hashin-Rosen upper bounds).
Correspondingly the highly non-uniform state of stress found for holes (the
upper halves of Figures 59 and 60) and the associated high stress-concentra-
tion factors (Table 16) bear out the finding that there is little relation be-
tween the effectiveness of binder material among holes and among filaments.
The ellipses loaded along their major axis produce an even more uniform
stress state than the round inclusions.

CONCLUDING REMARKS

Several studies relating to the mechanics of filament-reinforced composites have been reported herein. A prime motivation behind these studies derives from continuing investigations of efficiency of composite applications, because as noted in the section on shell efficiency such investigations emphasize the importance of adequate analysis of the role played by both binder and reinforcement in the attainment of the potentials of advanced composites. Thus the ultimate strength in both tension and compression, as well as the buckling resistance in compression have been shown in these studies to be profoundly influenced by both filamentary and binder material properties.

To further the understanding of the mechanics of reinforcement, an analysis of the visco-elastic response of composites has been accomplished and the influence of the viscous effects upon the individual properties has been identified. The transverse effectiveness of filamentary reinforcement has been studied experimentally, both mechanically and photoelastically, and the merits of triangular and elliptically-shaped filaments evaluated. An analytical procedure has been developed for the calculation of the elastic constants for three-dimensional reinforcement.

REFERENCES

1. Dow, N. F. & Rosen, B. W., "Evaluations of Filament-Reinforced Composites for Aerospace Structural Applications," Annual Report NASA Contract NASw-817, Oct. 1964.

2. Rosen, B. W.; Dow, N. F.; & Hashin, Z., "Mechanical Properties of Fibrous Composites," NASA CR-31, April, 1964.

3. Stein, M. & Mayers, J., "Compressive Buckling of Simply Supported Curved Plates and Cylinders of Sandwich Construction," NACA TN 2601, Jan. 1952.

4. Dow, N. F. & Rosen, B. W., "Structural Efficiency of Orthotropic Cylindrical Shells Subjected to Axial Compression," AIAA Preprint 65-73, Jan. 1965.

5. Rosen, B. W. & Dow, N. F., "Influence of Constituent Properties Upon the Structural Efficiency of Fibrous Composite Shells," AIAA Sixth Structures and Materials Conference, April, 1965.

6. Hashin, Z. & Rosen, B. W., "The Elastic Moduli of Fiber Reinforced Materials," Journal of Applied Mechanics, June, 1964.

7. _____, "Hollow Glass Fiber Reinforced Laminates," Final Report, Contract NOw-63-0674-c, General Electric Company, Aug. 1964.

8. Ambartsumian, S. A., "Contributions to the Theory of Anisotropic Layered Shells," Applied Mechanics Reviews, Vol. 15, No. 4, April 1962.

9. Habip, L. M., "A Review of Recent Work on Multilayered Structures," Int. J. Mech. Sci., Vol. 7, pp. 589-93, 1965.

10. Pickett, G., "Analytical Procedures for Predicting the Mechanical Properties of Fiber Reinforced Composites," AFML-TR-65-220, June 1965.

11. Tsai, S., "Procedures for Predicting Strength of Fiber-Reinforced Composites Based on Micromechanics Parameters," Contract No. AF 33(615)-2180, unpublished.

12. Sonneborn, R. H., "Fiberglass Reinforced Plastics," Reinhold, New York, N. Y., 1954.

13. Shaffer, B. W., "Stress-Strain Relations of Reinforced Plastics Parallel and Normal to Their Internal Filaments," AIAA Journal, February 1964.

14. Hashin, Z., "On Elastic Behavior of Fibre Reinforced Materials of Arbitrary Transverse Phase Geometry," J. Mech. Phys. Solids, Vol. 13, 1965.

15. Hill, R., "Theory of Mechanical Properties of Fiber-Strengthened Materials: I. Elastic Behavior," J. Mech. Phys. Solids, Vol. 12, pp. 199-212, 1964.

16. Tsai, S. W., "Structural Behavior of Composite Materials,"
    NASA CR-71, July 1964.

17. Nu, T. T., "On the Parametrization of the Elastic Moduli of
    Two Phase Materials, J. Appl. Mech., Vol. 32, pp. 211-214,
    1965.

18. Paul, B., "Prediction of Elastic Constants of Multiphase Ma-
    terials," Trans. AIME Vol. 219, February 1960, pp. 36-41.

19. Riley, M. B., & Whitney, J., to be published.

20. Filshtinskii, L. A., "Stresses and Displacements in an Elastic
    Sheet Weakened by a Doubly-Periodic Set of Equal Circular
    Holes., PMM-Journal of Appl. Math and Mech., Vol. 28, No.
    3, 1964.

21. Hashin, Z., "Theory of Mechanical Behavior of Heterogeneous
    Media," Appl. Mech. Reviews, Jan. 1964.

22. Dow, N. F., "Study of Stresses Near a Discontinuity in a Fila-
    ment-Reinforced Composite Material," General Electric Com-
    pany, Space Sciences Laboratory, Space Mechanics Memo #102,
    January 1961.

23. Sadowsky, M. A., "Transfer of Force by High Strength Flakes
    in a Composite Material," Watervliet Arsenal, WVT-RR-6105-R,
    June 1961.

24. Sadowsky, M. A., "Effect of Poisson's Ratio of an Elastic Filler
    on Force Transfer Between Embedded Microfibers," Watervliet
    Arsenal, WVT-RR-6108, September 1961.

25. Hedgepeth, J. M., "Stress Concentrations in Filamentary Struc-
    tures," NASA TN D-882, May 1961.

26. Machlin, E. S., "Status Report on Non-Metallic Fibrous Rein-
    forced Metal Composites, " Materials Research Corp., Sept.,
    1961.

27. Jech, R. W., McDaniels, D. L. & Weeton, J. W., "Fiber Re-
    inforced Metallic Composites," Proceedings of the Sixth Saga-
    more Ordnance Materials Research Conference, August 1959.

28. Parratt, N. J., "Defects in Glass Fibers and Their Effect on
    the Strength of Plastic Mouldings," Rubber and Plastics Age,
    March 1960, pp. 263-266.

29. Rosen, B. W., "Tensile Failure of Fibrous Composites," AIAA
    Journal, November 1964.

30. Kies, J. A. & Bernstein, H., "Recent Advances in Glass Fiber
    Reinforced Plastic Rocket Motors," 17th Annual Reinforced
    Plastics Conference, SPI, Section 6B, 1962.

31. Patrick, R. L., Ripling, E. J., & Mostovoy, S., "Fracture
    Mechanics Applied to Heterogeneous Systems," 19th Annual Rein-
    forced Plastics Conference, SPI, Section 3B, 1964.

32. Wu, E. M., "Application of Fracture Mechanics to Orthotropic
    Plates,"TAM Report No. 248, Univ. of Illinois, 1963, Contract
    Nonr 2947 (02)(X) with U. S. Naval Res. Lab.

33. Rosen, B. W., "Mechanics of Composite Strengthening in Fiber Composite Materials," ASM, Metals Park, Ohio, 1965.

34. Schuerch, H., "Boron Filament Composite Materials for Space Structures, Part I: Compressive Strength of Boron-Metal Composite," Astro Research Corporation, Report ARC-R-168, November 11, 1964.

35. Dow, N. F. & Gruntfest, I. J., "Determination of Most Needed Potentially Possible Improvements in Materials for Ballistic and Space Vehicles," General Electric Company, Space Sciences Laboratory, TIS R60SD389, June 1960.

36. Biot, M. A., "Mechanics of Incremental Deformations" John Wiley & Sons, New York, 1965.

37. Stavsky, Y and McGarry, F. J., "Investigation of Mechanics of Reinforced Plastics," WADD TR 60-746.

38. Timoshenko, S., "Theory of Elastic Stability," McGraw Hill, New York, New York, 1936.

39. _____, "Micromechanics of Fibrous Composites", Materials Advisory Board, MAB-207-M, National Academy of Sciences, May 1965.

40. Hashin, Z., "Viscoelastic Behavior of Heterogeneous Media," Journal of Applied Mechanics, Vol. 32, Trans. ASME, Vol. 87, Series E, 1965, pp. 630-636.

41. Gurtin, M. E., & Steinberg, E., "On the Linear Theory of Visco-elasticity", Archives for Rational Mechanics and Analysis, Vol. 11, 1962, p. 291.

42. Van der Pol, B., & Bremmer, H., "Operational Calculus", Second Edition, Cambridge University Press, Cambridge, England, 1955.

43. Schulgasser, K., to be published.

44. Dow, N. F., Libove, C., & Hubka, R. E., "Formulas for the Elastic Constants of Plates with Integral, Waffle-Like Stiffening", NACA TR-1195, 1954.

TABLE 1. COMPRESSIVE LOADINGS FOR LAUNCH VEHICLES

Vehicle	Thrust, kN (lbs.)	Radius, m. (in.)	Thrust / Circumference x Radius KN/m^2 (psi)
Redstone	347 (78,000)	0.889 (35)	70 (10)
Scout	383 (86,000)	0.4955 (39)	250 (36)
Thor	756 (170,000)	1.219 (48)	80 (12)
Atlas	1730-375* (389,000-80,000)	1.524 (60)	120-24 (17-3.5)
Minuteman	756 (170,000)	0.9015 (35.5)	150 (21.5)
Titan I	1334 (300,000)	1.524 (30)	90 (13)
Titan II	1913 (430,000)	1.524 (30)	130 (19)
Saturn V	33,360 (7,400,000)	5.08 (200)	200 (30)
Nova	11,200 (25,000,000)	12.19 (480)	120 (17)

*Lower value is that for sustainer engine-in this case perhaps more representative of the design condition.

142

TABLE 2. MECHANICAL PROPERTIES ASSIGNED TO IDEALIZED METALS FOR COMPARISON WITH COMPOSITES

Material	Density Mg/m^3 (pci)	Young's Modulus GN/m^2 (ksi)	Yield Stress GN/m^2 (ksi)	Poisson's Ratio
Steel	7.89 (0.285)	207 (30,000)	2.07 (300)	0.25
Titanium	4.82 (0.174)	103 (15,000)	1.38 (200)	0.145
Aluminum	2.80 (0.100)	73.8 (10,700)	0.483 (70)	0.315
Magnesium -Lithium	1.34 (0.0485)	42.75 (6200)	0.124 (18)	0.43
Beryllium	1.83 (0.066)	293 (42,500)	4.00 (58)	0.09

TABLE 3. MECHANICAL PROPERTIES USED FOR FILAMENTARY MATERIALS SURVEYED FOR COMPOSITES

	Young's Modulus GN/m^2 (ksi)	Density Mg/m^3 (pci)	Poisson's Ratio
Hollow E-Glass	72.45 (10,500)	2.56 (0.0914)	0.20
Solid E-Glass	72.45 (10,500)	2.56 (0.0914)	0.20
Hi-Modulus Glass	110 (16,000)	2.56 (0.0914)	0.20
Asbestos	183 (26,500)	2.44 (0.087)	0.20
Steel	207 (30,000)	7.9 (0.283)	0.25
Beryllium	276 (40,000)	1.85 (0.066)	0.09
Boron	414 (60,000)	2.32 (0.083)	0.20
Alumina	518 (75,000)	4.0 (0.143)	0.20

TABLE 4. MECHANICAL PROPERTIES USED FOR BINDER MATERIALS SURVEYED FOR COMPOSITES

"Epoxy"	3.45 (500)	1.40 (0.050)	0.35
"Light-Alloy I"	103.5 (15,000)	1.40 (0.050)	0.30
"Magnesium"	51.75 (7500)	2.10 (0.075)	0.30
"Light-Alloy II"	103.5 (15,000)	2.10 (0.075)	0.30
"Light-Alloy III"	207 (30,000)	2.10 (0.075)	0.30
"Boron"	414 (60,000)	2.10 (0.075)	0.30
"Titanium"	103.5 (15,000)	4.20 (0.150)	0.30
"Steel"	207 (30,000)	8.40 (0.300)	0.30

Table 5. Comparison of Elastic Moduli Predicted by the Methods of Pickett (Ref. 10) with those of Hashin/Rosen[*] (Ref. 6).

Case A:

$$E_f = 10.008 \times 10^6 \text{ psi} \qquad \nu_f = 0.20$$

$$E_b = 4.958 \times 10^6 \text{ psi} \qquad \nu_b = 0.34$$

$$v_f = 0.63$$

Property	Ref. 10 Value (case b 9 - p. 16)	Ref. 6 Value
E_1	6.4908×10^6	6.4913×10^6
ν_{21}	0.2428	0.2439
G_{12}	[†]0.6926×10^6	0.6886×10^6
K_{23}	1.5689×10^6	1.5598×10^6
G_{23}	0.6790×10^6	0.6870×10^6

Case B:

$$E_f = 10.008 \times 10^6 \text{ psi} \qquad \nu_f = 0.20$$

$$E_b = 4.958 \times 10^6 \text{ psi} \qquad \nu_b = 0.34$$

$$v_f = 0.8$$

Property	Ref. 10 Value (case c 2 - p. 17)	Ref. 6 Value
E_1	8.1037×10^6	8.1074×10^6
ν_{21}	0.2227	0.2228
G_{12}	-	1.1958×10^6

[*] Random array results with G_{23} value being the average of upper and lower bounds. Other bounds coincident.

[†] From run 6, p. 46.

146

| K_{23} | 2.5628×10^6 | 2.4873×10^6 |
| G_{23} | 1.2644×10^6 | 1.1828×10^6 |

$v_f = 0.7$

(case c4 - p. 17)

E_1	7.1596×10^6	7.1568×10^6
ν_{21}	0.2350	0.2350
G_{12}	-	0.8443×10^6
K_{23}	1.8645×10^6	1.8507×10^6
G_{23}	0.8496×10^6	0.8419×10^6

$v_f = 0.6$

(case c6 - p. 17)

E_1	6.2101×10^6	6.2060×10^6
ν_{21}	0.2482	0.2478
G_{12}	-	0.6354×10^6
K_{23}	1.4613×10^6	1.4591×10^6
G_{23}	0.6106×10^6	0.6334×10^6

$v_f = 0.5$

(case c8 - p. 17)

E_1	5.2535×10^6	5.2550×10^6
ν_{21}	0.2615	0.2612
G_{12}	-	0.4971×10^6

K_{23}	1.1936×10^6	1.1938×10^6
G_{23}	0.4631×10^6	0.4924×10^6

Case C:

$$E_f = \text{variable} \qquad \nu_f = 0.30$$

$$E_b = 0.2600 \times 10^6 \qquad \nu_b = 0.30$$

$$v_f = 0.63$$

$\underline{E_f = 0.2600 \times 10^6}$

Property	Ref. 10 Value (case d1 - p. 18)	Ref. 6 Value
E_1	0.2600×10^6	0.2600×10^6
ν_{21}	0.3000	0.3000
G_{12}	0.1000×10^6	0.1000×10^6
K_{23}	0.2500×10^6	0.2500×10^6
G_{23}	0.1000×10^6	0.1000×10^6

$\underline{E_f = 0.5200 \times 10^6}$

	(case d2 - p. 18)	
E_1	0.4421×10^6	0.4238×10^6
ν_{21}	0.3000	0.3000
G_{12}	–	0.1532×10^6
K_{23}	0.3943×10^6	0.3746×10^6
G_{23}	0.1593×10^6	0.1521×10^6

$$\underline{E_f = 1.5600 \times 10^6}$$

(case d 3 - p. 18)

E_1	1.1704	1.0790
ν_{21}	0.3000	0.3000
G_{12}	-	0.2636
K_{23}	0.6749	0.5892
$_{23}$	0.2907	0.2556

Table 6. - Equations for elastic constants for composites with unidirectional reinforcing filaments in the 1-direction.

$$A_1 = \frac{E_b(1-\nu_b)}{(1+\nu_b)(1-2\nu_b)}(1-V_f) + \frac{E_f(1-\nu_f)}{(1+\nu_f)(1-2\nu_f)}(V_f)$$

$$A_2 = \frac{\nu_b E_b}{(1+\nu_b)(1-2\nu_b)}(1-\beta_o V_f) + \frac{\nu_f E_f}{(1+\nu_f)(1-2\nu_f)}(\beta_o V_f)$$

$$A_3 = A_2$$

$$A_4 = \frac{E_b(1-\nu_b)}{(1+\nu_b)(1-2\nu_b)}(1-\beta_o V_f) + \frac{E_f(1-\nu_f)}{(1+\nu_f)(1-2\nu_f)}(\beta_o V_f)$$

$$A_5 = A_2$$

$$A_6 = A_4$$

$$A_7 = G_b(1-\beta_o' V_f) + G_f(\beta_o' V_f)$$

$$A_8 = G_b(1-\beta_o'' V_f) + G_f(\beta_o'' V_f)$$

$$A_9 = A_7$$

150

Table 7. - Equation for elastic constants for composites with orthogonal
reinforcing filaments in the 1- and 2-directions.

$$A_1 = \frac{E_b(1-\nu_b)}{(1+\nu_b)(1-2\nu_b)}\left(1-V_{f_1}-\beta_{2_0}V_{f_2}\right) + \frac{E_{f_1}(1-\nu_{f_1})}{(1+\nu_{f_1})(1-2\nu_{f_1})}\left(V_{f_1}\right) + \frac{E_{f_2}(1-\nu_{f_2})}{(1+\nu_{f_2})(1-2\nu_{f_2})}\left(\beta_{0_2}V_{f_2}\right)$$

$$A_2 = \frac{\nu_b E_b}{(1+\nu_b)(1-2\nu_b)}\left(1-\beta_{2_0}V_{f_1}-\beta_{2_0}V_{f_2}\right) + \frac{\nu_{f_1}E_{f_1}}{(1+\nu_{f_1})(1-2\nu_{f_1})}\left(\beta_{0_0}V_{f_1}\right) + \frac{\nu_{f_2}E_{f_2}}{(1+\nu_{f_2})(1-2\nu_{f_2})}\left(\beta_{0_2}V_{f_2}\right)$$

$$A_3 = A_2$$

$$A_4 = \frac{E_b(1-\nu_b)}{(1+\nu_b)(1-2\nu_b)}\left(1-\beta_{2_0}V_{f_1}-\beta_{2_0}V_{f_2}\right) + \frac{E_{f_1}(1-\nu_{f_1})}{(1+\nu_{f_1})(1-2\nu_{f_1})}\left(\beta_{0_1}V_{f_1}\right) + \frac{E_{f_2}(1-\nu_{f_2})}{(1+\nu_{f_2})(1-2\nu_{f_2})}\left(\beta_{0_2}V_{f_2}\right)$$

$$A_5 = A_2$$

$$A_6 = A_4$$

$$A_7 = G_b\left(1-\beta_{2_0}'V_{f_1}-\beta_{2_0}'V_{f_2}\right) + G_{f_1}\left(\beta_{0}'V_{f_1}\right) + G_{f_2}\left(\beta_{0}'V_{f_2}\right)$$

$$A_8 = G_b\left(1-\beta_{2_0}''V_{f_1}-\beta_{2_0}''V_{f_2}\right) + G_{f_1}\left(\beta_{0}''V_{f_1}\right) + G_{f_2}\left(\beta_{0}''V_{f_2}\right)$$

$$A_9 = A_7$$

Table 8. - Equations for elastic constants for composites with reinforcing filaments in the 1 - 2 plane and making angles of $\pm\,\theta$ degrees to the 1-direction.

$$A_1 = \frac{E_b(1-\nu_b)}{(1+\nu_b)(1-2\nu_b)}\left\{1-V_f\left[\cos^4\theta+\beta_{-\bullet}\sin^4\theta+\left(\nu_b\beta_{-\bullet}+\{1-2\nu_b\}\beta_{-\bullet}'\right)\frac{2\sin^2\theta\cos^2\theta}{1-\nu_b}\right]\right\}$$

$$+\frac{E_f(1-\nu_f)}{(1+\nu_f)(1-2\nu_f)}\left\{V_f\left[\cos^4\theta+\beta_{\bullet}\sin^4\theta+\left(\nu_f\beta_{\bullet}+\{1-2\nu_f\}\beta_{\bullet}'\right)\frac{2\sin^2\theta\cos^2\theta}{1-\nu_f}\right]\right\}$$

$$A_2 = \frac{\nu_b E_b}{(1+\nu_b)(1-2\nu_b)}\left\{1-V_f\left[\beta_{-\bullet}\left(\sin^4\theta+\cos^4\theta\right)+\left(\{1-\nu_b\}\left\{\frac{1+\beta_{-\bullet}}{2}\right\}-\{1-2\nu_b\}\beta_{-\bullet}'\right)\frac{2\sin^2\theta\cos^2\theta}{\nu_b}\right]\right\}$$

$$+\frac{\nu_f E_f}{(1+\nu_f)(1-2\nu_f)}\left\{V_f\left[\beta_{\bullet}\left(\sin^4\theta+\cos^4\theta\right)+\left(\{1-\nu_f\}\left\{\frac{1+\beta_{\bullet}}{2}\right\}-\{1-2\nu_f\}\beta_{\bullet}'\right)\frac{2\sin^2\theta\cos^2\theta}{\nu_f}\right]\right\}$$

$$A_3 = \frac{\nu_b E_b}{(1+\nu_b)(1-2\nu_b)}\left(1-\beta_{-\bullet}V_f\right)+\frac{\nu_f E_f}{(1+\nu_f)(1-2\nu_f)}\left(\beta_{\bullet}V_f\right)$$

$$A_4 = \frac{E_b(1-\nu_b)}{(1+\nu_b)(1-2\nu_b)}\left\{1-V_f\left[\sin^4\theta+\beta_{-\bullet}\cos^4\theta+\left(\nu_b\beta_{-\bullet}+\{1-2\nu_b\}\beta_{-\bullet}'\right)\frac{2\sin^2\theta\cos^2\theta}{1-\nu_b}\right]\right\}$$

$$+\frac{E_f(1-\nu_f)}{(1+\nu_f)(1-2\nu_f)}\left\{V_f\left[\sin^4\theta+\beta_{-\bullet}\cos^4\theta+\left(\nu_f\beta_{\bullet}+\{1-2\nu_f\}\beta_{\bullet}'\right)\frac{2\sin^2\theta\cos^2\theta}{1-\nu_f}\right]\right\}$$

$$A_5 = A_3$$

$$A_6 = \frac{E_b(1-\nu_b)}{(1+\nu_b)(1-2\nu_b)}\left(1-\beta_{-\bullet}V_f\right)+\frac{E_f(1-\nu_f)}{(1+\nu_f)(1-2\nu_f)}\left(\beta_{\bullet}V_f\right)$$

$$A_7 = G_b\left\{1-V_f\left[\{(1-\nu_b)+(1-3\nu_b)\beta_{-\bullet}\}\left\{\frac{2\sin^2\theta\cos^2\theta}{1-2\nu_b}\right\}+\beta_{-\bullet}'\cos^2 2\theta\right]\right\}$$

$$+G_f\left\{V_f\left[\{1-\nu_f\}+\{1-3\nu_f\}\beta_{\bullet}\}\left\{\frac{2\sin^2\theta\cos^2\theta}{1-2\nu_f}\right\}+\beta_{\bullet}'\cos^2 2\theta\right]\right\}$$

$$A_8 = G_b\left\{1-V_f\left[\beta_{-\bullet}'\sin^2\theta+\beta_{-\bullet}''\cos^2\theta\right]\right\}+G_f\left\{V_f\left[\beta_{\bullet}'\sin^2\theta+\beta_{\bullet}''\cos^2\theta\right]\right\}$$

$$A_9 = G_b\left\{1-V_f\left[\beta_{-\bullet}'\cos^2\theta+\beta_{-\bullet}''\sin^2\theta\right]\right\}+G_f\left\{V_f\left[\beta_{\bullet}'\cos^2\theta+\beta_{\bullet}''\sin^2\theta\right]\right\}$$

152

Table 9. - Equations for elastic constants for composites with reinforcing filaments in the 1-2 plane and making angles of ±30 degrees and 90 degrees with the 1-direction.

$$A_1 = \frac{E_b(1-\nu_b)}{(1+\nu_b)(1-2\nu_b)}\left\{1-V_f\left[\frac{3}{8}(1+\beta_\bullet)+\left(\nu_b\beta_\bullet+\{1-2\nu_b\}\beta'_{-\bullet}\right)\frac{\frac{1}{4}}{1-\nu_b}\right]\right\}$$

$$+\frac{E_f(1-\nu_f)}{(1+\nu_f)(1-2\nu_f)}\left\{V_f\left[\frac{3}{8}(1+\beta_\bullet)+\left(\nu_f\beta_\bullet+\{1-2\nu_f\}\beta'_\bullet\right)\frac{\frac{1}{4}}{1-\nu_f}\right]\right\}$$

$$A_2 = \frac{\nu_b E_b}{(1+\nu_b)(1-2\nu_b)}\left\{1-V_f\left[\frac{3}{4}\beta_{-\bullet}+\left(\{1-\nu_b\}\left\{\frac{1+\beta_\bullet}{2}\right\}-\{1-2\nu_b\}\beta'_{-\bullet}\right)\frac{\frac{1}{4}}{\nu_b}\right]\right\}$$

$$+\frac{\nu_f E_f}{(1+\nu_f)(1-2\nu_f)}\left\{V_f\left[\frac{3}{4}\beta_\bullet+\left(\{1-\nu_f\}\left\{\frac{1+\beta_\bullet}{2}\right\}-\{1-2\nu_b\}\beta'_\bullet\right)\frac{\frac{1}{4}}{\nu_f}\right]\right\}$$

$$A_3 = \frac{\nu_b E_b}{(1+\nu_b)(1-2\nu_b)}\left(1-\beta_{-\bullet}V_f\right)+\frac{\nu_f E_f}{(1+\nu_f)(1-2\nu_f)}\left(\beta_\bullet V_f\right)$$

$$A_4 = A_1$$

$$A_5 = A_3$$

$$A_6 = \frac{E_b(1-\nu_b)}{(1+\nu_b)(1-2\nu_b)}\left(1-\beta_{-\bullet}V_f\right)+\frac{E_f(1-\nu_f)}{(1+\nu_f)(1-2\nu_f)}\left(\beta_\bullet V_f\right)$$

$$A_7 = G_b\left\{1-V_f\left[\{(1-\nu_b)+(1-3\nu_b)\beta_{-\bullet}\}\left\{\frac{\frac{1}{4}}{1-2\nu_b}\right\}+\frac{1}{2}\beta'_{-\bullet}\right]\right\}$$

$$+G_f\left\{V_f\left[\{(1-\nu_f)+(1-3\nu_f)\beta_\bullet\}\left\{\frac{\frac{1}{4}}{1-2\nu_f}\right\}+\frac{1}{2}\beta'_\bullet\right]\right\}$$

$$A_8 = G_b\left\{1-V_f\left[\frac{1}{2}(\beta'_{-\bullet}+\beta''_{-\bullet})\right]\right\}+G_f\left\{V_f\left[\frac{1}{2}(\beta'_\bullet+\beta''_\bullet)\right]\right\}$$

$$A_9 = A_8$$

153

Table 10. - Equations for elastic constants for uni-directional triangular glass filaments in the 1-direction in epoxy binder.

$$A_1 = \frac{E_f(1-\nu_f)}{(1+\nu_f)(1-2\nu_f)}(V_f) + \frac{E_b(1-\nu_b)}{(1+\nu_b)(1-2\nu_b)}(V_b)$$

$$A_2 = \frac{\nu_f E_f}{(1+\nu_f)(1-2\nu_f)}(1-\beta_{-\bullet}V_b) + \frac{\nu_b E_b}{(1+\nu_b)(1-2\nu_b)}(\beta_\bullet V_b)$$

$$A_3 = A_2$$

$$A_4 = \frac{E_f(1-\nu_f)}{(1+\nu_f)(1-2\nu_f)}\left\{1-\frac{3}{4}V_b\left[\frac{1+\beta_{-\bullet}}{2}+\left(\nu_f\left\{\frac{1+\beta_{-\bullet}}{2}\right\}+\{1-2\nu_f\}\beta_\bullet'\right)\left(\frac{\frac{1}{3}}{1-\nu_f}\right)\right]\right\}$$
$$+\frac{E_b(1-\nu_b)}{(1+\nu_b)(1-2\nu_b)}\left\{\frac{3}{4}V_b\left[\frac{1+\beta_\bullet}{2}+\left(\nu_b\left\{\frac{1+\beta_\bullet}{2}\right\}+\{1-2\nu_b\}\beta_\bullet'\right)\left(\frac{\frac{1}{3}}{1-\nu_b}\right)\right]\right\}$$

$$A_5 = \frac{\nu_f E_f}{(1+\nu_f)(1-2\nu_f)}\left\{1-\frac{3}{4}V_b\left[\beta_{-\bullet}+\left(\{1-\nu_f\}\beta_{-\bullet}-\{1-2\nu_f\}\beta_\bullet'\right)\left(\frac{\frac{1}{3}}{\nu_f}\right)\right]\right\}$$
$$+\frac{\nu_b E_b}{(1+\nu_b)(1-2\nu_b)}\left\{\frac{3}{4}V_b\left[\beta_\bullet+\left(\{1-\nu_b\}\beta_\bullet-\{1-2\nu_b\}\beta_\bullet'\right)\left(\frac{\frac{1}{3}}{\nu_b}\right)\right]\right\}$$

$$A_6 = A_4$$

$$A_7 = G_f(\beta_\blacktriangle' V_f) + G_b(1-\beta_\blacktriangle' V_f)$$

$$A_8 = G_f(\beta_\blacktriangle'' V_f) + G_b\left\{V_b\left[(\{1-\nu_b\}+\{1-3\nu_b\}\beta_\bullet)\left(\frac{\frac{1}{4}}{1-2\nu_b}\right)+\frac{1}{2}\beta_\bullet'\right]\right\}$$

$$A_9 = A_7$$

with $\beta_\bullet$ for $E_f/E_b = 0.05$, $\beta_\blacktriangle$ for $E_f/E_b = 21$.

154

Table 11. - Equations for elastic constants for stretching for orthogonal, elliptical filaments aligned in the 1- and 2- directions and having their minor axes in the 3-direction.

$$A_1 = \frac{E_b(1-\nu_b)}{(1+\nu_b)(1-2\nu_b)}\left(1-\nu_{f_1}-\beta_{-\bullet}\nu_{f_2}\right) + \frac{E_f(1-\nu_f)}{(1+\nu_f)(1-2\nu_f)}\left(\nu_{f_1}+\beta_\bullet\nu_{f_2}\right)$$

$$A_2 = \frac{\nu_b E_b}{(1+\nu_b)(1-2\nu_b)}\left(1-\beta_{-\bullet}\nu_{f_1}-\beta_{-\bullet}\nu_{f_2}\right) + \frac{\nu_f E_f}{(1+\nu_f)(1-2\nu_f)}\left(\beta_\bullet\nu_{f_1}+\beta_\bullet\nu_{f_2}\right)$$

$$A_3 = \frac{\nu_b E_b}{(1+\nu_b)(1-2\nu_b)}\left\{1-\frac{\beta_{-\bullet}+\beta_\bullet}{2}(\nu_{f_1}) - \frac{\beta_{-\bullet}+\beta_\bullet}{2}(\nu_{f_2})\right\}$$
$$+ \frac{\nu_f E_f}{(1+\nu_f)(1-2\nu_f)}\left\{\frac{\beta_\bullet+\beta_\bullet}{2}(\nu_{f_1}) + \frac{\beta_\bullet+\beta_\bullet}{2}(\nu_{f_2})\right\}$$

$$A_4 = \frac{E_b(1-\nu_b)}{(1+\nu_b)(1-2\nu_b)}\left(1-\beta_{-\bullet}\nu_{f_1}-\nu_{f_2}\right) + \frac{E_f(1-\nu_f)}{(1+\nu_f)(1-2\nu_f)}\left(\beta_\bullet\nu_{f_1}+\nu_{f_2}\right)$$

$$A_5 = A_3$$

$$A_6 = \frac{E_b(1-\nu_b)}{(1+\nu_b)(1-2\nu_b)}\left(1-\beta_{-\bullet}\nu_{f_1}-\beta_\bullet\nu_{f_2}\right) + \frac{E_f(1-\nu_f)}{(1+\nu_f)(1-2\nu_f)}\left(\beta_\bullet\nu_{f_1}+\beta_\bullet\nu_{f_2}\right)$$

Table 12. - Equations for elastic constants for composites with orthogonal
reinforcing filaments in the 1-, 2-, and 3- directions.

$$A_1 = \frac{E_b(1-\nu_b)}{(1+\nu_b)(1-2\nu_b)}\left(1-V_{f_1}-\beta_{-\bullet}V_{f_2}-\beta_{-\bullet}V_{f_3}\right) + \frac{E_{f_1}(1-\nu_{f_1})}{(1+\nu_{f_1})(1-2\nu_{f_1})}\left(V_{f_1}\right)$$

$$+ \frac{E_{f_2}(1-\nu_{f_2})}{(1+\nu_{f_2})(1-2\nu_{f_2})}\left(\beta_{\bullet_2}V_{f_2}\right) + \frac{E_{f_3}(1-\nu_{f_3})}{(1+\nu_{f_3})(1-2\nu_{f_3})}\left(\beta_{\bullet_3}V_{f_3}\right)$$

$$A_2 = \frac{\nu_b E_b}{(1+\nu_b)(1-2\nu_b)}\left(1-\beta_{-\bullet}V_{f_1}-\beta_{-\bullet}V_{f_2}-\beta_{-\bullet}V_{f_3}\right) + \frac{\nu_{f_1}E_{f_1}}{(1+\nu_{f_1})(1-2\nu_{f_1})}\left(\beta_{\bullet_1}V_{f_1}\right)$$

$$+ \frac{\nu_{f_2}E_{f_2}}{(1+\nu_{f_2})(1-2\nu_{f_2})}\left(\beta_{\bullet_2}V_{f_2}\right) + \frac{\nu_{f_3}E_{f_3}}{(1+\nu_{f_3})(1-2\nu_{f_3})}\left(\beta_{\bullet_3}V_{f_3}\right)$$

$$A_3 = A_2$$

$$A_4 = \frac{E_b(1-\nu_b)}{(1+\nu_b)(1-2\nu_b)}\left(1-\beta_{-\bullet}V_{f_1}-V_{f_2}-\beta_{-\bullet}V_{f_3}\right) + \frac{E_{f_1}(1-\nu_{f_1})}{(1+\nu_{f_1})(1-2\nu_{f_1})}\left(\beta_{\bullet_1}V_{f_1}\right)$$

$$+ \frac{E_{f_2}(1-\nu_{f_2})}{(1+\nu_{f_2})(1-2\nu_{f_2})}\left(V_{f_2}\right) + \frac{E_{f_3}(1-\nu_{f_3})}{(1+\nu_{f_3})(1-2\nu_{f_3})}\left(\beta_{\bullet_3}V_{f_3}\right)$$

$$A_5 = A_2$$

$$A_6 = \frac{E_b(1-\nu_b)}{(1+\nu_b)(1-2\nu_b)}\left(1-\beta_{-\bullet}V_{f_1}-\beta_{-\bullet}V_{f_2}-V_{f_3}\right) + \frac{E_{f_1}(1-\nu_{f_1})}{(1+\nu_{f_1})(1-2\nu_{f_1})}\left(\beta_{\bullet_1}V_{f_1}\right)$$

$$+ \frac{E_{f_2}(1-\nu_{f_2})}{(1+\nu_{f_2})(1-2\nu_{f_2})}\left(\beta_{\bullet_2}V_{f_2}\right) + \frac{E_{f_3}(1-\nu_{f_3})}{(1+\nu_{f_3})(1-2\nu_{f_3})}\left(V_{f_3}\right)$$

$$A_7 = G_b\left(1-\beta_{-\bullet}'V_{f_1}-\beta_{-\bullet}'V_{f_2}-\beta_{-\bullet}''V_{f_3}\right) + G_{f_1}\left(\beta_{\bullet_1}'V_{f_1}\right) + G_{f_2}\left(\beta_{\bullet_2}'V_{f_2}\right) + G_{f_3}\left(\beta_{\bullet_3}''V_{f_3}\right)$$

$$A_8 = G_b\left(1-\beta_{-\bullet}''V_{f_1}-\beta_{-\bullet}'V_{f_2}-\beta_{-\bullet}'V_{f_3}\right) + G_{f_1}\left(\beta_{\bullet_1}''V_{f_1}\right) + G_{f_2}\left(\beta_{\bullet_2}'V_{f_2}\right) + G_{f_3}\left(\beta_{\bullet_3}'V_{f_3}\right)$$

$$A_9 = G_b\left(1-\beta_{-\bullet}'V_{f_1}-\beta_{-\bullet}''V_{f_2}-\beta_{-\bullet}'V_{f_3}\right) + G_{f_1}\left(\beta_{\bullet_1}'V_{f_1}\right) + G_{f_2}\left(\beta_{\bullet_2}''V_{f_2}\right) + G_{f_3}\left(\beta_{\bullet_3}'V_{f_3}\right)$$

156

Table 13. - Equations for elastic constants for composites with reinforcing filaments in the 1 -2, 2- 3, and 1 -3 planes and at three sets of equal angles $(\pm\Theta_1, \pm\Theta_2,$ and $\pm\Theta_3)$ to the 1-, 2-, and 3- directions.

$$A_1 = \frac{E_b(1-\nu_b)}{(1+\nu_b)(1-2\nu_b)}\left\{1-V_{f_1}\left[\cos^4\Theta_1+\beta_{-\circ}\sin^4\Theta_1+\left(\nu_b\beta_{-\circ}+\{1-2\nu_b\}\beta_{-\circ}'\right)\left(\frac{2\sin^2\Theta_1\cos^2\Theta_1}{1-\nu_b}\right)\right]-\beta_{-\circ}V_{f_2}\right.$$

$$\left.-V_{f_3}\left[\sin^4\Theta_3+\beta_{-\circ}\cos^4\Theta_3+\left(\nu_b\beta_{-\circ}+\{1-2\nu_b\}\beta_{-\circ}'\right)\left(\frac{2\sin^2\Theta_3\cos^2\Theta_3}{1-\nu_b}\right)\right]\right\}$$

$$+\frac{E_{f_1}(1-\nu_{f_1})}{(1+\nu_{f_1})(1-2\nu_{f_1})}\left\{V_{f_1}\left[\cos^4\Theta_1+\beta_\circ\sin^4\Theta_1+\left(\nu_{f_1}\beta_\circ+\{1-2\nu_{f_1}\}\beta_\circ'\right)\left(\frac{2\sin^2\Theta_1\cos^2\Theta_1}{1-\nu_{f_1}}\right)\right]\right\}$$

$$+\frac{E_{f_2}(1-\nu_{f_2})}{(1+\nu_{f_2})(1-2\nu_{f_2})}\left(\beta_{\circ_2}V_{f_2}\right)+\frac{E_{f_3}(1-\nu_{f_3})}{(1+\nu_{f_3})(1-2\nu_{f_3})}\left\{V_{f_3}\left[\sin^4\Theta_3+\beta_{\circ_3}\cos^4\Theta_3+\left(\nu_{f_3}\beta_{\circ_3}+\{1-2\nu_{f_3}\}\beta_{\circ_3}'\right)\left(\frac{2\sin^2\Theta_3\cos^2\Theta_3}{1-\nu_{f_3}}\right)\right]\right\}$$

$$A_2 = \frac{\nu_b E_b}{(1+\nu_b)(1-2\nu_b)}\left\{1-V_{f_1}\left[\beta_{-\circ}\left(\sin^4\Theta_1+\cos^4\Theta_1\right)+\left(\{1-\nu_b\}\left\{\frac{1+\beta_{-\circ}}{2}\right\}+\{1-2\nu_b\}\beta_{-\circ}'\right)\left(\frac{2\sin^2\Theta_1\cos^2\Theta_1}{\nu_b}\right)\right]-\beta_{-\circ}V_{f_2}-\beta_{\circ_3}V_{f_3}\right\}$$

$$+\frac{\nu_{f_1}E_{f_1}}{(1+\nu_{f_1})(1-2\nu_{f_1})}\left\{V_{f_1}\left[\beta_{\circ_1}\left(\sin^4\Theta_1+\cos^4\Theta_1\right)+\left(\{1-\nu_{f_1}\}\left\{\frac{1+\beta_{\circ_1}}{2}\right\}+\{1-2\nu_{f_1}\}\beta_{\circ_1}'\right)\left(\frac{2\sin^2\Theta_1\cos^2\Theta_1}{\nu_{f_1}}\right)\right]\right\}$$

$$+\frac{\nu_{f_2}E_{f_2}}{(1+\nu_{f_2})(1-2\nu_{f_2})}\left(\beta_{\circ_2}V_{f_2}\right)+\frac{\nu_{f_3}E_{f_3}}{(1+\nu_{f_3})(1-2\nu_{f_3})}\left(\beta_{\circ_3}V_{f_3}\right)$$

$$A_3 = \frac{\nu_b E_b}{(1+\nu_b)(1-2\nu_b)}\left\{1-\beta_{-\circ}V_{f_1}-\beta_{-\circ}V_{f_2}-V_{f_3}\left[\beta_{-\circ}\left(\sin^4\Theta_3+\cos^4\Theta_3\right)+\left(\{1-\nu_b\}\left\{\frac{1+\beta_{-\circ}}{2}\right\}+\{1-2\nu_b\}\beta_{-\circ}'\right)\left(\frac{2\sin^2\Theta_3\cos^2\Theta_3}{\nu_b}\right)\right]\right\}$$

$$+\frac{\nu_{f_1}E_{f_1}}{(1+\nu_{f_1})(1-2\nu_{f_1})}\left(\beta_\circ V_{f_1}\right)+\frac{\nu_{f_2}E_{f_2}}{(1+\nu_{f_2})(1-2\nu_{f_2})}\left(\beta_{\circ_2}V_{f_2}\right)$$

$$+\frac{\nu_{f_3}E_{f_3}}{(1+\nu_{f_3})(1-2\nu_{f_3})}\left\{V_{f_3}\left[\beta_{\circ_3}\left(\sin^4\Theta_3+\cos^4\Theta_3\right)+\left(\{1-\nu_{f_3}\}\left\{\frac{1+\beta_{\circ_3}}{2}\right\}+\{1-2\nu_{f_3}\}\beta_{\circ_3}'\right)\left(\frac{2\sin^2\Theta_3\cos^2\Theta_3}{\nu_{f_3}}\right)\right]\right\}$$

157

Table 13.- Continued.

$$A_4 = \frac{E_b(1-\nu_b)}{(1+\nu_b)(1-2\nu_b)}\left\{1-V_{f_1}\left[\sin^4\theta_1+\beta_{-_0}\cos^4\theta_1+\left(\nu_b\beta_{-_0}+\{1-2\nu_b\}\beta'_{-_0}\right)\left(\frac{2\sin^2\theta_1\cos^2\theta_1}{1-\nu_b}\right)\right]\right.$$

$$\left.-V_{f_2}\left[\cos^4\theta_2+\beta_{-_0}\sin^4\theta_2+\left(\nu_b\beta_{-_0}+\{1-2\nu_b\}\beta'_{-_0}\right)\left(\frac{2\sin^2\theta_2\cos^2\theta_2}{1-\nu_b}\right)\right]-\beta_{-_0}V_{f_3}\right\}$$

$$+\frac{E_{f_1}(1-\nu_{f_1})}{(1+\nu_{f_1})(1-2\nu_{f_1})}\left\{V_{f_1}\left[\sin^4\theta_1+\beta_{0_1}\cos^4\theta_1+\left(\nu_{f_1}\beta_{0_1}+\{1-2\nu_{f_1}\}\beta'_{0_1}\right)\left(\frac{2\sin^2\theta_1\cos^2\theta_1}{1-\nu_{f_1}}\right)\right]\right\}$$

$$+\frac{E_{f_2}(1-\nu_{f_2})}{(1+\nu_{f_2})(1-2\nu_{f_2})}\left\{V_{f_2}\left[\cos^4\theta_2+\beta_{0_2}\sin^4\theta_2+\left(\nu_{f_2}\beta_{0_2}+\{1-2\nu_{f_2}\}\beta'_{0_2}\right)\left(\frac{2\sin^2\theta_2\cos^2\theta_2}{1-\nu_{f_2}}\right)\right]\right\}+\frac{E_{f_3}(1-\nu_{f_3})}{(1+\nu_{f_3})(1-2\nu_{f_3})}\left(\beta_{0_3}V_{f_3}\right)$$

$$A_5 = \frac{\nu_b E_b}{(1+\nu_b)(1-2\nu_b)}\left\{1-\beta_{-_0}V_{f_1}-V_{f_2}\left[\beta_{-_0}\left(\sin^4\theta_2+\cos^4\theta_2\right)+\left(\{1-\nu_b\}\left\{\frac{1+\beta_{-_0}}{2}\right\}+\{1-2\nu_b\}\beta'_{-_0}\right)\left(\frac{2\sin^2\theta_2\cos^2\theta_2}{\nu_b}\right)\right]-\beta_{-_0}V_{f_3}\right\}$$

$$+\frac{\nu_{f_1}E_{f_1}}{(1+\nu_{f_1})(1-2\nu_{f_1})}\left(\beta_{0_1}V_{f_1}\right)+\frac{\nu_{f_2}E_{f_2}}{(1+\nu_{f_2})(1-2\nu_{f_2})}\left\{V_{f_2}\left[\beta_{0_2}\left(\sin^4\theta_2+\cos^4\theta_2\right)+\left(\{1-\nu_{f_2}\}\left\{\frac{1+\beta_{0_2}}{2}\right\}+\{1-2\nu_{f_2}\}\beta'_{0_2}\right)\left(\frac{2\sin^2\theta_2\cos^2\theta_2}{\nu_{f_2}}\right)\right]\right\}$$

$$+\frac{\nu_{f_3}E_{f_3}}{(1+\nu_{f_3})(1-2\nu_{f_3})}\left(\beta_{0_3}V_{f_3}\right)$$

$$A_6 = \frac{E_b(1-\nu_b)}{(1+\nu_b)(1-2\nu_b)}\left\{1-\beta_{-_0}V_{f_1}-V_{f_2}\left[\sin^4\theta_2+\beta_{-_0}\cos^4\theta_2+\left(\nu_b\beta_{-_0}+\{1-2\nu_b\}\beta'_{-_0}\right)\left(\frac{2\sin^2\theta_2\cos^2\theta_2}{1-\nu_b}\right)\right]\right.$$

$$\left.-V_{f_3}\left[\cos^4\theta_3+\beta_{-_0}\sin^4\theta_3+\left(\nu_b\beta_{-_0}+\{1-2\nu_b\}\beta'_{-_0}\right)\left(\frac{2\sin^2\theta_3\cos^2\theta_3}{1-\nu_b}\right)\right]\right\}$$

$$+\frac{E_{f_1}(1-\nu_{f_1})}{(1+\nu_{f_1})(1-2\nu_{f_1})}\left(\beta_{0_1}V_{f_1}\right)+\frac{E_{f_2}(1-\nu_{f_2})}{(1+\nu_{f_2})(1-2\nu_{f_2})}\left\{V_{f_2}\left[\sin^4\theta_2+\beta_{0_2}\cos^4\theta_2+\left(\nu_{f_2}\beta_{0_2}+\{1-2\nu_{f_2}\}\beta'_{0_2}\right)\left(\frac{2\sin^2\theta_2\cos^2\theta_2}{1-\nu_{f_2}}\right)\right]\right\}$$

$$+\frac{E_{f_3}(1-\nu_{f_3})}{(1+\nu_{f_3})(1-2\nu_{f_3})}\left\{V_{f_3}\left[\cos^4\theta_3+\sin^4\theta_3+\left(\nu_{f_3}\beta_{0_3}+\{1-2\nu_{f_3}\}\beta'_{0_3}\right)\left(\frac{2\sin^2\theta_3\cos^2\theta_3}{1-\nu_{f_3}}\right)\right]\right\}$$

Table 13. - Concluded.

$$A_7 = \frac{E_b(1-\nu_b)}{(1+\nu_b)(1-2\nu_b)}\left\{\frac{1-2\nu_b}{2(1-\nu_b)} - V_{f_1}\left[\left(1+\left\{\frac{1-3\nu_b}{1-\nu_b}\right\}\beta_{-\bullet}\right)\sin^2\theta_1\cos^2\theta_1 + \left(\frac{1-2\nu_b}{2\{1-\nu_b\}}\right)\beta'_{-\bullet}\cos^2 2\theta_1\right]\right.$$

$$\left. -\left[\frac{1-2\nu_b}{2(1-\nu_b)}\right]\left[V_{f_2}\left(\beta'_{-\bullet}\cos^2\theta_2+\beta''_{-\bullet}\sin^2\theta_2\right)+V_{f_3}\left(\beta'_{-\bullet}\sin^2\theta_3+\beta''_{-\bullet}\cos^2\theta_3\right)\right]\right\}$$

$$+\frac{E_{f_1}(1-\nu_{f_1})}{(1+\nu_{f_1})(1-2\nu_{f_1})}\left\{V_{f_1}\left[\left(1+\left\{\frac{1-3\nu_{f_1}}{1-\nu_{f_1}}\right\}\beta_{\bullet}\right)\sin^2\theta_1\cos^2\theta_1+\left(\frac{1-2\nu_{f_1}}{2\{1-\nu_{f_1}\}}\right)\beta'_{\bullet_1}\cos^2 2\theta_1\right]\right\}$$

$$+\frac{E_{f_2}}{2(1+\nu_{f_2})}\left\{V_{f_2}\left[\beta'_{\bullet_2}\cos^2\theta_2+\beta''_{\bullet_2}\sin^2\theta_2\right]\right\}+\frac{E_{f_3}}{2(1+\nu_{f_3})}\left\{V_{f_3}\left[\beta'_{\bullet_3}\sin^2\theta_3+\beta''_{\bullet_3}\cos^2\theta_3\right]\right\}$$

$$A_8 = \frac{E_b(1-\nu_b)}{(1+\nu_b)(1-2\nu_b)}\left\{\frac{1-2\nu_b}{2(1-\nu_b)}\left[1-V_{f_1}\left(\beta'_{-\bullet}\sin^2\theta_1+\beta''_{-\bullet}\cos^2\theta_1\right)\right]\right.$$

$$\left. -V_{f_2}\left[\left(1+\left\{\frac{1-3\nu_b}{1-\nu_b}\right\}\beta_{-\bullet}\right)\sin^2\theta_2\cos^2\theta_2+\left(\frac{1-2\nu_b}{2\{1-\nu_b\}}\right)\beta'_{-\bullet}\cos^2 2\theta_2\right]-\left[\frac{1-2\nu_b}{2(1-\nu_b)}\right]\left[V_{f_3}\left(\beta'_{-\bullet}\cos^2\theta_3+\beta''_{-\bullet}\sin^2\theta_3\right)\right]\right\}$$

$$+\frac{E_{f_1}}{2(1+\nu_{f_1})}\left\{V_{f_1}\left[\beta'_{\bullet_1}\sin^2\theta_1+\beta''_{\bullet_1}\cos^2\theta_1\right]\right\}+\frac{E_{f_2}(1-\nu_{f_2})}{(1+\nu_{f_2})(1-2\nu_{f_2})}\left\{V_{f_2}\left[\left(1+\left\{\frac{1-3\nu_{f_2}}{1-\nu_{f_2}}\right\}\beta_{\bullet_2}\right)\sin^2\theta_2\cos^2\theta_2+\left(\frac{1-2\nu_{f_2}}{2(1-\nu_{f_2})}\right)\beta'_{\bullet_2}\cos^2 2\theta_2\right]\right\}$$

$$+\frac{E_{f_3}}{2(1+\nu_{f_3})}\left\{V_{f_3}\left[\beta'_{\bullet_3}\cos^2\theta_3+\beta''_{\bullet_3}\sin^2\theta_3\right]\right\}$$

$$A_9 = \frac{E_b(1-\nu_b)}{(1+\nu_b)(1-2\nu_b)}\left\{\frac{1-2\nu_b}{2(1-\nu_b)}\left[1-V_{f_1}\left(\beta'_{-\bullet}\cos^2\theta_1+\beta''_{-\bullet}\sin^2\theta_1\right)-V_{f_2}\left(\beta'_{-\bullet}\sin^2\theta_2+\beta''_{-\bullet}\cos^2\theta_2\right)\right]\right.$$

$$\left. -V_{f_3}\left[\left(1+\left\{\frac{1-3\nu_b}{1-\nu_b}\right\}\beta_{-\bullet}\right)\sin^2\theta_3\cos^2\theta_3+\left(\frac{1-2\nu_b}{2\{1-\nu_b\}}\right)\beta'_{-\bullet}\cos^2 2\theta_3\right]\right\}$$

$$+\frac{E_{f_1}}{2(1+\nu_{f_1})}\left\{V_{f_1}\left[\beta'_{\bullet_1}\cos^2\theta_1+\beta''_{\bullet_1}\sin^2\theta_1\right]\right\}+\frac{E_{f_2}}{2(1+\nu_{f_2})}\left\{V_{f_2}\left[\beta'_{\bullet_2}\sin^2\theta_2+\beta''_{\bullet_2}\cos^2\theta_2\right]\right\}$$

$$+\frac{E_{f_3}(1-\nu_{f_3})}{(1+\nu_{f_3})(1-2\nu_{f_3})}\left\{V_{f_3}\left[\left(1+\left\{\frac{1-3\nu_{f_3}}{1-\nu_{f_3}}\right\}\beta_{\bullet_3}\right)\sin^2\theta_3\cos^2\theta_3+\left(\frac{1-2\nu_{f_3}}{2(1-2\nu_{f_3})}\right)\beta'_{\bullet_3}\cos^2 2\theta_3\right]\right\}$$

Table 14. - Generalized equations for elastic constants, like those of
Table 1 but with a variety of transverse effectiveness factors.

$$A_1 = \frac{E_b(1-\nu_b)}{(1+\nu_b)(1-2\nu_b)}(1-\beta_{\bullet_L}\,\nu_f) + \frac{E_f(1-\nu_f)}{(1+\nu_f)(1-2\nu_f)}(\beta_{\bullet_L}\,\nu_f)$$

$$A_2 = \frac{\nu_b E_b}{(1+\nu_b)(1-2\nu_b)}(1-\beta_{\bullet_{LT}}\,\nu_f) + \frac{\nu_f E_f}{(1+\nu_f)(1-2\nu_f)}(\beta_{\bullet_{LT}}\,\nu_f)$$

$$A_3 = A_2$$

$$A_4 = \frac{E_b(1-\nu_b)}{(1+\nu_b)(1-2\nu_b)}(1-\beta_{\bullet_T}\,\nu_f) + \frac{E_f(1-\nu_f)}{(1+\nu_f)(1-2\nu_f)}(\beta_{\bullet_T}\,\nu_f)$$

$$A_5 = \frac{\nu_b E_b}{(1+\nu_b)(1-2\nu_b)}(1-\beta_{\bullet_G}\,\nu_f) + \frac{\nu_f E_f}{(1+\nu_f)(1-2\nu_f)}(\beta_{\bullet_G}\,\nu_f)$$

$$A_6 = A_4$$

$$A_7 = G_b(1-\beta'_{\bullet}\,\nu_f) + G_f(\beta'_{\bullet}\,\nu_f)$$

$$A_8 = G_b(1-\beta''_{\bullet}\,\nu_f) + G_f(\beta''_{\bullet}\,\nu_f)$$

$$A_9 = A_7$$

$$(\beta_{\bullet} = \beta_{\bullet_T} \neq \beta_{\bullet_L} \neq \beta_{\bullet_{LT}} \neq \beta_{\bullet_G})$$

Table 15. - Interrelationships among elastic constants for use in evaluations of the various β's of Table 14.

$$A_1 = E_1 \left[\frac{1 - \nu_{23}}{1 - \nu_{23} - 2\nu_{12}\nu_{21}} \right]$$

$$A_2 = \frac{\nu_{21}E_2}{1 - \nu_{23} - 2\nu_{12}\nu_{21}}$$

$$A_3 = A_2$$

$$A_4 = \frac{E_2\left(1 - \nu_{12}\nu_{21}\right)}{\left(1 - \nu_{23} - 2\nu_{12}\nu_{21}\right)\left(1 + \nu_{23}\right)}$$

$$A_5 = A_4 - 2A_8$$

$$A_6 = A_4$$

$$A_7 = G_{12}$$

$$A_8 = G_{23}$$

$$A_9 = A_7$$

TABLE 16.-VALUES OF STRESS CONCENTRATION FACTOR FOR PHOTO-ELASTIC SPECIMENS

v_f	SPECIMEN	STRESS CONCENTRATION FACTOR		
		@0°[1]	45°	90°
0.30	Round Holes	-14.5	19	11.3
	Round Inclusions	0.5	1.4	0.6
.50	Round Holes	- 6.5	6.4	5.4
	Round Inclusions	0.5	1.6	0.5
	Elliptical Holes	-1.0	+2.7[2]	+1.3
	Elliptical Inclusions	0.4	0.5	0.1
.70	Round Holes	-2.7	2.6	3.7
	Round Inclusions	--	--	--

[1] On axis of load and holes

[2] Max. value
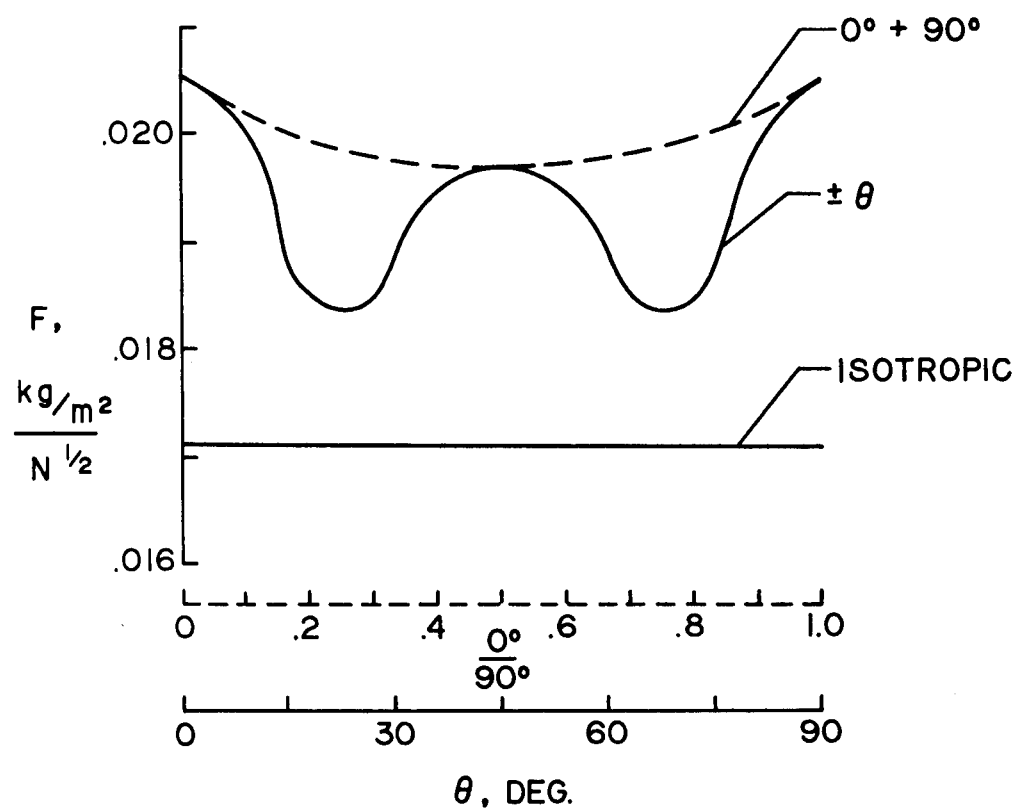
Figure 1. Variation of Elastic Structural Efficiency of Biaxial Laminates of E-Glass Fibers in an Epoxy Matrix
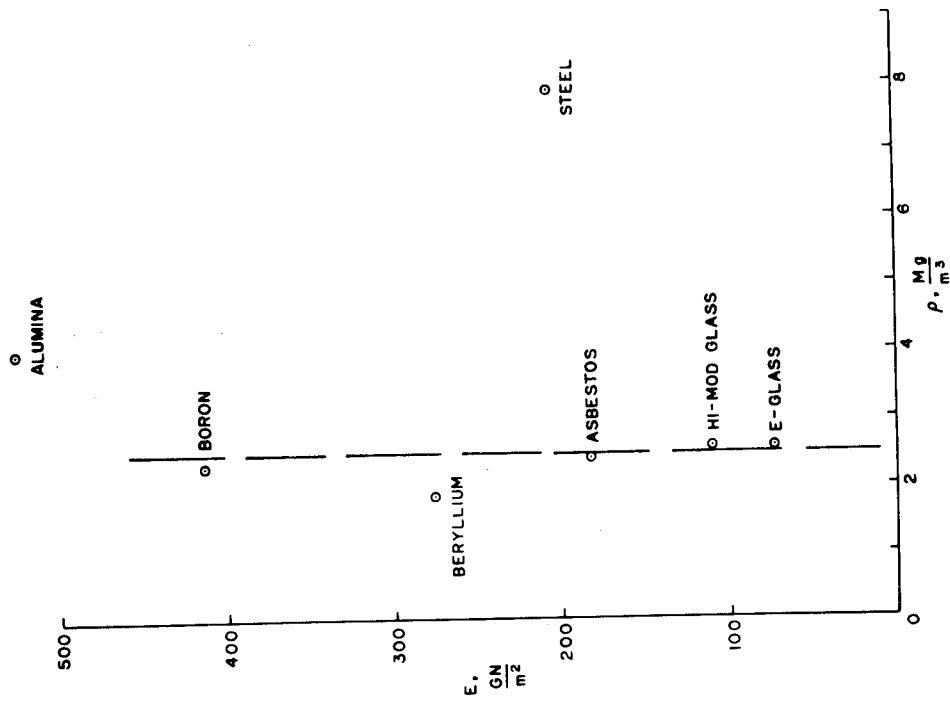
(b) Fiber Materials
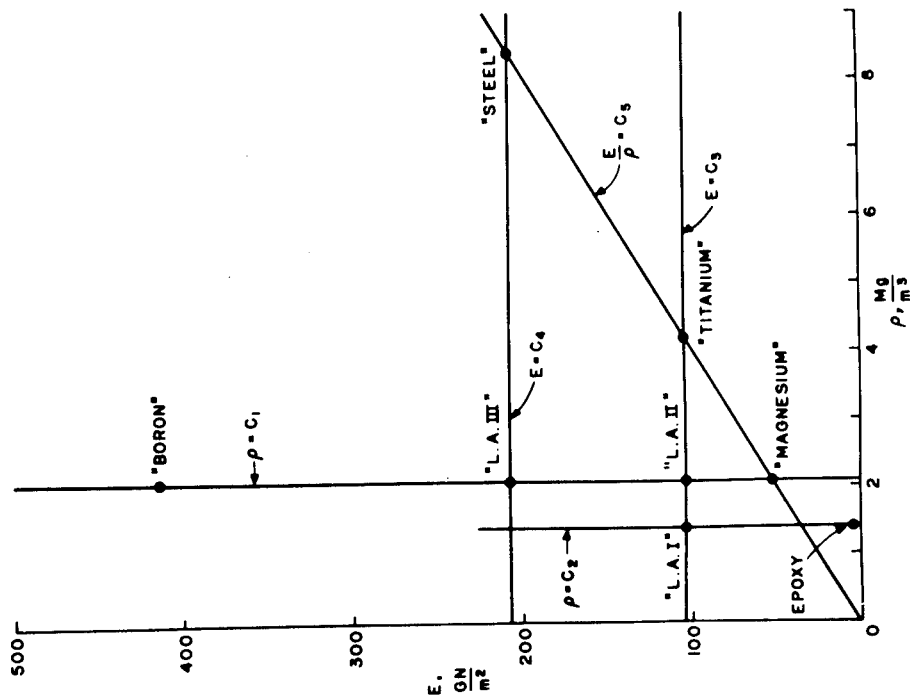
(a) Matrix Materials

Figure 2. Moduli and Densities of Matrix and Fiber Materials Studied
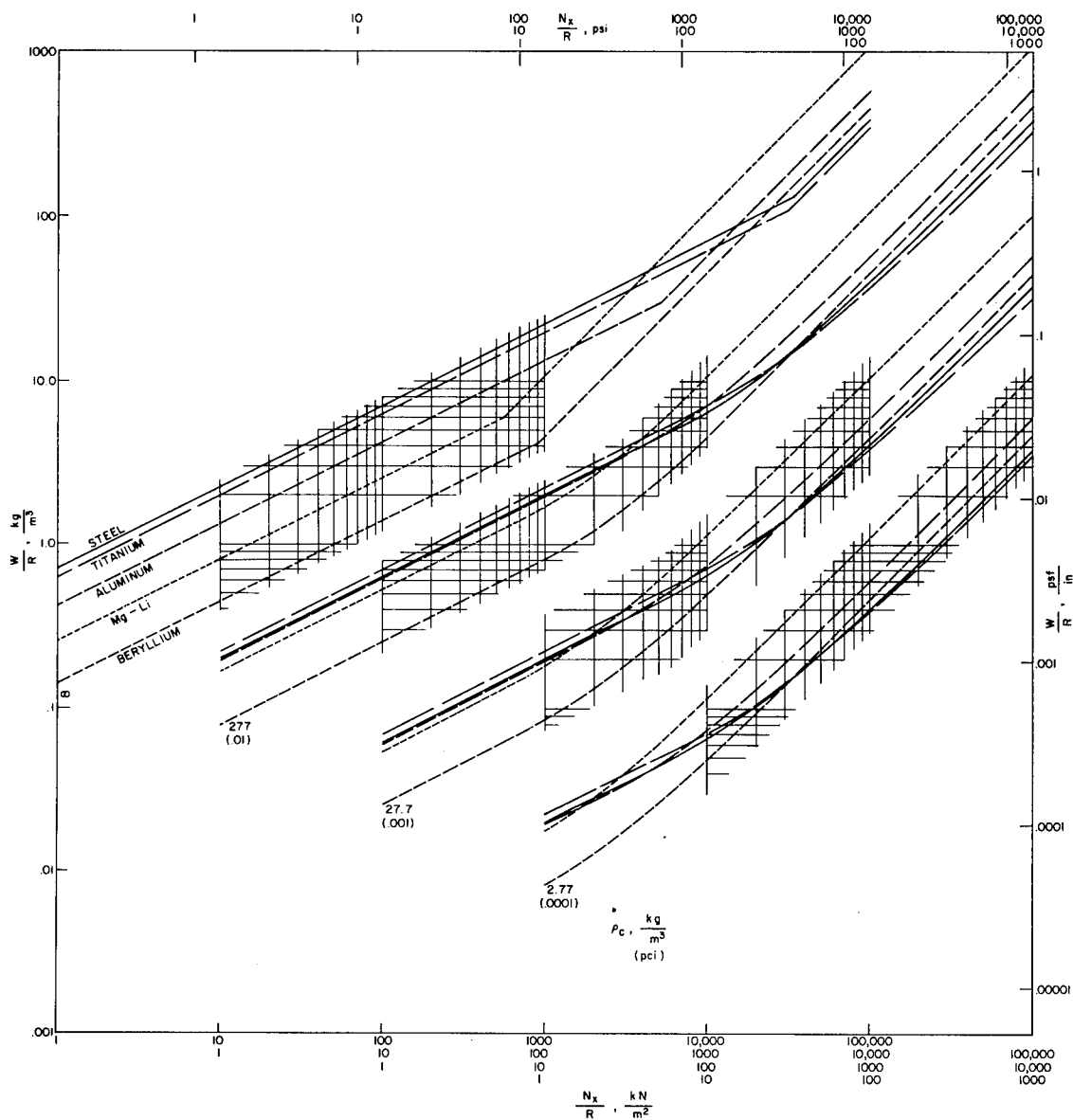
Figure 3. Reference Weight-Efficiencies of Idealized, Metal-Faced Sandwich,
Cylindrical Shells for Various Intensities of Axial Loading and
Various Densities of Hypothetical, Ideal Core Material
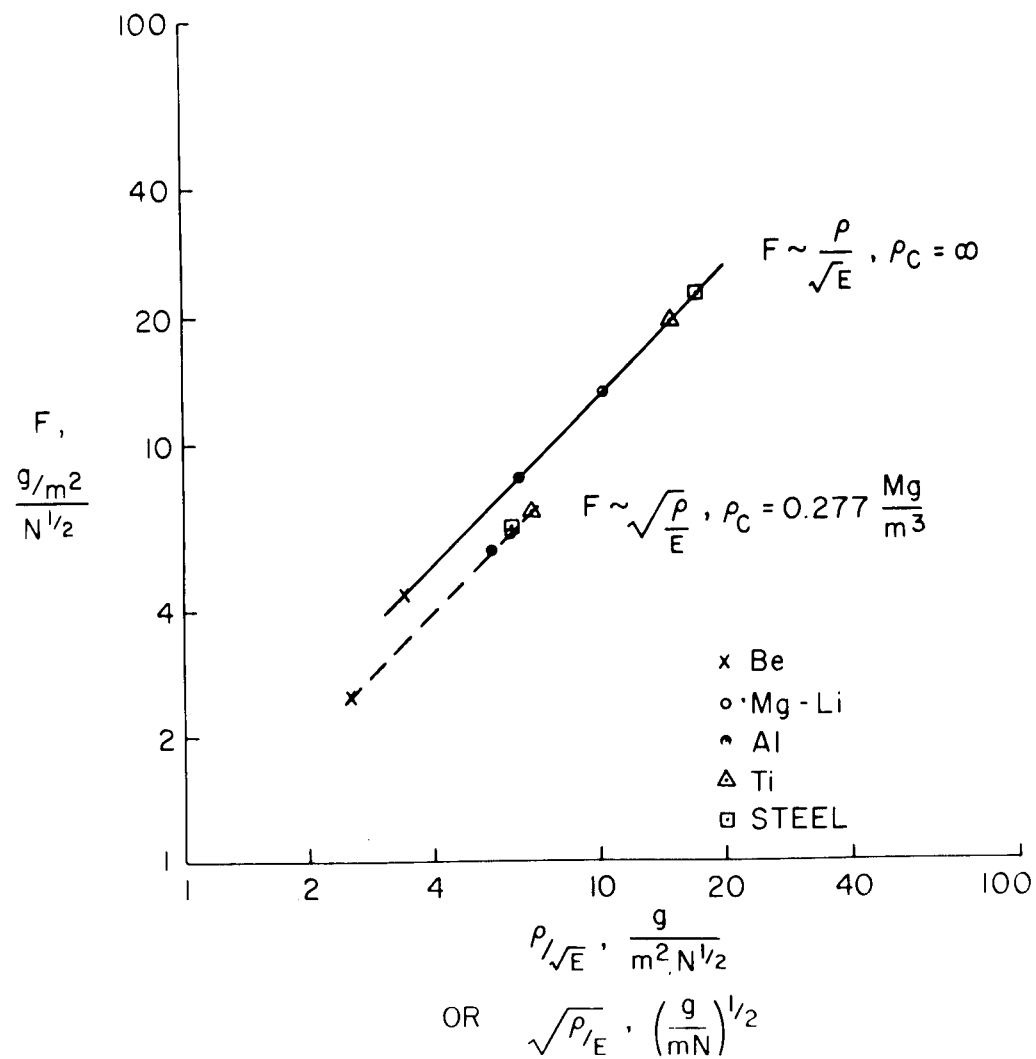
Figure 4. Elastic Buckling Efficiency of Metallic Monocoque and Sandwich Shells as a Function of Shell Material Properties
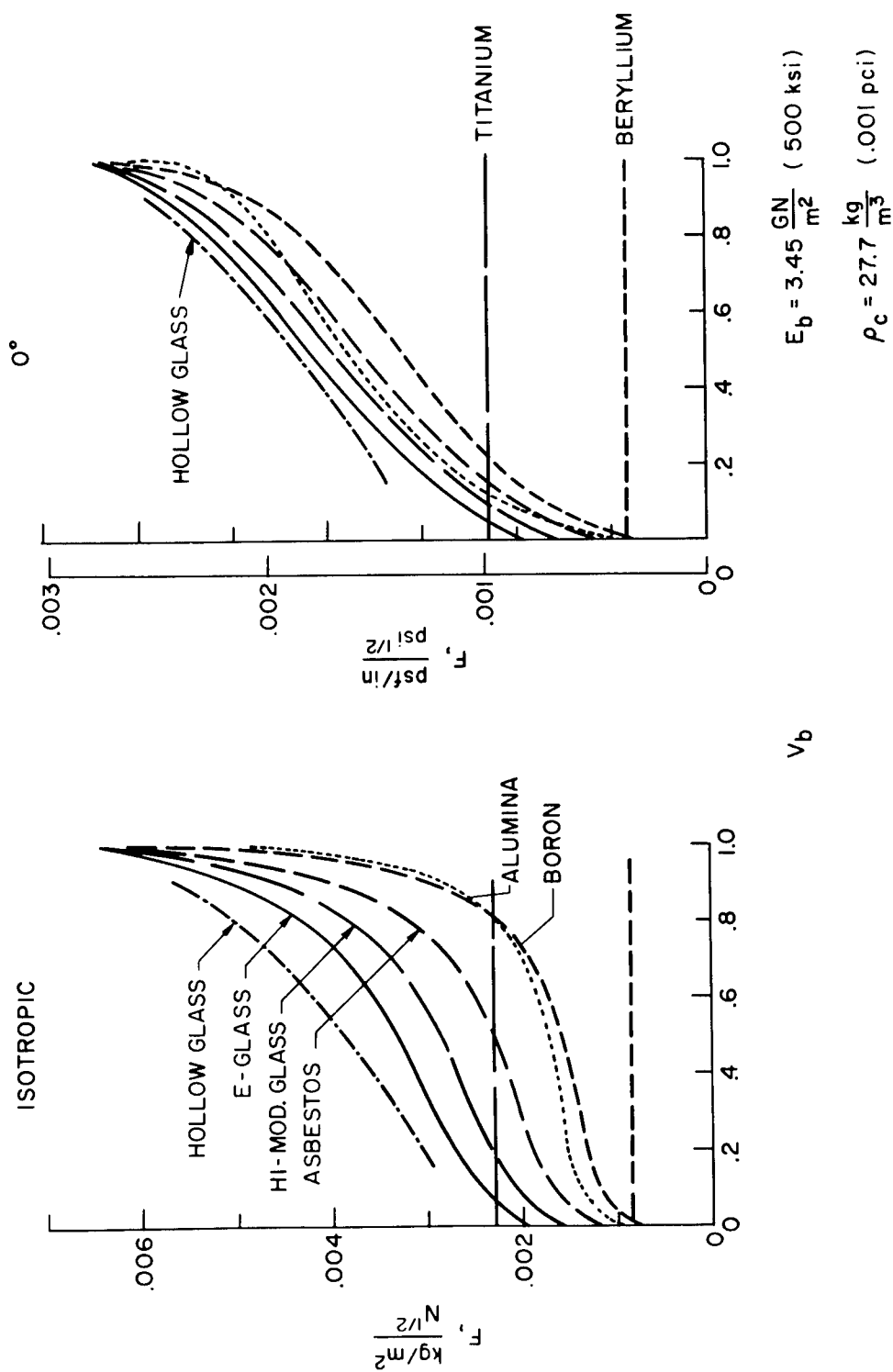
Figure 5. Elastic Buckling Efficiencies of Epoxy-Composite Sandwich Shells, and Comparison with Metal Efficiencies

167
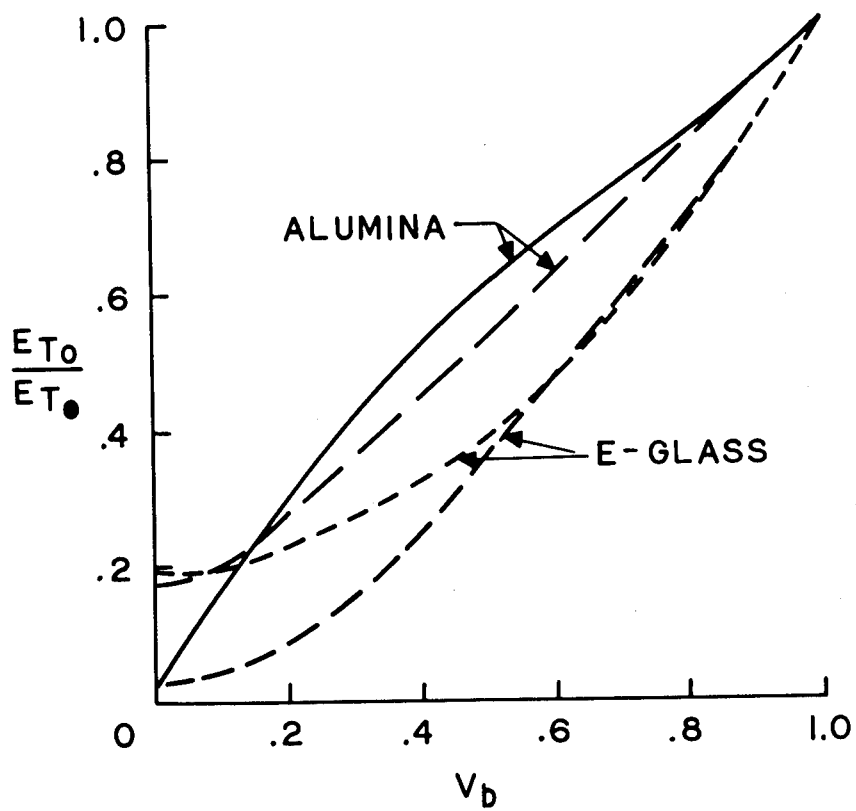
Figure 6. Ratio of Bounds for the Transverse Elastic Moduli of Hollow and Solid Fiber Composites
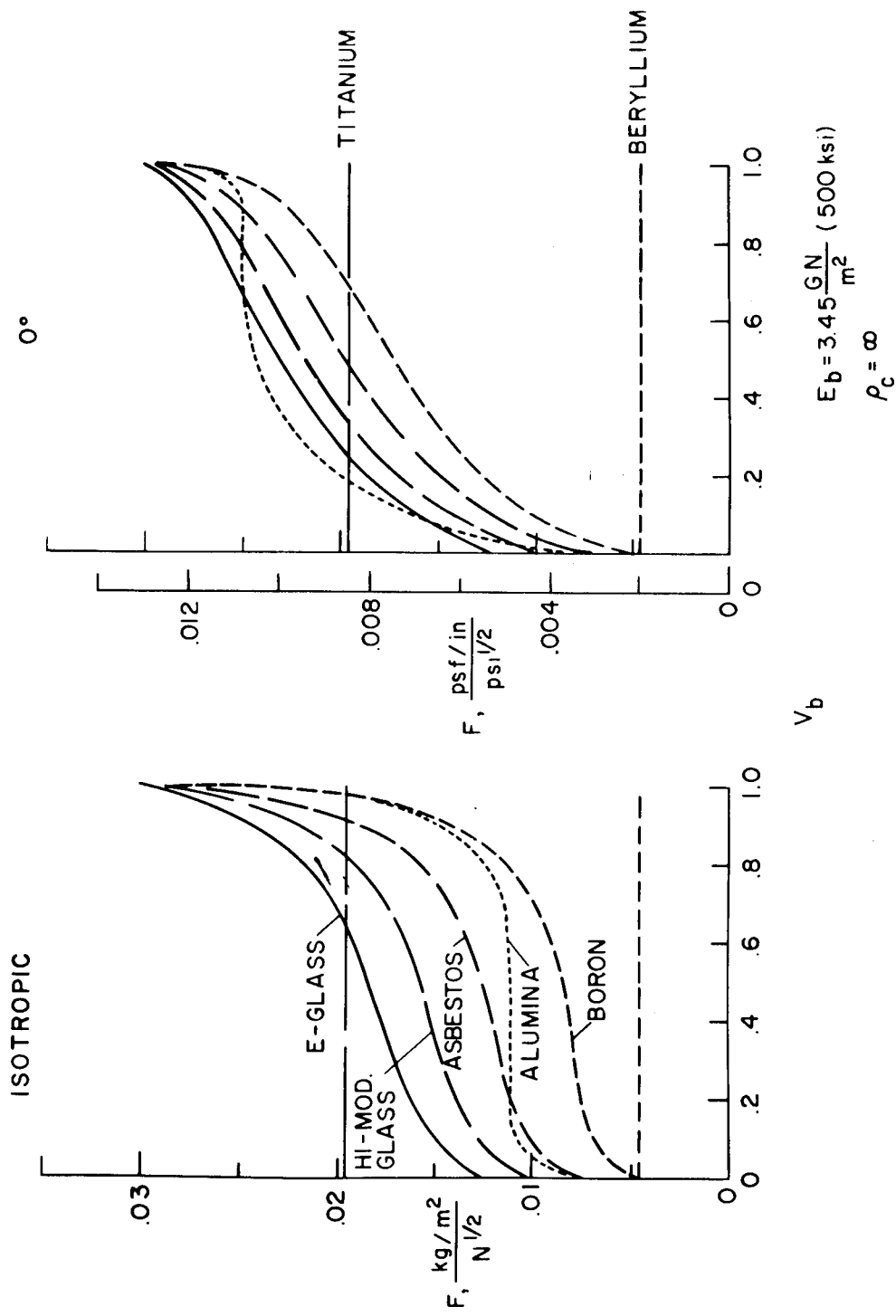
Figure 7. Elastic Buckling Efficiencies of Epoxy-Composite Monocoque Shells, and Comparison with Metal Efficiencies

169
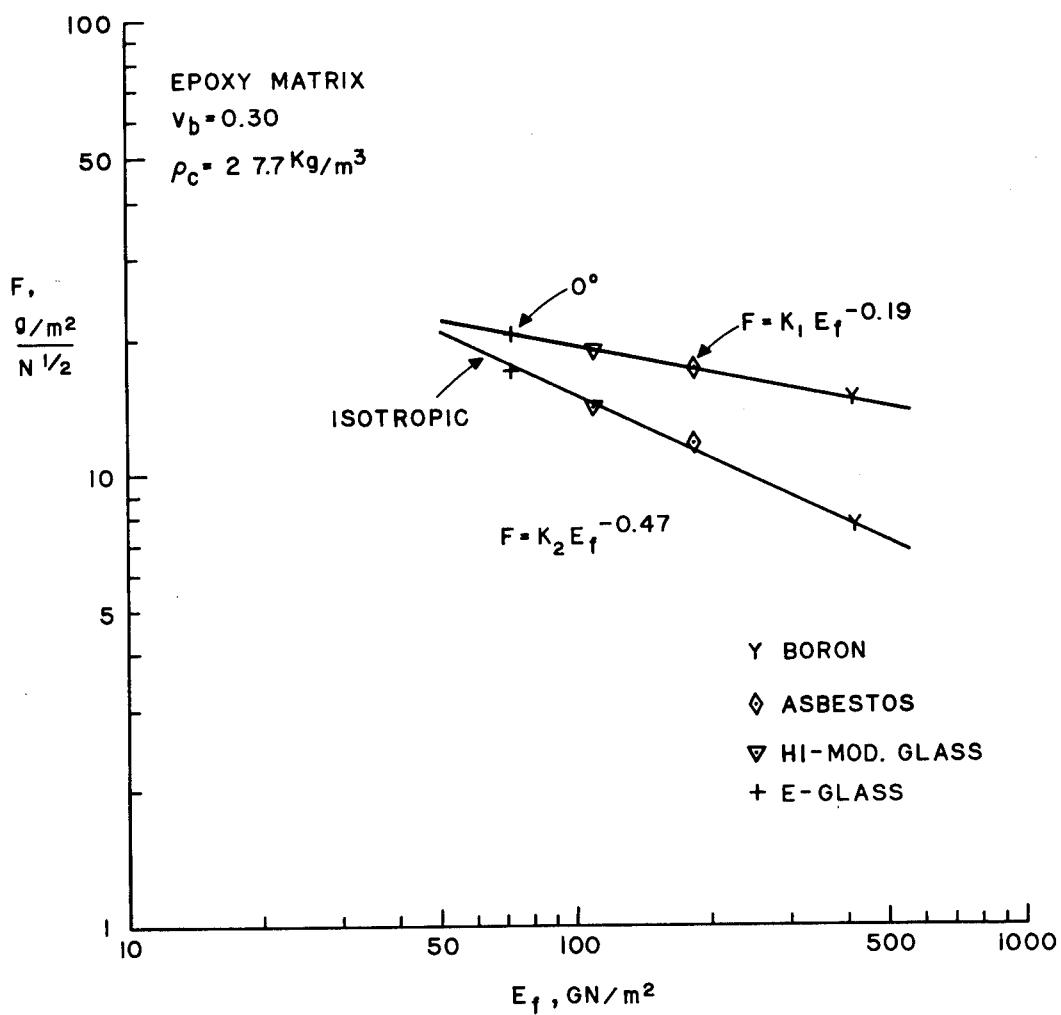
Figure 8. Elastic Buckling Efficiency of Epoxy Composite Sandwich Shells as a Function of Fiber Modulus
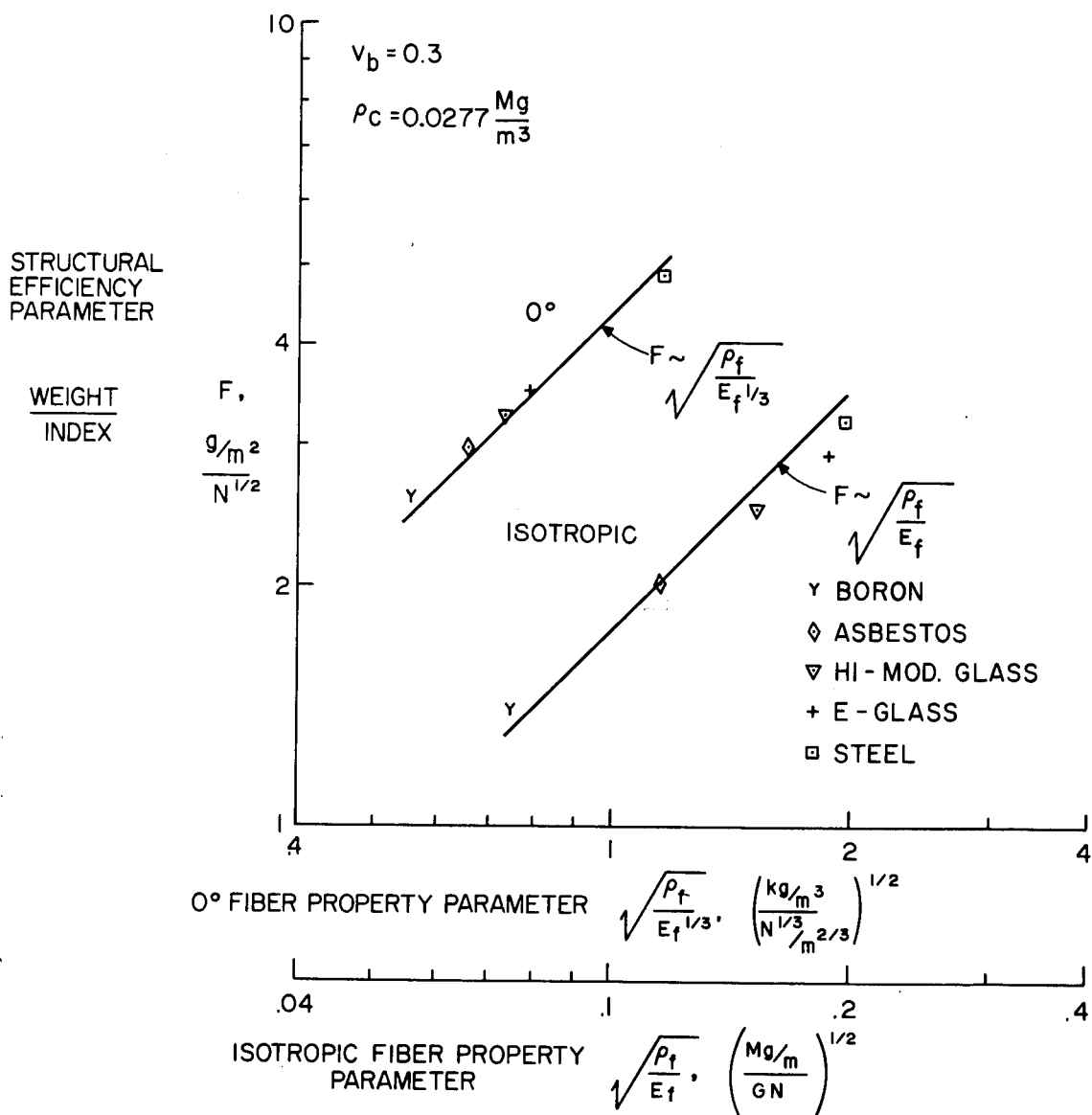
Figure 9.   Elastic Buckling Efficiency of Fiber-Epoxy Composite Sandwich
Shells as a Function of Fiber Properties
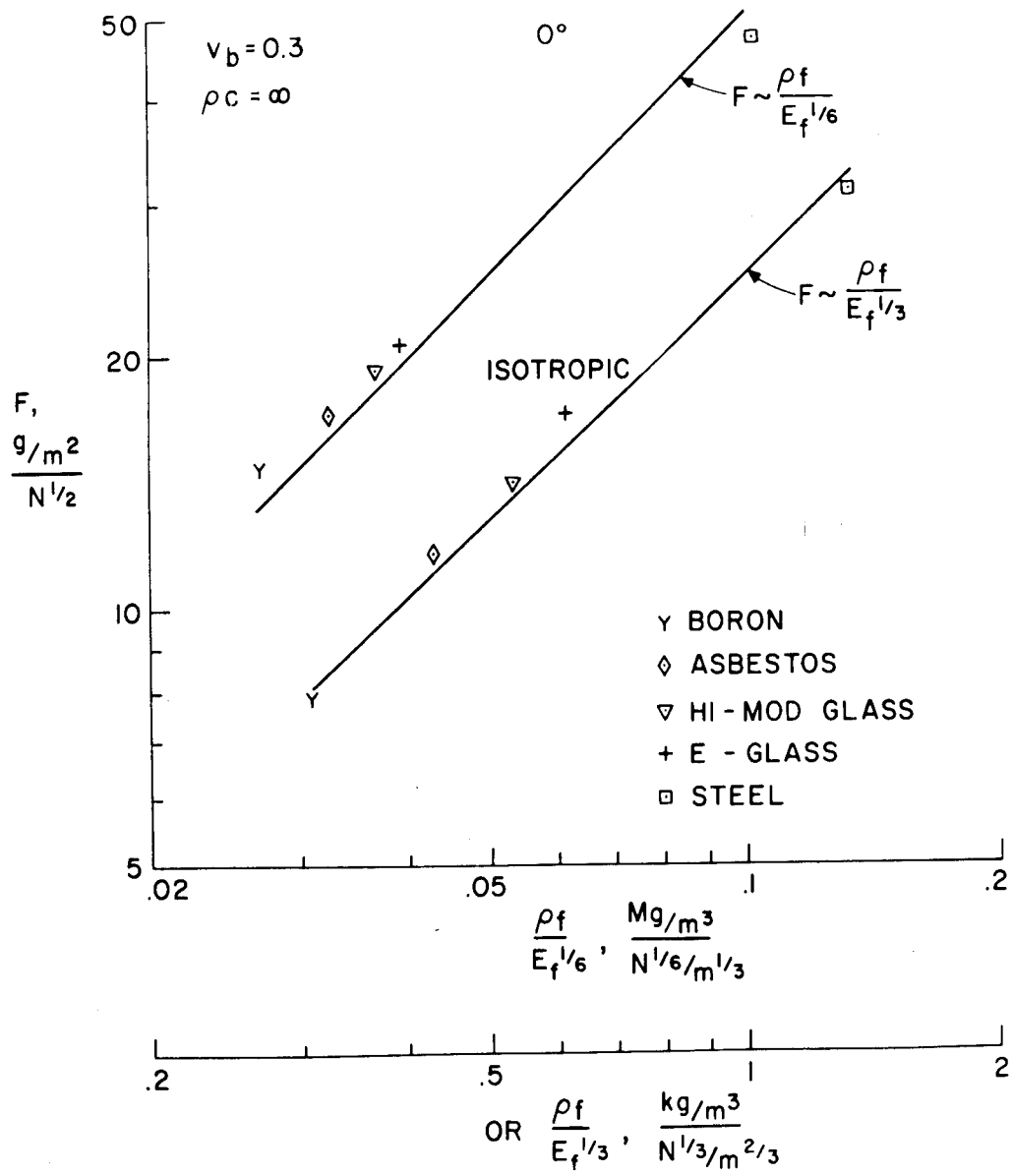
Figure 10. Elastic Buckling Efficiency of Fiber-Epoxy Composite Monocoque Shells as a Function of Fiber Properties
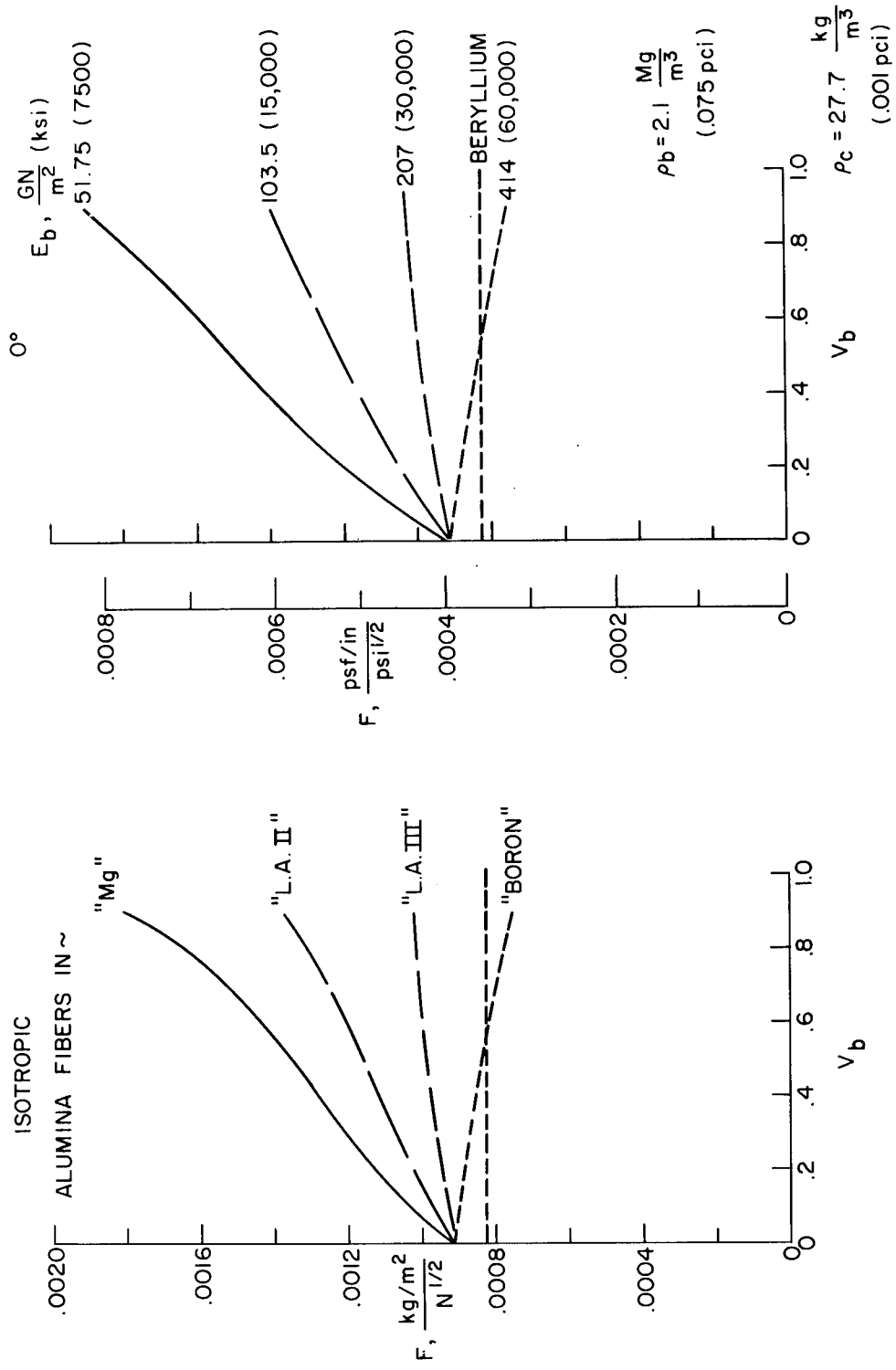
Figure 11. Elastic Buckling Efficiencies of Alumina-Fiber Reinforced Composite Sandwich Shells with Various Binders, and Comparison with Beryllium
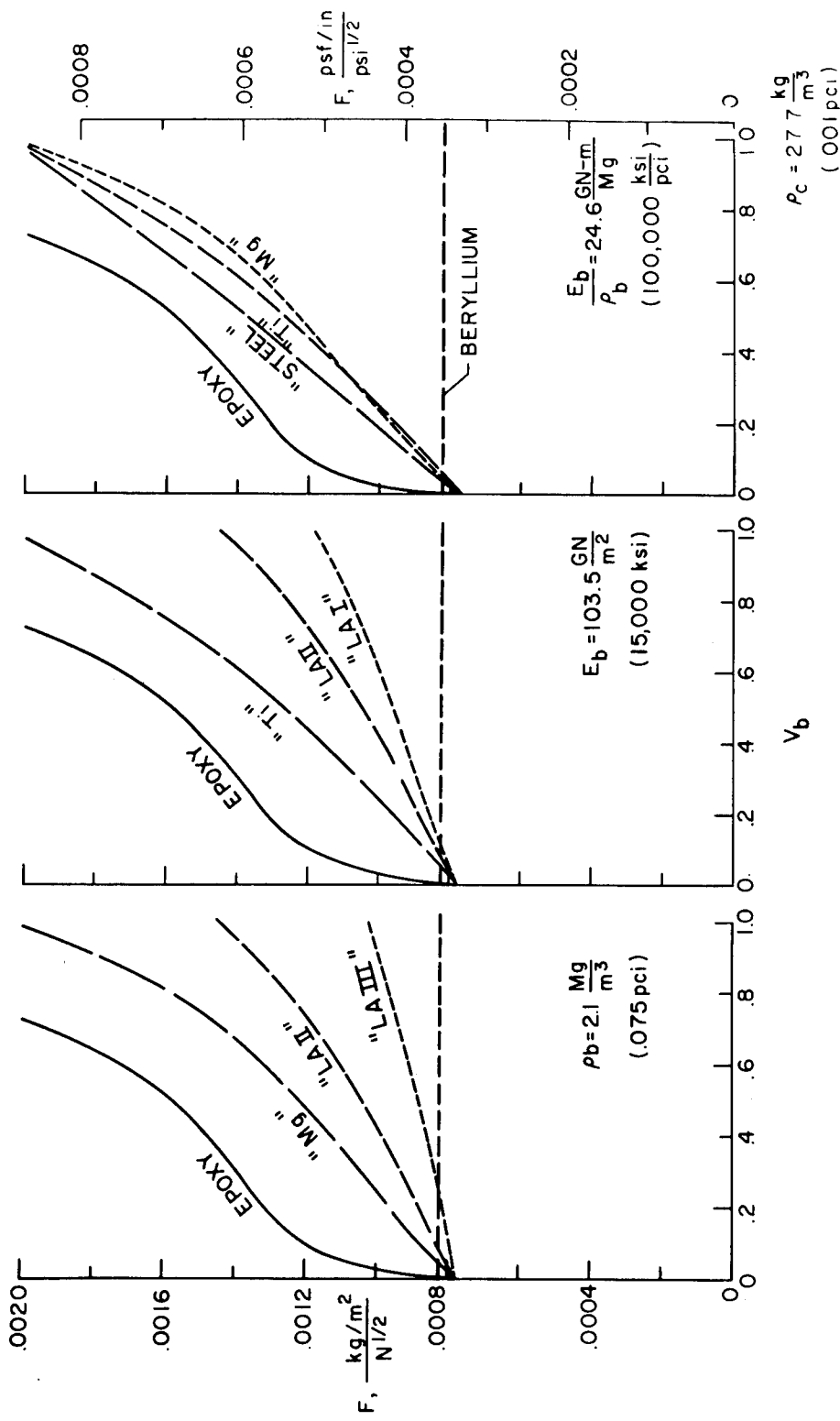
Figure 12. Effects of Variation in Binder Properties on Elastic Buckling Efficiency of $\pm$ 30°, 90° Boron Filament Reinforced Composite Sandwich Shells
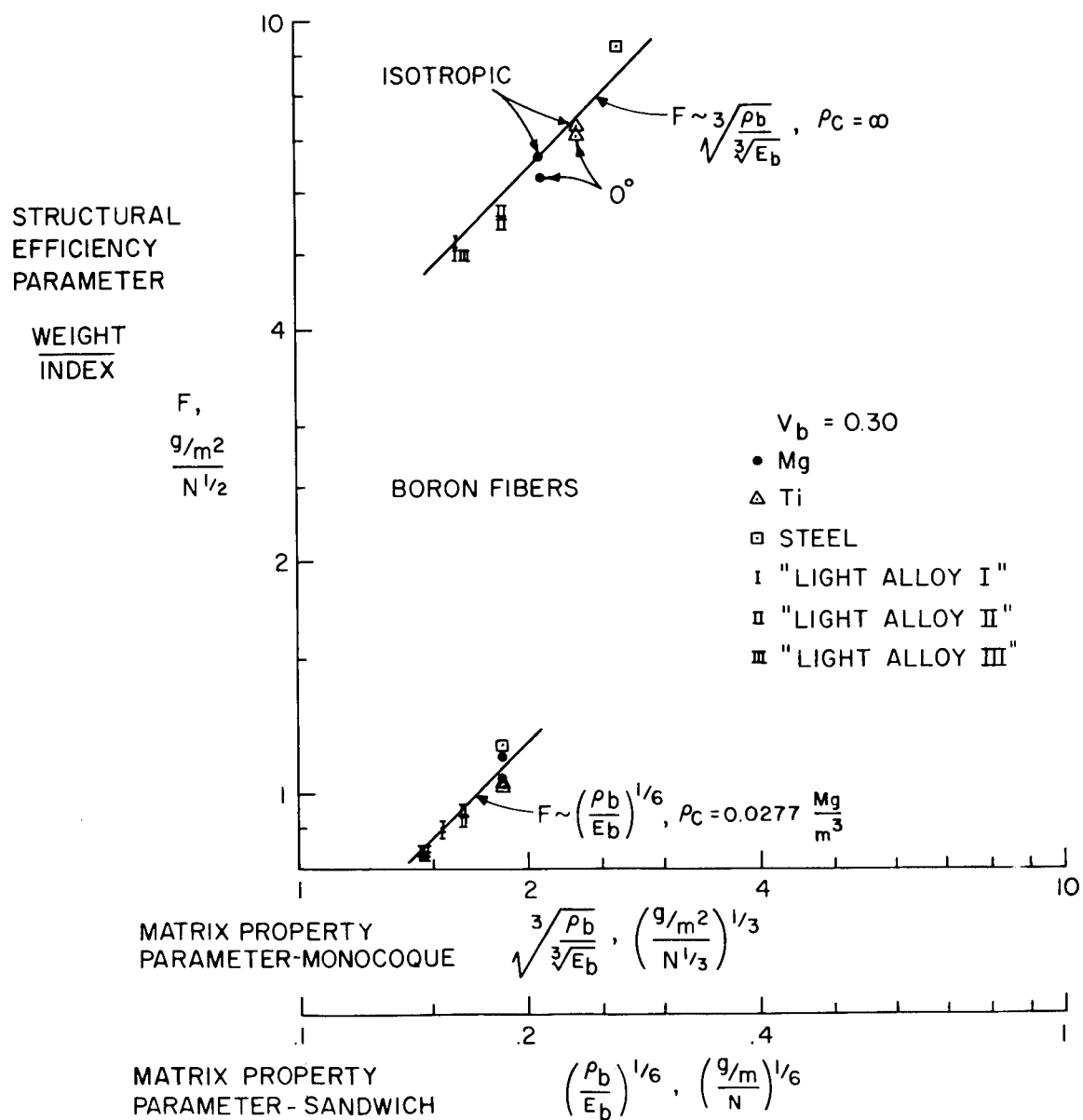
Figure 13. Elastic Buckling Efficiency of Fiber-Epoxy Composite Monocoque and Sandwich Shells as a Function of Binder Properties

CROSS - SECTION GEOMETRY
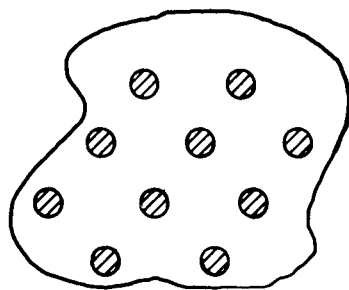
HEXAGONAL
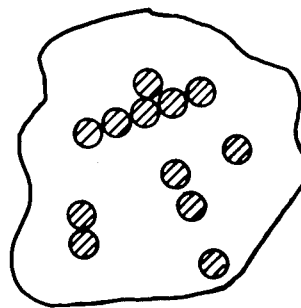
REAL
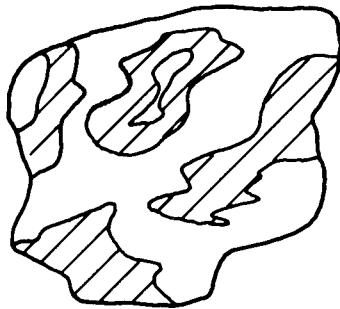
ARBITRARY
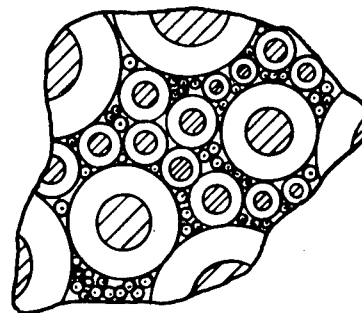
SPECIAL

Figure 14. Cross-sections of Uniaxial Fiber Composites Transverse to the Fiber Axes
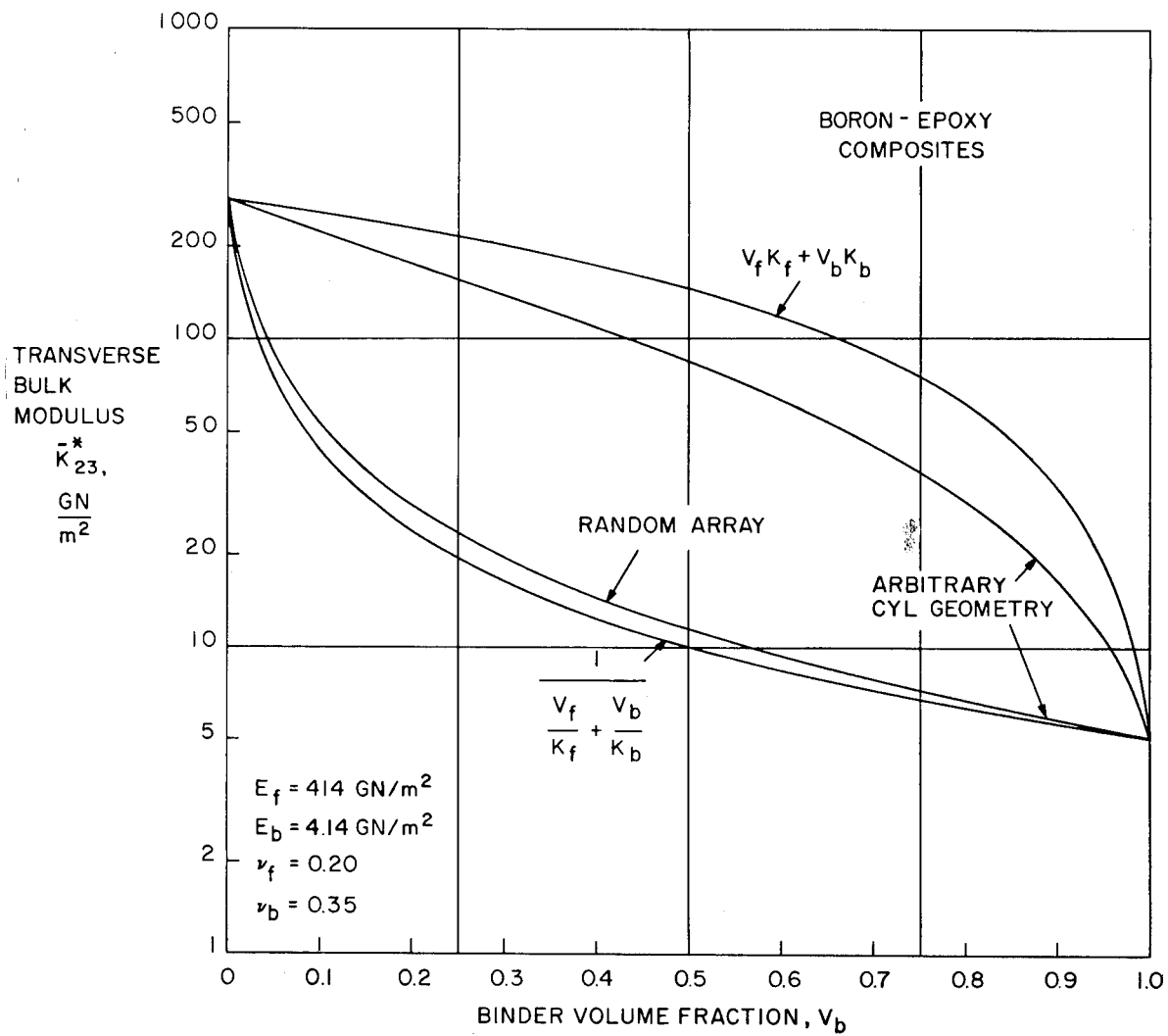
Figure 15. Analytical Bounds on the Transverse Plane Strain Bulk Modulus, $K_{23}{}^*$

177
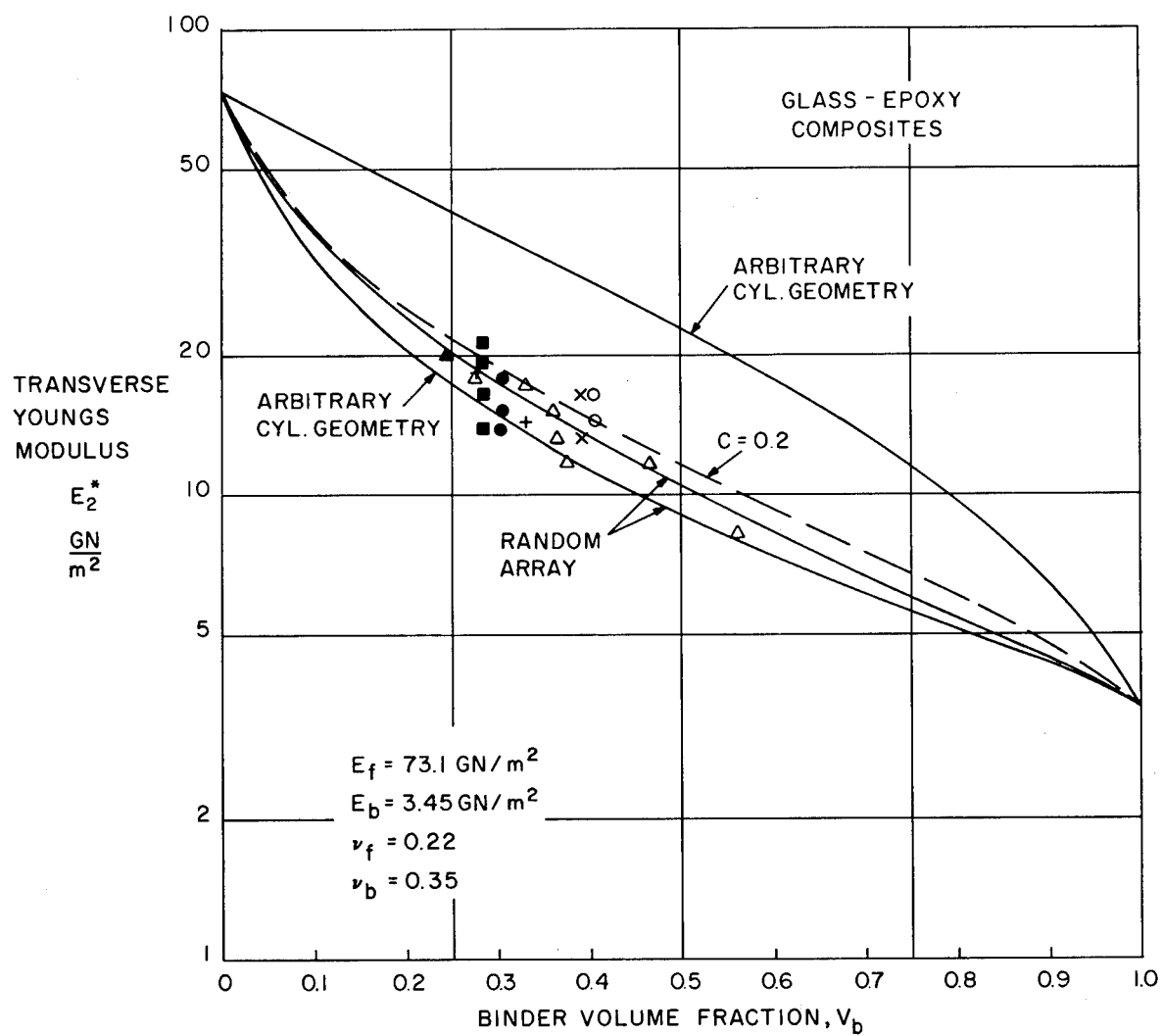
Figure 16. Transverse Young's Modulus, E_2^*, of Glass Reinforced
Epoxy–Comparison of Theory and Experiment

178
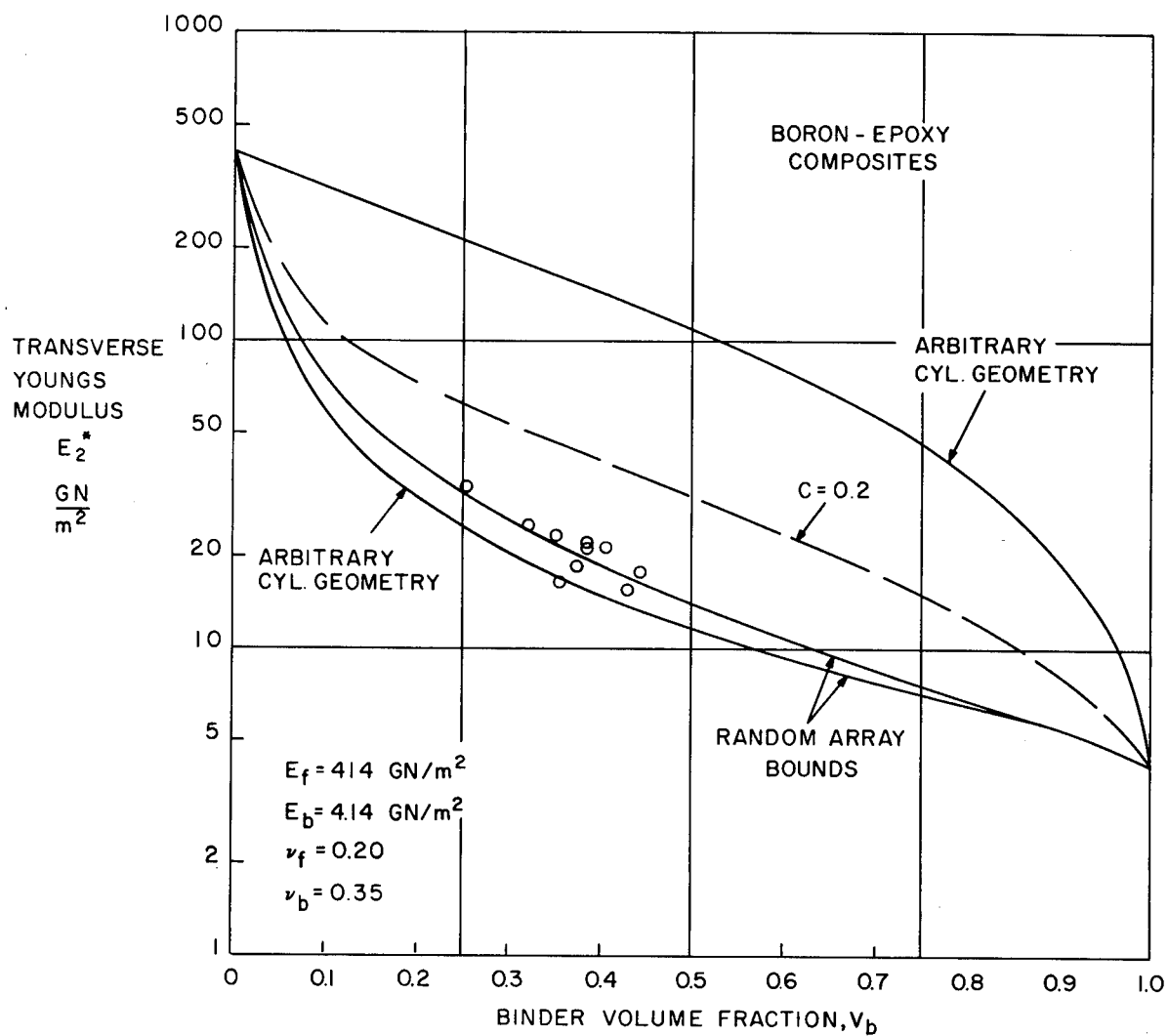
Figure 17. Transverse Young's Modulus, E_2^*, of Boron Reinforced Epoxy–Comparison of Theory and Experiment
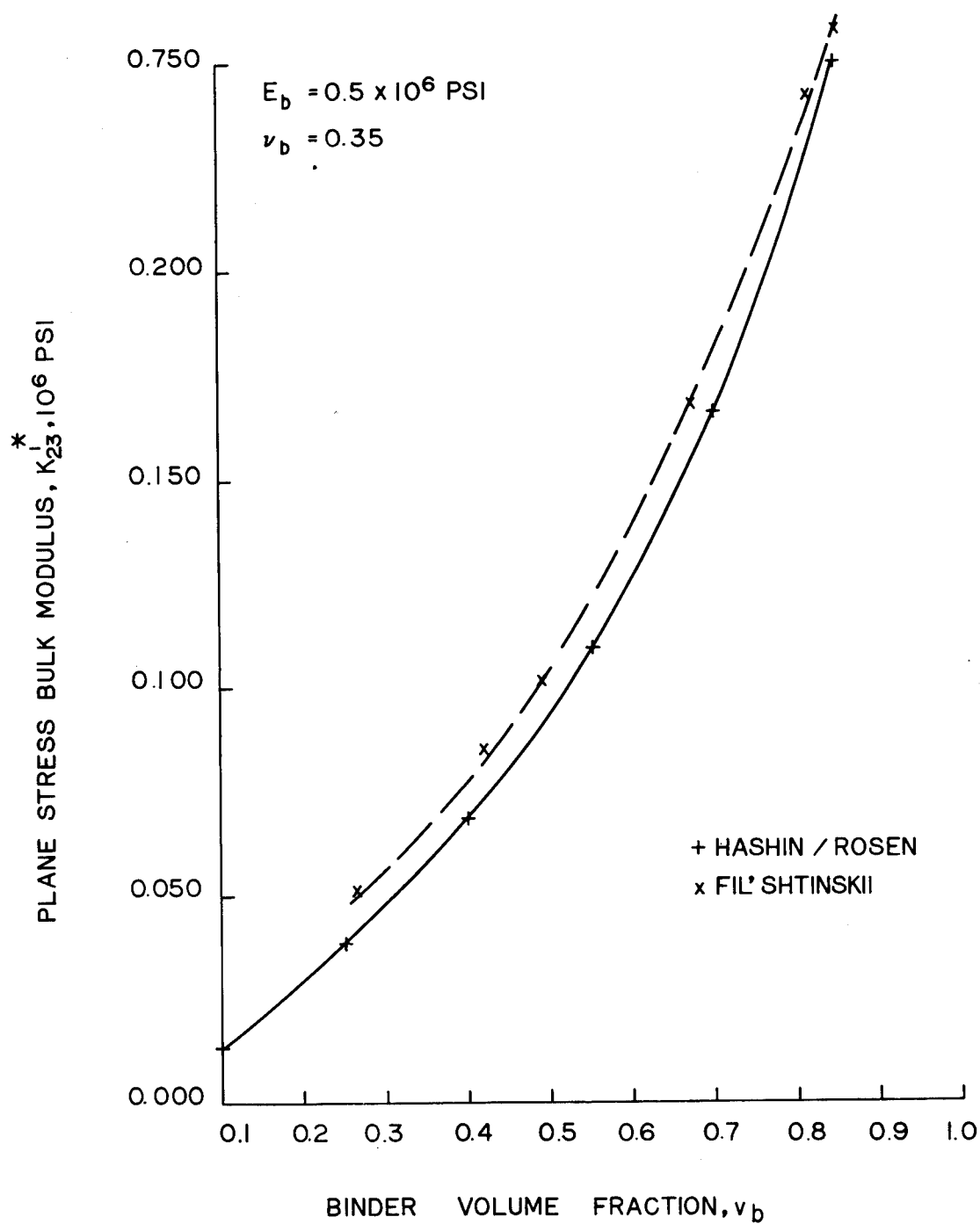
Figure 18. Comparison of Results for Elastic Constants Predicted by Fil'shtinskii (Ref. 20) with those Predicted by Hashin/Rosen (Ref. 6)
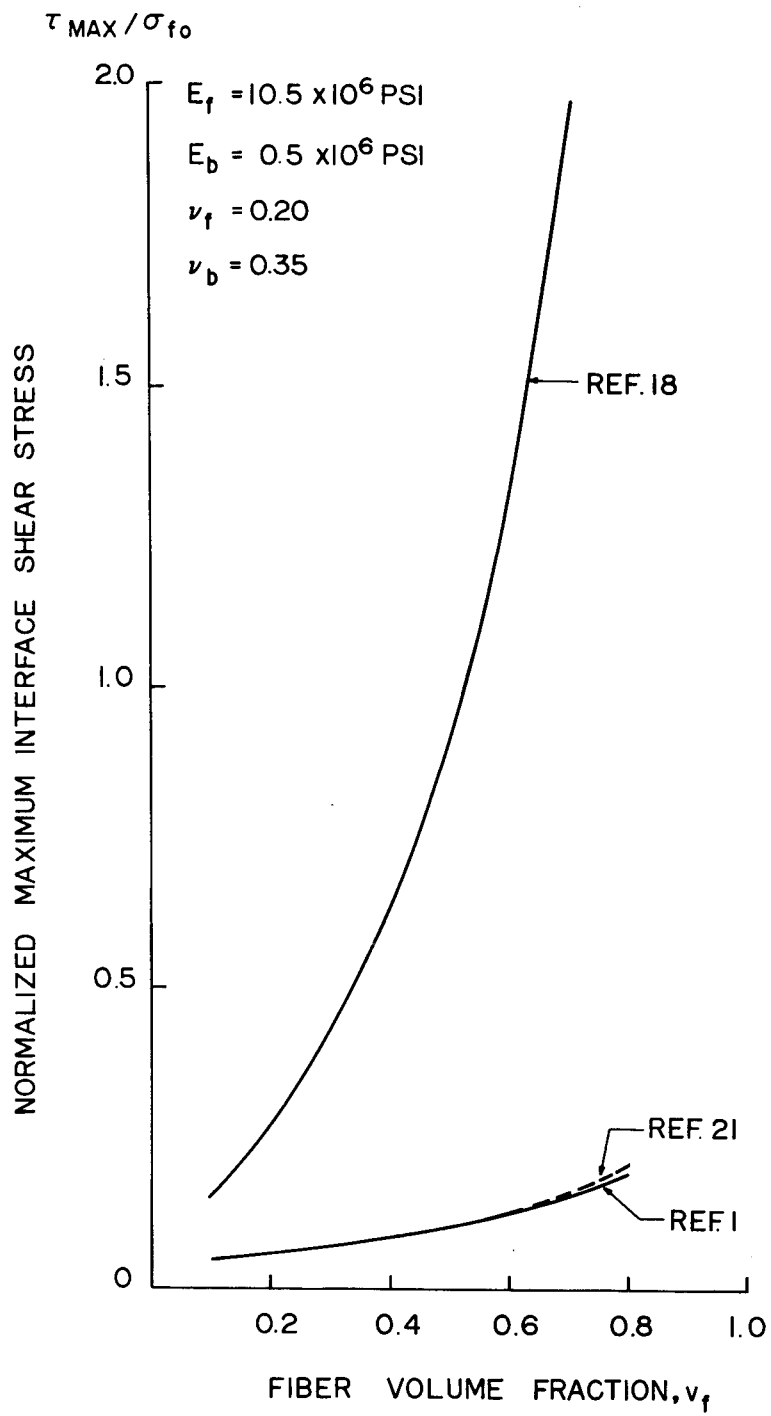
Figure 19. Maximum Fiber-Matrix Interface Shear Stress as a Function of Fiber Volume Fraction
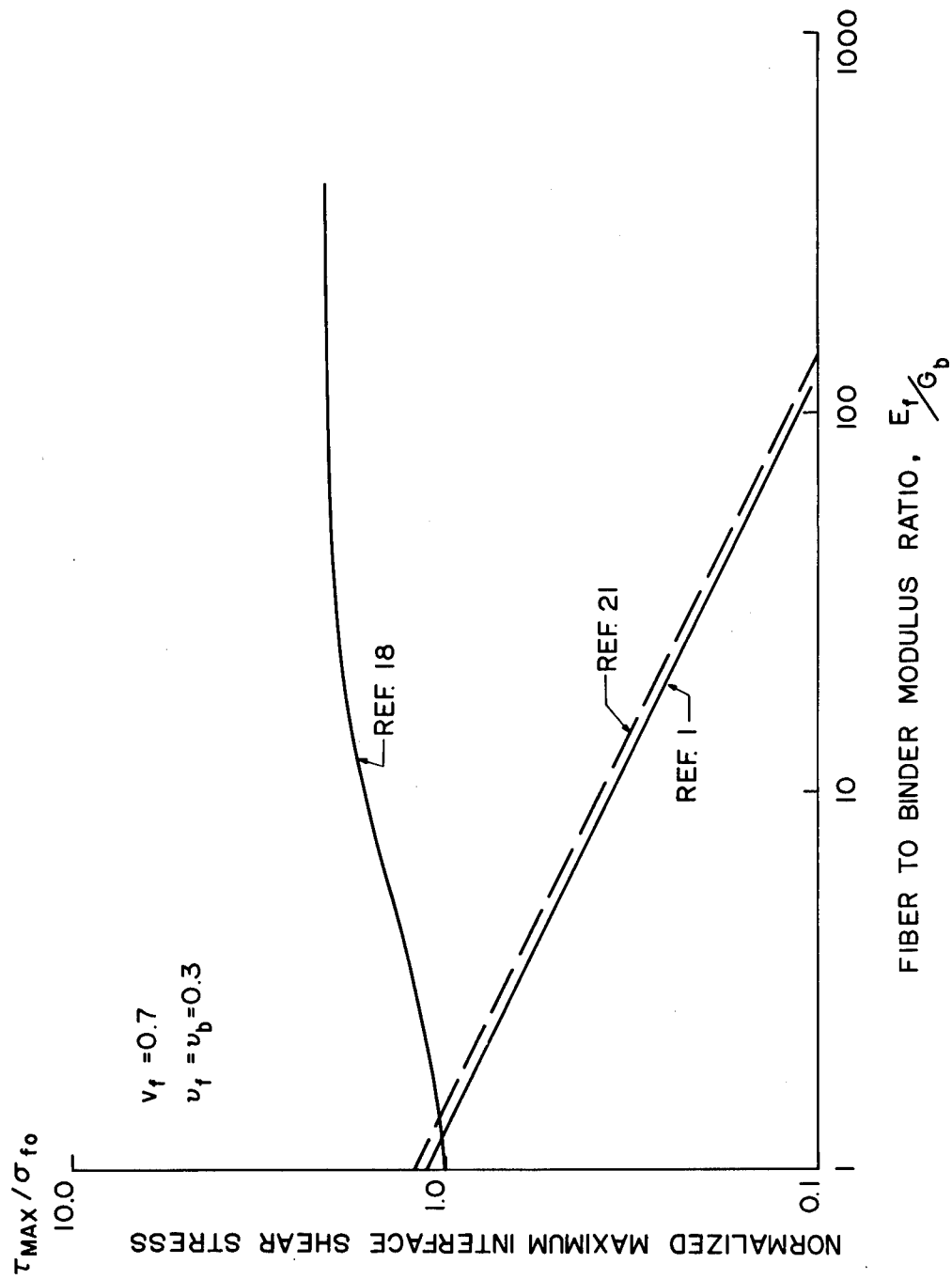
Figure 20. Maximum Fiber-Matrix Interface Shear Stress as a Function of Constituent Moduli Ratio
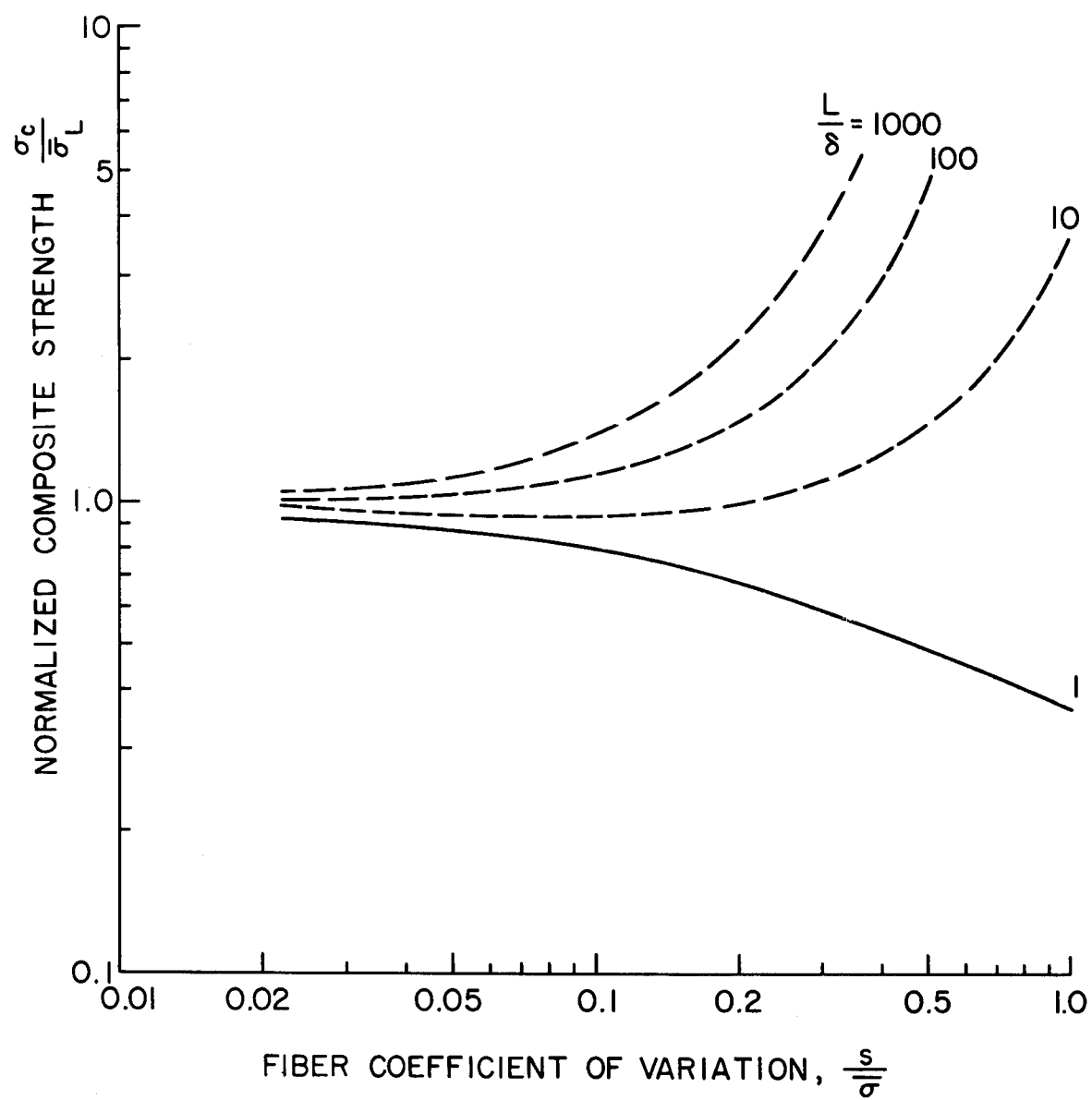
Figure 21. Effect of Fiber Strength Dispersion Upon Composite Tensile Strength
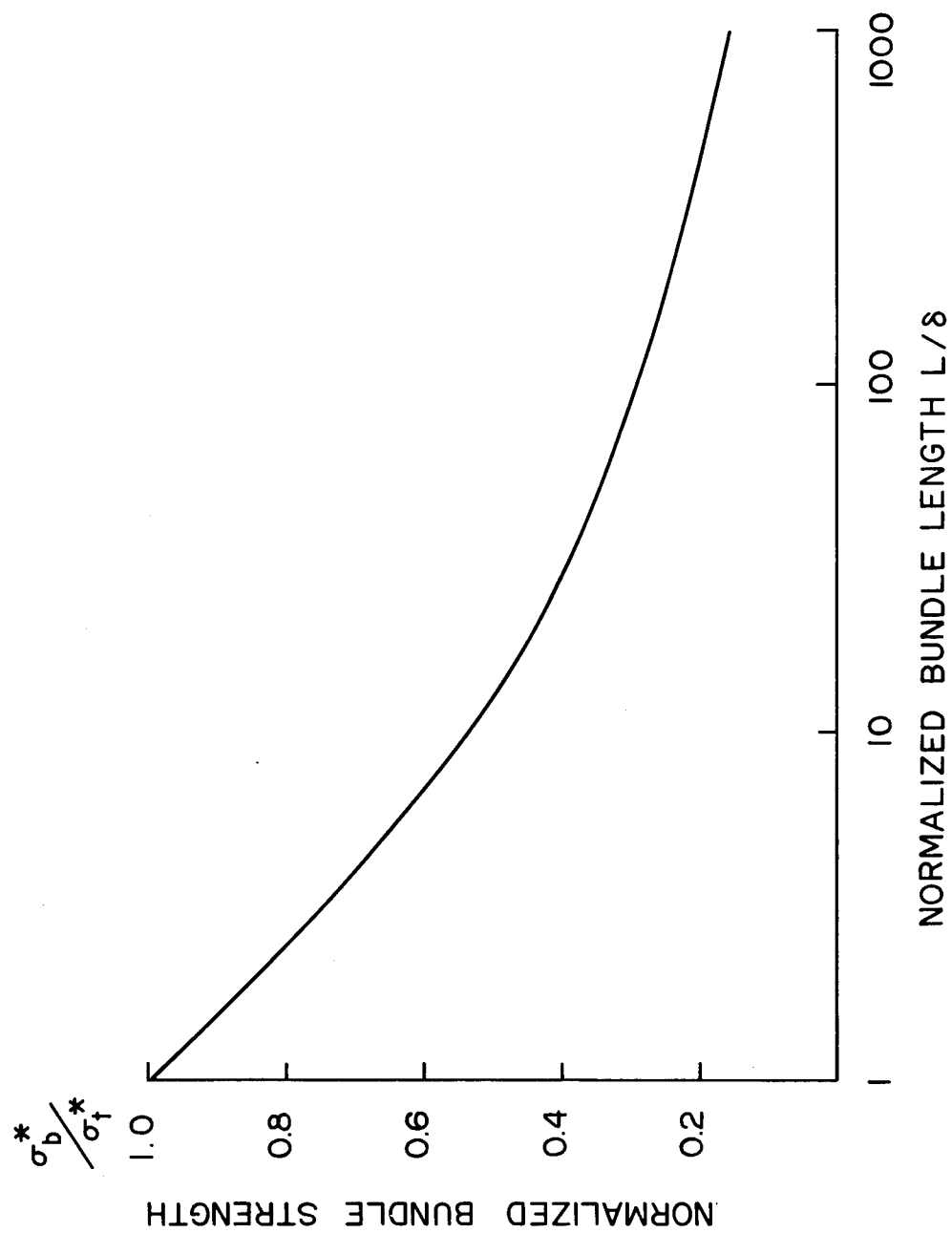
Figure 22. Effect of Length on Fiber Bundle Strength
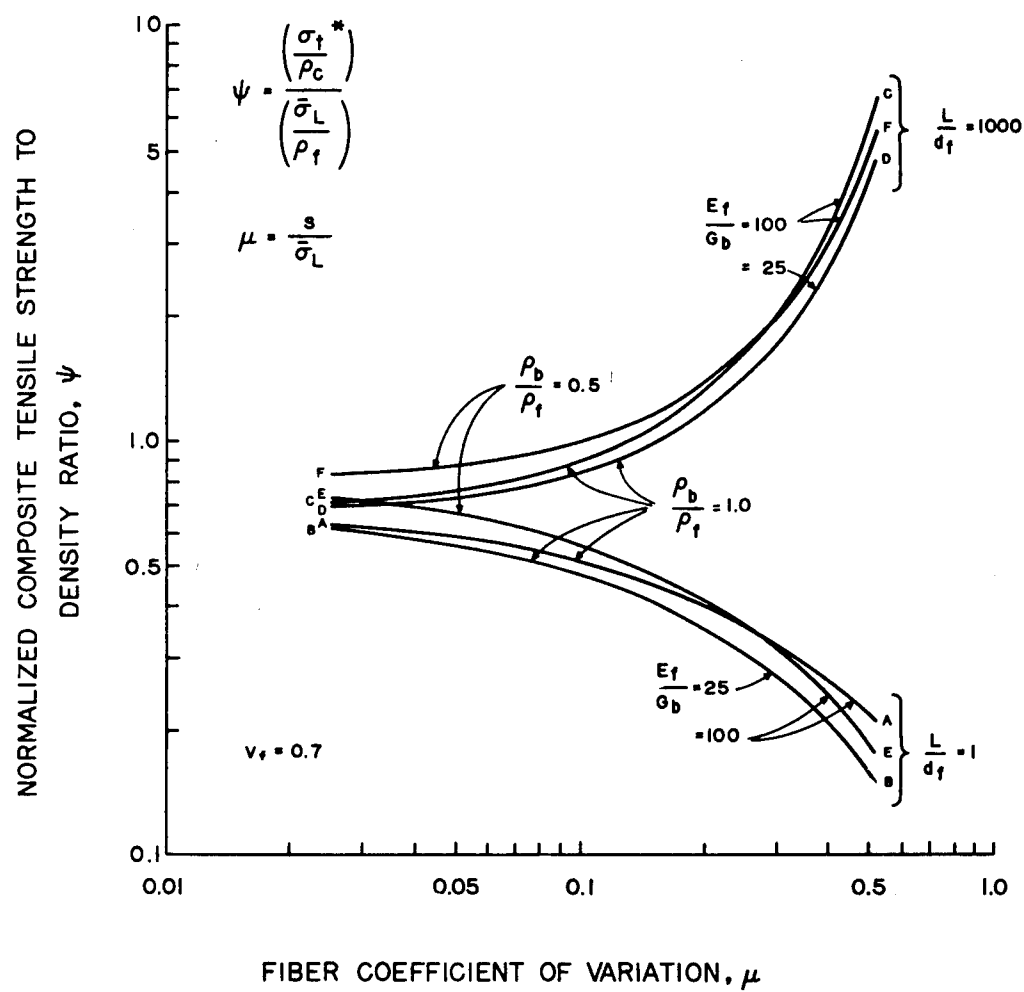
Figure 23. Strength to Density Ratio of Fibrous Composites for Tensile
Loading Parallel to Filaments

185
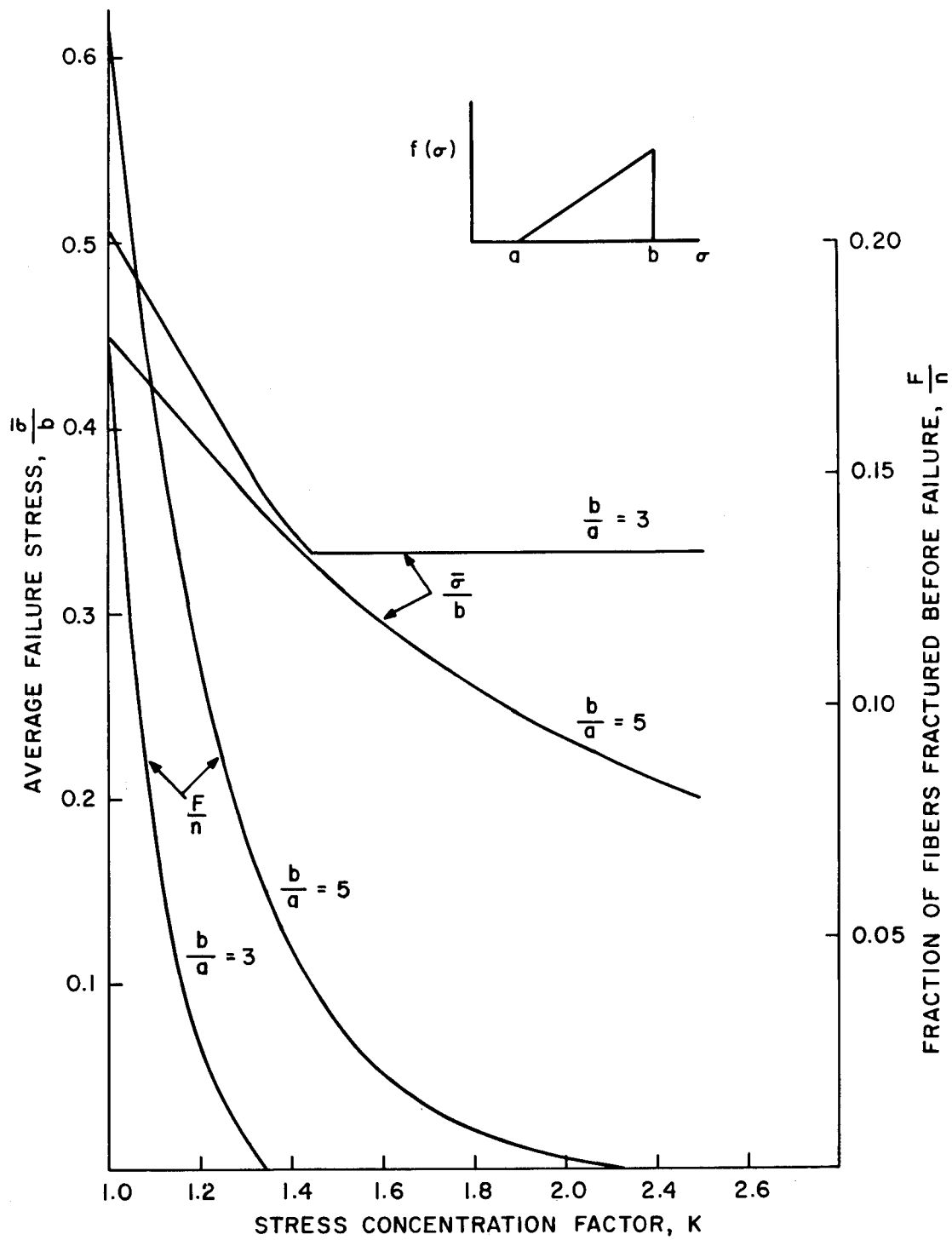
Figure 24. Effect of Stress Concentration on Tensile Strength of Fibrous Composites
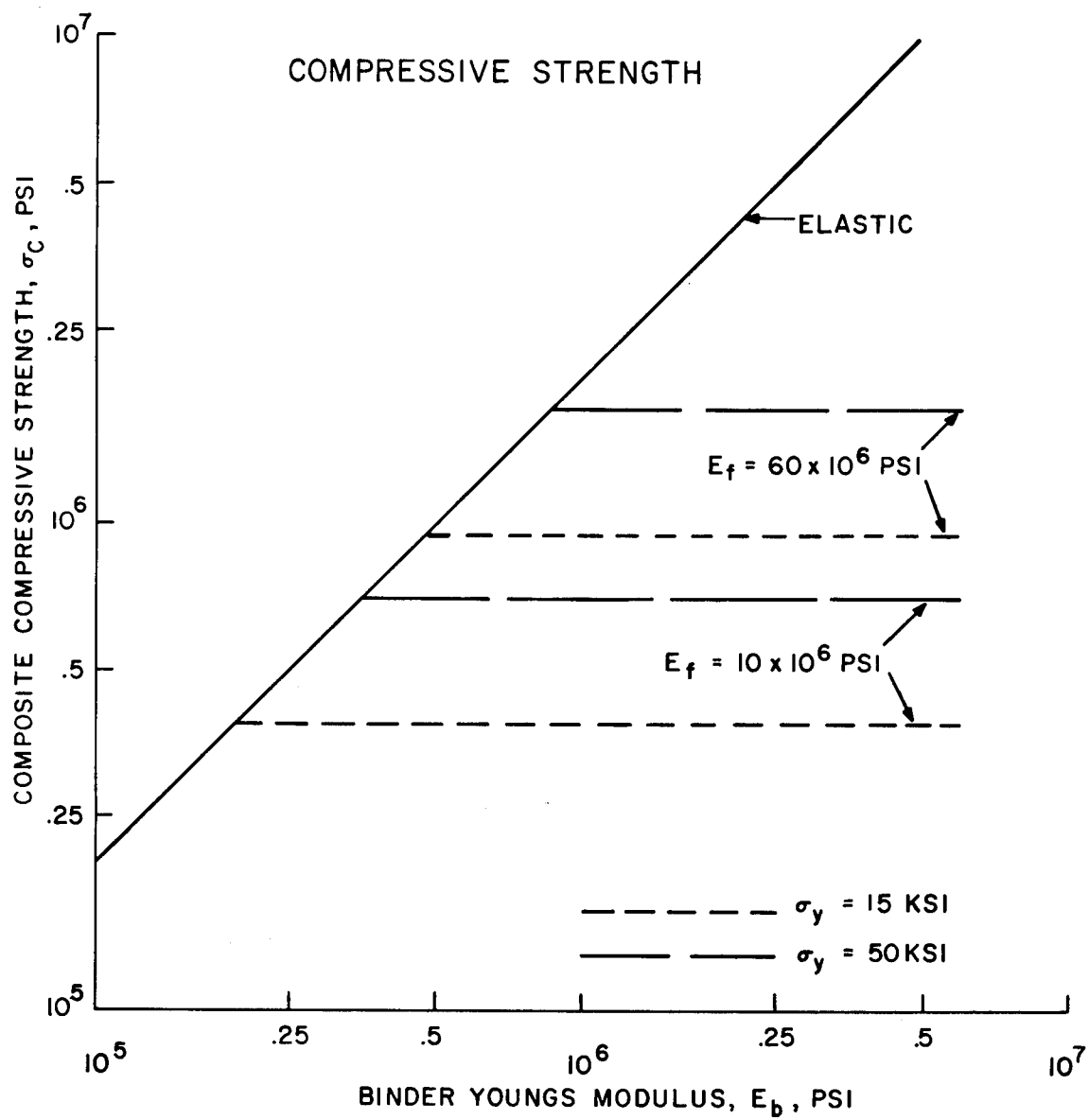
Figure 25. Influence of Matrix Properties Upon Composite Compressive Strength

a. 0.002" D TUNGSTEN
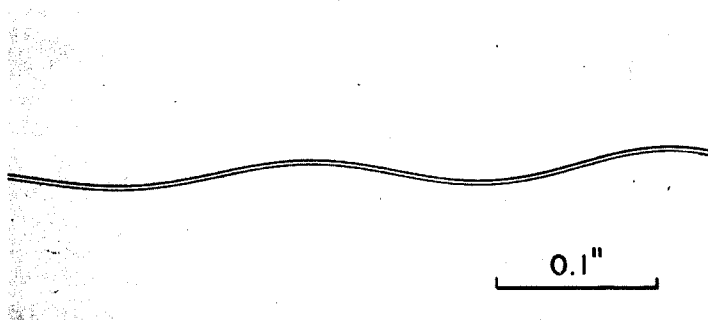
b. 0.0038" D GLASS
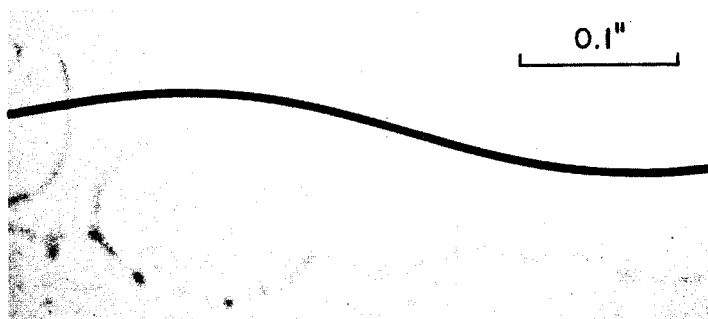
c. 0.0051" D BORON

Figure 26. Instability of Single Filaments Embedded in Silicone Rubber and Compressed in the Fiber Direction

188
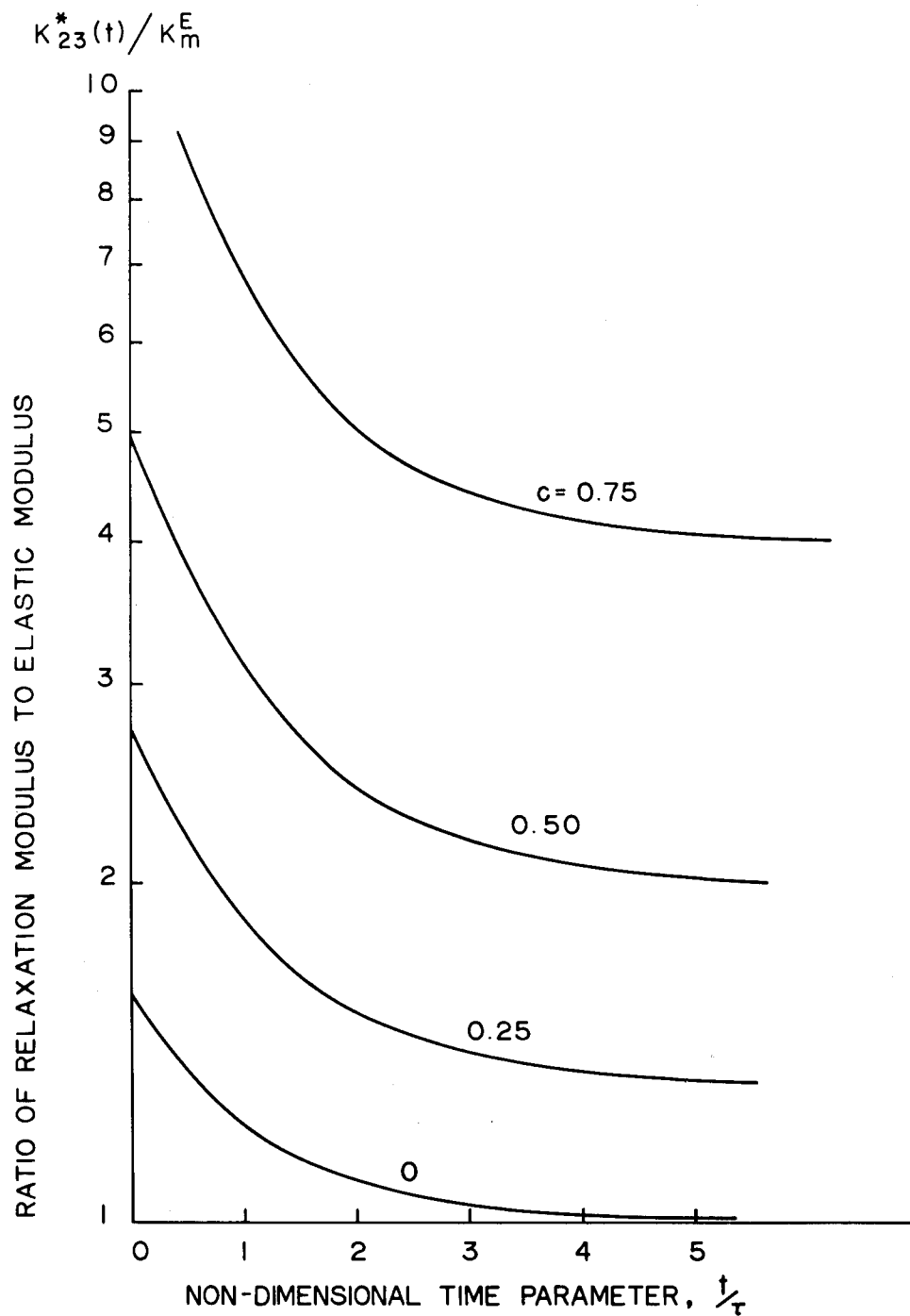
Figure 27. Transverse Plane Strain Bulk Relaxation Modulus, K_{23}^* (t) for Rigid Fiber Composites
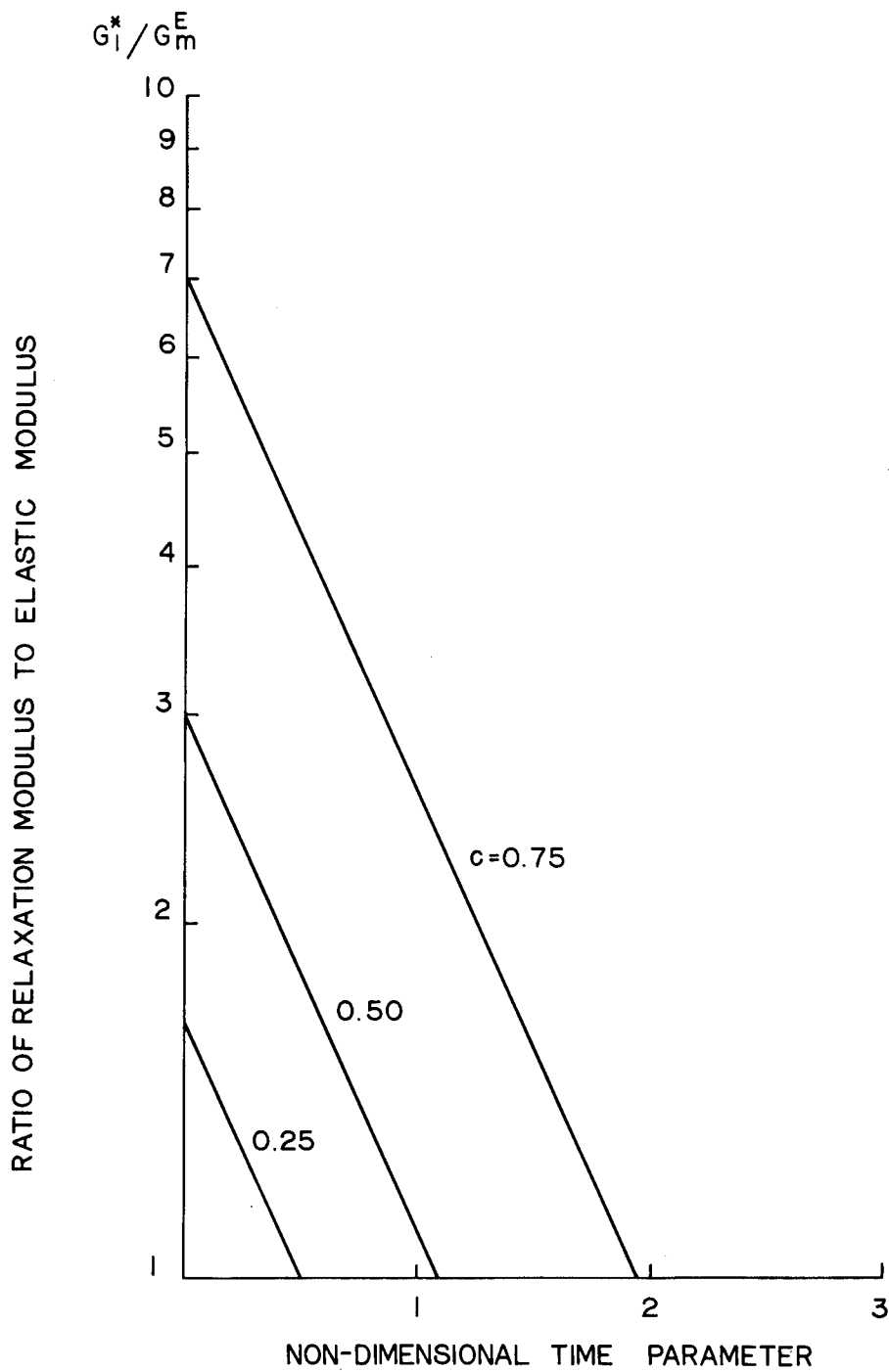
Figure 28. In-Plane Shear Relaxation Modulus, $G_1{}^*$ (t), for Rigid Fiber Composites
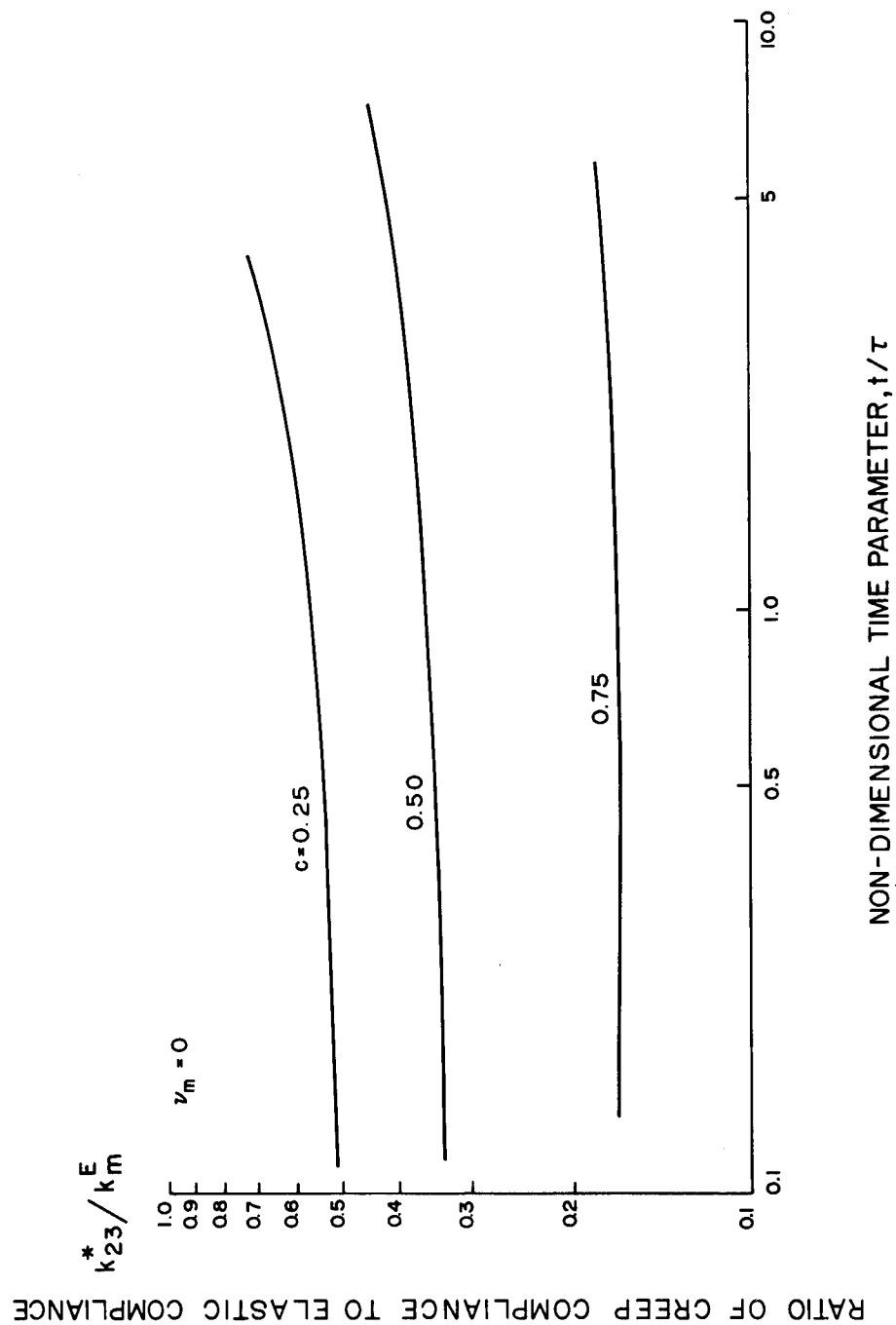
Figure 29. Transverse Plane Strain Bulk Creep Compliance, k_{23}^{*} (t), for Rigid Fiber Composites

191
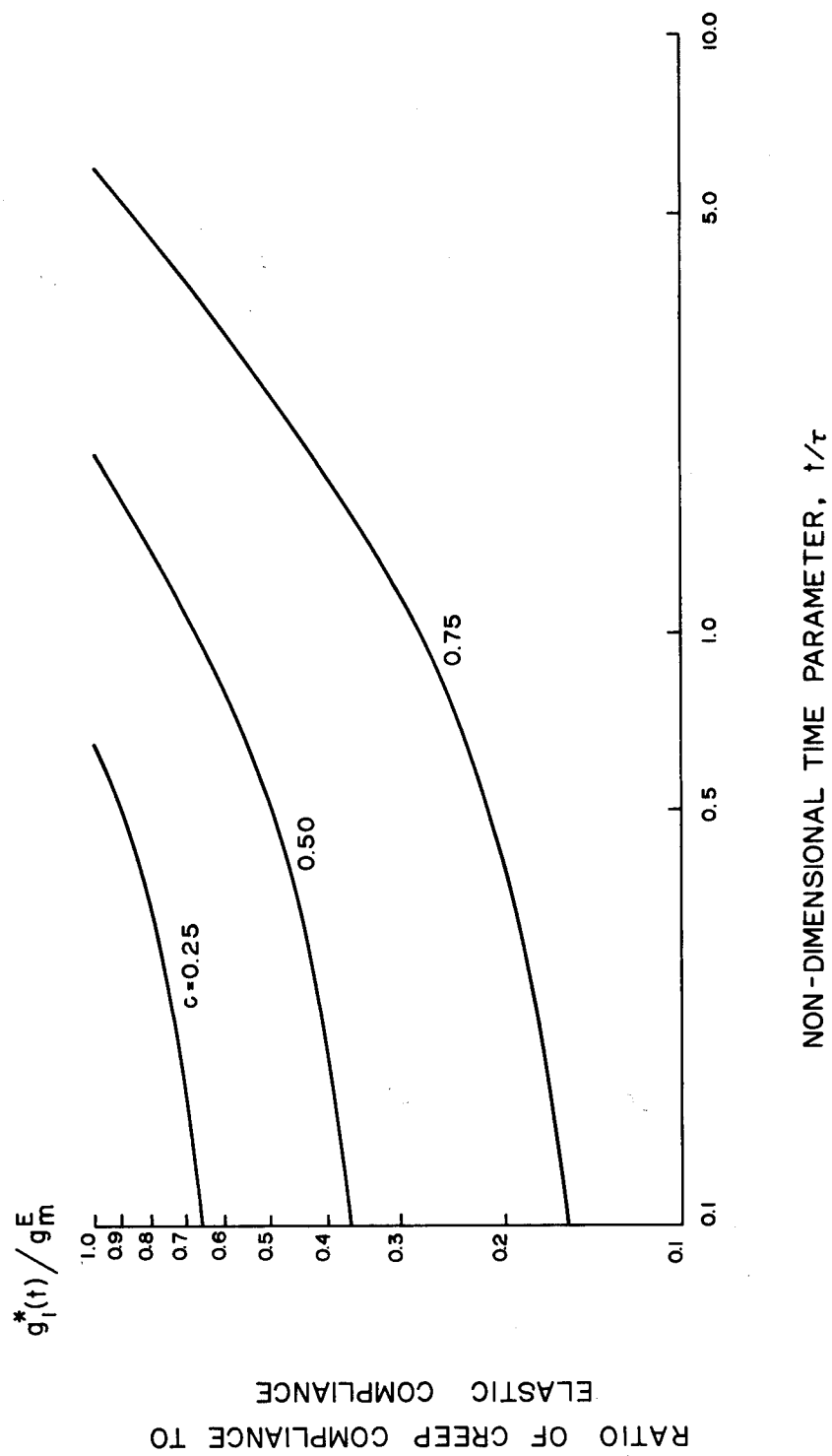
Figure 30. In-Plane Shear Creep Compliance, g_1^* (t), for Rigid Fiber Composites

192
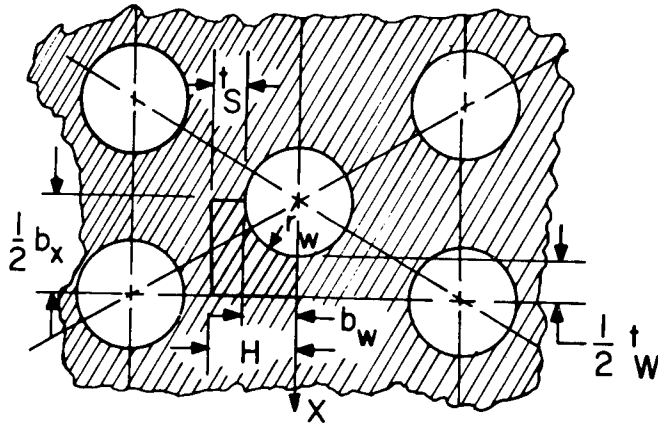
Figure 31. Repeating Element of Uni-Directionally Reinforced Composite
Corresponding to that for the Integrally Stiffened Plate of Ref. 44
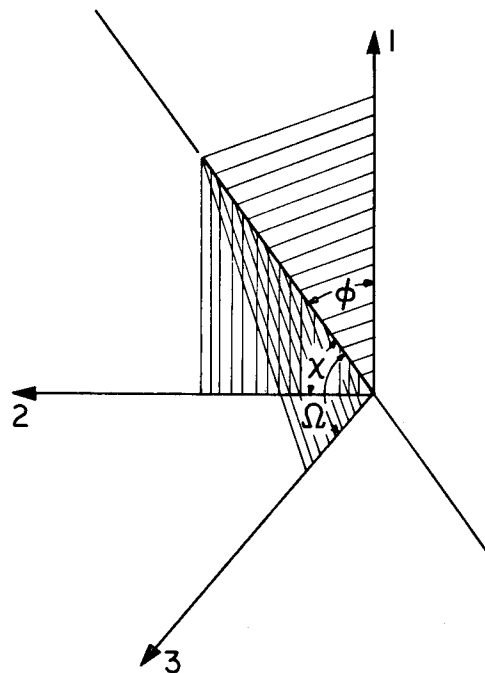
Figure 32. Three-Dimensional Angle Notation Used in Analysis.
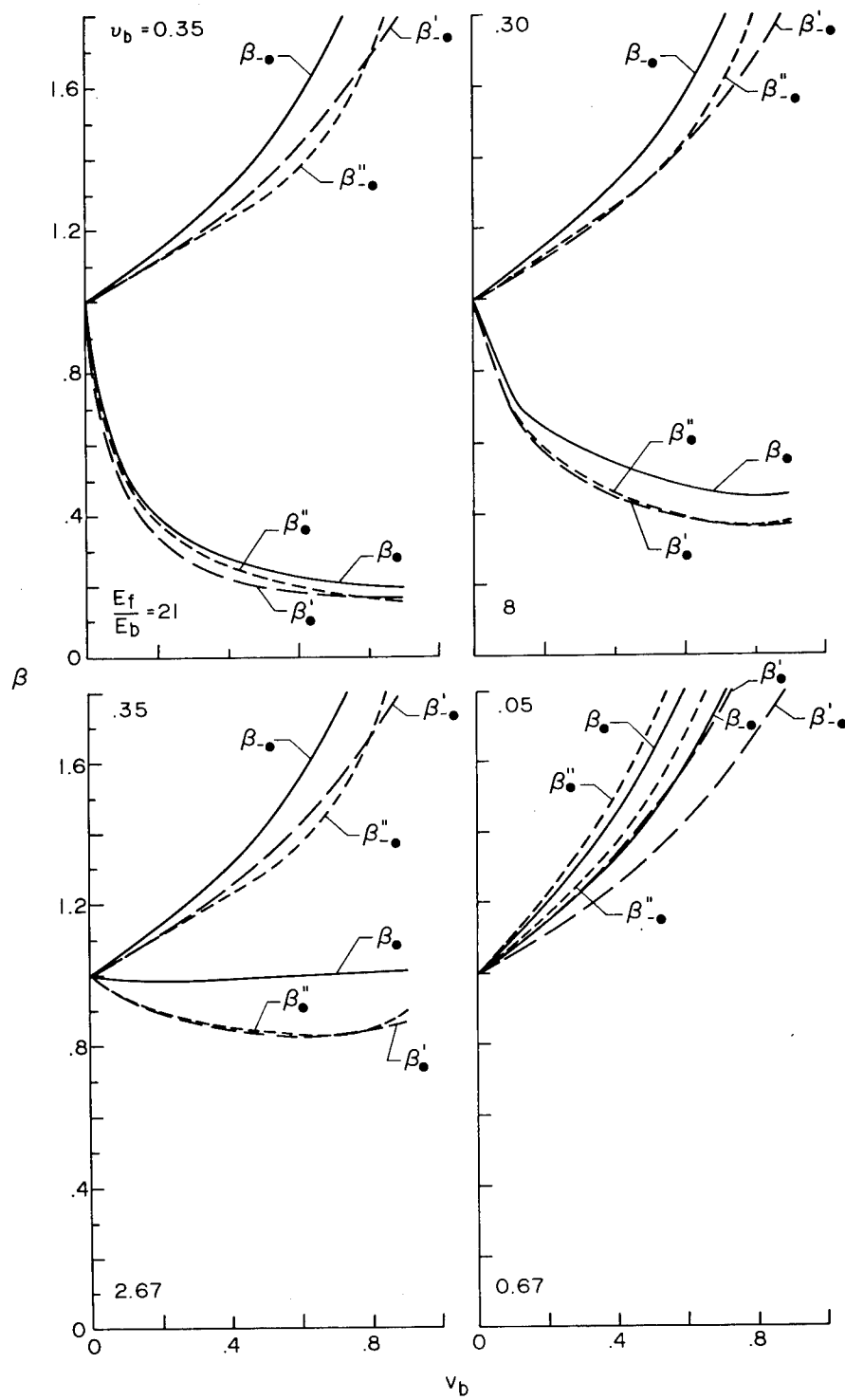
Figure 33. Values of Transverse Effectiveness Coefficients (β) Based on
Upper Bounds of Reference 6
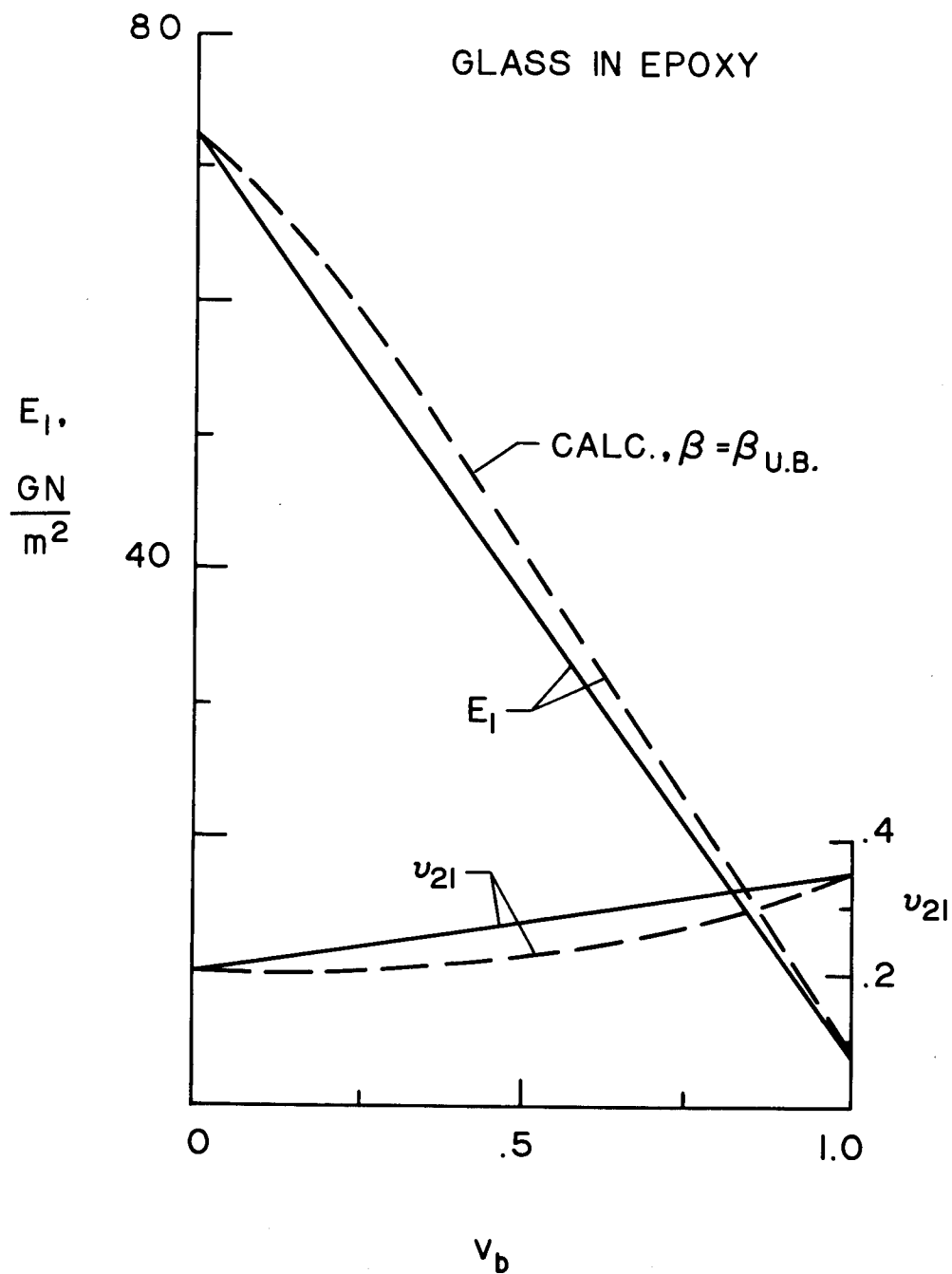
Figure 34. Comparison of Stretching Stiffness in the 1-direction E_1 and the Related Poisson's Ratio ν_{21} Calculated by the "Rule of Mixtures" or Laminate Analyses (Solid Curves) and by the Present Analysis (Dashed Curves) for Uni-Directional Reinforcement

195
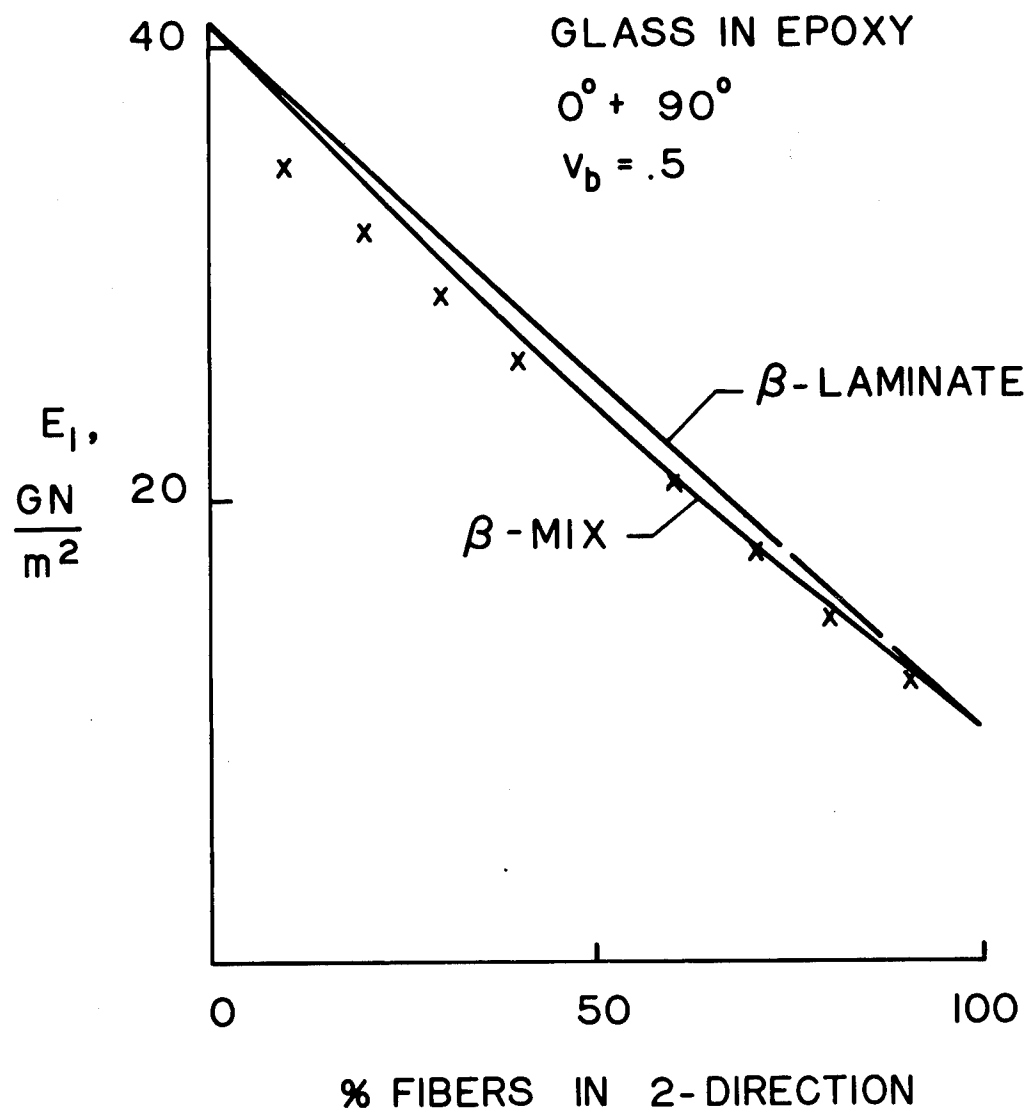
Figure 35. Comparison of Stretching Stiffness in the 1-Direction E_1 Calculated by Laminate Analysis (x-Points) and the Present Analysis (the Curves) for Orthogonal Filaments in the 1- and 2-Directions
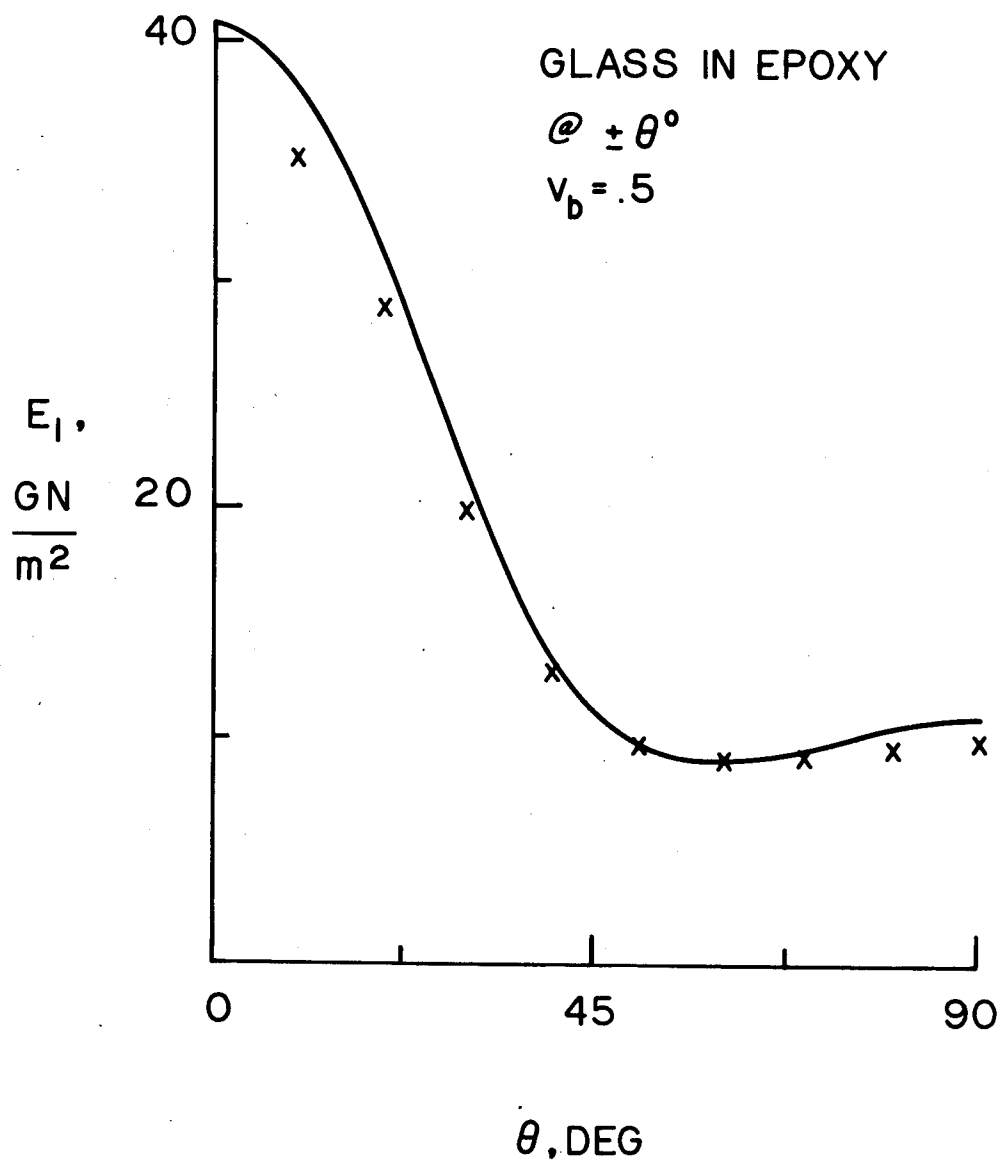
Figure 36. Comparison of Stretching Stiffness in the 1-Direction E_1 Calculated by Laminate Analysis (x-Points) and the Present Analysis (the Curve) for Bi-Directional Reinforcement in the 1-2 Plane with Filaments at Angles $\pm\theta$ to the 1-Direction
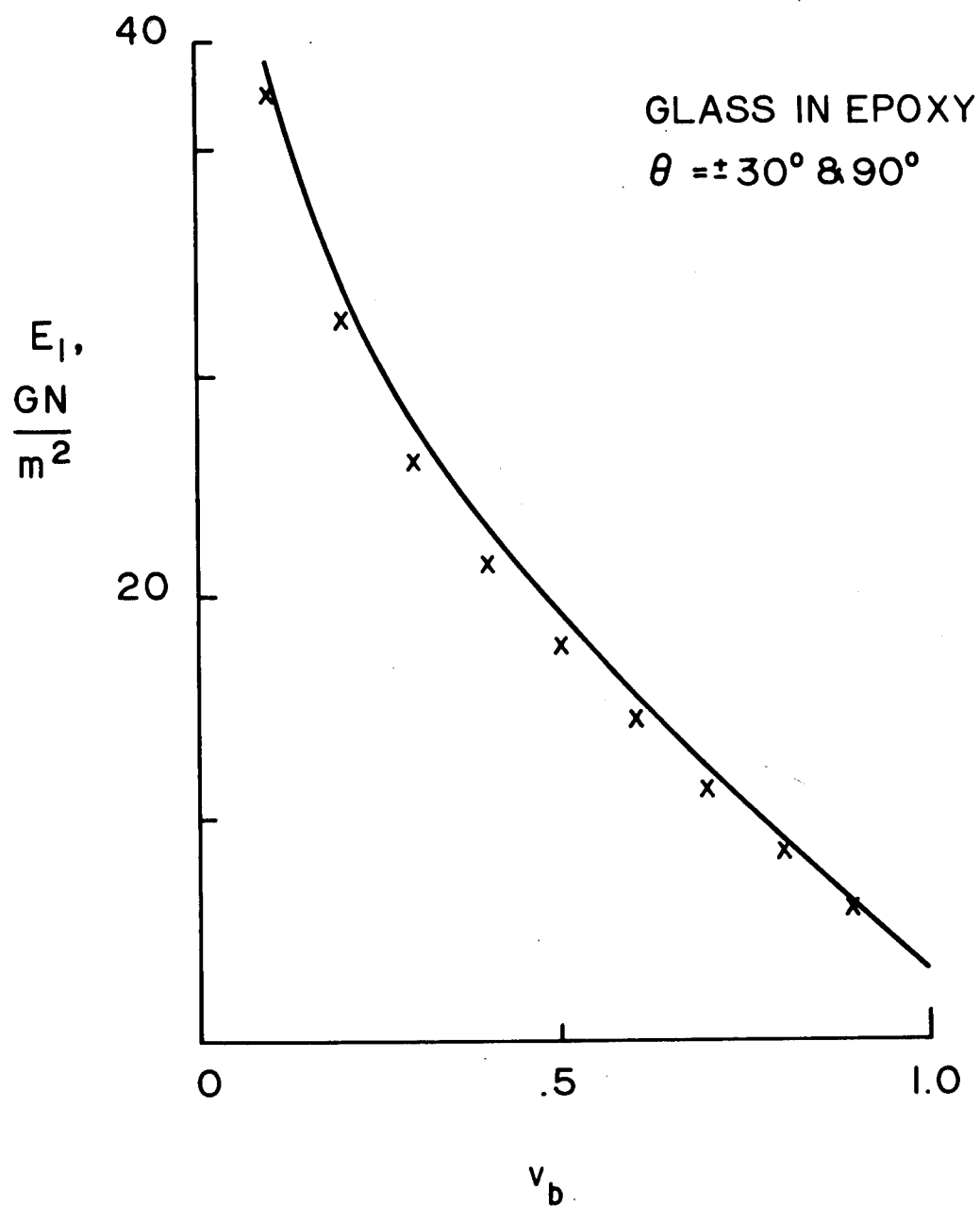
Figure 37. Comparison of Stretching Stiffness in the 1-Direction E_1 Calculated by Laminate Analysis (x-Points) and the Present Analysis (the Curve) for Three-Directional Reinforcement in the 1-2 Plane with Filaments at Angles of ± 30 Degrees and 90 Degrees in the 1-Direction

"BINDER" **"FIBER"**
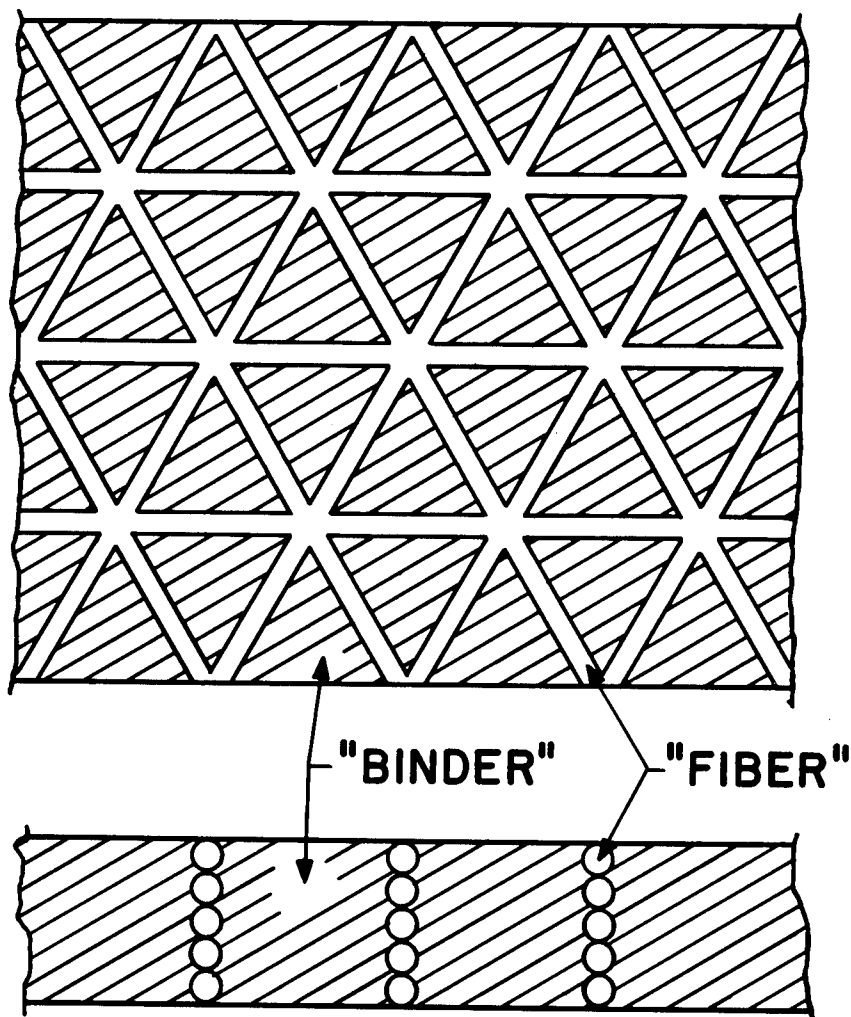
Figure 38. Schematic Representation of Straight-Line Binder Elements Possible Among Perfectly-Packed Equilateral Triangle Cross-Section Filaments, and of Closely-Packed Filamentary Binder Elements Postulated for Analysis
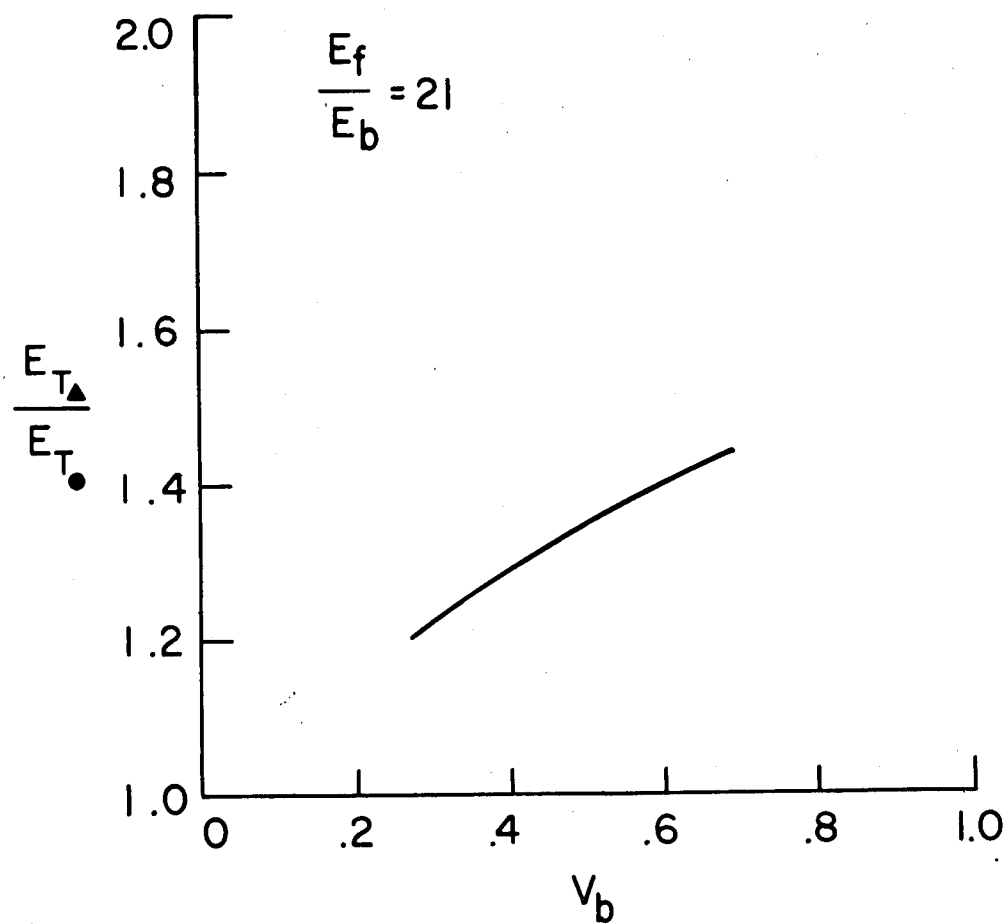
Figure 39. Ratio of Transverse Stiffnesses of Epoxy Composites Having
Uni-Directional Filamentary Glass Reinforcements of Triangular
and Circular Cross-Section

GLASS IN EPOXY
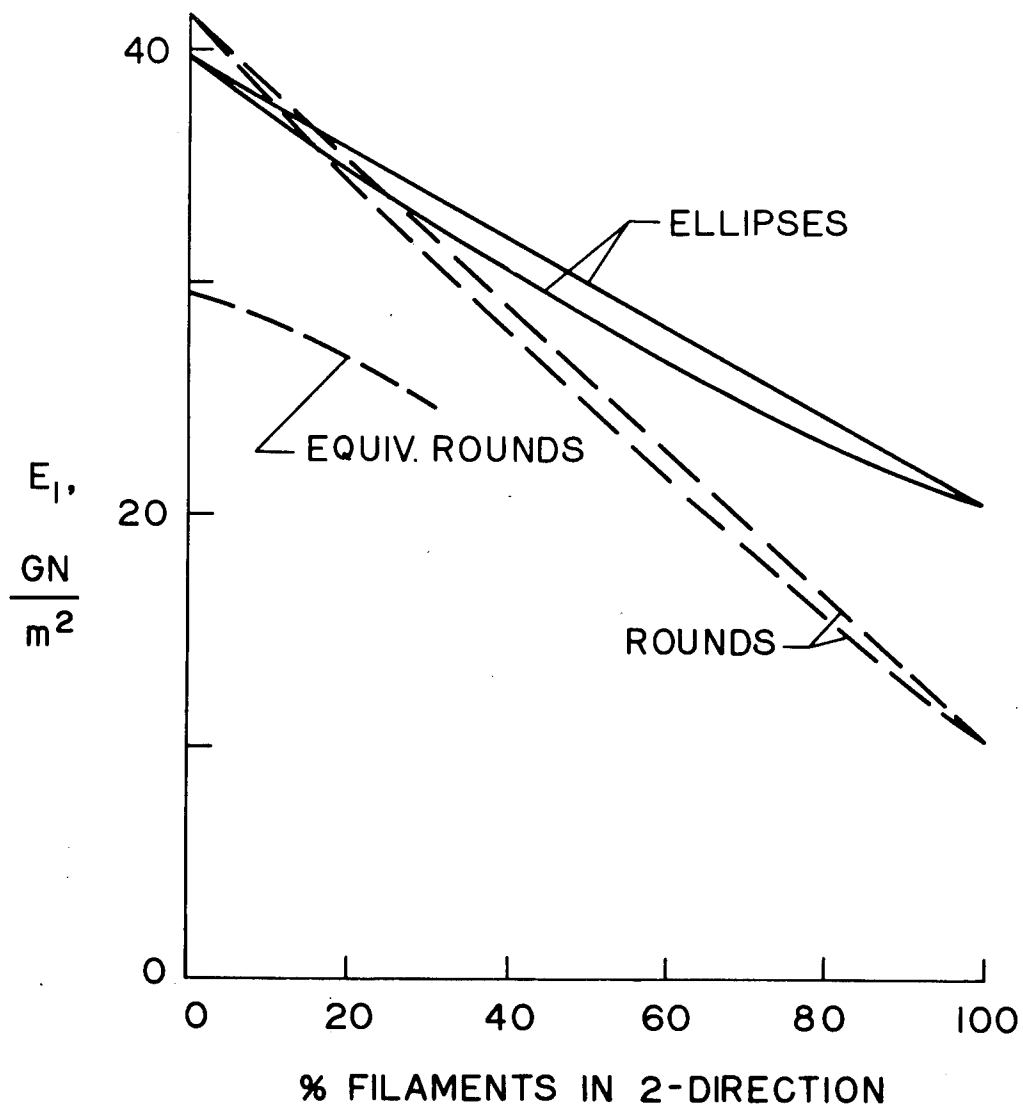
Figure 40. Evaluation of Enhancement of Transverse Stiffness Provided by
4 to 1 Aspect Ratio Elliptical Cross-Section Glass Filaments in
Epoxy Binder
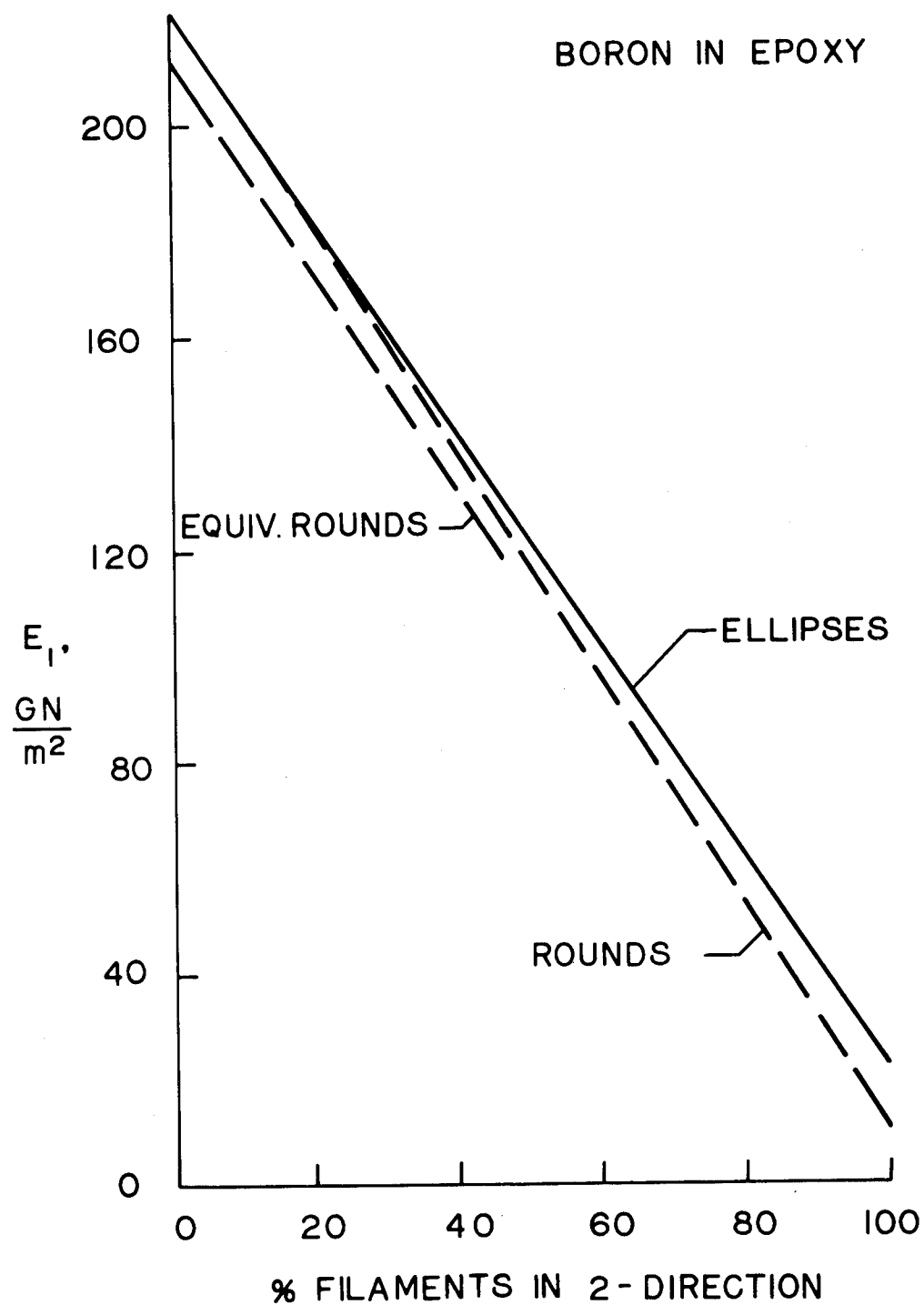
Figure 41. Evaluation of Enhancement of Transverse Stiffness Provided by 4 to 1 Aspect Ratio Elliptical Cross-Sectional Filaments of Boron in Epoxy
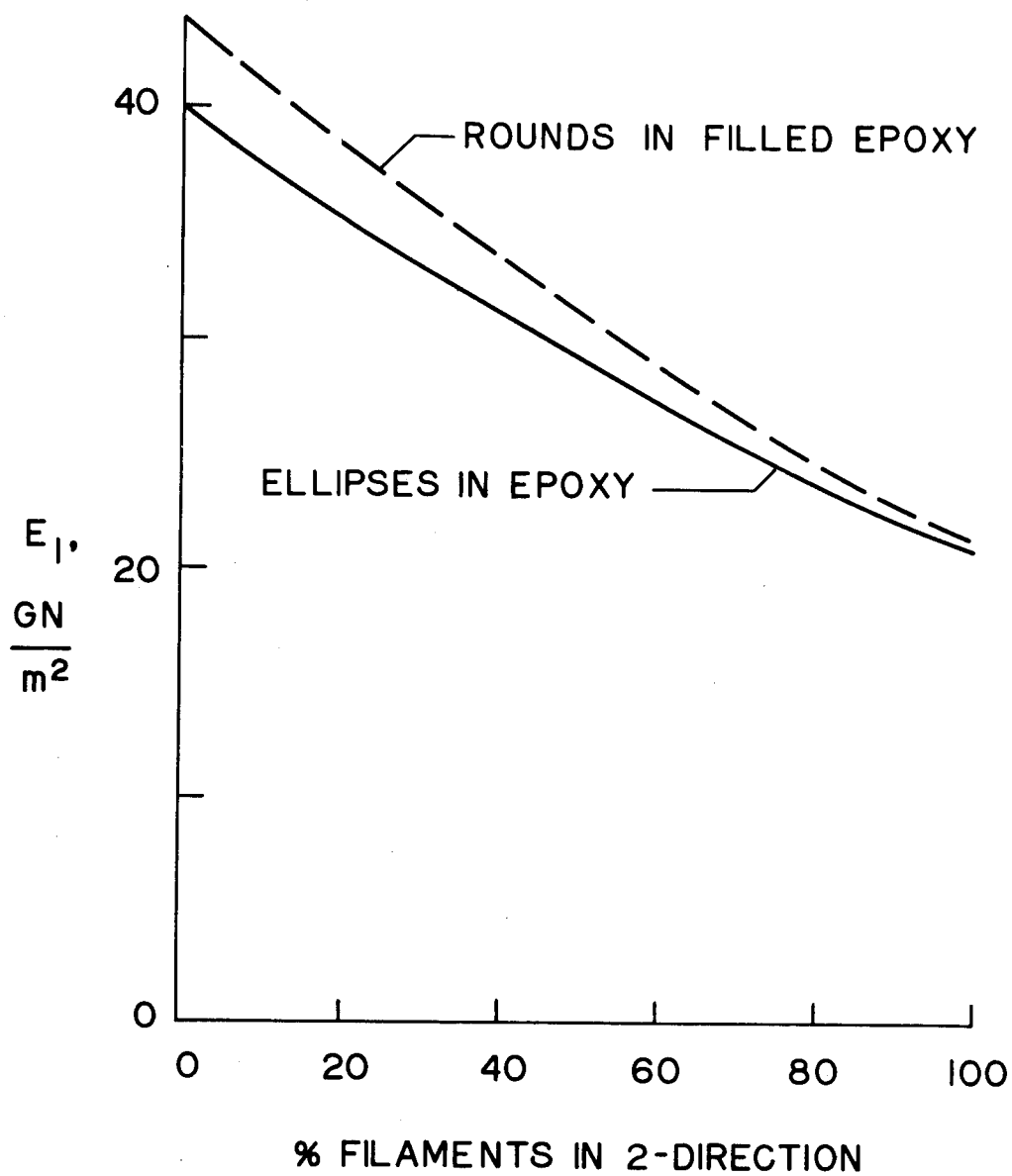
Figure 42. Evaluation of Enhancement of Transverse Stiffness Provided to Glass-Filament Reinforced Composites by a Filled Binder Having a Stiffness Increase of 160%
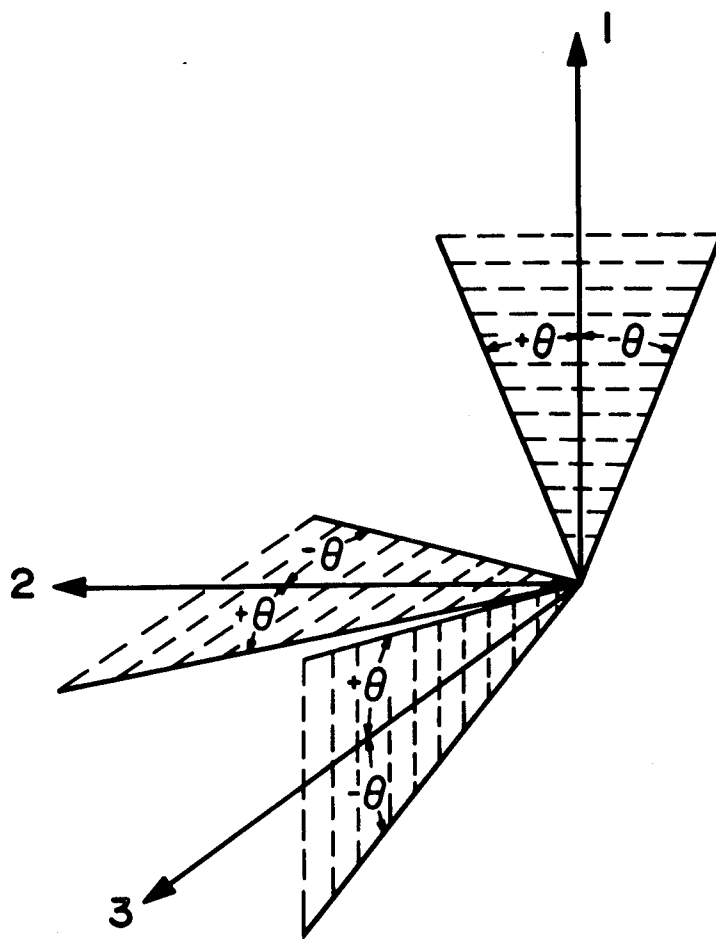
Figure 43. Schematic Representation of Orientations of Orthogonal, Skew
Pairs of Filamentary Reinforcements Considered in Figures 44-48

204
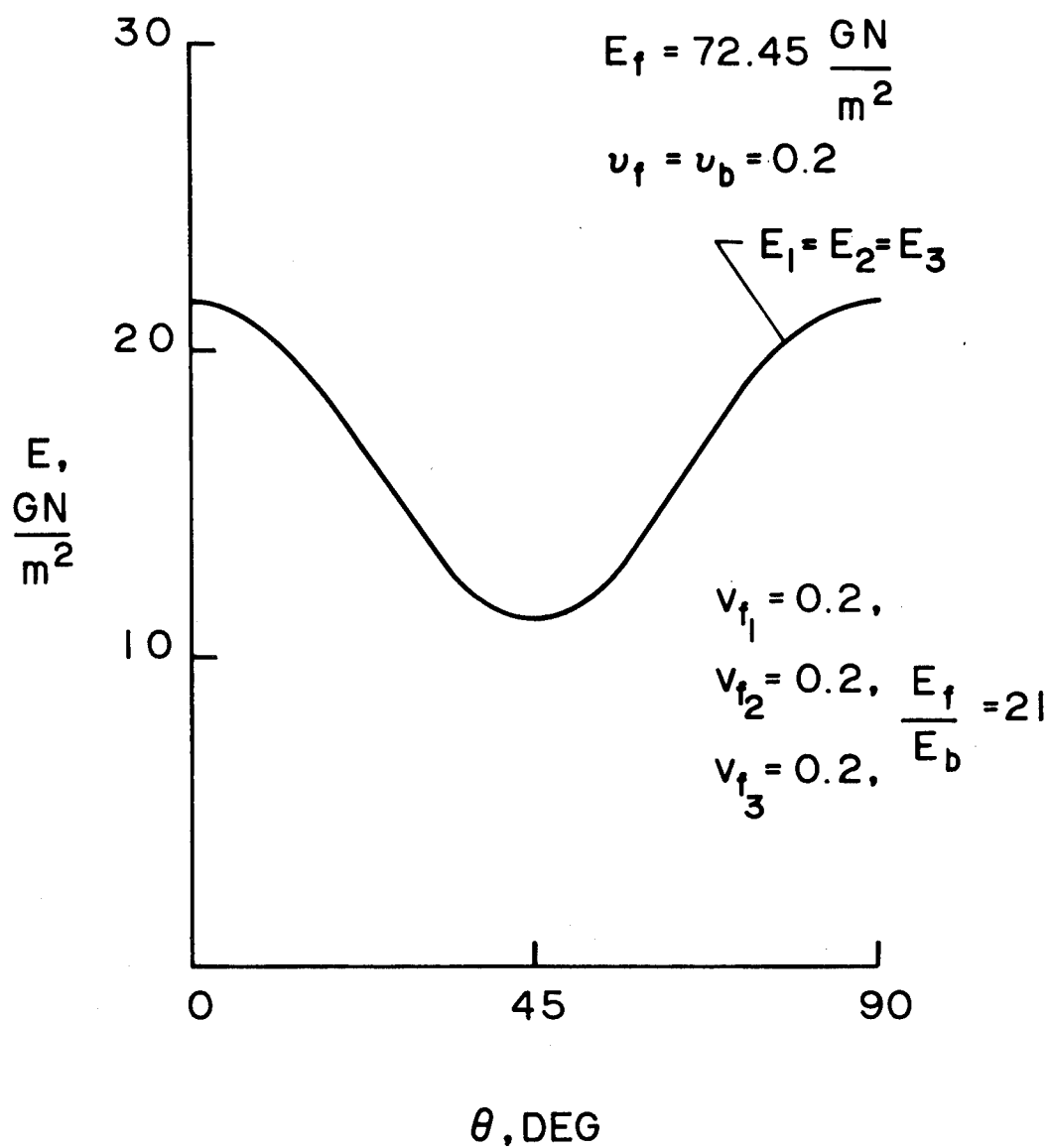
Figure 44. Stretching Stiffnesses of Composites with Three Orthogonal, Skew Pairs of Filamentary Reinforcements with Equal Volume ·Fractions in Each Direction
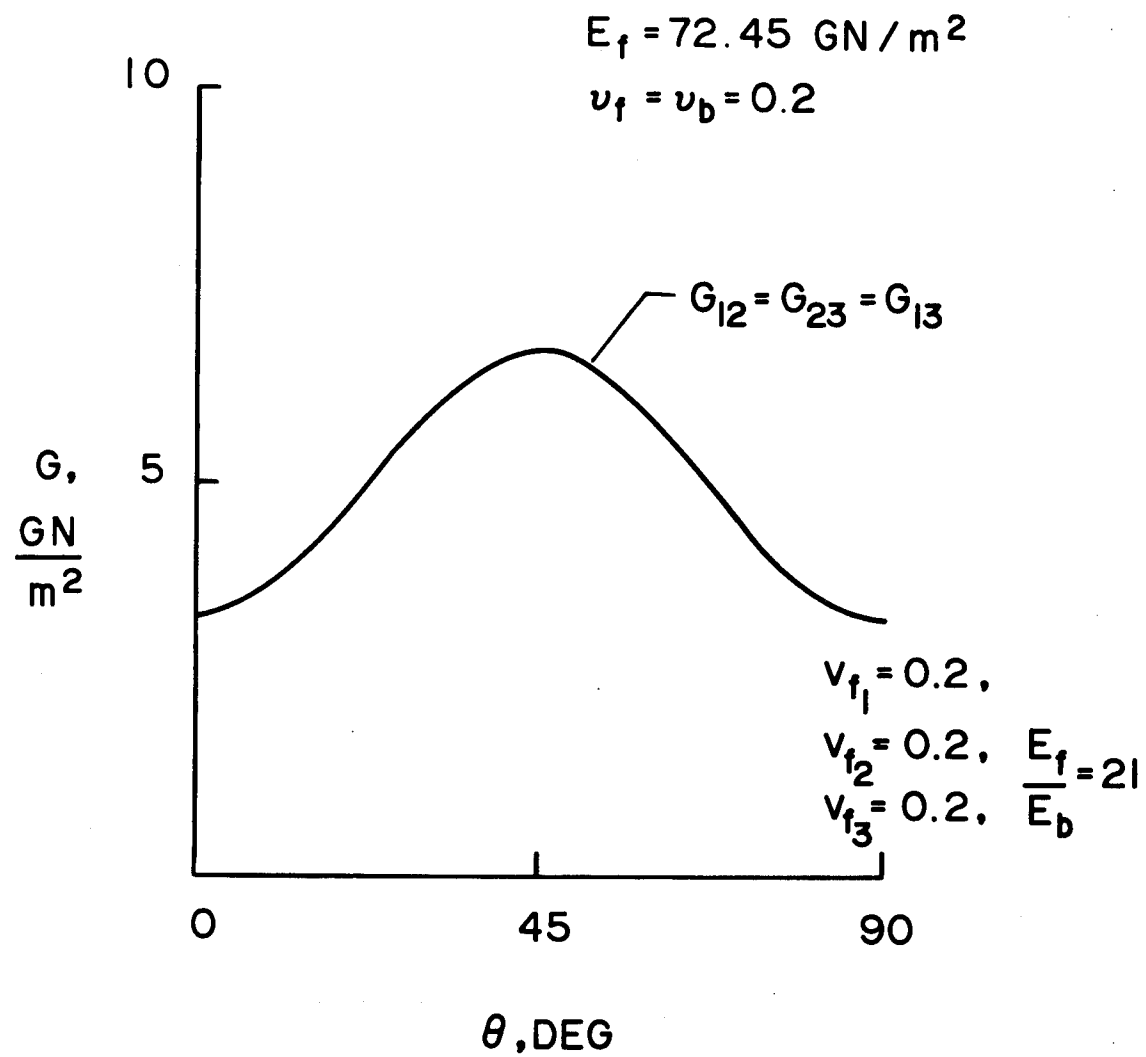
Figure 45. Shearing Stiffnesses of Composites with Three Orthogonal Skew
Pairs of Filamentary Reinforcements with Equal Volume Fractions
in Each Direction
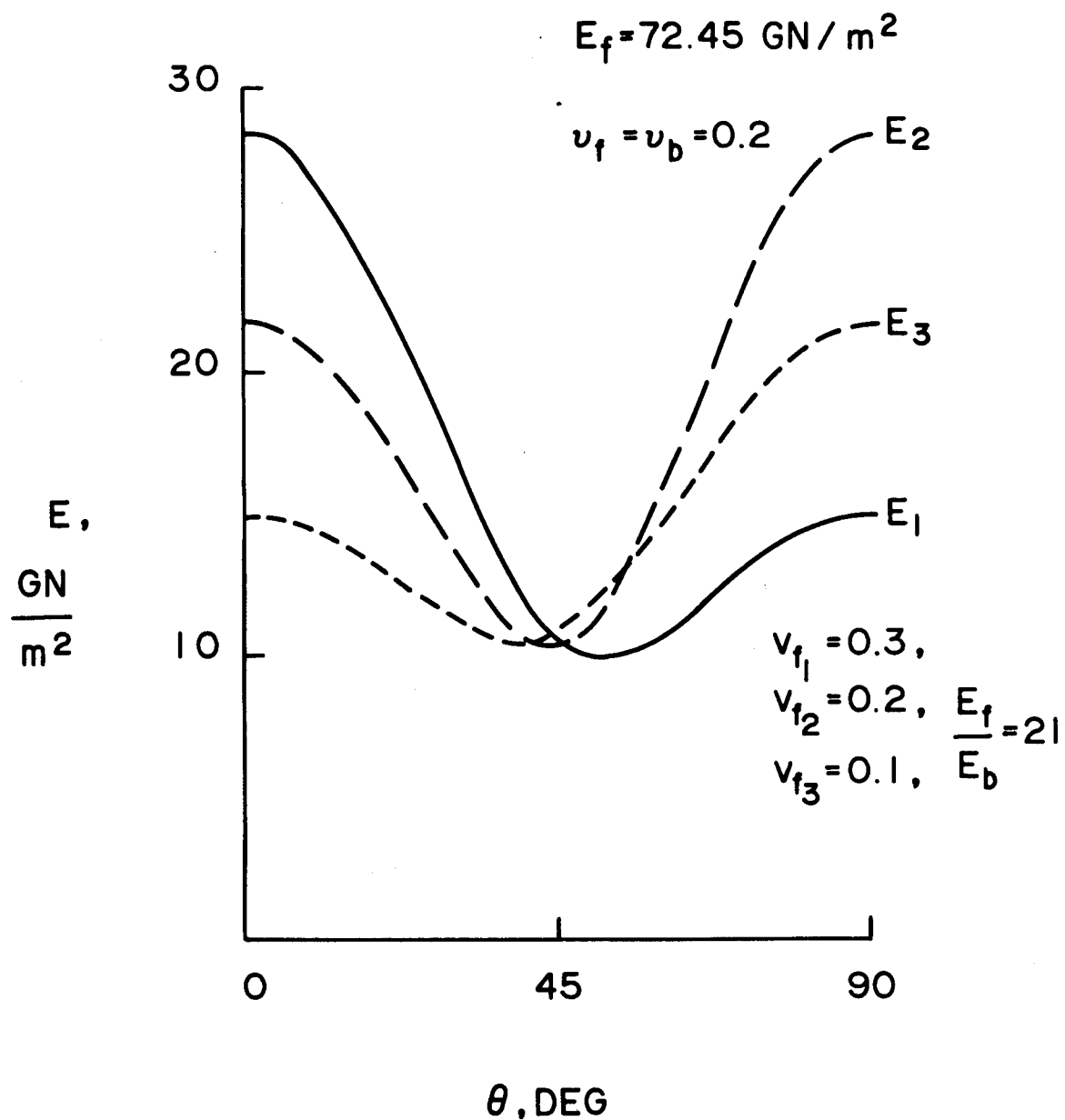
Figure 46. Stretching Stiffnesses of Composites with Three Orthogonal,
Skew Pairs of Filamentary Reinforcements, with Different
Volume Fractions in the Three Directions

$$E_f = 72.45 \ \frac{GN}{m^2}$$

$$v_f = v_b = 0.2$$
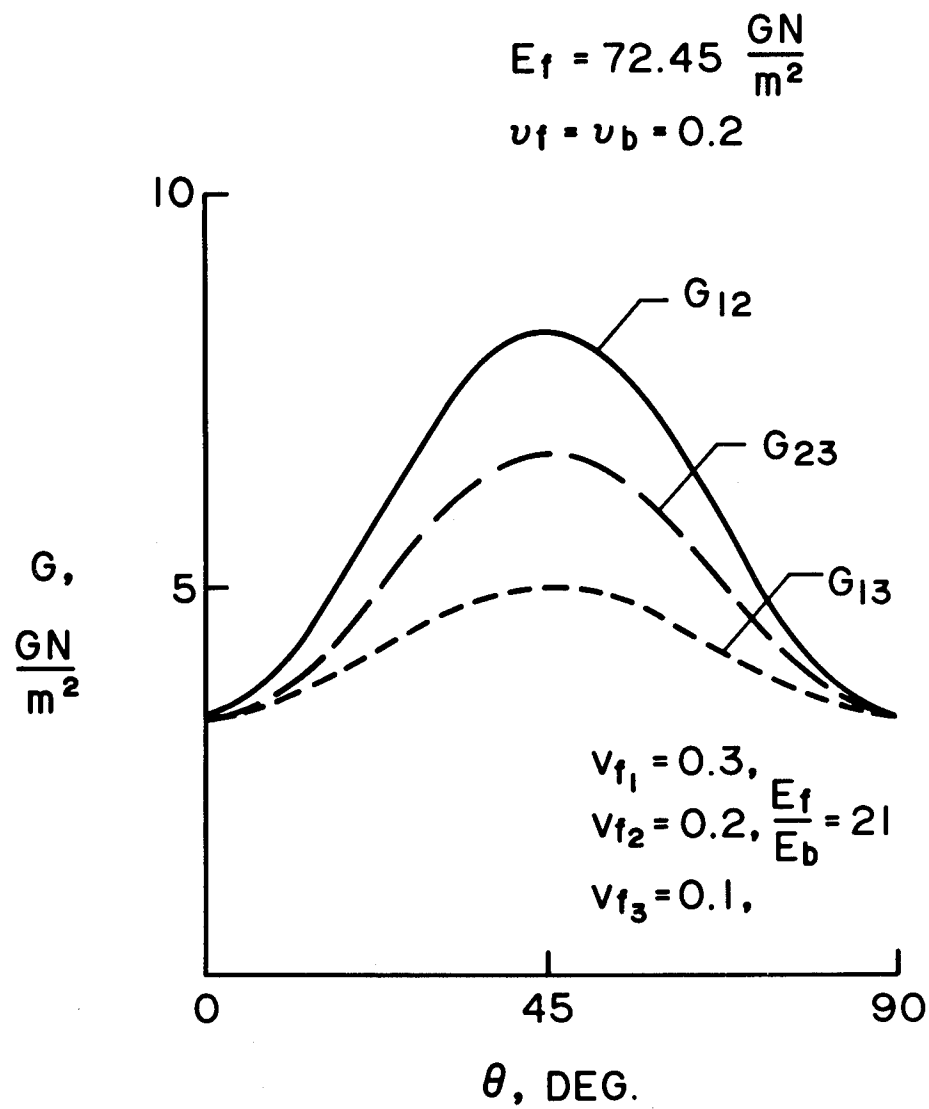
Figure 47. Shearing Stiffnesses of Composites with Three Orthogonal, Skew
Pairs of Filamentary Reinforcements, with Different Volume
Fractions in the Three Directions
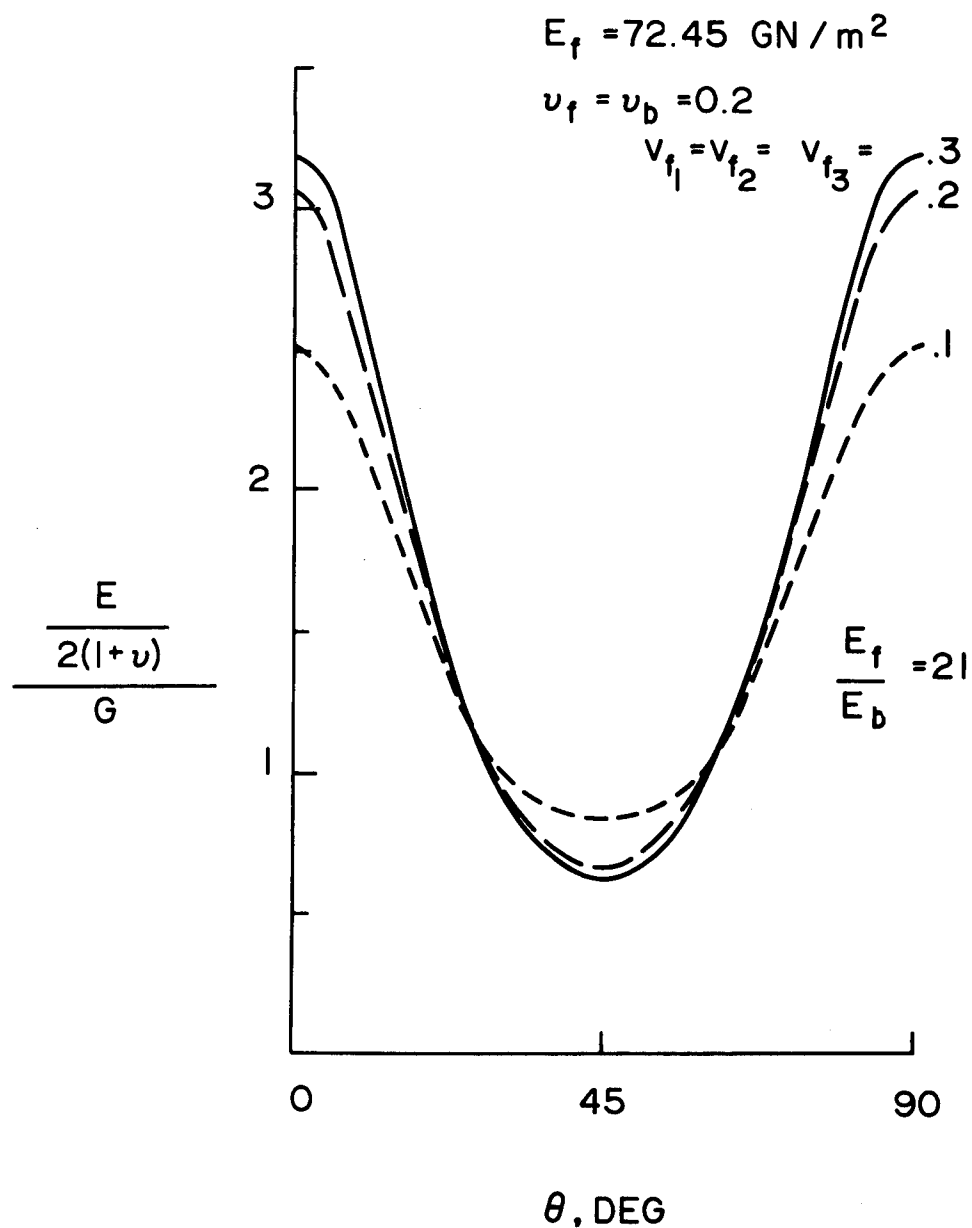
Figure 48. Ratio of Stretching Stiffness to Shearing Stiffness as Measured by

$$\frac{\dfrac{E_1}{2(1+\nu_{21})}}{G_{12}} = \frac{\dfrac{E_2}{2(1+\nu_{32})}}{G_{23}} = \frac{\dfrac{E_3}{2(1+\nu_{31})}}{G_{13}}$$

$$(E_1 = E_2 = E_3, \ G_{12} = G_{23} = G_{13}, \ \nu_{21} = \nu_{32} = \nu_{31})$$

for Composites with Three Orthogonal, Skew Pairs of Filamentary Reinforcements, with Equal Volume Fractions in the Three Directions

209
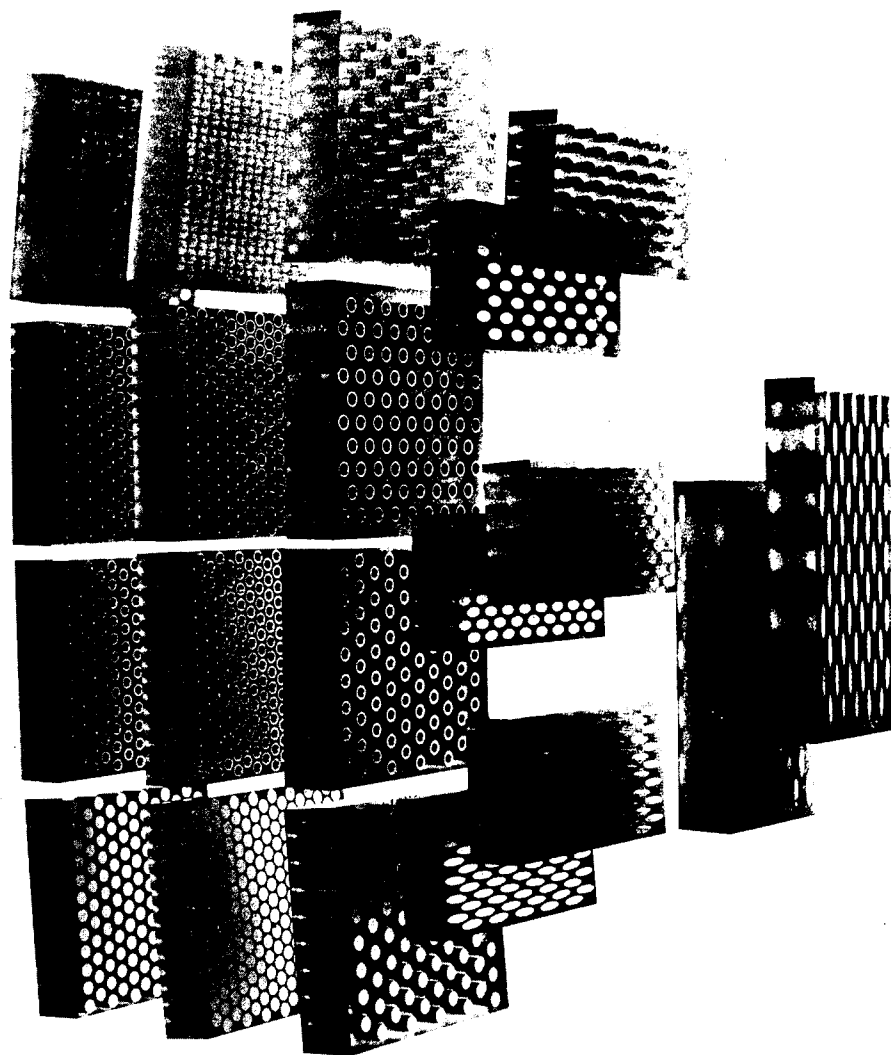
Figure 49. Epoxy Test Specimens with Aluminum Inclusions of Various Configurations Used to Measure Transverse Stiffnesses
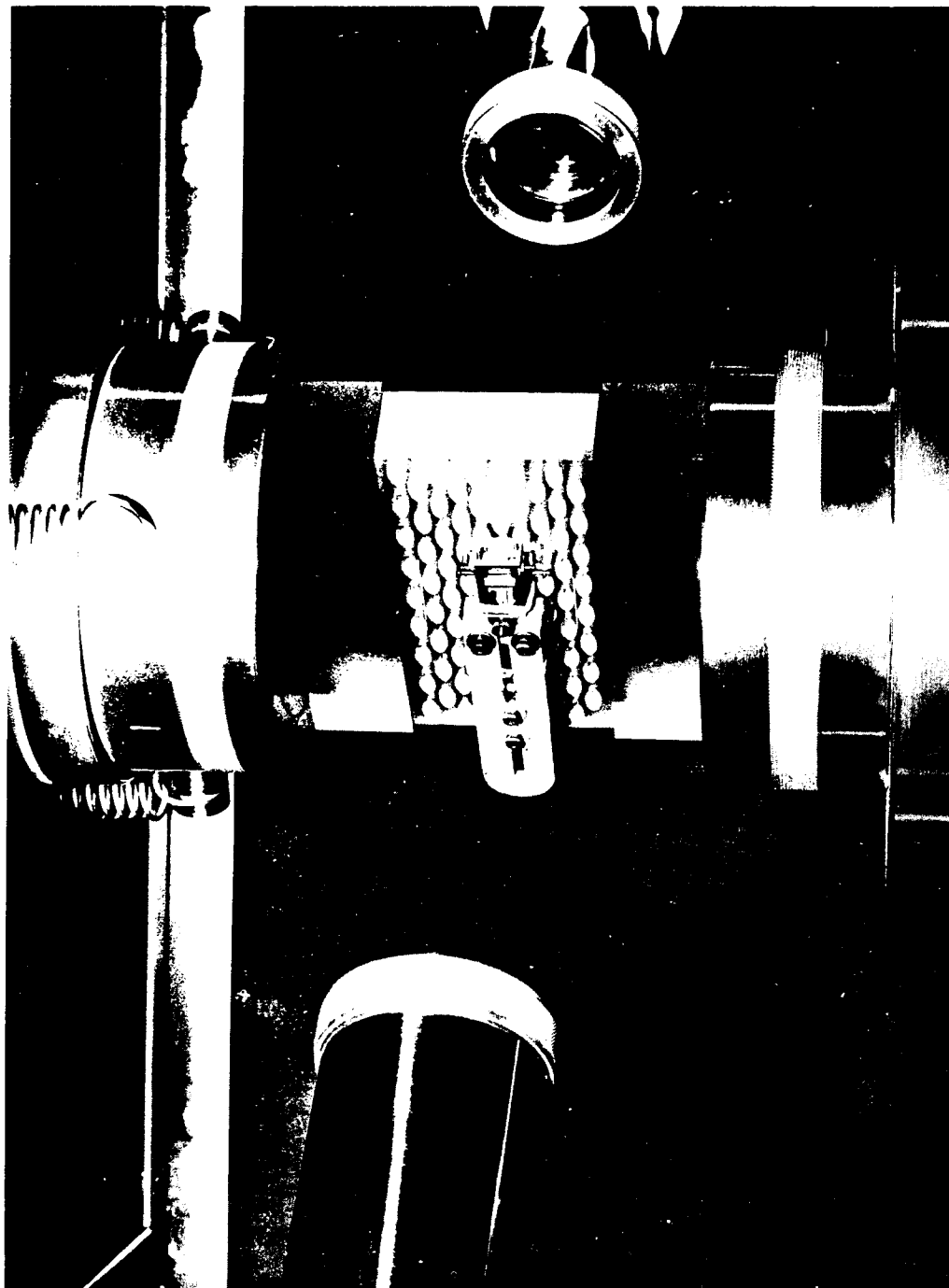
Figure 50. Typical Test Set-up for Measurement of Elastic Properties of Enlarged Models of Uni-Directionally Reinforced Composites
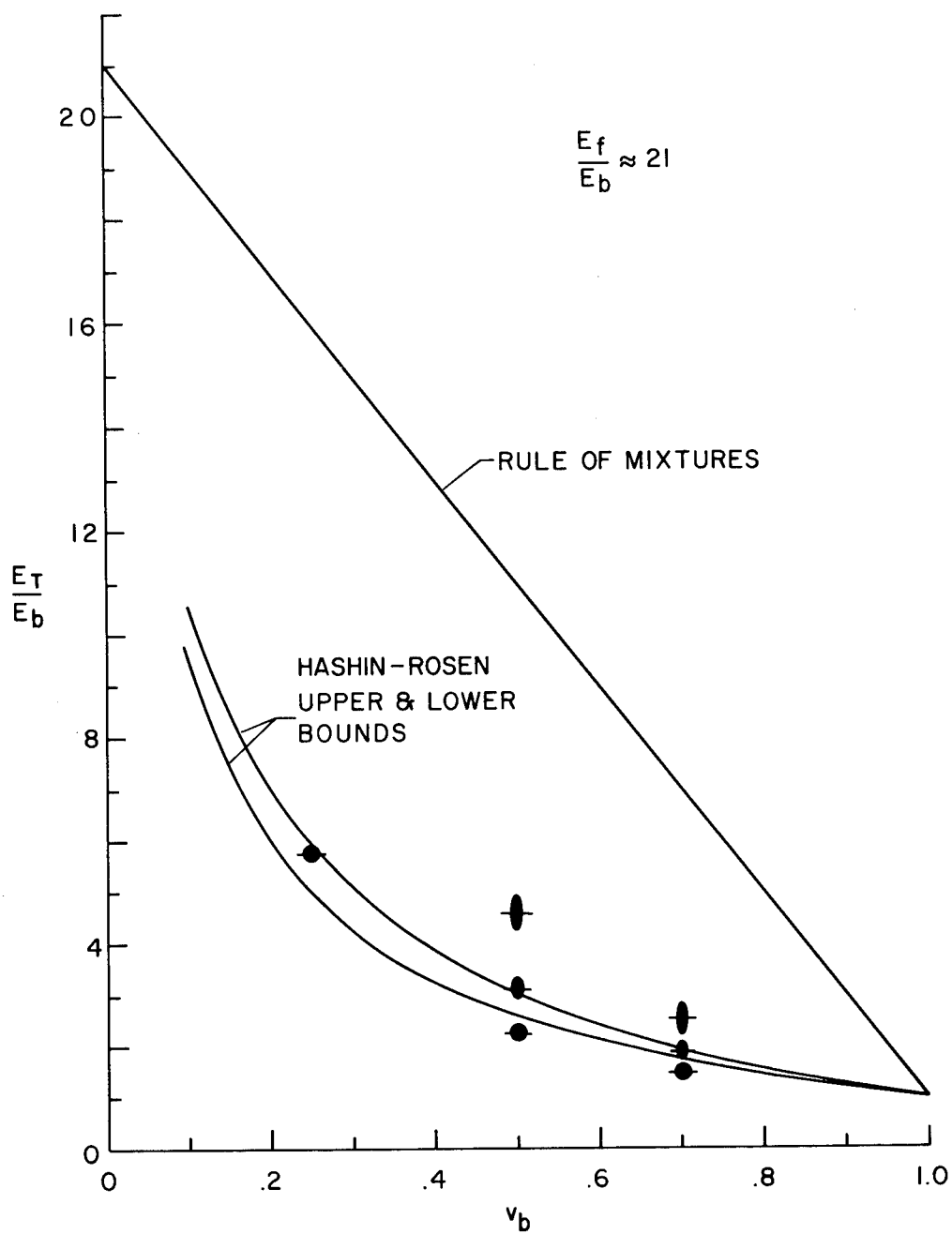
Figure 51. Transverse Stiffnesses of Solid, Round and Elliptical Aluminum
Inclusions in Epoxy, and Comparisons with Predictions. (Ellipses
Loaded in the Direction of the Major Axis.)
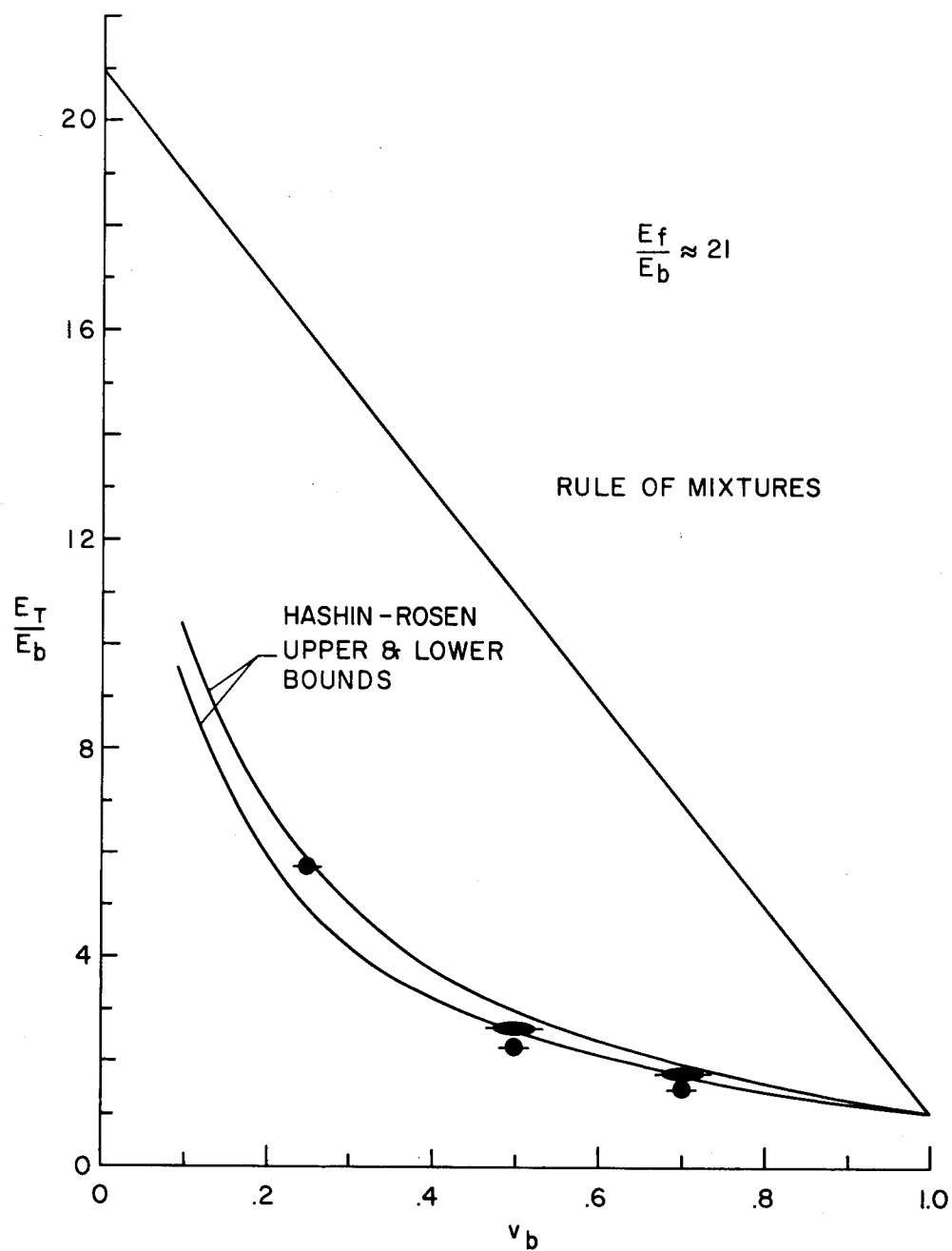
Figure 52. Transverse Stiffnesses of Elliptical Aluminum Inclusions in
Epoxy Loaded in the Direction of the Ellipse Minor Axis
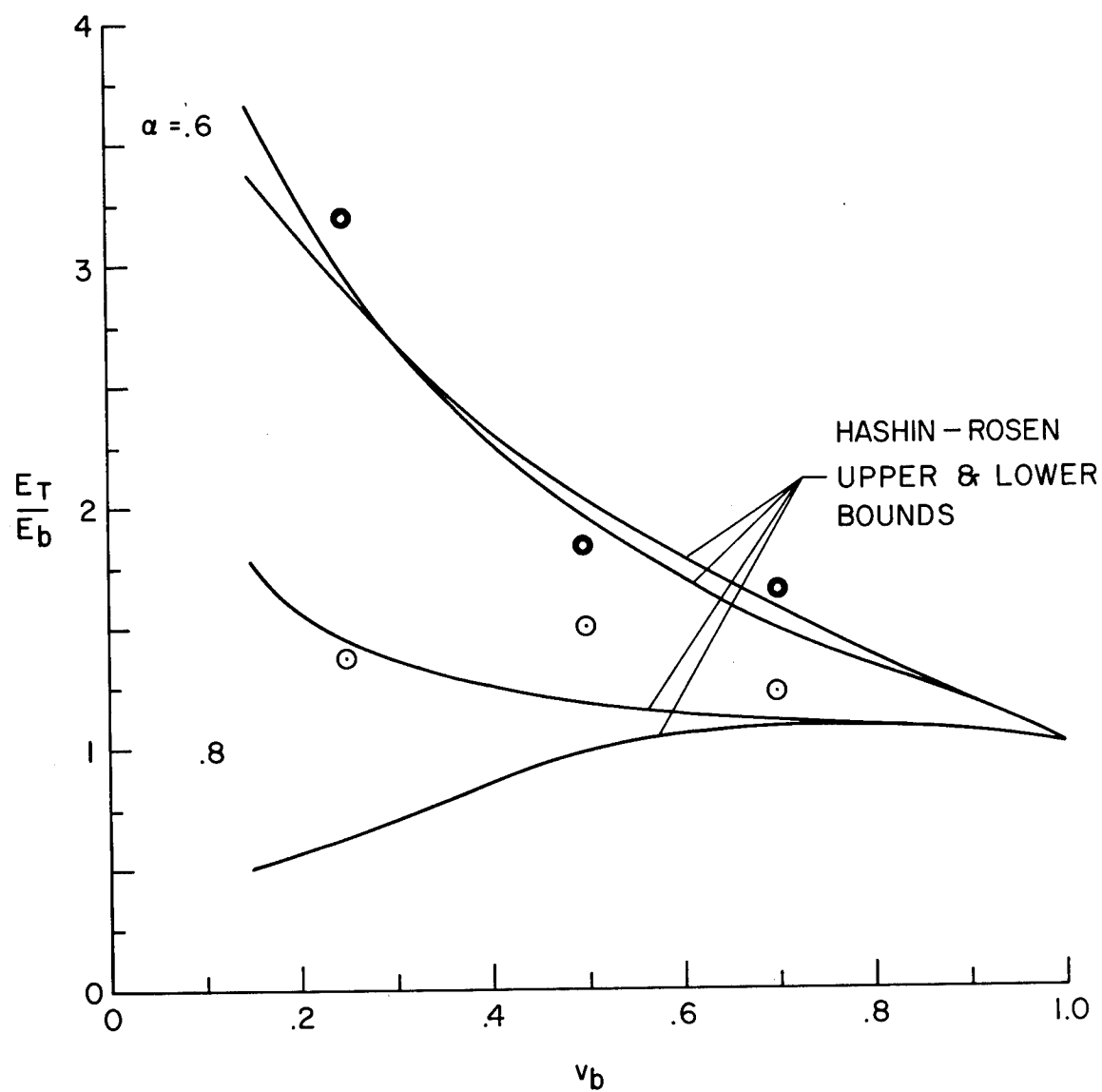
Figure 53. Transverse Stiffnesses of Round Aluminum Inclusions of Two
Hollowness Ratios (α), and Comparison with Predictions
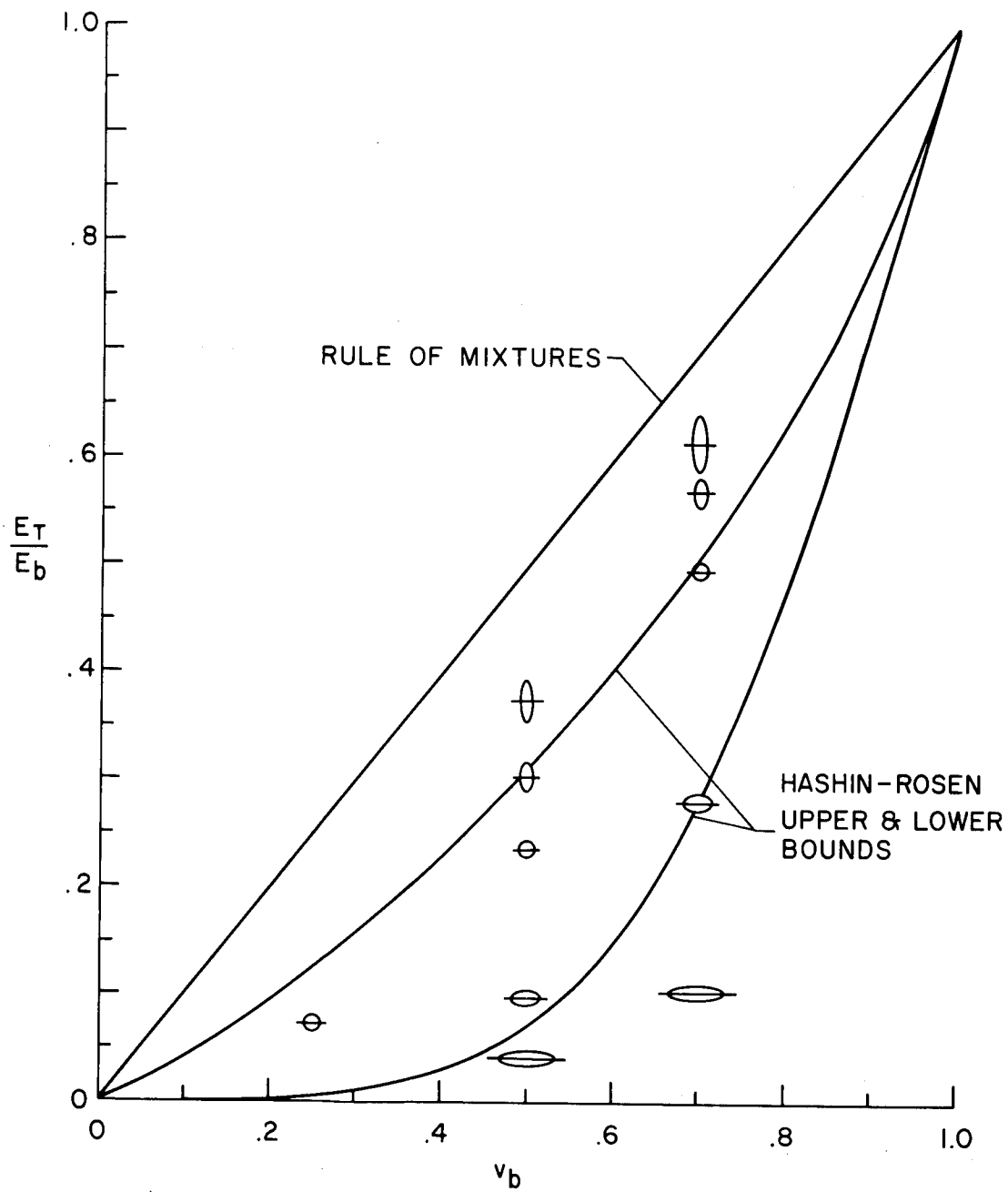
Figure 54. Transverse Stiffness of Epoxy with Holes of Various Shapes and
Volume Fractions, and Comparison with Predictions
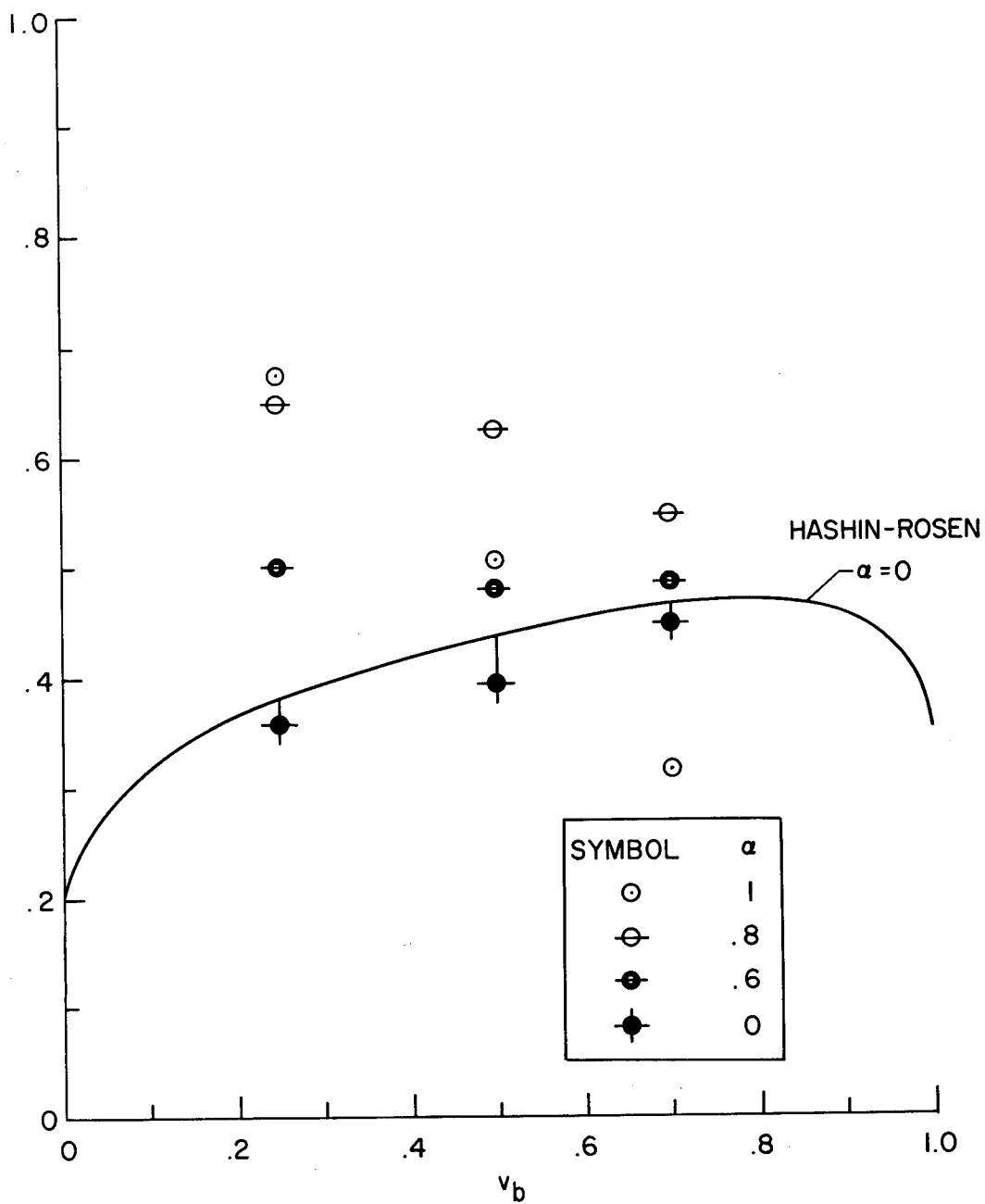
Figure 55. Poisson's Ratios for Aluminum Inclusions in Epoxy for Transverse
Loadings (Inclusion Shape Indicated by Plotted Symbols)

$V_f = 0.3$
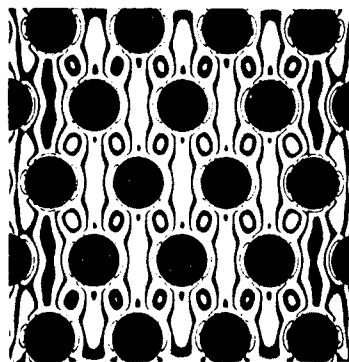
$.5$
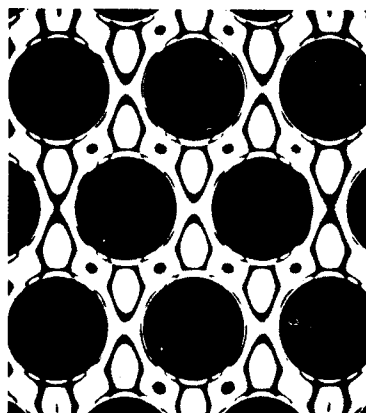
$.7$
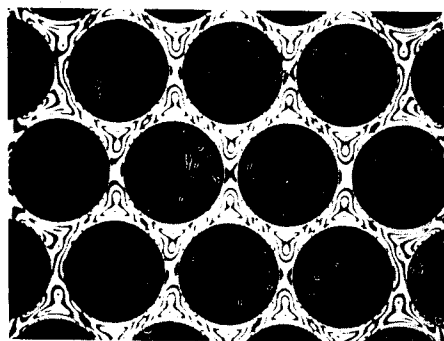
Figure 56. Photoelastic Patterns for Regular Arrays of Round Holes Loaded in Vertical Direction of Page

217

$V_f = 0.3$

.5

.7
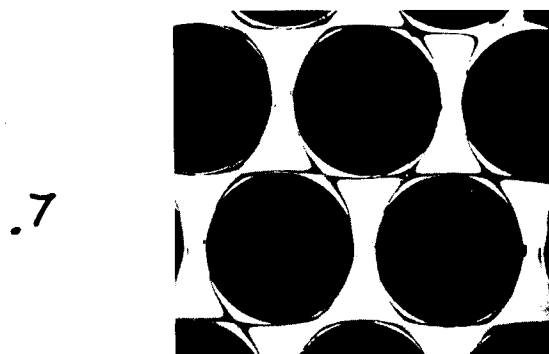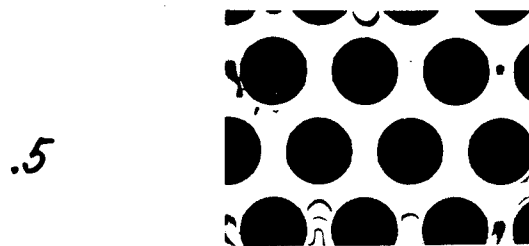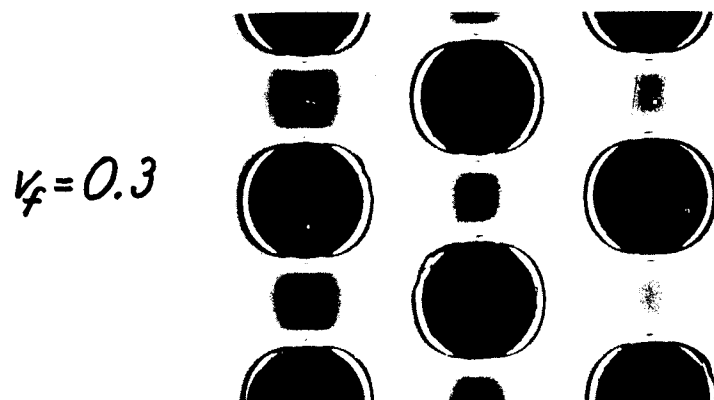
Figure 57. Photoelastic Patterns for Regular Arrays of Round, Solid
Inclusions Loaded in Vertical Direction of Page
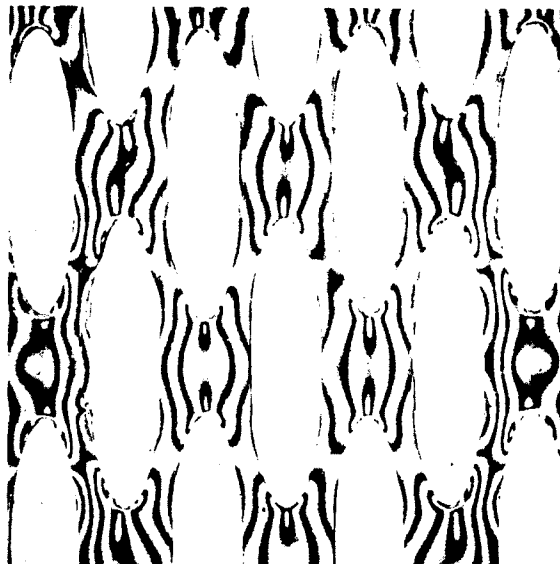
Holes

Inclusions

Figure 58. Photoelastic Patterns for Elliptical Holes and Solid Inclusions
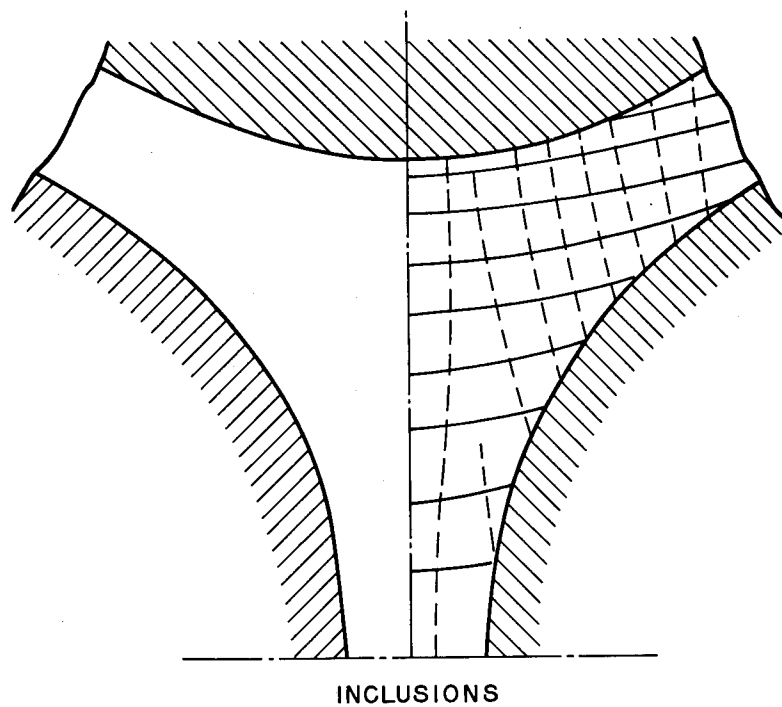(50% Volume Fraction) with Load Applied Along Major Axis
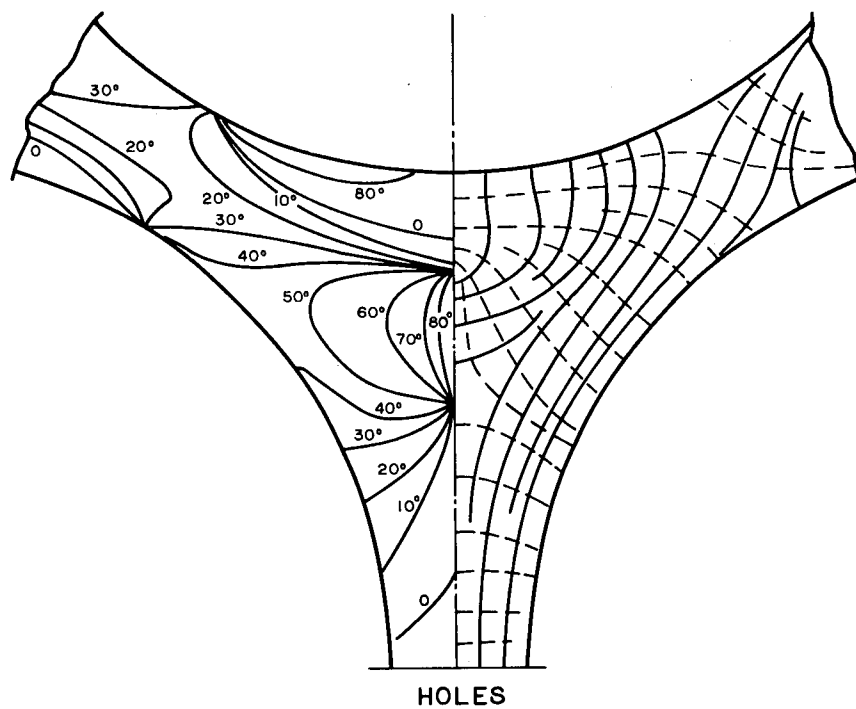Direction

HOLES

INCLUSIONS

Figure 59. Isoclinics and Isostatics Measured for Round Holes and Inclusions at v_f = 0.5. (Load in Vertical Direction of Page)
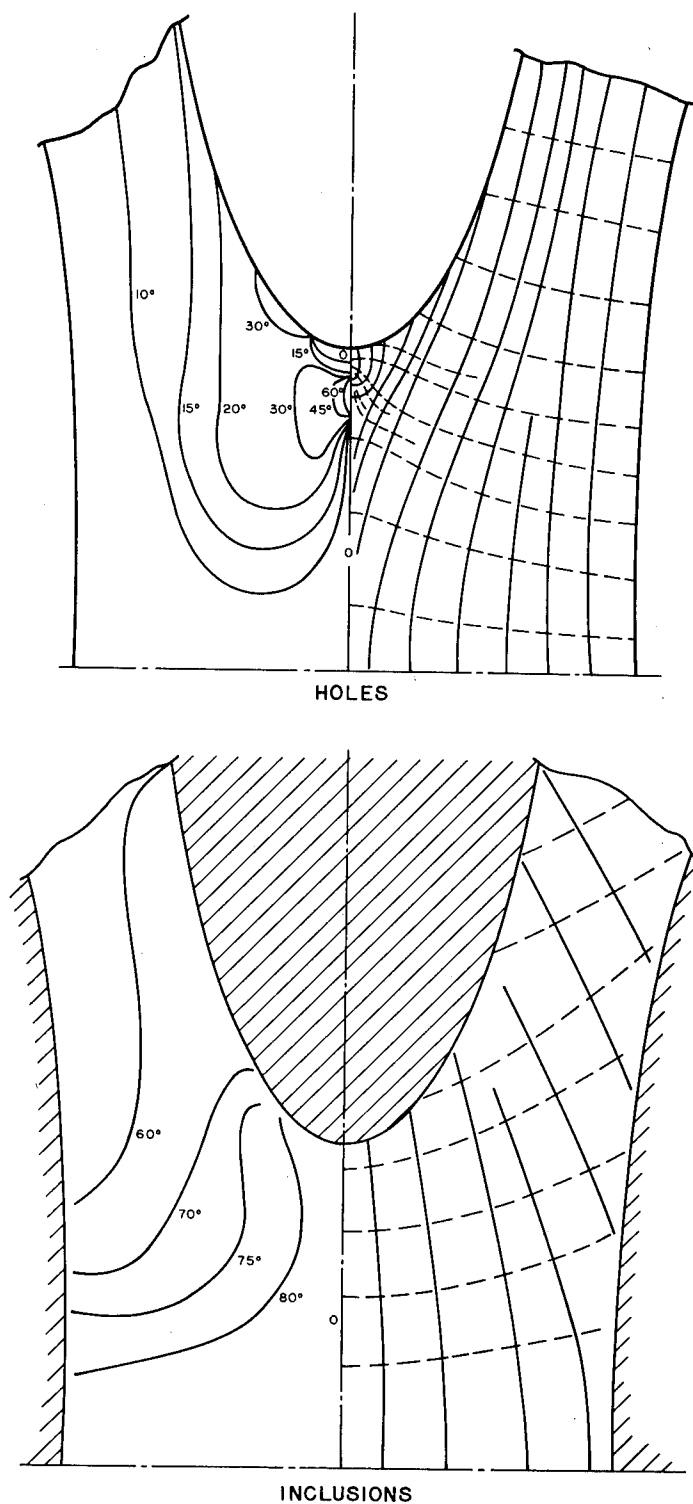
HOLES

INCLUSIONS

Figure 60. Isoclinics and Isostatics Measured for Elliptical Holes and Inclusions at v_f = 0.5. (Load in Direction of Ellipse Major Axis)